Vol. 64 March, 1960 No. 3

THE JOURNAL OF PHYSICAL CHEMISTRY

(Registered in U. S. Patent Office)

CONTENTS

SYMPOSIUM ON HIGH TEMPERATURE REACTIONS AND PHENOMENA, Boston, Mass, April 7–10, 1959

NOTES

COMMUNICATIONS TO THE EDITOR

THE JOURNAL OF PHYSICAL CHEMISTRY

(Registered in U. S. Patent Office)

W. Albert Noyes, Jr., Editor

Allen D. Bliss — Assistant Editors — A. B. F. Duncan

Editorial Board

A. O. Allen
C. E. H. Bawn
John D. Ferry
S. C. Lind
R. G. W. Norrish
R. E. Rundle
W. H. Stockmayer
G. B. B. M. Sutherland
A. R. Ubbelohde
E. R. Van Artsdalen
Edgar F. Westrum, Jr.

Published monthly by the American Chemical Society at 20th and Northampton Sts., Easton, Pa.

Second-class mail privileges authorized at Easton, Pa. This publication is authorized to be mailed at the special rates of postage prescribed by Section 131.122.

The *Journal of Physical Chemistry* is devoted to the publication of selected symposia in the broad field of physical chemistry and to other contributed papers.

Manuscripts originating in the British Isles, Europe and Africa should be sent to F. C. Tompkins, The Faraday Society, 6 Gray's Inn Square, London W. C. 1, England.

Manuscripts originating elsewhere should be sent to W. Albert Noyes, Jr., Department of Chemistry, University of Rochester, Rochester 20, N. Y.

Correspondence regarding accepted papers, proofs and reprints should be directed to Assistant Editor, Allen D. Bliss, Department of Chemistry, Simmons College, 300 The Fenway, Boston 15, Mass.

Business Office: Alden H. Emery, Executive Secretary, American Chemical Society, 1155 Sixteenth St., N. W., Washington 6, D. C.

Advertising Office: Reinhold Publishing Corporation, 430 Park Avenue, New York 22, N. Y.

Articles must be submitted in duplicate, typed and double spaced. They should have at the beginning a brief Abstract, in no case exceeding 300 words. Original drawings should accompany the manuscript. Lettering at the sides of graphs (black on white or blue) may be pencilled in and will be typeset. Figures and tables should be held to a minimum consistent with adequate presentation of information. Photographs will not be printed on glossy paper except by special arrangement. All footnotes and references to the literature should be numbered consecutively and placed in the manuscript at the proper places. Initials of authors referred to in citations should be given. Nomenclature should conform to that used in *Chemical Abstracts*, mathematical characters be marked for italic, Greek letters carefully made or annotated, and subscripts and superscripts clearly shown. Articles should be written as briefly as possible consistent with clarity and should avoid historical background unnecessary for specialists.

Notes describe fragmentary or incomplete studies but do not otherwise differ fundamentally from articles and are subjected to the same editorial appraisal as are articles. In their preparation particular attention should be paid to brevity and conciseness. Material included in Notes must be definitive and may not be republished subsequently.

Communications to the Editor are designed to afford prompt preliminary publication of observations or discoveries whose value to science is so great that immediate publication is imperative. The appearance of related work from other laboratories is in itself not considered sufficient justification for the publication of a Communication, which must in addition meet special requirements of timeliness and significance. Their total length may in no case exceed 500 words or their equivalent. They differ from Articles and Notes in that their subject matter may be republished.

Symposium papers should be sent in all cases to Secretaries of Divisions sponsoring the symposium, who will be responsible for their transmittal to the Editor. The Secretary of the Division by agreement with the Editor will specify a time after which symposium papers cannot be accepted. The Editor reserves the right to refuse to publish symposium articles, for valid scientific reasons. Each symposium paper may not exceed four printed pages (about sixteen double spaced typewritten pages) in length except by prior arrangement with the Editor.

Remittances and orders for subscriptions and for single copies, notices of changes of address and new professional connections, and claims for missing numbers should be sent to the American Chemical Society, 1155 Sixteenth St., N. W., Washington 6, D. C. Changes of address for the *Journal of Physical Chemistry* must be received on or before the 30th of the preceding month.

Claims for missing numbers will not be allowed (1) if received more than sixty days from date of issue (because of delivery hazards, no claims can be honored from subscribers in Central Europe, Asia, or Pacific Islands other than Hawaii), (2) if loss was due to failure of notice of change of address to be received before the date specified in the preceding paragraph, or (3) if the reason for the claim is "missing from files."

Subscription Rates (1960): members of American Chemical Society, $12.00 for 1 year; to non-members, $24.00 for 1 year. Postage to countries in the Pan-American Union $0.80; Canada, $0.40; all other countries, $1.20. Single copies, current volume, $2.50; foreign postage, $0.15, Canadian postage, $0.05; Pan-Aderican Union, $0.05. Back volumes (Vol. 56–59) $25.00 per volume; (starting with Vol. 60) $30.00 per volume; foreign postage per volume $1.20, Canadian, $0.15; Pan-American Union, $0.25. Single copies: back issues, $3.00; for current year, $2.50; postage, single copies: foreign, $0.15; Canadian, $0.05; Pan American Union, $0.05.

The American Chemical Society and the Editors of the *Journal of Physical Chemistry* assume no responsibility for the statements and opinions advanced by contributors to This Journal.

The American Chemical Society also publishes *Journal of the American Chemical Society, Chemical Abstracts, Industrial and Engineering Chemistry*, International Editon of *Industrial and Engineering Chemistry, Chemical and Engineering News, Analytical Chemistry, Journal of Agricultural and Food Chemistry, Journal of Organic Chemistry, Journal of Chemical and Engineering Data* and *Chemical Reviews*. Rates on request.

30 U.A. 2503

THE JOURNAL OF
PHYSICAL CHEMISTRY

(Registered in U. S. Patent Office) (© Copyright, 1960, by the American Chemical Society)

VOLUME 64 MARCH 29, 1960 NUMBER 3

THE HIGH TEMPERATURE THERMODYNAMIC FUNCTIONS OF CERIUM, NEODYMIUM AND SAMARIUM[1]

BY F. H. SPEDDING, J. J. MCKEOWN AND A. H. DAANE

Contribution No. 612 from the Institute for Atomic Research and Department of Chemistry, Iowa State College. Work was performed in the Ames Laboratory of the U. S. Atomic Energy Commission

Received March 13, 1959

The high temperature enthalpies of cerium, neodymium and samarium were measured from 0 to 1100° using a Bunsen ice calorimeter. The heat capacity and related thermodynamic quantities of the metals are tabulated at 50-degree intervals. The heats of transition and fusion were determined for these metals, with cerium having the lowest values and samarium the highest. Correlation has been made between the results of this study and calculated quantities contributing to the heat capacity of metals.

I. Introduction

As the rare earth metals have become available in quantity and in high purity, many of their physical properties are being determined. In studies in this Laboratory, thermal analyses to determine the melting points of some of these metals[2] showed the presence of a solid state transformation at temperatures near the melting points. The sizable heat effects associated with this transformation indicated a fundamental change in the nature of these metals, and this was confirmed by Barson, Legvold and Spedding[3a] in dilatometric studies and by Spedding, Daane and Herrmann[3b] in electrical resistivity studies. To examine this phenomenon in these metals and to determine their heat capacities, and heats of transition and fusion, a high temperature calorimetric study of the rare earth metals was begun. This paper describes the procedures used and the results obtained in a study of cerium, neodymium and samarium metals.

Equipment and Materials

Calorimeter.—A modification of the Bunsen ice calorimeter employed by Furukawa and others[4] was used in this investigation. A Teflon stopcock in the mercury accounting assembly was found to function satisfactorily instead of a paraffin-packed, soft iron needle valve. Grease for lubrication was not necessary and thus there was no contamination of the mercury from this source. To reduce thermal conduction out of the calorimeter along the central tube, the halves of the gate housing were separated by a rubber "O" ring, and screws holding the gate housing together passed through thermal insulators. The outer glass flask was attached to the metal head of the calorimeter by means of a collar seal. The open end of the flask had a ground glass flange which seated on a Neoprene gasket. A rubber "O" ring fitted on the outside of the flask on the top of the ground glass flange. A circular brass collar screwed on the brass head and compressed the "O" ring and flask against the Neoprene gasket. A vacuum was drawn between the chambers before the brass collar was screwed tightly into place. The inner glass flask was sealed to the head by means of a Kovar seal. The calorimeter was submerged in a constant temperature bath contained in a 30-gallon barrel; this bath contained crushed ice and a very dilute solution of methanol in water. It was found that by adding a few milliliters of methanol to the bath each morning before packing with ice, the heat leak could be adjusted to a low constant value for a period of 16 hours without any repacking of the ice. The space between the calorimeter chamber and the outer flask could be evacuated continuously, thus eliminating the task of evacuating this chamber and filling it with a dry insulating gas each day.

A new technique was employed for forming the ice mantle. Helium, previously cooled by passing through a copper coil immersed in liquid nitrogen, was passed down a tube inserted into the calorimeter well. Two different types of helium-dispersing tips were employed on this tube; one had an open end which localized freezing on the bottom plate while the other tube had a closed end with horizontal jets located near the bottom. By adjusting the height of the inserted tube and the rate of flow of helium, an ice mantle of the desired shape could be frozen at the desired rate. The shape of the mantle during freezing was observed by means of a simple glass periscope designed for this purpose. The usual precautions were observed in introducing outgassed conductivity water and mercury into the calorimeter.

(1) This paper is based in part on a Ph.D. Thesis presented to Iowa State College, February, 1958, by J. J. McKeown.

(2) F. H. Spedding and A. H. Daane, in "Progress in Nuclear Energy," ser. 5, Vol. 1, H. M. Finniston and J. P. Howe, Eds., Pergamon Press, London, 1956, p. 413.

(3) (a) F. Barson, S. Legvold and F. H. Spedding, *Phys. Rev.*, **105**, 418 (1957); (b) F. H. Spedding, A. H. Daane and K. W. Herrmann, *J. Metals*, **9**, 895 (1957).

(4) G. T. Furukawa, T. B. Douglas, R. E. McCoskey and D. C. Ginnings, *Bur. Standards J. Research*, **57**, 67 (1956).

The furnace employed was designed to determine the heats of fusion of the rare earth metals melting below 1200°. The main windings of the furnace consisted of #18 B and S gauge platinum (10% rhodium) wire. The power to these windings was supplied by an electronic temperature controller designed by Svec, Reade and Hilker.[5] The power to auxiliary windings on each end of the furnace tube was regulated by a voltage stabilizer and adjusted with a variable transformer. These end windings were used to minimize the thermal gradient in the center of the furnace where the sample was located. The dropping mechanism was a modification of the one described by Southard.[6] To attain thermal equilibrium in the furnace, the sample was held in position in the furnace by a string attached to the soft iron piston. The sample was dropped by releasing the soft iron piston from the core of a solenoid coil, after releasing the string. Reproducible dropping times were achieved by adjusting the weight of the falling assembly by addition of lead granules to the hollow soft iron piston. An empty platinum crucible of the same weight used to contain the corundum sample was dropped at 100° intervals as a blank; for the rare earth metal samples, the blank was an empty platinum crucible containing an empty tantalum crucible, both of the same weight used to contain the sample.

The temperature of the sample was measured with a platinum (10% rhodium)–platinum thermocouple whose hot junction was within a dummy platinum capsule inserted in the sample's position in the furnace. The calibration of this second thermocouple was checked frequently with the freezing point of samples certified by the National Bureau of Standards.

Materials.—To standardize the calorimeter a fused α-Al_2O_3 (corundum) sample 1'' long and $^1/_2$'' in diameter weighing 12.3136 g. was used; this was enclosed in a drawn platinum crucible. Spectrographic analyses indicated only a faint trace of silicon as an impurity in the corundum.

The rare earth metal samples were prepared from salts separated and purified by ion-exchange methods described by Spedding and Powell.[7] The anhydrous fluorides of cerium and neodymium were prepared by heating a mixture of the respective oxide with ammonium bifluoride to 400° in a stream of dry air. The metals were prepared by reducing these fluorides with calcium by methods described by Spedding and Daane.[2] The more volatile samarium metal was prepared by reducing its oxide with lanthanum metal *in vacuo* at 1400° as described by Daane, Dennison and Spedding.[8] The cerium and neodymium were melted down in their crucibles in a high vacuum at temperatures 100° above their melting points. Because of its high vapor pressure at its melting point, the samarium sample was melted into its crucible under an atmosphere of helium. Lids were welded on the tantalum crucibles under an atmosphere of helium; these were in turn forced into snugly fitting, drawn platinum crucibles which were welded closed in a helium atmosphere. The weights of the cerium, neodymium and samarium samples were 21.9943, 21.1556 and 22.5138 g., respectively. Table I indicates the results of spectrographic analyses of the metals.

TABLE I

SPECTROGRAPHIC ANALYSIS OF SAMPLES

Sample	Impurities,[a] %					
Cerium	Ca	La	Si			
	≤0.05	≤0.01	≤0.02			
Neodymium	Ca	Fe	Pr	Sm	Si	Ta
	~0.1	≤0.01	≤0.04	≤0.03	≤0.02	≤0.02
Samarium	Ca	Eu	Fe	La	Mg	Si
	≤0.05	≤0.2	~0.01	≤0.01	≤0.01	≤0.01

[a] The numbers with the symbol ≤ represent the lower limit of detection of the spectrographic method.

Results

The data for the heat content of α-Al_2O_3 (corundum) are compared in Table II with those of the National Bureau of Standards.[9] The maximum discrepancy between the two sets of data is 0.16% at 200°. The agreement between the two sets of data indicated that the apparatus was functioning properly.

TABLE II

HEAT CONTENT OF α-Al_2O_3

Furn. temp. (°C.)	Measured $H^0 - H^0_{273.15}$ (cal. g.$^{-1}$)	Reproducibility (%)	N.B.S. Meas. $H^0 - H^0_{273.15}$ (cal. g.$^{-1}$)	Dev. of meas. from N.B.S. (%)
100.5	19.70	0.21	19.69	+0.05
201.0	42.85	.07	42.92	− .16
301.5	68.41	.06	68.40	+ .01
402.1	95.29	.11	95.25	+ .04
500.9	122.42	.08	122.43	− .01
600.6	150.75	.06	150.80	− .03
698.2	178.94	.03	179.03	− .05
800.0	208.78	.06	208.97	− .10
901.6	239.13	.03	239.23	− .04
1001.5	268.77	.10		
1102.0	298.72	.07		

The enthalpies of cerium, neodymium and samarium were determined from 0 to 1100° at 100-degree intervals, except near the transition temperatures and melting points where more closely spaced measurements were made. To examine the possibility of quenching in any of the heat content in dropping to 0°, a small sample of neodymium metal was dropped into a copper block at the temperature of liquid nitrogen (−196°); this was then examined immediately in an X-ray diffractometer which showed only the room temperature form of the metal to be present. This suggested that the much less drastic quenching of the double clad samples to 0° in the actual measurements would not introduce significant error. The data in each case were fitted to an empirical equation utilizing a least-squares treatment. Three equations were needed: from 0° to the transition temperature, from the transition temperature to the melting point and for the liquid region.

The empirical equations for the enthalpy (cal. mole^{-1}) of cerium as a function of temperature are

$$H^0 - H^0_{273.15} = 6.366t + 1.474 \times 10^{-3}t^2 + 3.954 \times 10^{-2}t^3 \quad (0.14\%,\ 0\text{–}730^\circ) \quad (1)$$

$$H^0 - H^0_{273.15} = 9.047t - 318 \quad (0.02\%,\ 730\text{–}804^\circ) \quad (2)$$

$$H^0 - H^0_{273.15} = 9.345t + 680 \quad (0.04\%,\ 804\text{–}1100^\circ) \quad (3)$$

where the percentage listed after each equation refers to the average deviation of the calculated from the observed results. The mean heat capacity (cal. degree^{-1}mole^{-1}) from 0 to 730° can be expressed by the equation

$$C_p = 6.37 + 2.95 \times 10^{-3}t + 1.19 \times 10^{-6}t^2 \quad (4)$$

The heat capacities of the high temperature form and the liquid metal are constant at 9.05 and 9.35 cal. per degree per mole, respectively. The measured enthalpies with their corresponding reproducibilities and deviations are listed in Table III while Table IV gives derived thermodynamic functions at 50-degree intervals. The value of $S^0 - S^0_0$ at 298.15°K. was obtained from a private com-

(5) H. J. Svec, A. A. Reade and D. W. Hilker, U. S. Atomic Energy Commission Report ISC-585 (1955) (Iowa State College, Ames, Iowa. Office of Technical Services, Washington 25, D. C.).

(6) J. C. Southard, *J. Am. Chem. Soc.*, **63**, 3142 (1941).

(7) F. H. Spedding and J. E. Powell, *J. Metals*, **6**, 1131 (1954).

(8) A. H. Daane, D. H. Dennison and F. H. Spedding, *J. Am. Chem. Soc.*, **75**, 2272 (1953).

(9) D. C. Ginnings and R. J. Corruccini, *Bur. Standards J. Research*, **38**, 583 (1947).

munication from Jennings. The heats of transition and fusion of 700 ± 8 and 1238 ± 4 cal. per mole were obtained by evaluating the appropriate equations at the transition temperature and melting point. The errors in the heats of transition and fusion were computed from the average deviations of the empirical equations. Figure 1 is a plot of the enthalpy of cerium *versus* temperature into the liquid region.

TABLE III

HEAT CONTENT OF CERIUM

Furn. temp. (°C.)	Measured $H^0 - H^0_{273.15}$ (cal. mole^{-1})	Reproducibility (%)	Calcd. $H^0 - H^0_{273.15}$ (cal. mole^{-1})	Dev. of calcd. from obsd. (%)
100.3	652.4	0.20	653.7	+0.20
202.1	1348.3	.10	1350.1	+ .13
300.5	2060.8	.07	2056.8	− .19
400.3	2807.5	.04	2809.9	+ .09
500.7	3600.2	.07	3606.6	+ .18
600.7	4446.4	.05	4441.6	− .11
701.3	5323.2	.03	5325.7	+ .05
743.0	6402.8	.02	6403.8	+ .02
767.0	6622.2	.05	6620.9	− .02
789.7	6825.2	.04	6826.3	+ .02
811.4	8266.3	.03	8263.1	− .04
905.7	9140.9	.04	9144.4	+ .04
1002.2	10,043.8	.13	10,046.2	+ .02
1100.8	10,970.4	.06	10,967.7	− .02

TABLE IV

THERMODYNAMIC FUNCTIONS OF CERIUM (CAL. DEGREE^{-1} MOLE^{-1})

T, °K.	C_p	$S^0 - S^0_0$	$\frac{H^0 - H^0_{298.15}}{T}$[a]	$-\left(\frac{F^0 - H^0_{298.15}}{T}\right)$
298.15	6.44	18.12	0.0	18.12
300	6.45	18.16	0.040	18.12
350	6.60	19.16	0.966	18.19
400	6.76	20.06	1.680	18.38
450	6.92	20.86	2.253	18.61
500	7.10	21.60	2.729	18.87
550	7.27	22.29	3.134	19.16
600	7.46	22.93	3.487	19.44
650	7.65	23.53	3.799	19.73
700	7.84	24.10	4.081	20.02
750	8.04	24.65	4.338	20.31
800	8.25	25.18	4.576	20.60
850	8.46	25.68	4.798	20.88
900	8.68	26.17	5.008	21.16
950	8.90	26.65	5.207	21.44
1000	9.14	27.11	5.398	21.71
1003.15	9.15	27.14	5.409	21.73
1003.15	9.05	27.84	6.107	21.73
1050	9.05	28.25	6.238	22.01
1077.15	9.05	28.48	6.309	22.17
1077.15	9.35	29.63	7.458	22.17
1100	9.35	29.83	7.497	22.33
1150	9.35	30.24	7.577	22.66
1200	9.35	30.64	7.651	22.99
1250	9.35	31.02	7.719	23.30
1300	9.35	31.39	7.781	23.61
1350	9.35	31.74	7.839	23.90
1373.15	9.35	31.90	7.865	24.03

[a] $(H^0_{298.15} - H^0_0)/T$ = 7.63 cal. degree^{-1} mole^{-1} based on a private communication from Jennings.

The empirical equations which were fitted to the enthalpy values for neodymium are

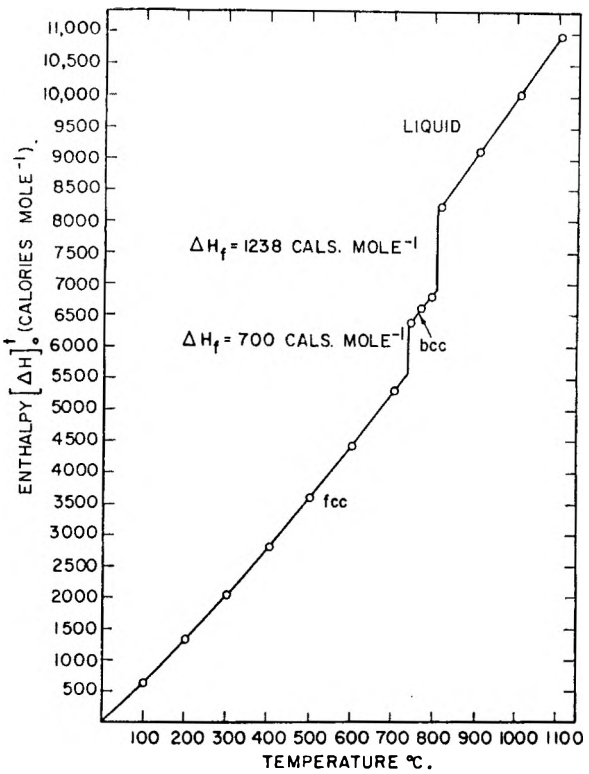

Fig. 1.—The high temperature enthalpy of cerium *versus* temperature. Typical of rare earths with a crystallographic transition below the melting point.

$$H^0 - H^0_{273.15} = 6.508t + 1.239 \times 10^{-3}t^2 + 1.085 \times 10^{-6}t^3 \quad (0.2\%,\ 0\text{–}862°) \quad (5)$$

$$H^0 - H^0_{273.15} = 10.654t - 1238 \quad (0.003\%,\ 862\text{–}1024°) \quad (6)$$

$$H^0 - H^0_{273.15} = 11.66t - 5641 \quad (0.17\%,\ 1024\text{–}1100°) \quad (7)$$

Upon differentiating equation 5 with respect to temperature, the heat capacity equation from 0 to 862° was found to be

$$C_p = 6.51 + 2.49 \times 10^{-3}t + 3.26 \times 10^{-6}t^2 \quad (8)$$

while the heat capacities in the transition region and liquid were constant at 10.65 and 11.66, respectively. Tables V and VI give measured enthalpies and calculated thermodynamic functions. The value of $S^0 - S^0_0$ for neodymium at 298.15°K. was taken from the data of Parkinson, Simon and Spedding.[10] The heats of transition and fusion were found to be 713 ± 15 and 1705 ± 19 cal. per mole.

It was more difficult to find an empirical equation to fit the samarium data below the transition temperature. The equations which fit the data in the three regions are

$$H^0 - H^0_{273.15} = 11.804t + 4.776 \times 10^{-4}t^2 - 3.477 \times 10^3 \log\left(\frac{t + 273.15}{273.15}\right) \quad (0.4\%,\ 0\text{–}917°) \quad (9)$$

$$H^0 - H^0_{273.15} = 11.216t - 538 \quad (0.06\%,\ 917\text{–}1072°) \quad (10)$$

$$H^0 - H^0_{273.15} = 14.041t - 1505 \quad (0.09\%,\ 1072\text{–}1125°) \quad (11)$$

The equation which defines the heat capacity as a function of temperature from 0 to 917° is

$$C_p = 11.80 + 9.55 \times 10^{-4}t - 1.51 \times 10^3 \frac{1}{t + 273.15} \quad (12)$$

(10) D. H. Parkinson, F. E. Simon and F. H. Spedding, *Proc. Roy. Soc. (London)*, **A207**, 137 (1951).

TABLE V

HEAT CONTENT OF NEODYMIUM

Furn. temp. (°C.)	Measured $H^0 - H^0_{273.15}$ (cal. mole^{-1})	Reproducibility (%)	Calcd. $H^0 - H^0_{273.15}$ (cal. mole^{-1})	Dev. of calcd. from obsd. (%)
99.3	657.0	0.25	659.5	+0.38
202.3	1381.7	.10	1376.2	− .40
300.5	2097.0	.06	2096.9	.00
400.6	2876.2	.01	2875.6	− .02
501.4	3708.6	.13	3711.2	+ .07
602.6	4607.6	.09	4608.9	+ .03
701.0	5545.1	.03	5544.5	− .01
801.2	6571.7	.05	6567.3	− .07
851.8	7105.3	.09	7112.8	+ .11
872.5	8058.2	.08	8057.7	− .01
938.9	8764.4	.05	8764.5	.00
984.8	9254.8	.08	9254.1	− .01
1030.2	11,431.8	.06	11,448.9	+ .15
1059.9	11,822.1	.08	11,795.3	− .23
1093.7	12,174.0	.08	12,189.4	+ .13

TABLE VI

THERMODYNAMIC FUNCTIONS OF NEODYMIUM (CAL. DEGREE^{-1} MOLE^{-1})

T, °K.	C_p	$S^0 - S^0_0$	$\frac{H^0 - H^0_{298.15}}{T}$[a]	$-\left(\frac{F^0 - H^0_{298.15}}{T}\right)$
298.15	6.57	17.50	0.0	17.50
300	6.58	17.54	0.041	17.50
350	6.72	18.56	0.984	17.58
400	6.87	19.47	1.710	17.76
450	7.05	20.29	2.294	18.00
500	7.24	21.04	2.778	18.26
550	7.44	21.74	3.193	18.55
600	7.67	22.40	3.556	18.84
650	7.90	23.02	3.882	19.14
700	8.16	23.62	4.178	19.44
750	8.43	24.19	4.452	19.74
800	8.72	24.74	4.710	20.03
850	9.02	25.28	4.954	20.33
900	9.34	25.81	5.189	20.62
950	9.68	26.32	5.416	20.90
1000	10.03	26.82	5.638	21.18
1050	10.40	27.32	5.856	21.46
1100	10.78	27.81	6.071	21.74
1135.15	11.06	28.16	6.221	21.94
1135.15	10.65	28.79	6.854	21.94
1150	10.65	28.93	6.905	22.02
1200	10.65	29.38	7.061	22.32
1250	10.65	29.82	7.205	22.61
1297.15	10.65	30.21	7.330	22.88
1297.15	11.66	31.52	8.644	22.88
1300	11.66	31.55	8.651	22.90
1350	11.66	31.99	8.763	23.23
1373.15	11.66	32.18	8.812	23.37

[a] $(H^0_{298.15} - H^0_0)/T$ = 6.01 cal. degree^{-1} mole^{-1} from Parkinson, Simon and Spedding.[10]

In the temperature ranges 917–1072° and 1072–1125°, the heat capacities have the constant values 11.22 and 11.80 cal. per degree per mole, respectively. Tables VII and VIII list the measured enthalpies and derived thermodynamic quantities. The value of $S^0 - S^0_0$ at 298.15°K. in Table VIII was obtained from the unpublished low temperature work on samarium by Jennings, Hill and Spedding.[11] The heats of transition and fusion are are 744 ± 36 and 2061 ± 15 cal. per mole.

TABLE VII

HEAT CONTENT OF SAMARIUM

Furn. temp. (°C.)	Measured $H^0 - H^0_{273.15}$ (cal. mole^{-1})	Reproducibility (%)	Calcd. $H^0 - H^0_{273.15}$ (cal. mole^{-1})	Dev. of calcd. from obsd. (%)
101.4	726.4	0.23	725.1	−0.18
200.6	1540.1	.05	1553.9	+ .89
293.7	2412.3	.10	2405.6	− .27
400.6	3482.5	.12	3442.1	−1.16
501.2	4438.8	.05	4462.2	+ .53
601.0	5492.8	.06	5510.2	+ .32
700.7	6592.7	.09	6586.6	− .09
799.4	7674.1	.05	7675.9	+ .02
899.8	8797.0	.04	8807.4	+ .12
928.2	9878.1	.11	9873.2	− .05
976.9	10,411.1	.07	10,419.4	+ .08
1038.0	11,108.7	.05	11,104.7	− .04
1078.9	13,636.1	.04	13,644.2	+ .06
1103.7	14,013.0	.09	13,992.5	− .14
1124.7	14,277.3	.04	14,287.3	+ .07

TABLE VIII

THERMODYNAMIC FUNCTIONS OF SAMARIUM (CAL. DEGREE^{-1} MOLE^{-1})

T, °K.	C_p	$S^0 - S^0_0$	$\frac{H^0 - H^0_{298.15}}{T}$[a]	$-\left(\frac{F^0 - H^0_{298.15}}{T}\right)$
298.15	6.76	16.64	0.0	16.64
300	6.80	16.68	0.042	16.64
350	7.56	17.79	1.064	16.73
400	8.15	18.84	1.914	16.93
450	8.62	19.83	2.634	17.20
500	9.00	20.76	3.252	17.51
550	9.32	21.63	3.790	17.84
600	9.60	22.45	4.263	18.19
650	9.84	23.23	4.683	18.55
700	10.05	23.97	5.059	18.91
750	10.25	24.67	5.399	19.27
800	10.42	25.34	5.707	19.63
850	10.58	25.97	5.989	19.98
900	10.73	26.58	6.248	20.33
950	10.86	27.16	6.487	20.67
1000	10.99	27.72	6.709	21.01
1050	11.11	28.26	6.916	21.34
1100	11.22	28.78	7.109	21.67
1150	11.33	29.28	7.290	21.99
1190.15	11.41	29.67	7.428	22.24
1190.15	11.22	30.30	8.055	22.24
1200	11.22	30.39	8.079	22.31
1250	11.22	30.85	8.204	22.65
1300	11.22	31.29	8.320	22.97
1345.15	11.22	31.67	8.417	23.25
1345.15	14.04	33.20	9.950	23.25
1350	14.04	33.25	9.964	23.29
1398.15	14.04	33.74	10.105	23.63

[a] $(H^0_{298.15} - H^0_0)/T$ = 6.07 cal. degree^{-1} mole^{-1} unpublished value according to Jennings, Hill and Spedding.

Discussion

The transition temperatures of 730° for cerium and 862° for neodymium were reported by Spedding, Daane and Herrmann[3b] who observed sharp breaks in the resistivity *versus* temperature curves at these temperatures. The melting points of cerium, neodymium and samarium were reported

(11) L. Jennings, E. Hill and F. H. Spedding, "The Low Temperature Heat Capacity of Samarium," to be published, Iowa State College, Ames, Iowa (1957).

by Spedding and Daane[2] to be 804, 1024 and 1052°, respectively, from thermal analyses of these metals; the transition in samarium was observed at 917°. In the present study, samarium was found to melt at 1072 ± 5° by dropping the sample at 5° increments above 1052°. This higher value for the melting point of samarium is believed to be due to the 0.2% europium in the samarium used by Spedding and Daane. The transition temperature was found to be 917° in both studies.

It should be noted that the last value of the enthalpy reported for neodymium in the transition region was at 985°, 40 degrees below the reported melting point. Above 985° the enthalpy deviated positively from the linear curve generated by the previous three points in this region. Through a comparison of the transition range for the other rare earths studied, it was assumed that the enthalpy varies linearly with temperature and the curve for neodymium generated by the three previous points was extrapolated to the melting point. The anamolous behavior between 985 and 1024° may be due to a premelting phenomenon although spectrographic analysis did not indicate any abnormally high metallic impurities.

Jaeger, Bottema and Rosenbohm[12,13] determined the heat capacity of cerium but reported sporadic results and gave an equation only between 380–480° to express their data. They found the value of C_p at 400° to be 7.43 cal. per degree per mole. They reported a melting point of 635° which is considerably lower than the presently accepted value. We found C_p to be 7.74 cal. per degree per mole at 400°. Stull and Sinke[14] and Brewer[15] estimated the heat of fusion to be 2.2 kcal. per mole; both had assigned too small a value for the heat of transition. The experimental values from this work are 700 and 1238 cal. per mole, respectively, for the heats of transition and fusion.

Jaeger, Bottema and Rosenbohm[13,16] measured the heat capacity of neodymium and gave two empirical equations for expressing the data in two temperature regions. Evaluating the appropriate equation at 400°, the value of 10.45 cal. per degree per mole was obtained. Although their sample was initially quite pure, they observed a reaction with their platinum container at about 600°. The heat capacity of neodymium was found to be 8.03 cal. per degree per mole in this study. Stull and Sinke[14] estimated the heats of transition and fusion to be 340 and 2600 cal. per mole, while our experimental values are 713 and 1705 cal. per mole.

The low temperature calorimetric group of this Laboratory[11] has determined the heat capacity of samarium and found the value at 340°K. to be 7.35 cal. per degree per mole. The value of 7.42 cal. per degree per mole at 340°K. from this work compares favorably with the low temperature work, as only a point at 100° was measured in this range. Stull and Sinke's[14] estimates of the heats of transition and fusion are 360 and 2650 cal. per mole, whereas our work shows these values to be 744 and 2061 cal. per mole.

Since the metals employed in this study were purer than those used by previous investigators and the calorimeter was found to function properly according to the comparison of the data on α-Al_2O_3 with the National Bureau of Standards, these data are considered to be more accurate.

If one considers the heat capacity to be the sum of various terms, one may write

$$C_p = C_{v(l)} + C_{e(i)} + C_{e(0)} + \delta C \qquad (13)$$

where C_p is the total measured heat capacity, $C_{v(l)}$ is the lattice contribution to the heat capacity from a Debye treatment, $C_{e(i)}$ is the inner electronic (4f) contribution, $C_{e(0)}$ is the outer or conduction electronic term and δC is the dilatation term. To obtain a qualitative comparison between total measured and estimated heat capacity, the various contributions were evaluated at some arbitrary temperature which, for convenience, was chosen to be 1000°K.

The lattice contributions at this temperature can be taken as the upper limit of the Debye equation, $3R$. The contributions of the 4f electrons by promotion to the next higher energy state within a multiplet can be approximated. The metals are looked upon as being trivalent ions which, of course, is not strictly true. The ground states of the trivalent species following Hund's rules are: cerium ($^2F_{5/2}$), neodymium ($^4I_{9/2}$) and samarium ($^6H_{5/2}$). The higher states of the multiplet in each case are denoted by unit increments of J from $J_{min} = L - S$ to $J_{max} = L + S$. The energy differences between states in the multiplet can be approximated according to the method outlined by Van Vleck.[17] Utilizing the energy differences, the partition function can be calculated. Employing the partition function's relationship to the heat capacity, the inner electronic contributions to the total heat capacity can be evaluated. At 1000°K. the promotion energy contributions were calculated to be: cerium (0.91), neodymium (1.22) and samarium (1.84) cal. per degree per mole.

Gerstein, *et al.*,[18] through a private communication with Boorse, reported the temperature coefficient for the conduction electronic contribution of lanthanum to be 2.4×10^{-3} (cal. degree^{-2} mole^{-1}). This value is used for evaluating the electronic contribution for neodymium. Clausius and Franzosini[19] measured the low temperature heat capacity of thorium and reported the coefficient equal to 1.6×10^{-3} (cal. degree^{-2} mole^{-1}). Because of the electronic and structural similarities between cerium and thorium, this value is used for the temperature coefficient for cerium. Jennings, Hill and Spedding[11] calculated the temperature co-

(12) F. M. Jaeger, J. A. Bottema and E. Rosenbohm, *Proc. Acad. Sci. Amsterdam*, **39**, 912 (1936).

(13) F. M. Jaeger, J. A. Bottema and E. Rosenbohm, *Rec. trav. chim.*, **57**, 1137 (1938).

(14) D. R. Stull and G. C. Sinke, "Thermodynamic Properties of the Elements," American Chemical Society, Washington, D. C., 1956.

(15) L. Brewer, in "The Chemistry and Metallurgy of Miscellaneous Materials," L. L. Quill, Ed., McGraw-Hill Book Co., Inc., New York, N. Y., 1950, p. 13.

(16) F. M. Jaeger, J. A. Bottema and E. Rosenbohm, *Proc. Acad. Sci. Amsterdam*, **41**, 120 (1938).

(17) J. H. Van Vleck, "The Theory of Electric and Magnetic Susceptibilities," Great Britain, Oxford at the Clarendon Press.

(18) B. C. Gerstein, M. Griffel, L. D. Jennings, R. E. Miller, R. E. Skochdopole and F. H. Spedding, *J. Chem. Phys.*, **27**, 394 (1957).

(19) K. Clausius and P. Franzosini, *F. Naturforsch.*, **11**, 957 (1956).

efficient for samarium from the low temperature work of Roberts[20] and found it to be 3.1×10^{-3} (cal. degree^{-2} mole^{-1}). The conduction electronic contributions to the heat capacity at 1000°K. are: cerium (1.6), neodymium (2.4) and samarium (3.1) cal. per degree per mole.

The dilatation differences were computed at room temperature by using the usual thermodynamic formula. The values for the compressibilities were obtained from the data of Bridgman.[21] The coefficients of expansion of cerium, neodymium and samarium were taken from the data of Barson, Legvold and Spedding.[2,22] The values of the X-ray density necessary to compute the molar volumes were obtained from the review of Spedding and Daane.[2] The value of C_p/C_v can be computed at any other temperature by means of the approximate equation

$$C_p/C_v = 1 + A\alpha_l T \qquad (14)$$

where A is a constant and α_l is the linear coefficient of expansion. The dilatation corrections at 1000°K. are: cerium (0.09), neodymium (0.13) and samarium (0.11) cal. per degree per mole. The total theoretical contributions and the experimental values are, respectively: cerium (8.54 and 9.12), neodymium (9.49 and 10.03) and samarium (10.99 and 10.96). Because of the qualitative nature of the calculations, little can be said regarding the discrepancies. The agreement for samarium is quite good and may be fortuitous. Factors which may contribute to these discrepancies are: anharmonicity of lattice vibrations, neglect of crystal field splitting, magnetic effects, analogies used to determine the outer electronic contributions for cerium and neodymium, and the treatment of the inner electronic promotion energies as trivalent species.

Acknowledgment.—The authors wish to express their thanks to J. E. Powell and coworkers for the pure rare earth oxides and G. F. Wakefield and C. E. Haberman for preparing the metals.

(20) L. M. Roberts, *Proc. Phys. Soc. London*, **B70**, 471 (1957).
(21) P. W. Bridgman, *Proc. Am. Acad. Sci.*, **83**, 1 (1954).
(22) F. Barson, unpublished work on the thermal expansion of samarium, Iowa State College, Ames, Iowa, 1957.

THE DENSITY AND ELECTRIC CONDUCTANCE OF THE MOLTEN SYSTEM CERIUM–CERIUM CHLORIDE

BY G. W. MELLORS AND S. SENDEROFF

Research Laboratories, National Carbon Company, Division of Union Carbide Corporation, Cleveland 1, Ohio

Received May 9, 1959

The density and electric conductance of the Ce–$CeCl_3$ system have been measured from the pure salt to the almost saturated solution (8 mole % Ce) from just above the melting point to 950°. The density of pure $CeCl_3$ is 3.216_0 g./cc. at 850°. It decreases by about 1.5% on addition of 0.3 mole % Ce metal after which an almost linear increase to 3.287_3 g./cc. at 8 mole % Ce is observed. The specific and equivalent conductances of pure $CeCl_3$ are 0.9600 ohm^{-1} cm.$^{-1}$ and 24.54 ohm^{-1} cm.^{2}, respectively, at 850°. Large increases in these values (43 and 46%, respectively) are observed on the initial addition of Ce metal corresponding to a concentration of 0.63 mole %. Beyond this initial addition the conductivity rises slowly to values of 1.8900 ohm^{-1} cm.$^{-1}$ and 48.26 ohm^{-1} cm.^{2} at 7.75 mole % Ce. The large effects of low concentration of Ce on the density and conductivity of the system are explained by postulating the existence of comparatively free electrons resulting from the reaction $Ce^0 \rightarrow Ce^{1+} + e^-$, some of which are trapped by the reaction $Ce^{3+} + 2e \rightleftarrows Ce^{1+}$. The comparatively free electrons in the systems dilute in Ce metal have large "molar volumes" and high mobilities as observed in Na–liquid ammonia systems. The electronic "molar volume" and mobility are reduced rapidly with increasing amounts of added cerium so that the conductivity mechanism at higher concentration becomes uncertain, although it is likely that even at the highest concentration there is still some component of electronic conductivity.

Introduction

Measurements of density and electric conductance have been but rarely reported for molten metal–metal halide systems, though such information exists on the one hand concerning molten metals and on the other molten halides. Aten[1] reported the density and conductance of the Cd–$CdCl_2$ system and the conductance and viscosity of Bi–$BiCl_3$ melts,[2] the density of which has been reported by Keneshea and Cubicciotti.[3] In both these systems the specific conductance decreases with increasing metal content, an effect which was observed also by Cubicciotti[4] for the molten Ca–$CaCl_2$ system. Aten attributed the decreasing conductance to the formation of the $(Cd_2)^{2+}$ cations (analogous to Hg_2^{2+}) the existence of which was postulated by Grjotheim, Gronwold and Krogh-Moe on the basis of magnetic susceptibility measurements.[5]

Bronstein and Bredig[6] measured conductances of alkali metal–alkali halide melts, but they did not measure densities and for the purpose of calculating equivalent conductances assumed additivity of equivalent volumes.

Greenwood and Worrall[7] measured the conductance and density of fused gallium dichloride and dibromide and found them to be typical molten salts with a conductance (and viscosity) characteristic of compounds in which the cation is considerably smaller than the anion. It had been shown earlier[8] on the basis of the Raman spectrum

(1) A. H. W. Aten, *Z. physik. Chem.*, **73**, 578 (1910).
(2) A. H. W. Aten, *ibid.*, **66**, 641 (1909).
(3) F. J. Keneshea, Jr., and D. D. Cubicciotti, THIS JOURNAL, **62**, 843 (1958).
(4) D. D. Cubicciotti, MDDC-1058, 1946–49, USAEC.
(5) K. Grjotheim, F. Gronwold and J. Krogh-Moe, *J. Am. Chem. Soc.*, **77**, 5824 (1955).
(6) H. R. Bronstein and M. A. Bredig, *ibid.*, **80**, 2077 (1958).
(7) N. N. Greenwood and I. J. Worrall, *J. Chem. Soc.*, 1680 (1958).
(8) L. A. Woodward, G. Garton and H. L. Roberts, *ibid.*, 3723 (1956).

of fused gallium dichloride that the structure was $Ga^{1+}[GaCl_4]^-$.

In the course of an e.m.f. investigation of the liquid Ce–$CeCl_3$ system,[9] it was established that a Ce^{3+}/Ce^{1+} oxidation–reduction system existed in $CeCl_3$ containing added Ce metal and measurements of density and electric conductance were undertaken to obtain further structural information on the system.

Experimental

Materials.—$CeCl_3$ and Ce metal were prepared as described in a previous paper.[9] All weighings and transfers were performed in a dry box. Argon was purified by passage through titanium chips at 900°.

Range of Experiments.—Measurements were made on the pure salt and on melts containing up to about 8 mole % cerium metal, the upper limit being imposed by the solubility of cerium in cerium chloride, *viz.*, 9 mole % at 950°.[10]

Apparatus. Furnace.—For both density and conductance work a tensile test furnace (Marshall Products) was used. The bore was $3^1/_2$'' and an iron tube $3^1/_4$'' o.d. $^1/_4$'' wall thickness served as a baffle between the furnace windings and the 51 mm. o.d. "Vycor" envelope containing the crucible.

For the measurement of electrical conductance, the melt was contained in a "Morganite" ΔRR XN100 alumina crucible. A molybdenum rod, threaded 6.32, passed through a hole in the base of the crucible and the crucible was rendered leakproof by tightening a stainless steel nut on the outside and a molybdenum nut on the inside of the crucible. The latter formed the fixed electrode. The upper electrode was a $^1/_8$'' diameter molybdenum rod raised and lowered by a rack and pinion mechanism provided with a pointer and scale. The cell was enclosed under purified argon atmosphere in a 51 mm. o.d. "Vycor" sheath, closed top and bottom with $10^1/_2$ rubber stoppers. This apparatus was modified as follows, in order to carry out density determinations. The upper electrode, alumina crucible and lower electrode were removed. The melt now was contained in a deep drawn molybdenum crucible (Fansteel Metallurgical Corporation) $1^5/_8$'' o.d., $2^5/_8$'' in height. Measurements were made by weighing submerged within the melt a tungsten bob (approximately 58 g.) suspended by a 10 mil. tantalum wire. The expansion of the bob was computed[11] in order to obtain the volume of the bob at each temperature.

Weighings were made with a modified Ainsworth balance. The left hand pan was removed and replaced by a small compensating weight; the tantalum suspension wire passed through a hole in the base of the balance made by removal of the left hand pan arrest.

Temperature Measurements for Density and Conductance Measurements.—Chromel–alumel thermocouples were used and sheathed in 6 mm. o.d. molybdenum thermowells. The methods of recording temperature and of controlling the furnace temperature were as described in a previous publication.[10]

During measurements of density or conductance the thermowell was raised above the melt surface in order to eliminate undesirable surface tension effects.

Electrical Circuit.—The resistance–capacitance bridge was of the conventional Wheatstone arrangement. An oscillator (Hewlett–Packard Model 200 CD) was used as signal source, usually at 1000 cycles/sec. The output from the bridge was fed *via* a low level battery powered amplifier (Tektronix Type 122) to the Y plates of an oscilloscope (Hewlett–Packard Model 130A) functioning as null indicator. A standard 1000 cycles/sec. signal was fed to the X-plates *via* an isolating transformer. The arrangement has been fully described elsewhere.[12] To avoid 60 cycles/sec. interference from the furnace current, the power supply was switched off temporarily during a measurement. The furnace insulation was adequate to maintain constant temperature during this period.

Cell Constant.—The cell constant was determined for different depths of liquid in the crucible, the depth of immersion of the upper electrode being maintained constant (0.30''). The molybdenum electrodes were sand-blasted to avoid polarization and with solutions of 0.1 and 0.01 *N* KCl the cell constants were found to range from 0.9 to 1.4 $cm.^{-1}$. The cell constants are valid at the temperature of measurement, because changes due to expansion were allowed for by raising and reinserting the upper electrode 0.30'' into the melt and also determining the total depth of liquid at each temperature where a measurement was to be made. With a cell constant of this magnitude a correction for lead resistance is required.

The resistance of the leads and electrodes was measured over the working range of temperatures, by welding together the two electrodes within the cell. It varied from 2.0×10^{-2} ohm at 800° to 2.6×10^{-2} ohm at 975°.

A quartz capillary conductance cell modified from that described by Van Artsdalen and Yaffe,[13] was used in some experiments with pure $CeCl_3$. The cell constants were measured at room temperature with 0.1 *N* KCl solution and found to be of the order of 330–380 $cm.^{-1}$. Allowance can be made for expansion of the quartz cells on raising the temperature, but such correction amounts to less than 0.05% and therefore was neglected. Molybdenum electrodes ($^1/_8$'' diam.), sand-blasted to eliminate polarization, were used in these experiments.

Polarization.—Measurements were made over the range 500–10,000 cycles/sec. Over this range, conductance was independent of frequency.

General Procedure of Conductance Measurements.—The melt was prepared as for the density measurements and held at 900° for 2 hours to homogenize. The electrode then was inserted, the position of the surface and the depth of the melt being accurately ascertained. A series of measurements at points on heating and cooling cycles was obtained, no measurements being taken unless thermal equilibrium had been attained.

The reproducibility was ±0.5% (±0.0095 ohm^{-1} $cm.^{-1}$) except near the liquidus region where small variations of temperature caused large variations of conductance.

Using the quartz cell an identical procedure was followed, the cell being lowered into the melt to the appropriate depth at 900–950°.

General Procedure of Density Measurements.—The apparatus was charged with sufficient materials to give a workable depth (about 2'') of melt in the crucible. All joints in the apparatus were sealed with "Unichrome Stop-off" (Metal and Thermite Corp.). The melt was homogenized for 2 hours at 900–950° and the bob inserted. A series of measurements both on heating and on cooling cycles was obtained. Measurements were not taken unless temperature equilibrium had been attained within the apparatus. The reproducibility was about ±0.25% (±8 mg./cc.) for melts of pure $CeCl_3$ and those containing more than 3 mole % Ce and ±0.75% (±24 mg./cc.) for melts containing between 0.07 and 3.0 mole % Ce.

Method of Calculation and Results. (a) **Density.**—For a solid suspended in a liquid the general relationship between the variables is

$$B = V\rho - \frac{2\pi r\gamma\cos\theta}{g}$$

where

B = bob buoyancy (≡ wt. in air − wt. in liquid)
V = vol. of bob at temp. of experiment
ρ = density of liquid at temp. of experiment
r = radius of wire
γ = surface tension of liquid
θ = contact angle between wire and liquid
g = gravitational constant

If the suspension wire is of small diameter, then we may write $\rho = B/V$ with very little loss of accuracy. The surface tension correction in the present work was negligible (approximately 0.04% when γ = 100 dyne $cm.^{-1}$) and the simple expression was employed.

The density–temperature plots for all compositions are straight lines. Figure 1 shows the density–composition

(9) S. Senderoff and G. W. Mellors *J. Electrochem. Soc.*, **105**, 224 (1958).

(10) G. W. Mellors and S. Senderoff, THIS JOURNAL, **63**, 1110 (1959).

(11) C. J. Smithells, "Tungsten," Chemical Publishing Co., Inc., New York, N. Y., 1953, pp. 171 and 188.

(12) G. W. Mellors, Thesis, London 1953; J. O'M. Bockris and G. W. Mellors, THIS JOURNAL, **60**, 1321 (1956).

(13) E. R. Van Artsdalen and I. S. Yaffe, *ibid.*, **59**, 118 (1955).

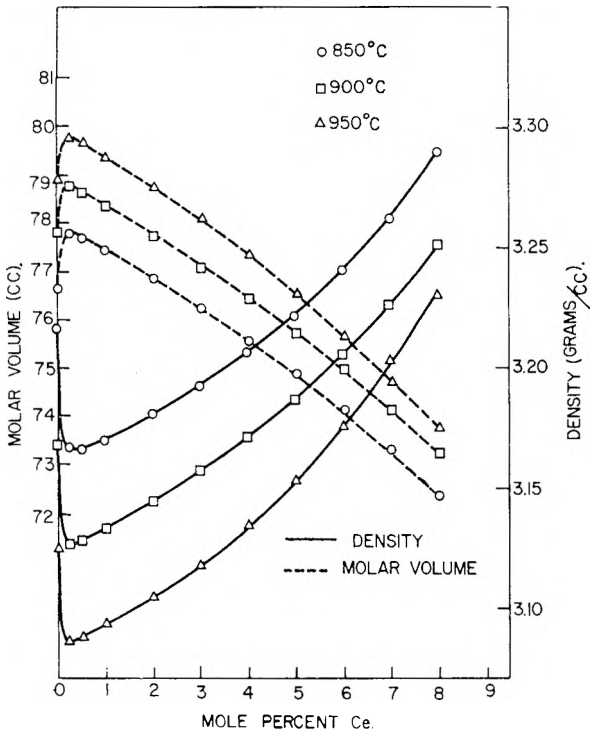

Fig. 1.—Molar volume and density *vs.* composition at 850, 900 and 950°.

and molar volume–composition relationship for three temperatures. The latter was calculated from the former on the basis of the equation

$$V_{T^\circ} = \frac{X_{CeCl_3}M_{CeCl_3} + X_{Ce}M_{Ce}}{\rho_{T^\circ}}$$

where

V_{T° = molar volume at temp. T°
ρ_{T° = density at temp. T°
X_{CeCl_3}, X_{Ce} = mole fractions of $CeCl_3$ and Ce, resp.
M_{CeCl_3}, M_{Ce} = mol. wt. of $CeCl_3$ and Ce, resp.

Interpolated values of the density and molar volume are collected in Table I.

TABLE I

Mole % Ce	Density, g./cc. 850°	900°	950°	Molar volume, cc. 850°	900°	950°
0.00	3.2160	3.1670	3.1240	76.68	77.87	78.94
.25	3.1659	3.1260	3.0868	77.81	78.80	79.80
.50	3.1655	3.1275	3.0877	77.73	78.68	79.69
1.00	3.1695	3.1327	3.0932	77.47	78.38	79.38
2.00	3.1800	3.1440	3.1040	76.87	77.75	78.76
3.00	3.1913	3.1566	3.1174	76.27	77.11	78.08
4.00	3.2055	3.1700	3.1333	75.60	76.45	77.34
5.00	3.2204	3.1860	3.1520	74.92	75.73	76.55
6.00	3.2390	3.2041	3.1740	74.16	74.97	75.68
7.00	3.2602	3.2247	3.2012	73.35	74.16	74.71
8.00	3.2875	3.2490	3.2288	72.42	73.28	73.74

(b) **Electrical Conductance.**—The specific conductance κ was calculated from the measured resistance by using the relationship

$$\kappa = \frac{C}{(R - r)}$$

where

κ = specific conductance
C = cell constant
R = measured resistance
r = leads resistance

The plots of specific conductance *versus* temperature are in all cases straight lines.

The equivalent conductance Λ was calculated from the relationship

$$\Lambda = \frac{\kappa\bar{e}}{\rho}$$

where the symbols κ and ρ have their usual meaning and $\bar{e}$ is the mean equivalent weight of the mixture given by[14]

$$\bar{e} = f_1e_1 + f_2e_2$$

where

e_1 = equiv. weight of component 1
e_2 = equiv. weight of component 2
f_1 = equiv. fraction of component 1
f_2 = equiv. fraction of component 2

Thus, for x mole fraction of $CeCl_3$ and $(1 - x)$ mole fraction of Ce

$$\bar{e} = \frac{3xe_{CeCl_3}}{3x + (1 - x)} + \frac{(1 - x)e_{Ce}}{3x + (1 - x)}$$

Experimental values of κ and Λ_{soln} are presented in Table II and the isotherms of κ and of Λ *versus* composition are shown in Fig. 2.

TABLE II

Mole % Ce	Specific conductance, κ, ohm^{-1} cm.$^{-1}$ 850°	900°	950°	Equiv. conductance of soln. Λ, ohm^{-1} cm.$^{-2}$ 850°	900°	950°
0.00[a]	0.9600	1.0670	1.1725	24.54	27.69	30.85
0.63	1.3730	1.5571	1.7400	35.70	40.97	46.37
1.51	1.4130	1.5980	1.7820	36.71	42.05	47.45
2.35	1.4700	1.6501	1.8303	38.16	43.33	48.68
2.73	1.5100	1.6850	1.8600	39.19	44.23	49.41
4.03	1.5600	1.7400	1.9200	40.40	45.56	50.85
5.15	1.6680	1.8520	2.0350	43.07	48.34	53.68
6.42	1.7150	1.9150	2.1170	44.08	49.76	55.49
7.75	1.8900	2.0870	2.2509	48.26	53.92	58.55

[a] The values for the conductivity of pure cerium chloride obtained with the capillary cell agree within 0.5% (±0.004 ohm^{-1} cm.$^{-1}$) with these values.

Discussion

The most interesting point common to the graphs of density, molar volume, specific and equivalent conductance *versus* composition (Figs. 1 and 2) is the sharp initial change in the function on adding a small amount of cerium metal.

The specific and equivalent conductance of the solution (Table II) increases with increasing metal content, the value of κ, *ca.* 8 mole % cerium metal, being about twice that of pure cerium chloride. This is in contradistinction to the behavior observed in the Cd–$CdCl_2$,[1] Bi–$BiCl_3$[2] and Ca–$CaCl_2$[4] systems where the measured specific conductance decreases with increasing metal content. In the Bi–$BiCl_3$ molten system[2] Keneshea and Cubicciotti observed a decrease in molar volume on adding Bi to pure $BiCl_3$. It will be observed that this behavior is exactly opposite to that of the Ce–$CeCl_3$ system where the molar volume and the conductance increase with the initial addition of cerium metal. On the other hand the increase in specific and equivalent conductance is very much smaller than that observed in the Na–NaCl, Na–NaBr, K–KCl and K–KBr molten systems by Bronstein and Bredig.[6] For example, the specific conductance of pure KCl is 2.69 ohm^{-1} cm.$^{-1}$ at 818°, while KCl containing 8.16 mole % K has a value of κ of 17.2 ohm^{-1} cm.$^{-1}$ at 823°, *i.e.*, a sevenfold increase. It appears on the basis

(14) H. Bloom, I. W. Knaggs, J. J. Molloy and D. Welch, *Trans. Faraday Soc.*, **49**, 1458 (1953).

of the change in specific and equivalent conductance with increasing metal content that the behavior of the Ce–$CeCl_3$ system is somewhat similar to that of the alkali metal–alkali halide systems, particularly in the dilute region, though with less spectacular increase in these parameters.

In Cd–$CdCl_2$ the decrease in conductance has been ascribed to the formation of complexes such as Cd_2^{2+},[1] but in spite of the observed large increase in the molecular conductance for the alkali-alkali halides, Bronstein and Bredig[6] state that the formation of Na_2^+ and K_2^+ cannot be ruled out. However, they feel that the decrease in conductance due to complexing would be more than balanced by the presence of a few comparatively mobile electrons.

However, the main point of difference from the alkali metal–halide melts is the fact that the isotherms of κ and Λ *vs.* composition show large initial increases followed by slight, almost linear increments with increasing metal content. Thus the behavior with respect to conductance of the alkali metal–halide melts over large composition ranges is restricted in the case of the Ce–$CeCl_3$ system to the first 0.2–0.3 mole % Ce.

In pure $CeCl_3$ it is certain that the conductance is purely ionic, but in the absence of transport number measurements the nature of the conducting entity or entities remains unknown. The conductance may be unipolar in nature involving the Ce^{3+} or the Cl^- ion, or bipolar involving both. However, it is probable that there will be few bare Ce^{3+} ions in the melt as these would readily coordinate with Cl^- ions and thus a complex ion of some type, *e.g.*, $[CeCl_2]^+$, $[CeCl_4]^-$ or $[CeCl_6]^{3-}$, might also contribute to the conductance. Further, it would be expected that the energy of activation for conductance by bare Ce^{3+} ions would be high, involving as it would the "squeezing" of a Ce^{3+} ion from an energy well associated with one group of Cl^- ions to another well. The value of 6.24 kcal. $mole^{-1}$ which is derived from the data in Table II is not excessively large compared with NaCl (3 kcal. $mole^{-1}$), KCl (3.5 kcal. $mole^{-1}$),[13] $BaCl_2$ (5.3 kcal. $mole^{-1}$) and $BaBr_2$ (5.4 kcal. $mole^{-1}$).[15] In the case of $PbCl_2$ (E_κ = 4.6 kcal. $mole^{-1}$)[16] it has been shown that t_{Cl^-} is 0.75 and $t_{Pb^{2+}}$ is 0.25,[17,18] so it may well be that in pure $CeCl_3$ the conductance is predominantly due to the Cl^- ions.

It has been shown previously[9] that on addition of cerium to cerium chloride the reaction $2Ce^0 + Ce^{3+} \rightarrow 3Ce^+$ occurs. Although one may expect Ce^{1+} to be more mobile than any of the ions in $CeCl_3$, this could not account for the very large increase in conductivity with the initial addition of Ce. At 850° the conductance increases 43% on the addition of 0.63 mole % cerium.

If this increase in conductance were to be ascribed to Ce^{1+} ions only, then, since conductance is equal to the product of valence, concentration and mobility, it would imply that Ce^{1+} ions had a very large mobility. At 0.63 mole % cerium metal it may be shown that the Ce^{3+}/Ce^{1+} ratio is about 160 and the Cl^-/Ce^{1+} ratio about 480. Suppose κ_1 is the specific conductance of pure cerium chloride, then it may be stated in general

$$\kappa_1 = e_0(N_+Z_+U_+ + N_-Z_-U_-)$$

where

e_0 = elementary change
N_+ and N_- = concentration
Z_+ and Z_- = valence
U_+ and U_- = mobility

} of positive and negative ions

Suppose κ_2 is the specific conductance at 0.63 molar % added Ce then

$$\kappa_2 = \kappa_1 + e_0[N_2Z_2U_2]$$

where N_2, Z_2 and U_2 represent the concentration, valence and mobility of the new added ion, provided that the conductance of the $CeCl_3$ remains virtually unchanged. Since there is one Ce^{1+} (assuming this to be the added species) per 640 other ions $[Ce^{3+} + Cl^-]$ the mobility of the Ce^{1+} to produce an increase of $\approx$ 50% in the conductance would have to be about 900 times the *average* mobility of the ions already present in $CeCl_3$. Such a conclusion is unreasonable and it is far more likely that the effect observed is due to conductance by electrons.

Although in the foregoing discussion the composition containing 0.63 mole % Ce was selected as the point of reference, this was merely because it was the lowest concentration of cerium for which reproducible data could be obtained. The exact point of inflection of the κ-composition and of Λ_{soln}–composition curves probably is between 0.25 and 0.63 mole % Ce, since at 0.25 mole % Ce the points, though scattered, were all below the conductance value at 0.63 mole %. The argument demonstrating that the increased conductance must be due to electrons at this composition remains valid at lower cerium compositions.

Since the initial sharp rise in conductivity is attributed to electrons generated in the melt on addition of cerium metal, the subsequent slow increase in conductivity can be accounted for only if the electrons generated on further additions of cerium are to a considerable extent trapped, or are of lower mobility.

To consider the electron-trapping effect in a very simple manner, we postulate an electron-generating reaction that goes to completion; *i.e.*

$$Ce^0 \longrightarrow Ce^{1+} + e \qquad (1)$$

and a reversible electron-trapping reaction, *i.e.*

$$Ce^{3+} + 2e \rightleftharpoons Ce^{1+} \qquad (2)$$

(Ce^{2+} apparently is not stable in this system[9] and is, therefore, ignored.) For reaction 2

$$K = \frac{[Ce^{1+}]}{[Ce^{3+}][e]^2} \qquad (3)$$

From equations 1 and 2 it may be seen that the total concentration of Ce^{1+} ions present in the

(15) J. O'M. Bockris, private communication, May, 1958.

(16) H. Bloom and E. Heymann, *Proc. Roy. Soc.* (*London*), **A188**, 392 (1946–47).

(17) F. R. Duke and R. W. Laity, THIS JOURNAL, **59**, 549 (1955); *J. Am. Chem. Soc.*, **76**, 4046 (1954).

(18) S. Karpachev and S. Palguev, *Zhur. Fiz. Khim.*, **23**, 942 (1949).

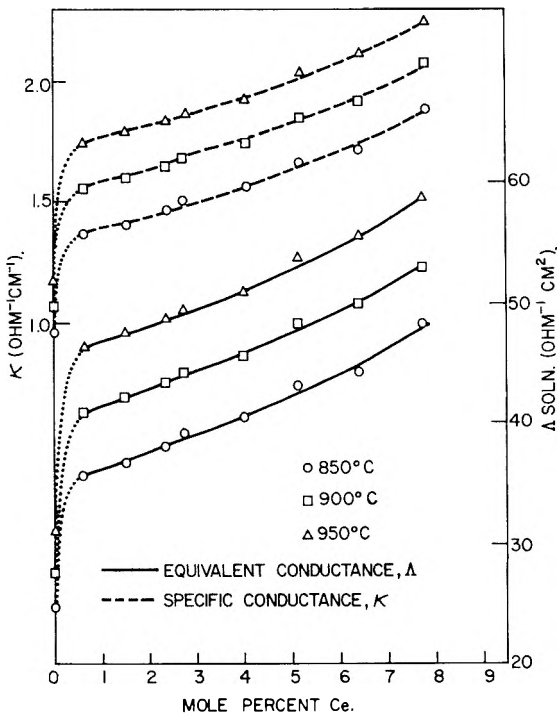

Fig. 2.—Equivalent and specific conductance *vs.* composition.

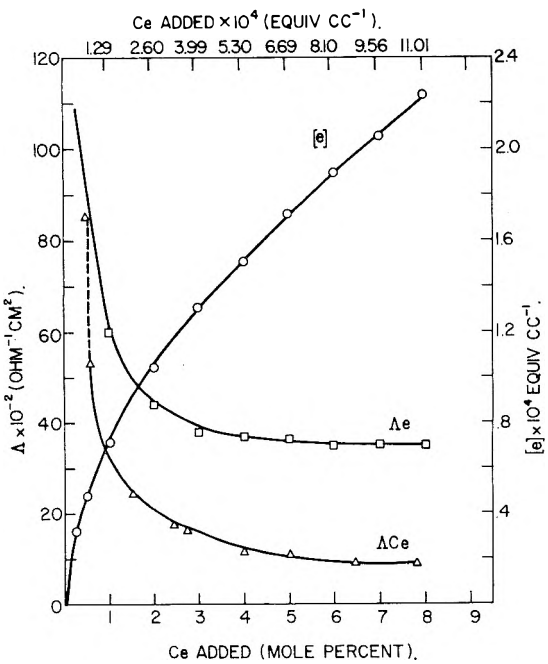

Fig. 3.—Λ_{Ce}, Λ_e and [e] as a function of cerium metal added.

system at a definite composition is given by

$$[Ce^{1+}] = \frac{3}{2}A - \frac{[e]}{2} \qquad (4)$$

where A is the amount of cerium metal added in equiv./cc.[19] The concentration of neutral cerium atoms in the solution, however, is zero at all times in view of the assumption that reaction 1 goes to completion. Substitution of (4) in (3) yields

$$K = \frac{3A - [e]}{2[Ce^{3+}][e]^2} \qquad (5)$$

(19) As can be seen from eq. 1, equiv./cc. = g. atoms/cc.

Since the maximum change in $[Ce^{3+}]$ is less than 10%, let $K' = 2K[Ce^{3+}]$ as a simplifying approximation

$$K' = \frac{3A - [e]}{[e]^2} \qquad (6)$$

or

$$K'[e]^2 + [e] - 3A = 0 \qquad (7)$$

$$\therefore [e] = \frac{-1 \pm \sqrt{1 + 12K'A}}{2K'} \qquad (8)$$

We now wish to assign a value to K' such that electron trapping be negligible at values of A at or slightly below the inflection points of Fig. 2. If electron trapping is negligible, then [e] is only slightly less than A, and as an approximation can be taken equal to A. Since the inflection point is between 0.25 and 0.63 mole % cerium added, we take the minimum value of the inflection point and require that $[e] = A$ at $A = 0.25$ mole % (0.322×10^{-4} equiv./cc.). This gives a value of K' of 6.2×10^4 equiv.$^{-1}$ cc. or a value of K ($K = K'/2[Ce^{3+}]$) of 8.0×10^5 equiv.$^{-2}$ cc.^{2}.[20]

One may use this value of K' in eq. 8 to calculate [e], and eq. 4 to calculate $[Ce^{1+}]$ for various values of A between 0.25 mole fraction and saturation near 8 mole %. This value for [e] may not be the actual concentration of electrons in the system, but rather, the highest concentration which can be attained on the basis of the assumptions and simple mechanism postulated above.

These assumptions then are made to assign to each species its contribution to the total conductivity

κ_{CeCl_3} = (specific conductance of pure $CeCl_3$) × mole fraction of $CeCl_3$

$\kappa_{"CeCl"}$ = (equiv. conductance of KCl[21]) × $[Ce^{1+}]$

$\kappa_{electron} = \kappa_{soln} - (\kappa_{CeCl_3} + \kappa_{"CeCl"})$

Finally, the mobility, μ_e, and equivalent conductance, Λ_e, of the electrons are calculated. The results, together with the electron concentration, [e], are shown in Fig. 3.

It can be seen that of the electrons derived from an addition of 8 mole % cerium metal, about 80% are trapped if one uses a value of K', chosen to make electron trapping negligible just below the inflection points in the curves of Fig. 2. However, even with this, the most favorable value of K' which could be chosen, the variation of the concentration of electrons with composition shown in Fig. 3 is insufficient to account for the observed variation of conductivity with composition and it is necessary to postulate a decrease of mobility (or equivalent conductance) with increasing concentration of the electrons by a factor of about one-third over the range studied.

As was noted above, attempts to obtain reproducible conductance data in the region of 0.25 mole % Ce were unsuccessful. If this difficulty were caused by the rapidly rising conductance with increasing metal content, then one may be certain that the inflection must fall between 0.25 and the first reproducible composition measured, *viz.*, 0.63 mole % Ce. Making the basic assumption

(20) The limits within whch this treatment is valid are: $[e] \leq A < 8$ mole %; with $A = [e]$ at the inflection point.

(21) Since the ionic sizes of Ce^{1+} and K^+ are not very different, it has been assumed that the hypothetical "CeCl" has the same equivalent conductance (*i.e.*, 108 Ω^{-1} cm.^{2}) as KCl.

that the amount of cerium added equals the electron concentration at 0.63 mole % Ce (instead of 0.25 mole %) leads to a value of K' of 2.47×10^4 equiv.$^{-1}$ cc. Using this K' to calculate Λ_e at 5 mole % Ce leads to a value of 23×10^{-2} ohm^{-1} cm.^{2} compared with 36×10^{-2} ohm^{-1} cm.^{2} for the prior case.

Another function, Λ_{Ce}, may be calculated from the formula

$$\Lambda_{Ce} = \frac{\Lambda_{soln} - X_{CeCl_3}\Lambda_{CeCl_3}}{X_{Ce}} \qquad (9)$$

where

Λ_{soln} = equiv. conductance of the soln.
Λ_{CeCl_3} = equiv. conductance of pure $CeCl_3$
X_{CeCl_3} = mole fraction of $CeCl_3$
X_{Ce} = mole fraction of Ce metal added

as was done by Bronstein and Bredig.[6]

In Fig. 3 the functions Λ_e and Λ_{Ce} are compared and the electron concentrations as a function of composition are shown. In both cases the contribution of the $CeCl_3$ to the conductance was assumed to that of the pure salt. Λ_{Ce} makes no distinction with regard to the type of carrier involved, but is sensitive to the assumption made regarding the nature of the solute. For instance, if the solute is taken to be $Ce^+[CeCl_4]^-$ instead of Ce,[9] the value of Λ_{solute} is found to be 545 at 850° and 7.75 mole % Ce instead of 897, and if the solute is taken to be $CeCl_2$ (for the existence of which there is no evidence), Λ_{solute} is as low as 173 for the same temperature and composition.

At a concentration of 0.63 mole % Ce and 850°, the Λ_{solute} values are approximately 5300, 3500, 900, for Ce, $Ce^+[CeCl_4]^-$, and $CeCl_2$, respectively, as the assumed solute. Λ_{Ce}, therefore, is the apparent equivalent conductance of the assumed solute, while Λ_e is the equivalent conductance of the electrons resulting from the assumed reactions between Ce and CeCl. Λ_e is considerably larger than Λ_{Ce} over most of the range, because the latter contains a contribution from the more abundant and slower carrier, $[Ce^{1+}]$. As an example, at 8 mole % added cerium the concentration of $[Ce^{1+}]$ is about seven times that of electrons, but its contribution to the conductance is about 20% that of the electrons.

Similar behavior is observed in the sodium–liquid ammonia system. If one plots Λ_{Na} *vs.* composition, an initial rapid decrease to a minimum at 500 ohm^{-1} cm.^{2} and 0.2 mole % Na is observed,[22] this is then followed by a rapid increase in Λ_{Na}. The Λ_e and Λ_{Ce} curves in Fig. 3 both seem to have reached a minimum, but the subsequent rise as in Na–NH_3 systems cannot be observed because of the solubility limit of the Ce at the temperature of this study.[10]

In Fig. 4 are shown the relative contributions of the $CeCl_3$, the electrons and the Ce^{1+} ions to the observed specific conductance. In the region near the initial additions of cerium the assumption of constancy of the conductance of $CeCl_3$ probably is justified. It probably is less justified at higher levels of cerium addition, since, as a result of the loosening of the structure, the conductance of the $CeCl_3$ itself may increase. To the extent which this may occur, there is introduced some ambiguity in the electronic contribution at high values of Ce^0. Further, the rather small values of Λ_e, at high values of Ce^0, (about one order of magnitude higher than typical ionic values) also make the decision as to the conductivity mechanism at higher concentrations of cerium somewhat difficult.

In the case of Na–liquid NH_3 systems, Ogg[23] has derived a "molar volume for electrons." This is defined as the excess volume above that of the NH_3 molecules and Na atoms. For example, at a concentration of 7.5×10^{-3} molar % Na in liquid NH_3 the volume of one mole of electrons was found to

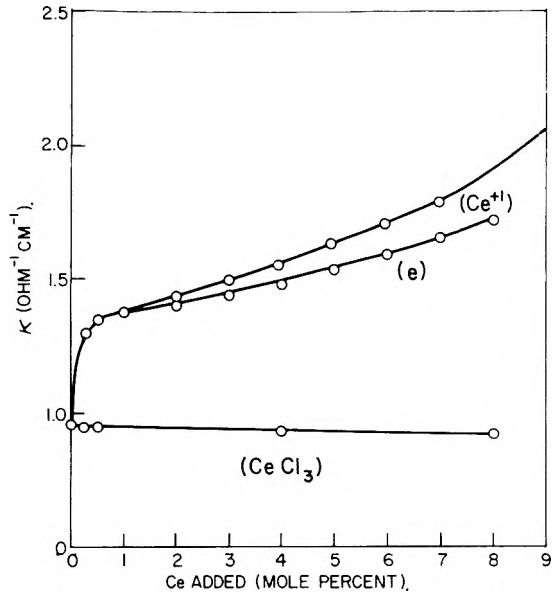

Fig. 4.—Contribution to conductance of electrons and Ce^{+1} at 850°.

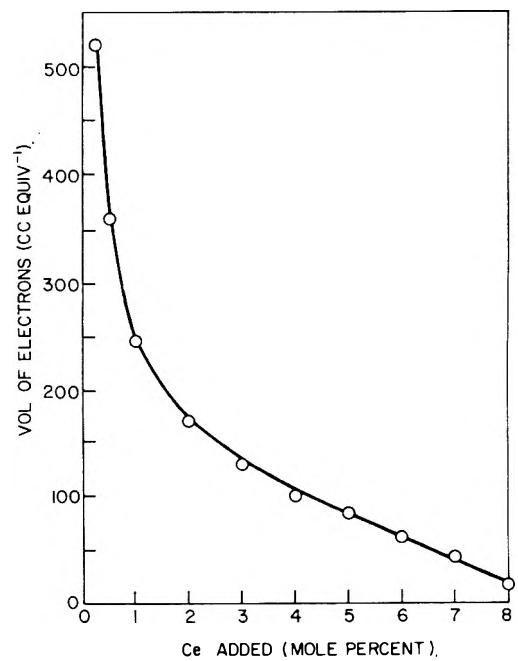

Fig. 5.—Excess volume due to electrons *vs.* cerium metal added.

(22) C. A. Kraus, *J. Am. Chem. Soc.*, **43**, 749 (1921); *J. Franklin Inst.*, **212**, 537 (1931).

(23) R. A. Ogg, *J. Am. Chem. Soc.*, **68**, 155 (1946).

be 700 cc.,[23] though this has been disputed by Stosick.[24] From 3 to 20 mole % the volume was estimated to be 41 to 43 cc.[25]

In the present system, the experimental molar volume may be considered to be made up of three components: (a) $CeCl_3$, (b) Ce^{1+} and (c) electrons. A reasonable approximation to the contribution of Ce^{1+} to the total volume is obtained by ascribing to Ce^{+1} the known volume of the added Ce metal. The contribution of $CeCl_3$ was assessed by taking the product of the molar volume of pure $CeCl_3$ and its mole fraction; the electron concentration was taken to be that shown in Fig. 3 and, hence, a volume per equivalent (mole) of electrons may be obtained. This is shown in Fig. 5 as a function of concentration. The values obtained are comparable with those observed for the Na–liquid NH_3 system, but it would be surprising if the values at the lower concentrations were identical. For example, about the same volume for electrons is obtained with 7.5×10^{-3} molar % Na in liquid NH_3 as with 2.5×10^{-1} molar % Ce in liquid $CeCl_3$, and in the more concentrated range (7 to 8 mole % Ce) the calculated volume for electrons is again of the same order of magnitude. One need not consider this volume as space occupied by the electrons, but rather as a volume increment of the system resulting from the presence of comparatively free electrons.

Acknowledgments.—The authors gratefully acknowledge enlightening and informative discussions with G. E. Blomgren and E. R. Van Artsdalen of these Laboratories.

(24) A. J. Stosick and E. B. Hunt, *ibid.*, **70**, 2826 (1948).

(25) C. A. Kraus, E. S. Carney and W. C. Johnson, *ibid.*, **49**, 2206 (1927).

THE EFFECT OF *p*H AND FLUORIDE ON THE FORMATION OF ALUMINUM OXIDES

BY RICHARD G. YALMAN, ELWOOD R. SHAW AND JAMES F. CORWIN

Chemistry Department, Antioch College, Yellow Springs, Ohio

Received September 3, 1959

At all *p*H's the first hydrothermal reaction of pseudoboehmite, $Al_2O_3 \cdot 1.3H_2O$, is the formation of boehmite. The rate of conversion of boehmite to diaspore and corundum at 350 and 400°, respectively, increases with increasing *p*H. In the neighborhood of 400° increasing temperatures have the same effect on the formation of corundum as increasing *p*H's. Neither corundum nor diaspore forms spontaneously in the presence of fluoride due to the stability of the fluoroaluminates and the precipitation of cryolites.

At 400° the hydrothermal conversion of silica glass to cristobalite and quartz depends upon the relative *p*H of the nutrient solution.[1] Although it has been suggested that the so-called "mineralizing" action of fluoride ion is due to the formation of fluorosilicate ions,[2] it has now been shown that the function of the fluoride ion is to control the relative *p*H of the nutrient solution by hydrolysis.[1]

The purpose of the present paper is to extend the *p*H and fluoride studies to the aluminum oxide system. In this system there are two trihydrates, two monohydrates and one anhydrous form which are hydrothermally stable.[3,4] The stability regions of these aluminas have been examined in detail.[5] Less well-defined hydrates have also been prepared.[6,7] Because there is no alumina glass it is necessary to use one of the hydrates as a source of aluminum. In order to avoid impurities, such as sodium, we chose to prepare a synthetic material by hydrolyzing aluminum isopropoxide.

(1) R. G. Yalman and J. F. Corwin, THIS JOURNAL, **61**, 1432 (1957).

(2) J. F. Corwin, R. G. Yalman, G. E. Owen and A. C. Swinnerton, *J. Am. Chem. Soc.*, **75**, 1581 (1953).

(3) For purposes of convenience the common names of these substances will be used.

(4) H. B. Weiser, "Inorganic Colloid Chemistry," Vol. II, John Wiley and Sons, New York, N. Y., 1935, p. 90.

(5) G. Erwin, Jr., and E. F. Osborn, *J. Geol.*, **59**, 381 (1951); G. C. Kennedy, *Am. J. Sci.*, **257**, 563 (1959).

(6) E. Calvet, P. Boivinet, M. Noel, H. Thibon, A. Maillard and R. Tertian, *Bull. soc. chim., France*, 99 (1953); R. Tertian and D. Papee, *J. chim. phys.*, 341 (1958).

(7) F. J. Shipko and R. M. Haag, KAPL-1740, July 10, 1957.

Experimental

The stainless steel autoclaves, the ovens and the controllers were identical to those previously described.[8] The design of the equipment limited the experiments to temperatures and pressures of 420° and 7200 p.s.i., respectively.

Unless otherwise indicated each autoclave contained 140 ml. of nutrient solution, 10 g. of corundum seed placed in the center of the autoclave and/or 3 g. of pseudo-boehmite on the floor of the autoclave. The seeds were cut from sapphire boule supplied by The Linde Air Products Co. In a few experiments seeds cut from clear diaspore obtained from Shortmann's Mineral Co. were used. Pseudo-boehmite was prepared by hydrolyzing purified aluminum isopropoxide at 85° in distilled water for one week. The product was air dried and stored in a desiccator over anhydrous calcium sulfate. The water content (analyzed as $Al_2O_3 \cdot 1.3H_2O$) and infrared analysis of this material agreed with that reported by Shipko and Haag.[7] All other reagents were A.C.S. reagent grade.

The relative *p*H of the nutrient solutions was controlled by the addition of potassium hydrogen sulfate, aluminum sulfate, potassium fluoride or sodium hydroxide. Although the initial and final *p*H of each run was determined, these measurements only confirm the order of increasing *p*H at 400°. However, both the *p*H measurements and the experiments themselves indicate that at higher temperatures the solutions of potassium hydrogen sulfate and aluminum sulfate are acidic while those of potassium fluoride and sodium hydroxide are basic.

Water was determined by dehydration at 1000°, aluminum as the hydroxyquinolate and potassium by flame-photometry. Optical measurements were made with a Bausch and Lomb Petrographic Microscope, infrared measurements were made by Dr. Harry Knorr, Kettering Foundation, Yellow Springs, Ohio, and X-ray analyses were performed

(8) A. C. Swinnerton, G. E. Owen and J. F. Corwin, *Disc. Faraday Soc.*, **5**, 172 (1948).

under the supervision of Dr. J. W. Edwards, Monsanto Chemical Co., Dayton, Ohio.

Results

The results of a number of growth experiments at 400° and 6200 p.s.i. are given in Table I. Because of their similarity the results of diaspore runs at 350° and 5000 p.s.i. are included. The growth on the diaspore seeds was in the form of whiskers. Although the spontaneous formation of diaspore has been observed at high pressures,[5b,9] it does not form readily at low pressures[5a,10] nor was it observed here. All of the residual material was converted into boehmite. In both series of experiments the seeds dissolved in acid solutions and grew in neutral and basic solutions.

The effect of *p*H on the *in situ* conversion of pseudo-boehmite to boehmite and corundum was determined at 380, 390, 400 and 420°. No seeds were present in these experiments. The results for five day runs are plotted as per cent. corundum formed against the logarithm of the composition of the nutrient solution on isotherms in Fig. 1. The values in the center of Fig. 1 indicated by the dotted line were obtained in distilled water. Values to the left and right of this line correspond to increasing aluminum sulfate and sodium hydroxide concentrations, respectively. Thus the abscissa is a relative *p*H scale.

TABLE I

GROWTH ON DIASPORE AND CORUNDUM SEEDS

Nutrient soln.	Concn., *M*	Growth, mg. Diaspore[a]	Corundum[b]
Potassium bisulfate	0.01	−20	−1.2
Aluminum sulfate	.01	−15	−0.9
Aluminum sulfate	.005	− 4	− .5
Aluminum sulfate	.002	− 2	− .2
Aluminum sulfate	.001	− 2	− .1
Distilled water		12	6
Sodium hydroxide	.001	40	12
Sodium hydroxide	.01	55	120
Sodium hydroxide	.1	75	304

[a] Av. of duplicate 30 day runs at 350° and 5000 p.s.i. [b] Av. of duplicate five day runs at 400° and 6200 p.s.i.

The effect of longer and shorter runs is to shift the isotherms up and down, respectively. This was particularly true in those solutions where partial conversion to corundum had occurred in five days. Data in Table II are typical of these time studies. In every experiment including those in sodium hydroxide at 420° where the bombs were just brought to temperature and then cooled, only boehmite was observed.

In all of these experiments the pressure varied from 3700 p.s.i. at 380° to 7100 p.s.i. at 420°. A few experiments with different degrees of filling showed that within this narrow pressure range the results depend more upon the total amount of electrolyte present than upon the total pressure. This is more apparent from solubility studies of corundum in sodium hydroxide. Preliminary experiments showed that equilibrium was reached within five days, that the solubility of corundum was independent of the position of the seed in the autoclave (above the critical point) and that there was no transfer of alumina to the walls of the autoclave.

(9) R. A. Laudise and A. A. Ballman, *J. Am. Chem. Soc.*, **80**, 2655 (1958).

(10) A. W. Laubengayer and R. S. Weisz, *ibid.*, **65**, 247 (1943).

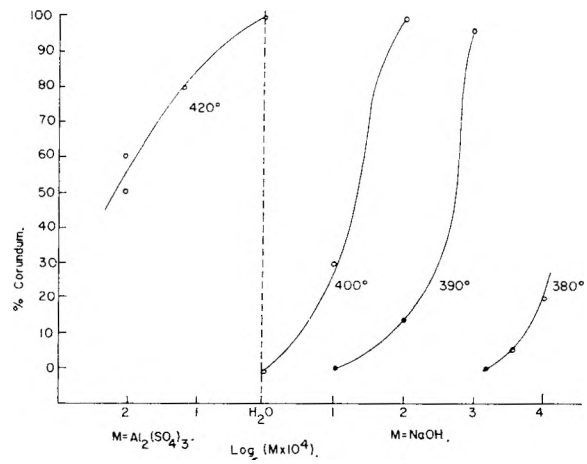

Fig. 1.—The effect of relative *p*H on the hydrothermal formation of corundum.

TABLE II

FORMATION OF CORUNDUM IN 0.001 *M* NaOH AT 400°

Time, days	Per cent.[a]
0.1	0.00
0.25	1
1	5
2	10
5	31
10	100

[a] Best estimate from index of refraction measurements, the remainder is boehmite.

Typical results at two different pressures at 380, 400 and 420° are given in Table III. The ratio of the number of gram atoms of aluminum dissolved to the number of gram moles of sodium hydroxide added, Al:NaOH, are given in column five. These values, which have been corrected for the solubility of corundum in water, show that the relative solubility of corundum in water and sodium hydroxide solutions is virtually constant over the small temperature and pressure ranges investi-

TABLE III

SOLUBILITY OF CORUNDUM IN 0.1 *M* SODIUM HYDROXIDE

Nutrient soln.	Ml.	Pressure, p.s.i.	Solubility, g.	Al:NaOH
	A.	380°		
Distilled water	140	3600	0.001	
Distilled water	160	4300	.001	
Sodium hydroxide	140	3600	.504	0.72
Sodium hydroxide	160	4300	.592	0.705
	B.	400°		
Distilled water	70	4000	0.0015	
Distilled water	140	5100	.003	
Sodium hydroxide	70	4000	.265	0.74
Sodium hydroxide	140	5100	.537	0.75
	C.	420°		
Distilled water	50	4000	0.004	
Distilled water	140	7100	.013	
Sodium hydroxide	50	4000	.188	0.72
Sodium hydroxide	140	7100	.519	0.71

gated here. The small variations observed are within the error of the experiments themselves.

TABLE IV

SOLUBILITY OF CORUNDUM AT 400°

Concn. NaOH, *M*	Solubility, g./140 ml.	Al:NaOH
0.000	0.003	
.01	.055	0.73
.02	.105	.72
.05	.265	.74
.10	.530	.74
.20	1.090	.76
.50	2.820	.79

The solubility data for corundum at 400° (Table IV) correspond to the over-all reaction

$$Al_2O_3 + 7H_2O + 2OH^- = 2Al(H_2O)_2(OH)_4^-;$$
$$K = [Al(H_2O)_2(OH)_4^-]/[OH^-] \quad (1)$$

It can be shown easily that

$$K = R/(1 - R)$$

where R is the value of Al:NaOH in Tables III and IV. At 400° and infinite dilution K has a value of 2.64.

Fluoride Runs.—The results of growth experiments in potassium fluoride solutions at 400° are summarized in Table V. Although the amount of growth increases with increasing concentration, there was no comparable increase with time. In the thirty-day run in 1 *M* KF the deposit consisted almost entirely of potassium cryolite; in the other runs well developed faces of corundum formed on the seeds. There was no evidence for the formation of corundum *in situ* in these experiments nor at 420°. Instead the residual material consisted of boehmite, potassium cryolite and an unidentifiable material of variable composition (index of refraction 1.48–50). The latter material disappeared in the longer runs.

There was no evidence for the growth of spontaneous formation of diaspore at 350° in potassium fluoride solutions.

TABLE V

GROWTH IN POTASSIUM FLUORIDE SOLUTIONS

400° 6200 p.s.i.

Concn. KF, *M*	Length of run, days	Growth, mg.	Products (*in situ*)
0.01	2	3	Boehmite
.01	2	15	Boehmite
.1	2	6	Boehmite
.1	5	93	Boeh., K_3AlF_6, Un. Mat.
.1	5	120	Boeh., K_3AlF_6, Un. Mat
.1	10	70	Boeh., K_3AlF_6, Un. Mat
.1	14	146[a]	Boeh., K_3AlF_6, Un. Mat.
.1	20	40	Boeh., K_3AlF_6, Un. Mat.
1.0	5	93	Boeh., K_3AlF_6, Un. Mat.
1.0	30	398[b]	Boeh., K_3AlF_6, Un. Mat.

[a] Traces of K_3AlF_6 on the seed. [b] All growth material was K_3AlF_6.

At 400° 45 mg. of corundum dissolved in 140 ml. of 0.01 *M* KF and 94.5 mg. dissolved in 140 ml. of 0.02 *M* KF. This is less than the amount of corundum which dissolved in the corresponding sodium hydroxide solutions (see Table IV). Solubility experiments at higher potassium fluoride concentrations were complicated by the formation of solid phases of variable composition.

If the hydrolysis of the fluoride ion were complete at 400°, then the solubility of corundum in potassium fluoride solutions would be the same as that in sodium hydroxide solutions. The lower solubility in the former solutions indicates that the hydrolysis of the fluoride ion is not complete at 400°. In addition the formation of potassium cryolite in the more concentrated potassium fluoride solutions indicates that some of the soluble aluminum is present as fluoroaluminate complexes.

Discussion

The hydrothermal transformations in the alumina system differ from those in the silica system in several respects. In the silica system cristobalite and quartz can be formed *simultaneously* in weakly alkaline solutions from silica glass.[1] The stability of cristobalite in acid and neutral solutions and the ease of formation of quartz in alkaline solutions suggests that the crystallization processes involve a neutral molecule and a silicate ion in the formation of cristobalite and quartz, respectively. Thus the hydrothermal formation of these polymorphs depends more upon their rate of crystallization from the nutrient solution than upon their thermodynamic stability.

Our experiments show that boehmite is the first product in the hydrothermal crystallization of pseudo-boehmite. Similar observations have been made on the hydrothermal formation of boehmite from other aluminas.[5b,11,12] At a given temperature and pressure the rate of formation of diaspore and corundum from boehmite increases with increasing alkalinity. Below 400° the rate-determining step may involve the aluminate ion while above 400° both the ion and the aluminum molecule may contribute to the growth process. However, in contrast to the silica system, *p*H is a less important factor here than the temperature of the reaction and the thermodynamic stability of the oxides themselves.

The solubility of quartz has been investigated over a wide range of temperatures and pressures[13] and under the conditions of our experiments (350–420° and 3700–7100 p.s.i.) the most important species is the monomer.[14] Although similar data are not available for the aluminas, the solubility of corundum in sodium hydroxide indicates that the aluminate ion is a monomer. It seems likely that the neutral molecule would also be a monomer.

In equation 1 the aluminate ion was written as a hexacoördinated complex. The only justification for this formula is the octahedral arrangement of water, hydroxyl and oxide ions in the various hydrates and oxides of aluminum. Aluminum also occurs with a tetrahedral arrangement in feldspars and other aluminosilicates. This is explained by the fact that the radius ratio of Al^{3+}:$O^{=}$ is 0.41, the limiting value for the tetrahedral configura-

(11) H. B. Weiser, ref. 4, p. 94.

(12) H. Ginsburg and M. Koster, *Z. anorg. allgem. Chem.*, **271**, 41 (1952).

(13) G. C. Kennedy, *Econ. Geol.*, **451**, 629 (1950).

(14) John A. Woods, Jr., *Am. J. Sci.*, **256**, 40 (1958).

tion.[15] This same argument can be used to justify the formula $Al(OH)_4^-$ for the aluminate ion. It seems very likely that in the aluminum system equilibria exist between tetra- and hexacoördinated molecules and ions. Such equilibria would explain the incorporation of aluminum in quartz crystals[16,17] under conditions suitable for the formation of boehmite, diaspore and corundum as well as the occurrence of both tetra- and hexacoördinated aluminum in mica, clays and related minerals.[18]

Finally the effect of the fluoride ion is different in the two systems. In the silica system the hydrolysis of the fluoride ion and the subsequent formation of hydroxide ion promotes the spontaneous formation of quartz. In the alumina system the stability of fluoroaluminate ions[19] represses the hydrolysis of the fluoride ion and thus inhibits the formation of corundum. Consequently corundum is only formed by seeding in potassium fluoride solutions. The stability of the fluoroaluminate ions also accounts for the successful growth of radiograde quartz from quartzites in sodium carbonate solutions containing small amounts of sodium fluoride.[17]

(15) L. Pauling, "Nature of the Chemical Bond," 2nd Ed., Cornell University Press, Ithaca, N. Y., 1940, p. 382.

(16) J. M. Stanley and S. Theokritoff, *Am. Min.*, **41**, 527 (1956).

(17) C. S. Brown, R. C. Kell, P. Middleton and L. A. Thomas, *Nature*, **176**, 602 (1955).

(18) L. Pauling, ref. 15, p. 391.

(19) Equilibrium experiments carried out in this Laboratory show that at 25° the fluoroaluminate ion, AlF^{2+}, is ninety times more stable than the corresponding fluorosilicate ion, SiF^{2+}.

ABSORPTION SPECTRA IN FUSED SALTS

By Norman W. Silcox and Helmut M. Haendler[1]

Department of Chemistry, University of New Hampshire, Durham, N. H.

Received September 3, 1959

The absorption spectra of eight anhydrous metal chlorides dissolved in a magnesium chloride–potassium chloride–sodium chloride eutectic have been observed at 430° in the spectral region from 230 to 400 mμ. The chlorides used were those of copper(II), nickel(II), cobalt(II), manganese(II), iron(III), uranium(III), uranium(IV) and uranyl.

Absorption spectra have been reported recently for a number of fused salt systems.[2-5] In general, the emphasis has been on the use of spectra to determine the species present. The use of spectra for analytical purposes is also worthy of consideration. We have attempted to consider both aspects of the problem, and this paper reports on the experimental procedure and the ultraviolet absorption spectra of a series of chlorides in fused salt solution. Visible spectra of these chlorides have also been measured and will be reported subsequently.

Experimental

Chemicals.—Anhydrous copper(II), cobalt(II) and nickel(II) chlorides were prepared by the dehydration of the hydrated salts at 185° for 24 hours. Anhydrous sublimed iron(III) chloride was reagent grade. Manganese(II) chloride was prepared by passing dry hydrogen chloride gas over manganese(II) carbonate at 300°. Uranium(III), uranium(IV) and uranyl chlorides were prepared according to the directions in Inorganic Syntheses.[6] The chlorides were analyzed for metal content and found to be satisfactory. They were used without further purification.

The ternary eutectic was supplied by the Brookhaven National Laboratory Nuclear Engineering Department. Its nominal composition was 58% magnesium chloride, 24% sodium chloride and 18% potassium chloride, by weight. The melting point of the mixture is about 400°. The melt is clear and colorless, and remains so as long as hydrolysis does not occur. Due to its hygroscopic nature, the eutectic was always handled in a dry box.

The Furnace.—A copper rod was cut and reassembled to leave a hole to accept a one cm. path square cell. The block was 10 cm. high and 5 cm. in diameter and was nickel plated to retard oxidation. A ceramic tube was cut to fit around the block and wound with No. 18 Kanthal wire. The furnace was insulated with No. 1500 Sauereisen cement, a vermiculite type. It can operate satisfactorily to 700°. In the work described, temperature was kept at 430 ± 3°. This fluctuation in temperature had negligible effects on absorbance measurements. Temperatures were controlled and recorded with a Leeds and Northrup Micromax recorder. A metal clip held the cell in a fixed reproducible position, and the furnace assembly was placed as close as possible to the entrance slit of the monochromator.

The Spectrometer.—A Perkin-Elmer Model 12-C spectrometer, with quartz optics, was used in conjunction with an 1P-28 photomultiplier tube detector. The chopped beam and tuned amplifier of this instrument prevent interference by the radiant energy of the furnace and sample, particularly at higher temperatures. The instrument was calibrated with mercury vapor and hydrogen lamps. A hydrogen lamp was used as the source.

The Optical Cells.—Measurements were made in square quartz cells, with one cm. path length, supplied by the Pyrocell Manufacturing Co. The optical surface was four cm. high. A side arm permits passage of argon over the surface of the melt. The argon was dried with magnesium perchlorate, "Molecular Sieves," and phosphorus pentoxide. The flow of argon is monitored between 20–80 cc./min., and a cell cap reduces atmospheric contamination. After the cells have been in use for some time, etching appears at the gas-melt interface, but very slight attack occurs on the optical surfaces. Care in transfer and high quality of eutectic minimize the attack. Immediate removal of the eutectic while still molten is imperative at the end of a run.

The Density.—A standard Westphal specific gravity balance was modified to permit direct determination of the density of molten eutectic or solutions. A nickel plummet was used as a bob. A set of weights was constructed to accompany the bob to make the balance direct reading. The density of the eutectic was found to be 2.05 g./cc. at 420°. The deviation from the value at 430° is outside the experimental error of the method.[7] There is some attack on the

(1) To whom communications should be addressed. Research supported by Brookhaven National Laboratory and taken in part from the Ph.D. Thesis of N. W. Silcox.

(2) C. R. Boston and G. P. Smith, This Journal, **62**, 409 (1958).

(3) B. R. Sundheim and M. Greenberg, *J. Chem. Phys.*, **28**, 439 (1958).

(4) D. M. Gruen, *J. Inorg. Nucl. Chem.*, **4**, 74 (1957).

(5) D. M. Gruen and R. L. McBeth, *ibid.*, **9**, 290 (1959).

(6) "Inorganic Syntheses," Vol. V. T. Moeller, Editor, McGraw-Hill Book Co., New York, N. Y., 1957 pp. 143–150.

(7) E. R. van Artsdalen and I. S. Yaffe, This Journal, **59**, 118 (1955).

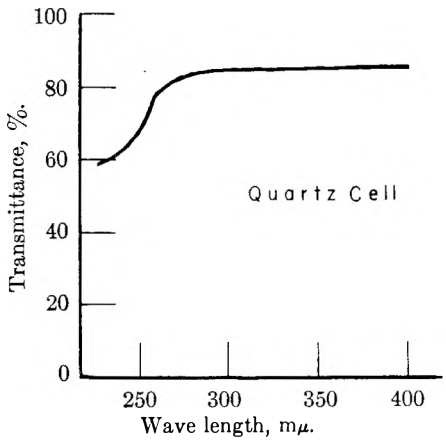

Fig. 1.—Transmittance of quartz cell.

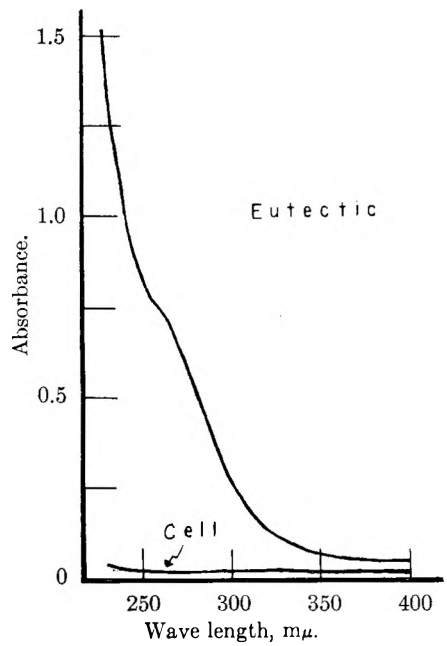

Fig. 2.—Absorbance (optical density) of $MgCl_2$-KCl-NaCl eutectic at 430°.

nickel, but the resultant density change is negligible.

Procedure.—Eutectic was transferred to a cell in the dry box, the cell stoppered, and weighed to determine the amount of eutectic taken. Samples of solute were weighed directly on a Berman Torsion micro-balance in the dry box, on platinum weighing pans. The samples were kept suspended in stoppered tubes in a desiccator until needed for addition to the molten eutectic in the cell. These additions were made as successive increments, permitting consecutive measurements on solutions of different concentrations. In some cases a "master solution" of metal chloride in eutectic was prepared and used as the sample to attain greater dilution or to slow down hydrolysis of the sample. This was the case with copper(II) and iron(III) chlorides. No vaporization of metal chloride was observed.

The capped cell and eutectic were placed in the furnace and clipped in place. Argon was passed through the cell side arm and the eutectic allowed to melt. The spectrum of the solvent was taken with narrow slit widths, the practical lower limit being that obtainable with the maximum gain setting at which accompanying noise can be tolerated. A sample of solute was added directly from the balance pan and the mixture stirred with a "flamed" Vycor stirrer until uniform. The spectrum was rerun with the same gain and slit settings as for the solvent alone. The same procedure was followed for the second sample. The absorption spectrum then must be calculated on a point-to-point basis.

The eutectic was used as the reference for all spectral

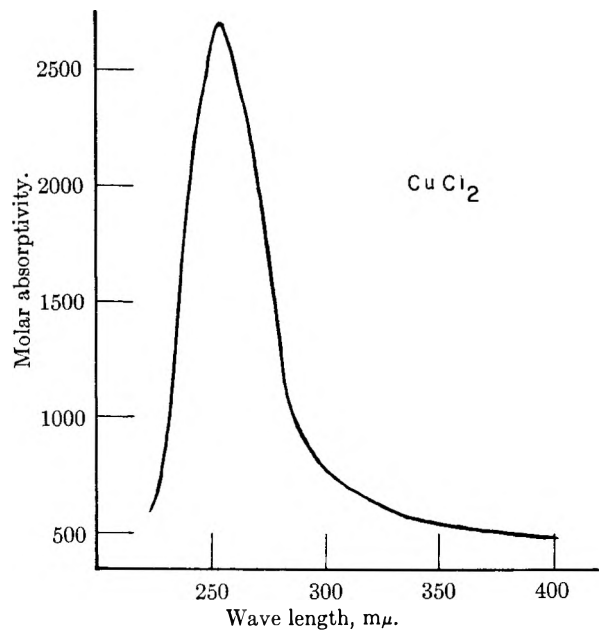

Fig. 3.—Absorption spectrum of copper(II) chloride in $MgCl_2$-KCl-NaCl eutectic at 430°.

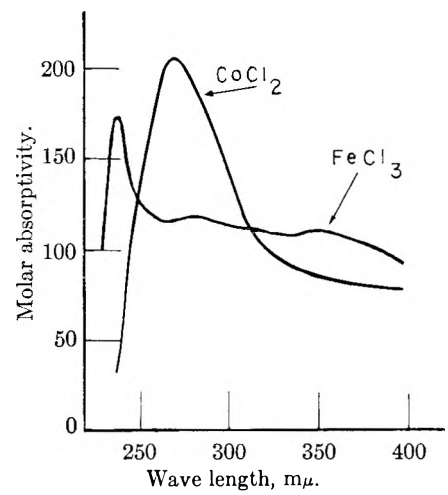

Fig. 4.—Absorption spectra of $FeCl_3$ and $CoCl_2$ in $MgCl_2$-KCl-NaCl eutectic at 430°.

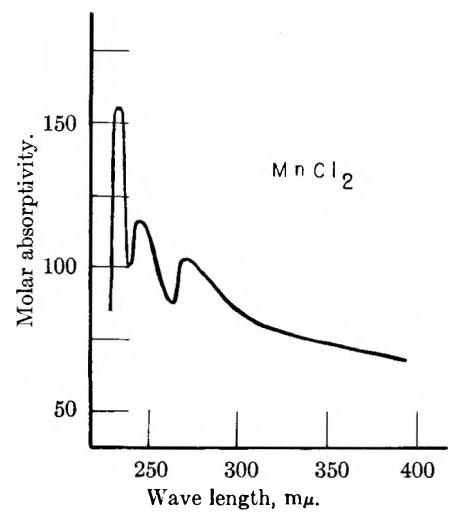

Fig. 5.—Absorption spectrum of $MnCl_2$ in $MgCl_2$-KCl-NaCl eutectic at 430°.

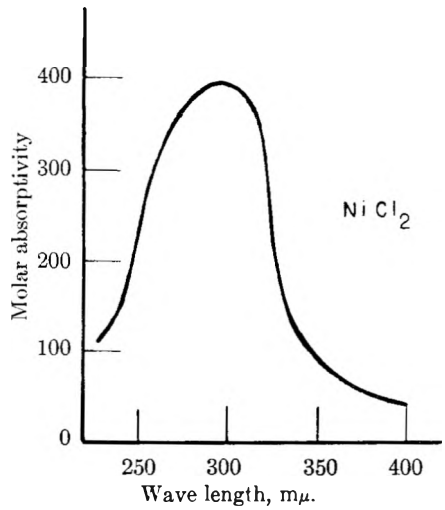

Fig. 6.—Absorption spectrum of $NiCl_2$ in $MgCl_2$–KCl–NaCl eutectic at 430°.

measurements. At 225 mμ the eutectic itself is highly absorptive, but this absorption drops off rapidly near 300 mμ, and is very small at 400 mμ. Since the concentration of the solutions is low, the density was taken as that of the pure solvent in computing the molar absorptivities. Only absorbance values between 0.1 and 1.0 were used in the computations.

Results

The solute concentrations, absorption maxima and corresponding molar absorptivities (molar extinction coefficient) for the metal chlorides dissolved in the ternary eutectic, at 430°, are listed in Table I. The transmittance of a typical cell, and the absorbance of the pure eutectic, are shown in Fig. 1 and 2. The observed spectra are shown in Fig. 3 to 8. The molar absorptivities are reproducible to 2–3% for values of 1000 l./mole-cm. or greater, and 7–8% for values between 100 and 500 l./mole-cm. Data are based on an average of 3–6 separate interconsistent runs.

TABLE I

ABSORPTION MAXIMA AND MOLAR ABSORPTIVITIES

Salt	Solute concn., wt. %	Wave length of maximal absorption, mμ	Molar absorptivity, l./mole-cm.
$CoCl_2$	0.001–0.002	266	203
$CuCl_2$	.001– .002	254	2770
$FeCl_3$	.01 – .03	238	174
$MnCl_2$	.01 – .03	233, 246, 272	135, 102, 92
$NiCl_2$	.004– .01	295	398
UCl_3	.004– .01	242, 330	1656, 1219
UCl_4	.01 – .07	235	349
UO_2Cl_2	.004– .01	250	1804

Discussion

All the chlorides studied show absorption in the lower ultraviolet region, with considerable variation in the magnitude of the molar absorptivity. The absorption in this region appears to be related to some common property of these systems rather than to some unique property of individual metal ions or complexes present. The most probable explanation seems to involve "charge transfer" spectra,[8] the absorption being due to electron transfer from one ionic species in the solution to another.

The order of magnitude of the molar absorptivity

(8) L. E. Orgel, *Quart. Revs., London*, **8**, 422 (1954).

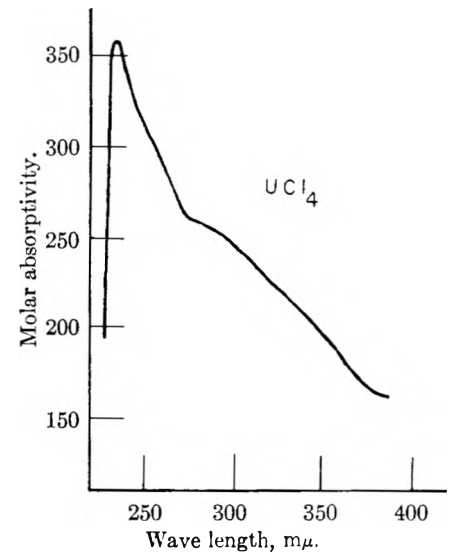

Fig. 7.—Absorption spectrum of UCl_4 in $MgCl_2$–KCl–NaCl eutectic at 430°.

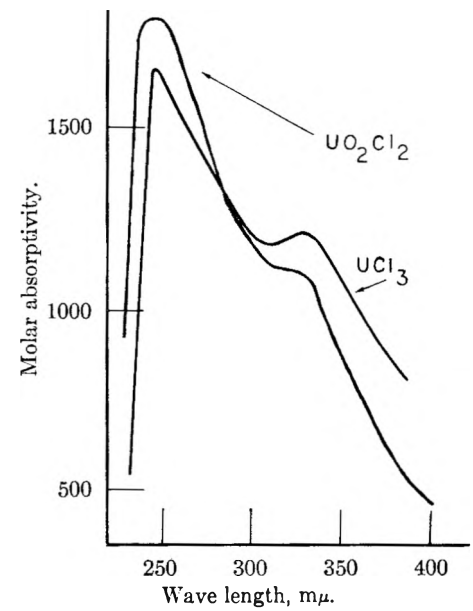

Fig. 8.—Absorption spectra of UCl_3 and UO_2Cl_2 in $MgCl_2$–KCl–NaCl eutectic at 430°.

is also more characteristic of charge transfer than electron transitions in the metal or complex. Further support is given by the intense absorption of the eutectic itself, when compared to air, Fig. 2. Sundheim's observations[3] on pure salts in the ultraviolet have shown a region of sharp demarcation between absorption and transmission. This he identifies as due to charge transfer phenomena. Smith[2] has attributed his first nickel(II) chloride band to charge transfer. It is therefore not unreasonable to assume that we are dealing with the same situation. The analysis of the nickel chloride spectrum has been amplified by Sundheim and Harrington.[9]

Jorgensen[10] has reported red solutions are formed by aqueous uranium(III) in the presence of 12 *M*

(9) B. R. Sundheim and G. Harrington, *J. Chem. Phys.*, **31**, 700 (1959).

(10) Chr. K. Jorgensen, *Acta Chem. Scand.*, **10**, 1503 (1956).

hydrochloric acid. The presence of UCl_4^- or higher complexes has been implied. Solutions of uranium(III) chloride in lithium chloride–potassium chloride solution at 400° show the tail of what may be a charge transfer band at 360–400 mμ, with a molar absorptivity greater than 250 l./mole-cm.

The salt spectra which are observed in solution are detected as differences measured against a rapidly changing background. This greatly increases the difficulty of obtaining high precision on individual runs when compared to other runs. It should not, however, materially affect accuracy, if the background can be held constant. In considering the possible analytical application of these ultraviolet spectra it should be noted that sensitivity is high, but selectivity is low. The greatest sensitivity is shown by copper(II), uranium(III) and uranyl chlorides. A change in transmittance from 100%, for eutectic alone, to an assumed 98%, for a solution of copper(II) chloride in eutectic, would correspond to a concentration change of about 0.1 p.p.m. of copper. A similar transmittance change would be equivalent to about 0.6 p.p.m. of uranium(III), as chloride.

The ideal condition for selectivity would be completely different and unique spectra for the species to be analyzed. This is only seldom attainable, but if there be sufficient distinction at several wave lengths, calculation by simultaneous equations often can be made. The ultraviolet spectra are not, in general, as suitable in this respect as are visual spectra. There must, therefore, be a compromise between selectivity and sensitivity.

A rough test of the uranium(III)–uranium(IV) combination was made by measurements at 240 and 330 mμ of a mixture of the two chlorides in eutectic. Comparison of results is shown

UCl_3

Present:	4.8×10^{-4} mole/l.	5.0×10^{-4} mole/l.
Found:	1.3×10^{-4} mole/l.	2.4×10^{-4} mole/l.

UCl_4

Present:	6.8×10^{-4} mole/l.	8.3×10^{-4} mole/l.
Found:	1.7×10^{-4} mole/l.	2.0×10^{-4} mole/l.

The order of magnitude is appropriate.

SOLUBILITY OF PLUTONIUM TRIFLUORIDE IN FUSED-ALKALI FLUORIDE–BERYLLIUM FLUORIDE MIXTURES[1]

BY C. J. BARTON

Reactor Chemistry Division, Oak Ridge National Laboratory,[2] Oak Ridge, Tennessee

Received September 3, 1959

The solubility of PuF_3 in five LiF–BeF_2 mixtures, three NaF–BeF_2 mixtures and two NaF–LiF–BeF_2 mixtures was determined at temperatures ranging from about 550 to 650° because of interest in the possibility of fueling a fused salt power reactor with plutonium. The solvents examined varied in BeF_2 content from 26 to 50 mole %. Solubility determinations were made in nickel filter apparatus. Liquid salt mixtures saturated with PuF_3 were forced through sintered nickel filters and the cooled filtrate was analyzed chemically for total plutonium content. The data appear to follow a linear relationship within the experimental accuracy of the measurements when plotted as log of molar concentration of PuF_3 *versus* $1/T(°K.)$. The solubility of PuF_3 in these solvents is rather low, varying from about 0.4 to 2.5 mole % at 650°, and from 0.16 to 1.0 mole % at 550°. Minima in solubility–composition diagrams for the binary systems at 565° occur at 63 mole % LiF (0.3 mole % PuF_3) and 57 mole % NaF (0.18 mole % PuF_3). The observed solubilities are believed to be adequate for some types of fused salt reactors. The effect of ThF_4, BaF_2 and CeF_3 in diminishing the solubility of PuF_3 in LiF–BeF_2 (63-37 mole %) was determined. The solubility of PuF_3 in the mixture LiF–BeF_2–UF_4(70-10-20 mole %) was found to be higher than in an LiF–BeF_2 solvent having the same concentration of LiF.

Introduction

Studies conducted at the Oak Ridge National Laboratory have demonstrated that UF_4 can be dissolved in a number of molten-fluoride solvents to provide fuel for fused-salt reactors.[3,4] Consideration of UF_3 for this purpose was discontinued when this compound was found to be unstable in fused-salt mixtures in contact with structural metals at elevated temperatures.[5] The Aircraft Reactor Experiment,[6,7] the only fused-salt reactor that is known to have operated, used $U^{235}F_4$ as fissionable material and a mixture of NaF and ZrF_4 as the solvent. Some thought has been given to the use of $U^{235}Cl_3$ or $U^{235}Cl_4$ as fissionable materials in a fast-neutron fused-salt reactor[8] and to the promising possibility of a $Th^{232}F_4$–$U^{233}F_4$ breeder reactor.[9] Consideration of use of plutonium in molten-fluoride reactors has been limited by lack of information on the high-temperature behavior of fluoride mixtures containing plutonium fluorides. This paper gives the results of a preliminary investigation of the possibility of using $Pu^{239}F_3$ as the fissionable species in a molten-fluoride reactor.

Equipment and Apparatus.—All high-temperature operations with plutonium were performed in a stainless steel glove box. The heating well, surrounded by a 2700-watt, 5-inch-tube furnace beneath the box, consisted of a

(1) This paper was presented at the 135th Meeting of the American Chemical Society, Boston, April 5–10, 1959.

(2) Operated for the United States Atomic Energy Commission by the Union Carbide Corporation.

(3) "Fluid Fuel Reactors," James A. Lane, H. G. MacPherson and Frank Maslan, Editors, Addison-Wesley Publishing Co., Inc., Reading, Mass., 1958, Chapter 12.

(4) W. R. Grimes, *et al.*, "Reactor Handbook," Vol. 2, Section 6, AECD-3646, May, 1955.

(5) Ref. 3, p. 577.

(6) A. M. Weinberg and R. C. Briant, *Nuclear Sci. Eng.*, **2**, 797 (1957).

(7) E. S. Bettis, *et al.*, *ibid.*, **2**, 841 (1957).

(8) Ref. 4, Chapter 6.2.

(9) Ref. 3, Chapter 14.

1.5 inch length of 6-inch i.d. pipe welded around an opening in the bottom of the box and connected to an 8-inch length of 4-inch i.d. pipe closed at the bottom. The furnace was mounted on a jack so that it could be lowered to facilitate rapid cooling of the well. The box was kept cool while the furnace was in operation by water flowing through a copper coil soldered to the bottom of the box around the well. Bellows-type valves mounted on a panel below the front face of the box controlled admission of argon, 95% argon–5% hydrogen mixture and HF to apparatus within the box from gas tanks located outside the laboratory. A similar valve provided connection to a vacuum pump adjacent to the gas tanks. HF-containing gas mixtures were passed through two 30-inch lengths of 3-inch o.d. copper tubing filled with NaF pellets to remove HF before discharging into the exhaust system. The first of the two traps which were placed in series was maintained at about 100° in order to avoid formation of semiliquid HF-rich NaF complexes while the second trap was kept at room temperature in order to effect more nearly complete removal of HF from the gas stream.

A Zeiss polarizing microscope, mounted in a glove box connected to the stainless-steel box through an interchange chamber, was used to identify the compounds present in fused mixtures. The microscope box was connected to another glove box containing a torsion balance used for weighing solvent mixtures or PuF_3 to the nearest milligram.

All of the boxes were maintained at a pressure of approximately one inch of water below that of the laboratory by means of an exhaust system equipped with air filters.

The filtration apparatus for this investigation was a modification of that used earlier at ORNL for solubility determinations.[10] The filter medium consisted of a small disc of sintered nickel (0.0004-inch porosity) welded into one end of a 14-inch length of $^3/_8$-inch nickel tubing. The filter tube was inserted into the filter bottle through a copper bellows that permitted the filter medium to be kept out of contact with the charge material prior to filtration in order to minimize clogging of the filter medium. A nickel tube ($^1/_4$-inch o.d.) ending in a Swagelok connection extended just through the top of the filter bottle and a thin-wall nickel thermowell extended from the top to within approximately $^1/_8$ inch of the bottom. The first apparatus of this type was assembled by Heliarc welding. An improved version having a thin wall thermowell was assembled by brazing with gold–nickel alloy in a hydrogen atmosphere at 1000°. This assembly method effectively removed oxide film from the nickel surfaces of the apparatus.

The temperature of the melt surrounding the tip of the thermocouple well was measured by means of a platinum–platinum 10% rhodium thermocouple, and recorded on a 300–1000° recorder. Temperature control was maintained by means of a Brown proportional controller.

Materials.—Plutonium trifluoride used in these studies was supplied by Los Alamos Scientific Laboratory. Chemical and spectroscopic analyses furnished by the supplier showed that the plutonium content of the material was very close to the theoretical value and the total of metallic impurities was less than 0.1 weight %. Optical microscopic examination showed less than 1% of other compounds present. Some solvent mixtures were purified prior to being introduced into the glove box by treatment with gaseous HF and H_2 at about 800°, followed by cooling under an inert atmosphere. The compositions of these mixtures were determined by chemical analysis. Other solvent mixtures were produced in the glove box by addition of LiF, NaF or crystalline BeF_2 to one of the purified mixtures and their compositions were calculated from the weights of materials used.

Experimental Procedure.—The filtration apparatus was first connected to the gas tanks and vacuum pump through a manifold system below the stainless-steel glove box and vacuum tested at room temperature. After a vacuum of about 50μ was obtained the filter stick was removed and a long-neck metal funnel inserted in its place through which 5.0 to 5.5 g. of solvent mixture and enough PuF_3 to give 6.0 g. total was transferred to the filter bottle from weighed plastic vials. The ratio of solvent to PuF_3 was adjusted to provide at least twice the amount of PuF_3 that was expected to be dissolved. After the filter apparatus was reassembled and vacuum tested a second time, it was filled with argon–hydrogen mixture or pure argon and a slow flow of gas was introduced under a positive pressure of 1 to 3 lb. of argon through the filter stick which was positioned with the filter medium close to the salt mixture. Argon–hydrogen mixture was used during a large part of the investigation to provide a reducing atmosphere but this mixture was replaced with pure argon when it was concluded that the hydrogen present in HF, together with the nickel surfaces of the filter apparatus, would reduce any PuF_4 present in the fused-salt mixture to PuF_3. Gaseous HF was added to the argon or argon–hydrogen mixture in the filter apparatus before the temperature reached 250° in order to minimize hydrolysis resulting from adsorbed water on the surfaces of the solvent or PuF_3 crystals.

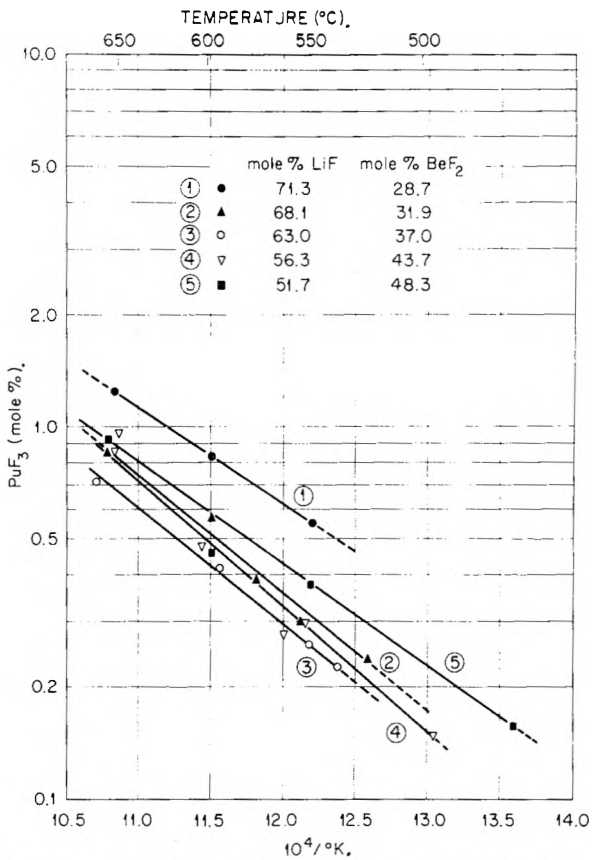

Fig. 1.—Solubility of PuF_3 as a function of temperature for LiF–BeF_2 solvents.

The filter bottle and contents were held at the desired filtration temperature ±5° for two hours while a slow flow of mixed gases was maintained over the surface of the liquid. Filtration then was effected by evacuating the interior of the filter stick and applying an argon pressure of 3 to 6 lb. to the surface of the liquid while the bellows was compressed to bring the filter medium in contact with the liquid for a period of 5 to 10 minutes. After the filtrate and residue had cooled to room temperature in an argon atmosphere, the filter stick was removed and sectioned for recovery of the filtrate. The entire filtrate was ground to pass a 65-mesh sieve and a portion of the thoroughly mixed material was submitted for chemical analysis. Fresh portions of solvent and PuF_3 were added to the residue from the previous filtration, a new filter stick was inserted in the apparatus and the above filtration procedure was repeated at a different temperature. After the required number of filtrations had been completed with each solvent composition, the filter bottle usually was cut open and the residue from the final filtration experiment was removed for examination and analysis. In some instances, it was found possible to remove practically all of the residue without sacrificing the filter bottle, permitting it to be reused with a different solvent composition.

(10) Designed by B. H. Clampitt, formerly a member of the Chemistry Division, Oak Ridge National Laboratory.

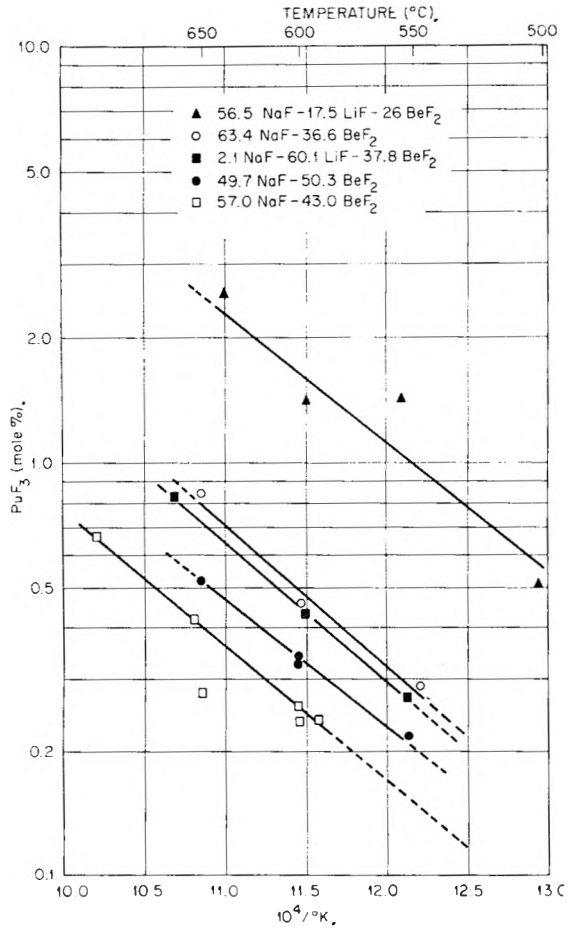

Fig. 2.—Solubility of PuF_3 as a function of temperature for $NaF-BeF_2$ and $NaF-LiF-BeF_2$ solvents.

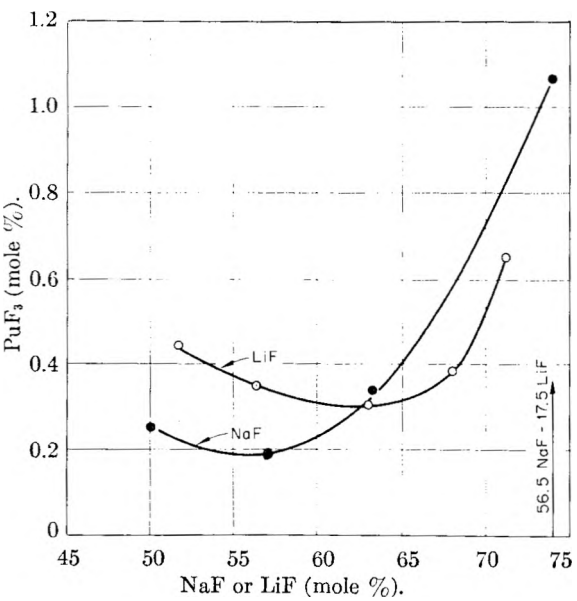

Fig. 3.—Solubility of PuF_3 in $LiF-BeF_2$ and $NaF-BeF_2$ at 565°.

Results and Discussion

Solubility data obtained with $LiF-BeF_2$ mixtures are shown in Fig. 1, plotted as log of molar concentration of PuF_3 *vs.* $1/T$ (°K.). Similarly, solubility values obtained with $NaF-BeF_2$ compositions and data on the solubility of PuF_3 in two $NaF-LiF-BeF_2$ mixtures are displayed in Fig. 2. It is clear from these figures that about 25% of the trials gave erratic results. The scatter in data is believed to be due principally to experimental difficulty encountered in accurately determining the temperature of the molten materials. The linearity of the solubility–temperature relationship indicates that the heat of solution of PuF_3 in these solvents is essentially constant for the temperature range covered in this investigation. It varied from about 12,000 to 16,800 cal. per mole.

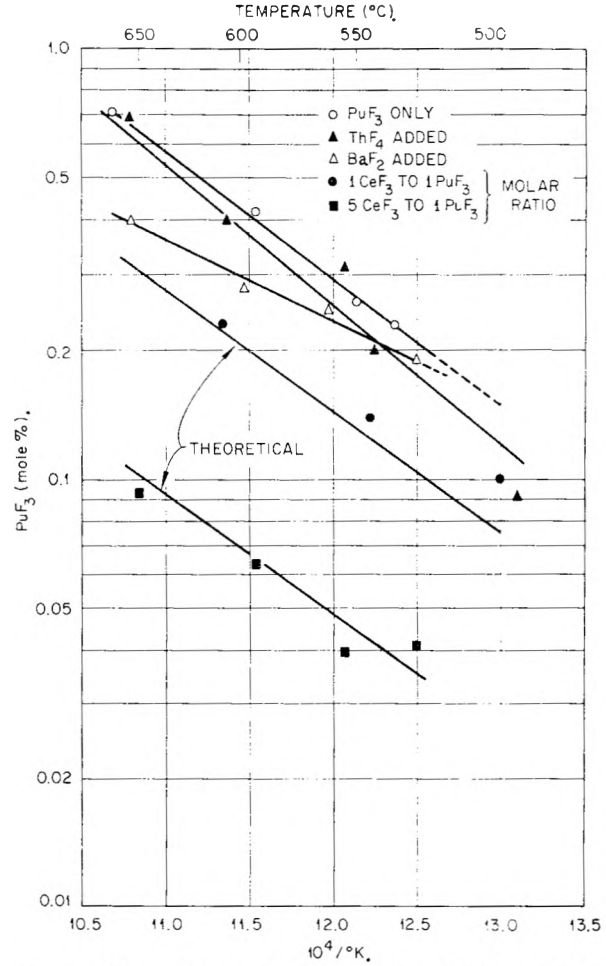

Fig. 4.—Effect of other fluorides on the solubility of PuF_3 in $LiF-BeF_2$ (63–37 mole %).

The relationship between solubility and solvent composition at 565° is shown in Fig. 3. A minimum in the $LiF-BeF_2$ solubility–composition curve occurs at approximately 63 mole % LiF (0.31 mole % PuF_3) while in the NaF–BeF system the minimum solubility (0.18 mole % PuF_3) occurs at about 57 mole % NaF. The minimum PuF_3 solubility values observed are believed to be adequate to exceed the critical concentration in some molten-fluoride reactor designs. If concentrations in excess of the minimum values appear desirable for circulating fuel reactors, viscosity considerations dictate a decrease in the BeF_2 content of the solvent mixture.

Interest in the possibility of converting $Th^{232}F_4$ to $U^{233}F_4$ in a plutonium-fueled molten-fluoride

reactor led to a determination of the effect of ThF_4 on the solubility of PuF_3 in the solvent mixture 63 LiF–37 BeF_2 (mole %). The effect of BaF_2 on the solubility of PuF_3 in the same solvent composition was investigated as an example of the possible effect of divalent fission products formed in long-term operation of a power reactor. The data shown graphically in Fig. 4 indicate that one mole per cent. ThF_4 has very little effect on PuF_3 solubility in this solvent. The same amount of BaF_2 diminished the solubility of PuF_3 in a manner not clearly understood. The saturating phase in these experiments quite possibly was not pure PuF_3 but a solid solution of BaF_2 and PuF_3 and since the molar ratio of BaF_2 and PuF_3 varied in these experiments, the solid phase or phases in equilibrium with the liquid may have varied in composition. Microscopic examination of the mixtures indicated the probable existence of two different BaF_2–PuF_3 solid solutions. The magnitude of the effect indicates that the concentration of divalent fission products likely to be encountered in reactor operation would be unlikely to affect the solubility of PuF_3 significantly.

The effect of CeF_3 on the solubility of PuF_3 was examined as an example of the effect of trivalent fission products and also because coprecipitation of CeF_3 and PuF_3 might be useful as a means of removing plutonium from solution in the fused-salt medium as the first step in a reprocessing scheme. Data obtained with CeF_3–PuF_3 solute mixtures in the solvent 63 LiF–37 BeF_2 (mole %) are displayed graphically in Fig. 4. The theoretical curves for CeF_3–PuF_3 mixtures shown in Fig. 4, which agree reasonably well with the experimental data, were calculated by use of the equation

$$N_{PuF_3(d)} = S^0_{PuF_3} N_{PuF_3(ss)}$$

where $N_{PuF_3(d)}$ is the mole fraction of PuF_3 in solution, $S^0_{PuF_3}$, the mole fraction (solubility) of PuF_3 in the solvent at a specified temperature (shown labeled "PuF_3 only" in Fig. 4), while $N_{PuF_3(ss)}$ is the mole fraction of PuF_3 in the solute mixture. This equation was adapted from the solubility relation developed by other investigators at this Laboratory.[10] Agreement between experimental and calculated solubility values in the majority of the experiments performed probably indicates that PuF_3 and CeF_3 form solid solutions. Confirmation of this belief was found in the optical properties of crystalline filtrates.[11] The solutes were found to be single-phase materials with optical properties intermediate between those of CeF_3 and PuF_3.

Data on the solubility of PuF_3 in the solvent mixture 70 LiF–10 BeF_2–20 UF_4 (mole %) are contained in Table I. These data, when plotted on a log concentration *vs.* reciprocal temperature graph, fall on a straight line. The data in Table I seem to indicate that operation of a plutonium-producing molten fluoride reactor would not be limited by low solubility of PuF_3 in a solvent of this type.

TABLE I

SOLUBILITY OF PuF_3 IN LiF–BeF_2–UF_4 (70-10-20 MOLE %)

Filtration temp., °C.	Plutonium in filtrate	
	Wt. % Pu	Mole % PuF_3
558	3.43	1.27
600	4.57	1.70
658	6.50	2.48

Acknowledgments.—The writer is grateful to F. N. Case, Isotopes Division, Oak Ridge National Laboratory, for help in designing the glove boxes used in this investigation; to R. J. Sheil, Reactor Chemistry Division, Oak Ridge National Laboratory, for designing the gas manifold system; to members of the Analytical Division, Oak Ridge National Laboratory, who performed the numerous analyses required in these studies under the direction of L. T. Corbin, J. H. Cooper and W. R. Laing; to R. A. Strehlow, Reactor Chemistry Division, Oak Ridge National Laboratory, who identified the crystalline components of many of the fused mixtures by microscopic examination; and to personnel of the Los Alamos Scientific Laboratory, including R. D. Baker, W. J. Maraman, Charles Metz and K. W. R. Johnson for helpful advice during the planning stage of the project and for furnishing high purity PuF_3.

(10) W. T. Ward, R. A. Strehlow, W. R. Grimes and G. M. Watson, "Solubility Relations Among Some Fission Product Fluorides in NaF–ZrF_4–UF_4 (50-46-4 mole %)," ORNL-2421, January 15, 1958.

(11) Determined by R. A. Strehlow, Oak Ridge National Laboratory.

THE ELECTRICAL CONDUCTIVITY OF CRYOLITE AND NaF–AlF_3 MELTS[1]

BY W. B. FRANK AND L. M. FOSTER

Alcoa Research Laboratories, Aluminum Company of America, New Kensington, Pennsylvania

Received September 3, 1959

The electrical conductivity of cryolite and NaF–AlF_3 melts is analyzed with the objective of determining the mechanism of conductance and obtaining correlation with information on constitution and transport processes. The constitution of the melts is described by the equilibrium between cryolite and its dissociation products, thus $Na_3AlF_6 \leftrightarrows 2NaF + NaAlF_4$. Conductance is attributed entirely to sodium and fluoride ions. Two conductance mechanisms are considered: (1) complete ionization of all species to sodium and the respective anions; (2) incomplete ionization of the sodium fluoride. Only Case 2—incomplete ionization of sodium fluoride—gives good agreement on all counts with other information. This result is interpreted from the standpoint of the "defect" liquid structure. The "un-ionized" sodium fluoride is considered to be Na^+F^- ion pairs that diffuse *via* paired cation–anion vacancies and thus do not contribute to conductivity. This is competitive with the process of cation and anion diffusion *via* single cation or anion vacancies, which is responsible for conductance. Sodium fluoride was found to be 68% "ionized" at 1000°. That is, for every 68 sodium or fluoride ions that diffuse *via* single ion vacancies, 32 diffuse *via* paired vacancies. With a sixfold coördination in the melt, it is thereby estimated that 6% of all sites are vacant. Equivalent conductances of 96.4 and 67.5 for sodium and fluoride are determined. Transference numbers of $t_{Na^+} = 0.91$ and $t_{F^-} = 0.09$ at the cryolite composition are obtained.

Introduction

Cryolite, Na_3AlF_6, comprises about 85–91% of a "neutral" electrolyte for the commercial production of aluminum. The balance in a typical case might be 7% calcium fluoride and 2–8% aluminum oxide. In practice, "alkaline" or "acid" electrolytes might be employed, which are rich in sodium fluoride or aluminum fluoride, respectively, over the stoichiometric cryolite composition. Other additions might be made for specific purposes.

The electrical conductivity of the molten electrolyte is only mildly altered by the usual additions, but is particularly sensitive to the weighed-in NaF–AlF_3 ratio, being greater for sodium fluoride-rich melts.

This paper attempts to correlate the electrical conductivity of cryolite, and NaF–AlF_3 melts in general, with information on the constitution and transport processes described elsewhere.[2,3]

The composition of molten sodium fluoride–aluminum fluoride systems is taken to be that determined by Frank and Foster[2] where cryolite, sodium fluoride and sodium tetrafluoroaluminate are present according to the dissociation scheme

$$Na_3AlF_6 \rightleftharpoons 2NaF + NaAlF_4 \qquad (1)$$
$$(K_{1000^\circ} = 0.09)$$

All of the calculations given here are for melts at 1000°, with compositions given in Fig. 1.

The electrical conductivity of sodium fluoride–aluminum fluoride melts was measured by Edwards, *et al.*,[4] Yim and Feinleib,[5] and Winterhager and Werner.[6] These data are shown in Fig. 2. Agreement between the three investigators is generally good, except at the pure sodium fluoride point, where Edwards' value is appreciably higher. Conductivities employed here are the averages shown by the solid line.

Two conductivity schemes are considered. In both cases, conductivity is attributed entirely to sodium and fluoride ions. (That this is approximately true had been indicated by the transport work and is reasonable in view of the relative ion sizes.) In the first case, the simplest mechanism is considered, where all molecular species are completely ionized to sodium and the respective anions. In this case, all of the sodium is free to conduct, whereas the greater part of the fluorine is tied up in the immobile fluoroaluminate ions.

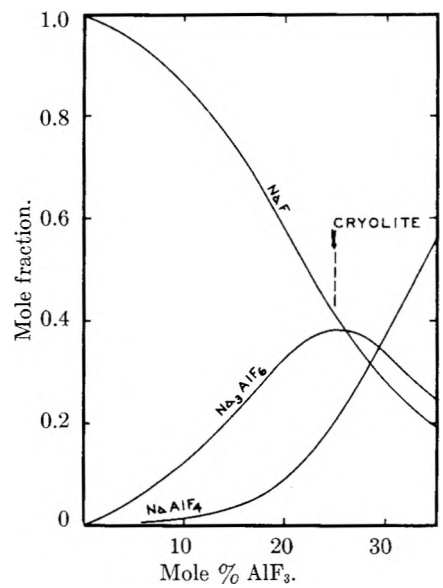

Fig. 1.—Equilibrium composition of NaF–AlF_3 melts at 1000°.

In the second case, sodium fluoride is considered to be only partially ionized. As will be pointed out further on, this case provides a means of mathematically treating the situation where part of the sodium fluoride is in some manner tied up and does not contribute to conductivity.

Case 1. Complete Ionization of Sodium Fluoride.—From the melt compositions from Fig. 1 and the density data of Edwards, *et al.*,[4] the composition on a milliliter volume basis is calculated for a range of compositions. This is expressed as equivalents of sodium and fluoride ion per milliliter. The equivalent conductances of sodium and fluoride ion are calculated by solving the relation (eq. 2) simultaneously for Λ_{Na^+} and Λ_{F^-} at two

(1) Presented at the Symposium on High Temperature Chemistry of the American Chemical Society, April 9, 1959, Boston, Massachusetts.

(2) W. B. Frank and L. M. Foster, *J. Phys. Chem.*, **64**, 95 (1960).

(3) W. B. Frank and L. M. Foster, THIS JOURNAL, **61**, 1531 (1957).

(4) J. D. Edwards, C. S. Taylor, L. A. Cosgrove and A. S. Russell, *J. Electrochem. Soc.*, **100**, 508 (1953).

(5) E. W. Yim and M. Feinleib, *ibid.*, **104**, 622 (1957).

(6) H. Winterhager and L. Werner, Forschungsber. Nr. 31 Wirtsch. u. Verkehrsmin. Nordrh.-Westf. (1956).

TABLE I

THE CONDUCTIVITIES OF SODIUM AND FLUORIDE ION WITH COMPLETE AND INCOMPLETE IONIZATION

Composition, NaF →		100	86.4	80.0	75.0	71.1		
Mole %, AlF_3 →		0	13.6	20.0	25.0	28.9		
Specific conductance, L		5.19	3.84	3.24	2.80	2.54	Mean	$\Lambda_{F^-}/\Lambda_{Na^+}$
				Case 1				
($\alpha_0 = 1.00$)	Λ_{F^-}	..[7]	21.2	23.4	23.2	21.5	22.3 ± 1.0	
	Λ_{Na^+}	..	90.1	91.6	88.1	89.9	89.9 ± 0.9	0.25
				Case 2				
$\alpha_0 = 0.80$	Λ_{F^-}	..	42.8	46.2	48.5	47.5	46.2 ± 1.8	
	Λ_{Na^+}	..	96.4	93.0	90.7	91.7	93.0 ± 1.8	0.50
$\alpha_0 = 0.75$	Λ_{F^-}	..	49.9	54.1	57.0	56.2	54.3 ± 2.3	
	Λ_{Na^+}	..	98.6	94.4	91.5	92.3	94.2 ± 2.3	0.58
$\alpha_0 = 0.68$	Λ_{F^-}	..	61.5	67.1	70.8	70.4	67.5 ± 3.1	
	Λ_{Na^+}	..	102.3	96.7	93.0	93.4	96.4 ± 3.2	0.70
$\alpha_0 = 0.65$	Λ_{F^-}	..	67.2	73.6	77.7	77.5	74.0 ± 3.6	
	Λ_{Na^+}	..	104.2	97.8	93.6	93.8	97.4 ± 3.6	0.76

different compositions where the specific conductance, L, is known, from Fig. 2

$$C_{Na^+}\Lambda_{Na^+} + C_{F^-}\Lambda_{F^-} = L \qquad (2)$$

where C_{Na^+} and C_{F^-} are the ion concentrations, in equivalents per milliliter. Table I (Case 1) gives these conductances calculated for a range of melt compositions by employing the data for pure sodium fluoride together with each other composition in the solutions of equation 2.

Case 2. Incomplete Ionization of Sodium Fluoride.—Let α_0 be the degree of ionization of the sodium fluoride. Then, the number of moles (or gram ions) resulting from one starting mole of NaF at equilibrium is

$$\begin{aligned} N_{Na^+} &= \alpha_0 \\ N_{F^-} &= \alpha_0 \\ N_{NaF} &= 1 - \alpha_0 \\ \text{Total moles} &= 1 + \alpha_0 \end{aligned} \qquad (3)$$

and the activities, taken as the mole or ion fractions, become

$$\begin{aligned} a_{Na^+} &= \frac{\alpha_0}{1 + \alpha_0} \\ a_{F^-} &= \frac{\alpha_0}{1 + \alpha_0} \\ a_{NaF} &= \frac{1 - \alpha_0}{1 + \alpha_0} \end{aligned} \qquad (4)$$

and

$$K = \frac{[a_{Na^+}][a_{F^-}]}{[a_{NaF}]} \frac{\alpha_0^2}{1 - \alpha_0^2} \qquad (5)$$

where K is the ionization constant of sodium fluoride.

In NaF–AlF_3 melts, sodium ion is contributed by the complete ionization of the fluoroaluminate species, in addition to the partial ionization of the sodium fluoride. Fluoride ion comes only from the sodium fluoride. Therefore, at any composition designated by the subscript n

$$\begin{aligned} \text{Moles } Na^{+[8]} &= 3a + b\alpha_n + c \\ \text{Moles } F^- &= b\alpha_n \\ \text{Moles NaF} &= b(1 - \alpha_n) \\ \text{Moles } AlF_4^- &= c \\ \text{Moles } AlF_6^{---} &= a \\ \text{Total moles} &= 4a + b(1 + \alpha_n) + 2c \end{aligned}$$

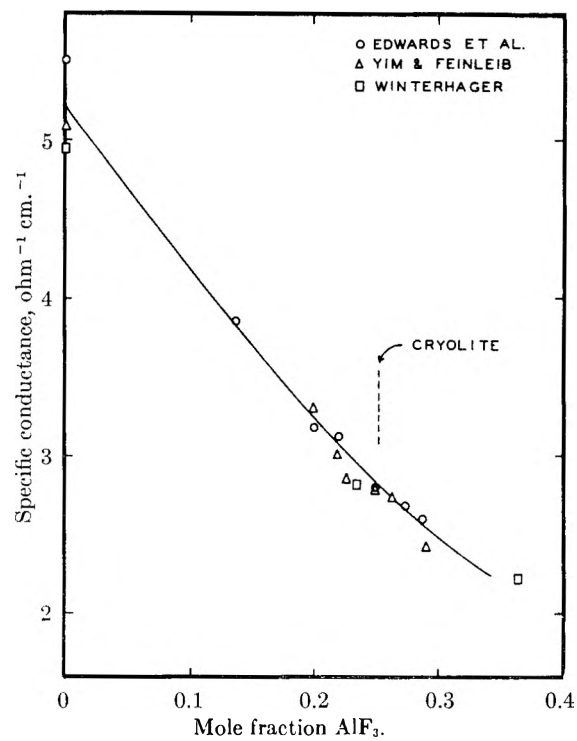

Fig. 2.—Electrical conductivity of NaF–AlF_3 melts at 1000°.

where a, b and c are the mole fractions of Na_3AlF_6, NaF and $NaAlF_4$ at composition n, disregarding ionization (from Fig. 1), and α_n is the degree of ionization of the sodium fluoride at that composition.

As before, activities are equated to mole fractions. Although the anions, AlF_4^- and AlF_6^{---}, do not influence the ionization of NaF, they must be included in determining the activities of the participating species, thus

$$a_{Na^+} = \frac{3a + b\alpha_n + c}{4a + b(1 + \alpha_n) + 2c} \qquad (6)$$

(7) Since the data for pure sodium fluoride were used in each case in the solution of the pairs of simultaneous equations for Λ_{F^-} and Λ_{Na^+}, there is no entry in this column. Other pairs of values could have been used just as well.

(8) Hereafter, for simplicity in writing, "moles" will be used interchangeably for moles of molecular species or gram ions of ionic species.

$$a_{F^-} = \frac{b\alpha_n}{4a + b(1 + \alpha_n) + 2c} \quad (7)$$

$$a_{NaF} = \frac{b(1 - \alpha_n)}{4a + b(1 + \alpha_n) + 2c} \quad (8)$$

From (5), after substitution of (6), (7) and (8) for activities and simplifying

$$K = \frac{(3a + b\alpha_n + c)\alpha_n}{[4a + b(1 + \alpha_n) + 2c](1 - \alpha_n)} \quad (9)$$

Since there is no *a priori* information at this point to suggest the magnitude of the degree of ionization of sodium fluoride, α_0 must be chosen arbitrarily. Using this arbitrary value, the corresponding K is calculated from (5). This is substituted into (9), which then is solved for α_n at each melt composition. This process is repeated for other arbitrary values of α_0, to give additional sets of α_n's.

The concentrations of the conducting species (Na^+ and F^-) can now be obtained in useful units from the values determined for α_n and the experimental melt densities of Edwards, *et al.*,[4] as

$$C_{n(Na^+)} = \frac{d_n(3a + b\alpha_n + c)}{210a + 42b + 126c} \quad (10)$$

$$C_{n(F^-)} = \frac{d_n b\alpha_n}{210a + 42b + 126c} \quad (11)$$

where $C_{n(Na^+)}$ and $C_{n(F^-)}$ are the concentrations in moles per milliliter of sodium and fluoride ion, and d_n is the melt density.

For pure sodium fluoride, the specific conductance L_0 is the sum of the separate conductances of Na^+ and F^-, thus

$$C_{0(Na^+)}\Lambda_{Na^+} + C_{0(F^-)}\Lambda_{F^-} = L_0 \quad (12)$$

and at any other melt composition n for which the specific conductance is known

$$C_{n(Na^+)}\Lambda_{Na^+} + C_{n(F^-)}\Lambda_{F^-} = L_n \quad (13)$$

Using the C_n's calculated from (10) and (11), Equations 12 and 13 are solved simultaneously over the range of compositions, n, for the equivalent conductances of sodium and fluoride, Λ_{Na^+} and Λ_{F^-}.

Table I (Case 2) gives the experimental specific conductances and the equivalent conductances calculated over a range of α_0's.

Discussion

It is not a purpose of this paper to defend the application of the mass action principle to molten salts. This has some historical basis. Moreover, the concept of individual ion activities that was used here is recognized as a mathematical device without physical significance, which, nevertheless, yields useful end results. The use of simple mole and ion fractions as activities may appear somewhat naive in view of the detailed treatments of Temkin,[9] Flood, Fykse and Urnes[10] and Flood, Forland and Grjotheim.[11] It is pointed out, however, that in mixtures of components with a common ion—sodium in the present case—Temkin's ion fraction product reduces to the simple mole fraction, as employed here.

It is imperative that the species be properly identified if activity coefficients are to be disregarded. The stable AlF_6^{---} ion might be described as an AlF_4^- ion "solvated" by two fluoride ions, and the extent of solvation might be related to concentration through an activity coefficient. This is a cumbersome procedure, however.

It is seen that the information obtained from the calculations is a description of molten sodium fluoride. The additions of aluminum fluoride serve only to adjust the activity of the sodium fluoride in a known manner, and the concentrations of the conducting species.

Several factors enter into the selection of the best model for molten sodium fluoride. The data are examined with the following criteria in mind: (1) The equivalent conductance of the sodium and fluoride ions should be reasonably constant regardless of the composition at which the calculation was made. (2) The diffusion coefficients, and hence the equivalent conductances of Na^+ and F^-, should be in the inverse ratio of their ionic radii, as stated by the Stokes–Einstein relation, $D = kt/6\pi\eta r$. (3) The transference number for the fluoride ion, t_{F^-}, at the cryolite composition must be low to give general agreement with the experimental transport measurements in cryolite–alumina melts.[3]

The simplest picture of sodium fluoride, with complete ionization and all sodium and fluorine conducting (Case 1), is not acceptable because of the very low equivalent conductance of the fluoride, and hence the low $\Lambda_{F^-}/\Lambda_{Na^+}$ ratio. Employing Pauling radii in the Stokes–Einstein relation should give a mobility ratio of fluorine to sodium of $\Lambda_{F^-}/\Lambda_{Na^+} \propto r_{Na^+}/r_{F^-} = 0.95/1.36 = 0.7$. Calculations for Case 1 give only 0.25 (see Table I). The calculations for this case are particularly straightforward, and the difference could not possibly come from the uncertainty in the gross composition of the melt.

Case 2, considering incomplete ionization of sodium fluoride, seems illogical on the surface. The high dielectric constant of the melts and the high temperature both should work toward complete ionization; however, very little information is available on this.

Actually, Case 2 only requires that there be some mechanism by which part of the sodium and fluoride ions are not available for conductance, and does not necessarily require that there be neutral molecules present. The work of Borucka, Bockris and Kitchener[12] suggests such a mechanism. They found that, for molten sodium chloride, approximate agreement could be obtained between the observed equivalent conductance and that calculated from diffusion data if, in the application of the Nernst–Einstein relation, part of the diffusion was attributed to "neutral" particles. These neutral particles were considered to be Na^+Cl^- ion pairs, moving into coupled

(9) M. Temkin, *Acta Physicochim. U.R.S.S.*, **20**, 411 (1945).

(10) H. Flood, O. Fykse and S. Urnes, *Z. Elektrochem.*, **59**, 364 (1955).

(11) H. Flood, T. Forland and K. Grjotheim, *Z. anorg. allgem. Chem.*, **276**, 289 (1954).

(12) A. Z. Borucka, J. O'M. Bockris and J. A. Kitchener, *Proc. Roy. Soc. (London)*, **241**, 554 (1957).

cation–anion vacancies. Seitz[13] and Dienes[14] calculated that the activation energy for this duffusion is less than that for individual ion diffusion *via* single vacancies—the process responsible for conductivity. This simultaneous diffusion of a cation and an anion gives a bulk diffusion that does not contribute to the electrical conductivity.

In the present case, since Na^+ and F^- must occupy the paired vacancies together, the filling of these vacancies will conform to mass action law that determines the amount of both ions present. In effect, therefore, a fraction of the sodium and fluoride ions diffuse in pairs independent of the mild electric field gradient and, in the calculations of Case 2, appear as un-ionized NaF molecules.

The paired vacancies might also be filled by Na^+–AlF_4^- ion pairs. This situation would remove a conducting species, Na^+, and a non-conducting species, AlF_4^-, and would not be properly described by the calculations. In this respect the calculations would be misleading. It is highly unlikely, however, that a large fluoroaluminate ion would occupy the vacancy in preference to a fluoride ion.

From Table I, Case 2, it is seen that the ratio of Λ_{F^-} to Λ_{Na^+} becomes about 0.7, to satisfy the Stokes–Einstein relation, when sodium fluoride is 68% ionized ($\Lambda_{F^-} = 67.5$, $\Lambda_{Na^+} = 96.4$). This implies that at any given time, for every 68 sodium or fluoride ions that diffuse by a single vacancy mechanism to provide the electrical conductivity, 32 ion pairs occupy paired ion vacancies and do not contribute to conductivity.

Following the reasoning of Borucka, *et al.*,[12] if each cation site has six adjoining anion sites, and *vice versa*, the probability that at least one anion vacancy will occur next to a given cation vacancy is $1 - x^6 = p$, where x is the fraction of sites occupied. With the derived probability of 0.32 in the present case, x becomes about 0.94; or 6% of all sites are vacant. These authors further estimate that such vacancies comprise perhaps half of the free volume of a melt.

Whereas these calculations on the structure of the melt are very approximate, it is seen that this interpretation of the situation in Case 2 is not inconsistent with the novel hole theory of the structure of fused salts.

Conclusions

The simplest, and heretofore generally accepted, view that alkali halides exist and conduct as simple, singly charged anions and cations is not acceptable without introduction of the "hole" theory of fused salts. Incorporation of this theory to account for the depressed conductance of sodium fluoride results in a model (Case 2) in which the mobilities of the conducting species are in the ratio required by the Stokes–Einstein relation. This model is in good agreement with that proposed by Borucka, Bockris and Kitchener[12] and Bockris and Richards,[15] considering the approximations involved in each case.

For the degree of ionization that satisfies the Stokes–Einstein relation, the transference number t_{F^-} of the fluoride ion at the cryolite composition is 0.09. Work in progress by the present authors shows that the addition of alumina to cryolite lowers the fluoride ion activity appreciably more than the sodium ion activity. This will lower t_{F^-} and give reasonable agreement with the transport results of Frank and Foster in cryolite–alumina melts.[3]

The diffusion of Na^+F^- ion pairs *via* paired ion vacancies is proposed here to explain the suppressed conductivity of sodium fluoride. The same end effect would be achieved, however, if sodium fluoride were partially dimerized in its melts, with ionization of the dimers to NaF_2^- and Na^+, or possibly to Na_2F^+ and F^-. The evidence for dimerization of alkali halides will be discussed in a future paper.

(13) F. Seitz, *Rev. Mod. Phys.*, **18**, 384 (1946).
(14) G. J. Dienes, *J. Chem. Phys.*, **16**, 620 (1948).
(15) J. O'M. Bockris and N. E. Richards, *Proc. Roy. Soc.* (*London*), **241**, 44 (1957).

แผนกห้องสมุด กรมวิทยาศาสตร์
กระทรวงอุตสาหกรรม

THE INFRARED SPECTRUM OF THE GASEOUS LITHIUM FLUORIDE (LiF) MOLECULE[1]

BY GUIDO L. VIDALE

General Electric Company, Aerosciences Laboratory, Philadelphia 24, Pa.

Received September 26, 1959

The infrared spectrum of the vapor over LiF in a carbon resistor furnace has been obtained. The rotational structure in the region of the fundamental vibration of the gaseous LiF monomer molecule has been resolved and the assignment of the rotational lines has been derived. Because of an unresolved uncertainty in the assigned value of the J quantum number, two sets of molecular parameters are equally probable, and a third set is perhaps possible. The last column gives the best value now available which was obtained by averaging the first two sets. If any of these parameters should be obtained by another method, a unique choice could be made between these sets, and the probable error could be reduced by approximately a factor of ten.

	Probable sets		Best value at this date and probable error			Probable sets		Best value at this date and probable error
ω_e, cm.$^{-1}$	904.85	907.64	906.2	$\pm$ 1.5	B_e, cm.$^{-1}$	1.3881	1.3676	1.378 $\pm$ 0.010
$\omega_e\chi_e$, cm.$^{-1}$	7.889	7.910	7.900	$\pm$ 0.010	r_e, Å.	1.5397	1.5512	1.545 $\pm$ 0.006
α_e, cm.$^{-1}$	0.019556	0.019856	0.01971	$\pm$ 0.00016				

Introduction

The only values of the molecular parameters of the gaseous LiF molecule which can be found in the literature have been obtained either from theoretical consideration alone[2] or indirectly from the results of a resonance beam experiment.[3] The values so obtained for B_e and ω_e are obviously of limited accuracy.

A study of the emission and absorption spectrum of the LiF molecule has been undertaken in the region of its fundamental vibration frequency. In order to resolve the rotational and vibrational fine structure of the fundamental band, relatively high resolution was required.

Experimental Method

The furnace used for generating the vapor was a carbon resistor furnace capable of maintaining 3000°, of the type first described by King[4] but partly modified as described by Zeeman.[5] The heating element consisted of a National Carbon AUC grade graphite tube, approximately 24″ long, having a wall diameter of 0.060″ to 0.100″ in the central 16″ which comprises the hot zone of the tube. The inner diameter of the tube is $1^3/_8$″. The only insulation used in the furnace consists of a series of nine concentric AUC graphite radiation shields. The optical arrangement used in this work is essentially that described by Klemperer.[6]

The spectrometer used was a standard Perkin–Elmer 12G grating monochromator, which utilizes a potassium bromide foreprism and a 75 lines/mm. grating. The instrument was calibrated in the spectral region of interest by observing, in the second order, the position of lines belonging to the water vapor 6 μ band, using the values of Dalby and Nielsen.[7] These values have been shown to be sufficiently accurate for this purpose.[8] Approximate temperature measurements were made with a Pyro Micro-optical Pyrometer.

A more complete description of the experimental equipment has been published elsewhere.[9]

Results

At the beginning of the experiment, a few grams of Baker Reagent Grade lithium fluoride was placed in a graphite boat in the center of the heater tube. The furnace then was evacuated, and the temperature raised to 800° while pumping. Pumping was stopped after approximately one hour, and Air Reduction welding grade argon was introduced into the furnace without purification until its pressure was approximately one atmosphere. The furnace temperature then was raised until the bands due to gaseous LiF became sufficiently intense. The optimum temperature was found to be 1450–1475°.

An extensive band was observed which contained resolvable structure and which extended from 730 to 973 cm.$^{-1}$. The maximum resolution in this region was obtained with a slit width of 0.12 mm., which corresponds to 0.5 at 900 cm.$^{-1}$. In practice, peaks approximately 0.6 cm.$^{-1}$ apart could be resolved.

This band was observed both in emission and in absorption. When relatively wide slits were used, the only visible features were a series of band heads, the most pronounced of which were observed at 973.19 and 956.1 cm.$^{-1}$.

Under higher resolution, many of the more intense individual lines became resolved, as seen in Figs. 1, and 2 and 3. Their frequencies were measured on a minimum of three different spectra. It was found that most of these lines belonged to a regular progression of the type expected for the rotational structure of a band due to a linear molecule in the $^1\Sigma$ state. Individual line frequencies are listed in Table I; most of these lines were obtained in both emission and absorption.

The frequency of this band system and the spacing of the individual lines pointed to the LiF monomer as the most likely emitter of the band.

The temperature dependence of these bands, and their absence when no lithium fluoride was present in the furnace, provided further confirma-

(1) This work was performed under Contract No. AF 04(647)-269 with the U. S. Air Force Ballistic Missiles Division.

(2) (a) A. Honig, M. Mandel, M. L. Stitch and C. H. Towns, *Phys. Rev.*, **96**, 629 (1954); (b) E. S. Rittner, *J. Chem. Phys.*, **19**, 1030 (1951).

(3) R. Braunstein and J. W. Trischka, *Phys. Rev.*, **98**, 1092 (1955).

(4) A. S. King, *Trans. Am. Electrochem. Soc.*, **56**, 97 (1929).

(5) P. B. Zeeman, *Can. J. Phys.*, **32**, 9 (1954).

(6) W. Klemperer, *J. Chem. Phys.*, **24**, 353 (1956).

(7) F. W. Dalby and H. H. Nielsen, *ibid.*, **25**, 934 (1956).

(8) K. N. Rao, L. R. Ryan and H. H. Nielsen, *J. Opt. Soc. Amer.*, **49**, 216 (1959).

(9) G. Vidale, "The Infrared Spectrum of the Gaseous LiF Molecule," General Electric Company, Missile and Space Vehicle Department, TIS Report R59SD359.

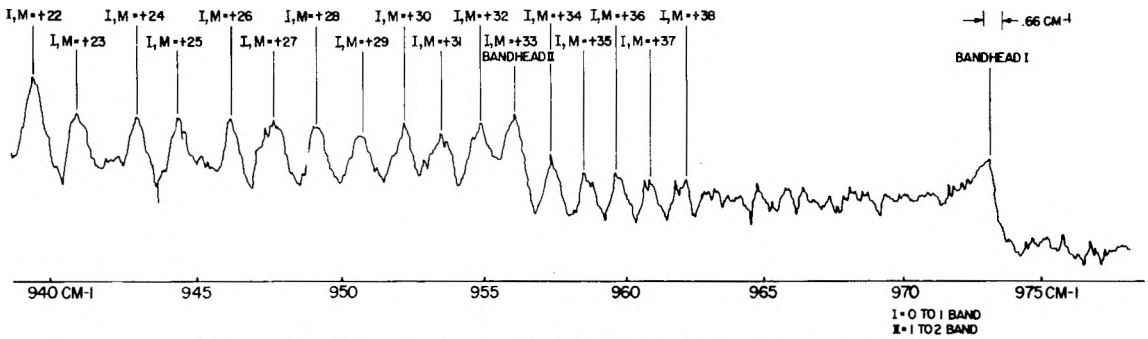

Fig. 1.—Absorption spectrum of LiF, including the 0–1 and 1–2 band heads.

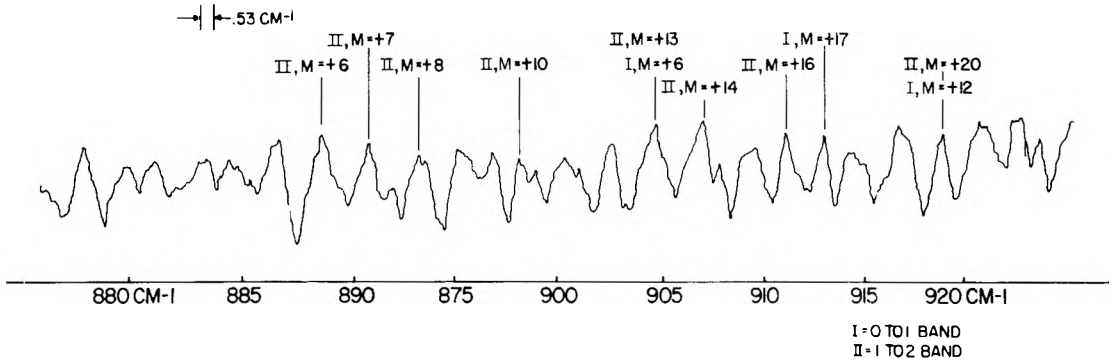

Fig. 2.—Absorption spectrum of LiF in the region of the band origin.

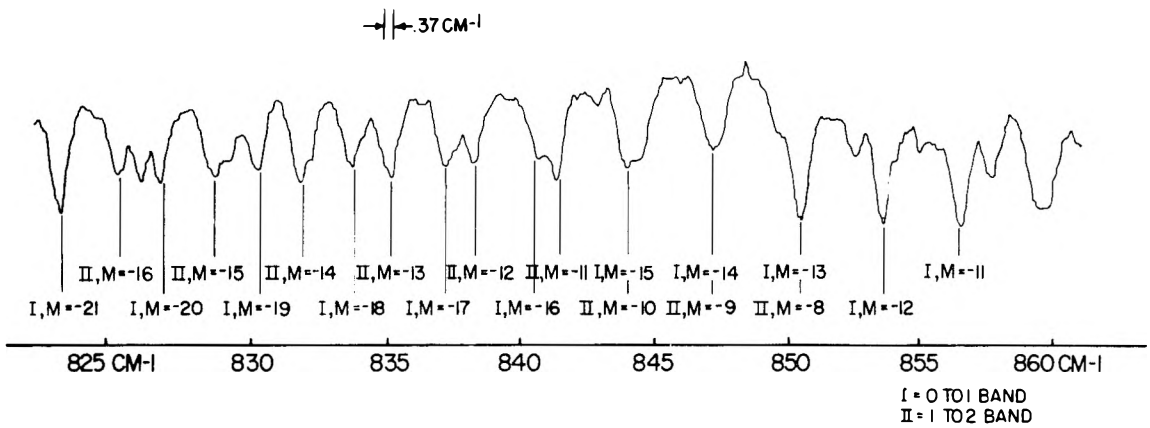

Fig. 3.—Emission spectrum of LiF: P branch.

tion for their assignment. The same bands were also observed recently with lower resolution by Klemperer,[10] who generated them in a wire-wound, ceramic core furnace. He also attributed them to the LiF molecule.

An attempt also was made to observe the first overtone bands and bands due to Li^6F^{19}. None were observed under the conditions of this study.

Theoretical

An expression for the rotational levels of a diatomic molecule, as found in standard texts,[11] is

$$E_{vJ}/hc = \omega_e(v + 1/2) - \omega_e\chi_e(v + 1/2)^2 + B_vJ(J + 1) - D_vJ^2(J + 1)^2 + H_vJ^3(J + 1)^3 \quad (1)$$

This expression neglects the third and higher order terms of $(v + 1/2)^n$ and the fourth and higher order terms of $J^m\,(J + 1)^m$.

(10) W. Klemperer, private communication.

(11) G. Herzberg, "Spectra of Diatomic Molecules," D. Van Nostrand Co., New York, N. Y., 1950.

While the values of ω_e and $\omega_e\chi_e$ are independent of J, B_v, D_v and H_v are functions of v. This dependence is approximated by the equations[11]

$$B_v = B_e - \alpha_e(v + 1/2) \quad (2)$$

$$D_v = D_e + \beta_e(v + 1/2) \quad (3)$$

$$H_v = H_e \quad (4)$$

where now B_e, D_e, α_e, β_e and H_e are constants. On substituting equations 2, 3 and 4 into equation 1, one obtains

$$E_{vJ}/hc = \omega_e(v + 1/2) - \omega_e\chi_e(v + 1/2)^2 + [B_e - \alpha_e(v + 1/2)]\,J(J + 1) - [D_e + \beta_e(v + 1/2)]J^2(J + 1)^2 + H_eJ^3(J + 1)^3 \quad (5)$$

A particular line, observed in the region of the fundamental, represents a transition between an upper level (primed) and a lower level (doubly primed) which obeys the selection rules

$$v' = v'' + 1$$

$$J' = J'' \pm 1 \quad (6)$$

In the case $J' = J'' + 1$, the frequency of the line in question is given by

$$\nu\,(\text{cm.}^{-1}) = \omega_e - 2\omega_e\chi_e v' + 2(B_e - \alpha_e v')J' - (\alpha_e + \beta_e)J'^2 - 4(D_e + \beta_e v' - H_e/2)J'^3 - \beta_e J'^4 + 6H_e J'^5 \quad (7)$$

where J' can take on any positive integral value greater than 0. When an equivalent expression is obtained for the case $J' = J'' - 1$, the general equation is obtained

$$\nu(\text{cm.}^{-1}) = \omega_e - 2\omega_e\chi_e v' + 2(B_e - \alpha_e v')M - (\alpha_e + \beta_e)M^2 - 4(D_e + \beta_e v' - H_e/2)M^3 - \beta_e M^4 + 6H_e M^5 \quad (8)$$

where $M = J'$ for $J' = J'' + 1$ and $M = -J''$ for $J' = J'' - 1$, and M may now take on any positive or negative integral value, but may not be zero.

Treatment of Data

The complex appearance of the band envelope, and the prominence of several band heads, indicated that the intensity of "hot bands" is rather high. This is also predicted from the simple harmonic oscillator theory expression[11,12]

$$I_{v'} \sim v' e^{-v' h\omega_e c/kT} \quad (9)$$

On substituting $\omega_e = 900$ cm.$^{-1}$ and $T = 1748$°K., it is found that the 0–1 band accounts for only 28% of the total energy, and that the 1–2 band is only 5% weaker than the 0–1.

Furthermore, the energy of a single vibrational band is distributed over many individual rotational lines.

The formula giving the intensity of rotational lines for a rigid rotor is[11]

$$I_J \sim (J' + J'' + 1)e^{-B_e hcJ''(J''+1)/kT} \quad (10)$$

If B_e is given a value of 1.37, and $T = 1748$°K., the most intense line should be found at approximately $J = 20$, and the intensity has fallen to 50% at $J = 40$ and to 7.6% at $J = 60$. The frequency dependence of the intensity has been ignored in all cases.

It is not surprising that most of the observed lines are broad, since the resolution achieved was not sufficient to separate the individual components of lines belonging to the higher "hot bands." Hence, the frequency measurements given in Table I in many cases must correspond to frequencies where several weaker lines happen to bunch.

It was necessary to select the strongest and sharpest lines which seem to form a regular sequence, and to fit only these lines to one or more suitable expressions having the form

$$\nu = a + bM + cM^2 + dM^3 + eM^4 + fM^5 \quad (11)$$

where M may take on only integral values.

The first sequence found was reconstructed upon realizing that the resolved lines close to the highest frequency band head could only be assigned to the 0–1 vibrational band. These lines are those listed as Set I in Table II, which have an M value between 28 and 38, and are shown in Fig. 1. Other lines belonging to this sequence were sought in the region where the 0–1 band is expected to be considerably more intense than other bands, that is, at M values between −11 and −21. These lines were found and are shown in Fig. 3. A numbering sequence was worked out after finding several other lines of this Set I at M values between 18 and 28. Altogether, 40 lines were found which could be assigned without ambiguity to the 0–1 band.

(12) L. Pauling and E. B. Wilson, "Introduction to Quantum Mechanics," McGraw-Hill Book Co., New York, N. Y., 1935.

TABLE I

973.19	band head	925.72	888.89	849.42	812.04	771.55
964.12		923.77	886.70	847.06	810.57	769.47
963.06		922.82	884.67	844.37	808.54	767.67
962.06		921.23	883.44	843.87	807.39	766.10
960.98		918.88	881.06	842.72	805.49	765.15
959.97		917.04	879.76	841.33	804.04	763.59
958.77		915.92	877.84	840.65	803.02	762.54
957.52		915.06	875.12	838.18	801.86	761.28
956.13	band head	914.38	873.09	837.21	800.77	759.51
954.95		913.06	871.93	835.18	800.05	758.73
953.56		912.09	871.22	833.81	799.21	757.47
952.15		911.24	870.44	832.09	798.19	755.72
950.75		909.69	869.01	830.32	797.33	755.01
949.14		908.05	867.84	829.26	796.08	753.65
947.65		907.01	866.01	828.73	794.55	752.31
946.13		904.76	864.69	826.92	792.87	751.39
944.34		902.71	862.99	826.23	790.89	749.66
942.83		900.74	862.23	825.44	789.70	748.68
940.93		900.11	861.07	823.38	787.22	747.48
939.36		898.92	859.71	822.14	785.05	745.65
937.22		898.31	857.77	820.02	783.64	744.98
935.51		897.05	856.50	818.89	781.84	743.55
933.71		895.42	855.10	816.94	780.09	742.13
932.44		893.58	853.53	815.42	776.63	739.85
931.65		892.16	852.46	814.45	775.49	739.10
929.56		891.11	851.19	813.74	774.13	737.82
927.68		890.55	850.43	812.82	772.98	735.93
						735.12

A tentative M value then was chosen on the basis of the relative intensity of the lines associated with Set I, and of the expected theoretical intensity. The M values listed in Table II are these approximate values, which could be in error by as much as ±2. This uncertainty is present because, as seen in Fig. 2, the high intensity of the "hot bands" around the 0–0 gap made the estimation of the intensity of the Set I lines difficult in this region.

A second set of lines, recorded as Set II in Table II, was obtained by looking for an almost identical set shifted toward lower frequencies by about 17 cm.$^{-1}$, which is the difference between the first two observed band heads. These lines, which must be associated with the 1–2 band, were found most clearly resolved in the part of the spectrum shown in Fig. 3. Only 23 lines were found which are definitely associated with this set. In the case of Set II, the choice of an M value consistent with those assigned to Set I was easy, since it became apparent that a unique set of values was necessary in order to avoid grotesque values of the various coupling constants.

Thus, while these tentative assignments of M for Set I and Set II may be in error, both must be in error by the same amount.

TABLE II

M	Set I (0–1), cm.$^{-1}$	M	Set II (1–2), cm.$^{-1}$
38	962.06	20	918.88
37	960.98	17	913.06
36	959.97	16	911.24
34	957.52	14	907.01
32	954.95	13	904.76
30	952.15	7	891.11
28	949.14	6	888.89
26	946.13	− 8	850.43
25	944.34	−12	838.18
24	942.83	−13	835.18
23	940.93	−15	828.73
22	939.36	−16	825.44
20	935.51	−17	822.14
19	933.71	−18	818.89
17	929.56	−19	815.42
16	927.68	−24	798.19
12	918.88	−27	787.22
6	904.76	−29	780.09
− 6	871.93	−33	765.15
− 7	869.01	−34	761.28
− 8	866.01	−35	757.47
− 9	862.99		
−11	856.50		
−12	853.53		
−13	850.43		
−15	843.87		
−17	837.21		
−18	833.81		
−19	830.32		
−21	823.38		
−24	812.82		
−28	798.19		
−31	787.22		
−34	775.49		
−35	771.55		
−36	767.67		
−37	763.59		
−39	755.72		
−40	751.39		
−41	747.48		

The various parameters which appear in equation 8 were computed with the aid of a Royal McBee digital computer in the following way.

It was decided to evaluate the four parameters ω_e, $\omega_e\chi_e$, α_e and B_e directly from the experimental data, while D_e, β_e and H_e could be obtained more accurately from the three equations[11]

$$D_e = \frac{4B_e^3}{\omega_e^2} \tag{12}$$

$$\beta_e = D_e\left(\frac{8\omega_e\chi_e}{\omega_e} - \frac{5\alpha_e}{B_e} - \frac{\alpha_e^2\omega_e}{24B_e^3}\right) \tag{13}$$

$$H_e = \frac{2D_e}{3\omega_e^2}(12B_e^2 - \alpha_e\omega_e) \tag{14}$$

Approximate values of ω_e, $\omega_e\chi_e$, α_e and B_e were chosen, and β_e, D_e and H_e were calculated from equations 12, 13 and 14.

After setting $v' = 1$, these values of β_e, D_e and H_e were substituted into equation 8, and $(\omega_e - 2\omega_e\chi_e)$, B_e and α_e were evaluated by least squaring with respect to the data for the 0–1 transition, given in Set I. Thus, a better value was obtained for $(\omega_e - 2\omega_e\chi_e)$, B_e and α_e.

The same approximate values of D_e, β_e and H_e and the newly obtained value of α_e were then substituted into equation 8, and, after setting $v' = 2$, $(\omega_e - 4\omega_e\chi_e)$ and a new value of B_e were calculated by least squaring the first two coefficients to 1–2 band data given by Set II.

The magnitude of ω_e and $\omega_e\chi_e$ then were determined by comparing the values of $(\omega_e - 2\omega_e\chi_e)$ from Set I and of $(\omega_e - 4\omega_e\chi_e)$ from Set II. The B_e calculated from the data given in Set II, which is listed in Table III as $B_e^{(2)}$ was not used further except to compare with B_e obtained from Set I (listed in Table III as $B_e^{(1)}$).

New values of β_e, D_e and H_e then were calculated from equations 12, 13 and 14 using these new ω_e, $\omega_e\chi_e$, $B_e^{(1)}$ and α_e, and the calculation was iterated as many times as necessary to establish the value of all parameters to the desired degree of accuracy. The results of the successive iterations are listed in Table III, in the section labeled $M = M$ orig.

Finally, the calculation was repeated for the other likely assignments of J values in exactly the same fashion. These results also are given in Table III.

Discussion

No unambiguous choice of the correct assignment of the J value can be made on the basis of the data given in Table III. The root mean square deviation of the experimental points from the fitted expression differs only very slightly in the four sets, and is, in all cases, of the order of magnitude expected from the accuracy of measurements and the method of calculation.

The agreement between the two calculated values of B_e is only fair, although a distinct improvement is noticed as the assigned J value is lowered. The discrepancy between the two B_e values can be attributed perhaps in part to the neglect of higher order terms in the expansion of B_v as a function of v, and in part to the lower accuracy of values obtained from Set II. This lower accuracy is the result of the absence of any regions where only peaks due to this band are present. Notice that a change in B_e of 0.004 cm.$^{-1}$ leads to a maximum shift in the frequency of the Set II values of less than 0.15 cm.$^{-1}$.

This is the reason that it was decided to make use of the value of B_e obtained from Set I, so that the frequency of lines associated with Set II was used only to determine the value of ω_e and $\omega_e\chi_e$.

A better indication of the correct J value assignment is obtained by calculating the position of the band head from the parameters given in Table III for each of the considered choices of J value assignment, and then comparing these values to the experimentally obtained frequency at the band head. These values are given in Table IV. Notice that the neglect of higher order terms in the expansion for B_v and possible inaccuracy associated with results obtained from Set II do not affect sensibly the predicted position of the band head.

The agreement between values of the band head

TABLE III[a]

M value	Iteration	σ Set I	σ Set II	ω_e	$\omega_e x_e$	$B_e^{(1)}$	$B_e^{(2)}$	α_e	$D \times 10^5$	$\beta_e \times 10^7$	$H_e \times 10^{11}$	$\frac{B_e^{(1)} - B_e^{(2)}}{B_e^{(1)}}$
M orig	1			905.06	7.911	1.3870		0.01969	1.303	− 0.8498		
	2			904.85	7.889	1.3880	1.3843	.019557	1.307	− .7950		
	3	0.09	0.08	904.85	7.889	1.3881	1.3843	.019556	1.307	− .7951	5.77	0.00274
M orig + 1	1			904.81	7.875	1.387		.01953	1.304	+17.55		
	2			901.48	7.863	1.4053		.01673	1.366	+ 0.8834		
	3			902.04	7.871	1.4088		.01928	1.375	− .4976		
	4			902.08	7.872	1.4091	1.4044	.019492	1.375	− .6135	7.03	
	5			902.09	7.872	1.4091	1.4044	.019509	1.375	− .6233		
	6	.11	.07	902.09	7.872	1.4091	1.4044	.019511	1.375	− .6241	7.02	.00334
M orig − 1	1			904.81	7.875	1.387		.01953	1.304	− .804		
	2			907.65	7.915	1.3689		.01984	1.245	− 1.060		
	3			907.64	7.910	1.3677		.019854	1.242	− 1.079	4.45	
	4			907.64	7.910	1.3676	1.3642	.019856	1.242	− 1.081		
	5	.09	.09	907.64	7.910	1.3676	1.3642	.019856	1.242	− 1.080	4.41	.00249
M orig − 2	1			910.44	7.930	1.3470		.02010	1.179	− 1.321		
	2			910.35	7.924	1.3469	1.3439	.02001	1.179	− 1.277		
	3	.09	.09	910.34	7.929	1.3468	1.3439	.02000	1.179	− 1.273	3.38	.00215

[a] $\sigma_{\text{Set I}}$ = root mean square deviations of Set I from final curve; $\sigma_{\text{Set II}}$ = root mean square deviations of Set II from final curve; $B_e^{(1)}$ = value of B_e obtained by least squaring Set I; $B_e^{(2)}$ = value of B_e obtained by least squaring Set II.

position is most gratifying, because the original estimate of the M value was made before any calculations were carried out on the predicted position of the band head.

TABLE IV

	Band head, cm.$^{-1}$ Calcd.	Exper.	Difference
$M = M$ orig + 1	972.22	973.19	−0.97
$M = M$ orig	973.02	973.19	− .17
$M = M$ orig − 1	973.12	973.19	− .07
$M = M$ orig − 2	973.58	973.19	+ .39

TABLE V

MOLECULAR PARAMETERS OF Li^7F^{19}

	This study		BT[3]		R[2]	HMST[1]
ω_e, cm.$^{-1}$	906.2	± 1.5	646	± 32		
$\omega_e x_e$, cm.$^{-1}$	7.900	± 0.010				
α_e, cm.$^{-1}$	0.01971	± .00016				
B_e, cm.$^{-1}$	1.378	± .010				
r_e, Å.	1.545	± .006	1.51 ± 0.08 1.57 ± 0.08		1.53	1.527

Conclusions

On the basis of the results given in Table IV, $M = M$ orig + 1 can be ruled out, and $M = M$ orig − 2 is possible, but much less likely than the other two M assignments. Thus, it is concluded that one of the two sets of parameters associated with $M = M$ orig and $M = M$ orig − 1 are most probably the correct set. A choice between these will have to be made through an accurate independent determination of any one of the parameters considered here.

In the meantime, however, the value of the average of the two probable sets is considerably more accurate than other available values. These recommended results are listed in Table V, together with literature values.

Acknowledgments.—The author wishes to acknowledge the able help of Mr. Roy Freides, who carried out most of the experimental work mentioned here, and of Mr. Sheldon Blecher, who programmed and carried out the computations.

The valuable advice and criticism of Prof. R. S. Mulliken, Prof. R. W. Klemperer and several members of the Aerophysics Operation staff also contributed to the success of this study.

THE REACTIONS OF ACTIVE NITROGEN WITH NITRIC OXIDE AND NITROGEN DIOXIDE[1]

BY G. J. VERBEKE[2] AND C. A. WINKLER

Upper Atmosphere Chemistry Research Group, Physical Chemistry Laboratory, McGill University, Montreal, Canada

Received February 16, 1959

Both reactions have been studied over a range of reactant flow rates. N_2O has been found as a product of the NO_2, but not of the NO, reaction. The NO_2 reaction also yielded NO. The chemical activity in the active nitrogen, inferred from the amount of NO destroyed, has been found to be approximately 1.5 times that indicated by the maximum yield of HCN in the active nitrogen–ethylene reaction, for a wide range of flow rates of active nitrogen. Moreover, the ratio of the activities measured in these two ways increased with total pressure. These observations might imply that NO reacts with more than one reactive species in active nitrogen and that measurement of the nitrogen *atom* concentration by the extent of the NO reaction might be subject to considerable error.

In previous studies in this Laboratory, it has been assumed frequently that active nitrogen concentrations could be taken to correspond to the essentially constant limiting yield of hydrogen cyanide produced in the reactions of active nitrogen with various hydrocarbons at elevated temperatures.[3,4] On the other hand, the concentration of active nitrogen so estimated was much higher than that indicated by the amount of ammonia destroyed under comparable conditions, and it was suggested that ammonia reacted with one, and ethylene reacted with a second reactive species in the active nitrogen.

Since earlier work by other investigators[5-7] had indicated that the extent of the active nitrogen–NO reaction might be used as a measure of the active nitrogen concentration, it was decided to re-investigate the reactions of active nitrogen with NO and NO_2, in the hope of obtaining more definitive information about the composition of active nitrogen.

The reactions of active nitrogen with oxides of nitrogen have been the subject of a number of recent investigations.[8-11] The reactions of nitrogen dioxide are necessarily complex and will be discussed further when the results of the present study have been presented. It was, however, generally concluded that nitric oxide reacts completely with atomic nitrogen by the fast reaction

$$N + NO \rightarrow N_2 + O$$

the extent of which could be used to measure the concentration of nitrogen atoms. This "titration" actually has been used to study the kinetics of recombination of nitrogen atoms.[12-14]

Experimental

Nitrogen was removed from commercial NO (Matheson Co.) by evacuation while the NO was kept at liquid nitrogen temperature, and then by repeated distillation (three times) from a frozen pentane bath (−130°). Infrared analysis showed the product to contain no traces of higher oxides and less than 0.3% of N_2O.

NO_2 was prepared by treating purified NO with excess oxygen. When the deep blue color of N_2O_3 was no longer visible in the condensed material, excess oxygen was pumped off. The NO_2 was kept frozen when not in use to prevent photochemical decomposition. When traces of N_2O_3 were found to be present, the oxidation procedure was repeated. Halocarbon stopcock grease was used in all parts of the system in contact with NO_2.

Ethylene, ammonia and nitrogen were of the grades, and were purified by the methods, described in previous papers.

Active nitrogen was formed in a condensed discharge through nitrogen in an apparatus that was essentially similar to that used in earlier investigations of active nitrogen reactions in this Laboratory (*e.g.*, ref. 1). For some experiments the spherical, 300-cc. reaction vessel generally used was replaced by a tube 140 cm. long, 18 mm. i.d., into the side of which were sealed 6 reactant inlet jets at intervals down the length of the tube. Furnaces were provided so that the spherical or tubular reaction vessels could be heated as desired, and the discharge tube and reaction vessels were poisoned with metaphosphoric acid to minimize wall deactivation of the active nitrogen.

The products of the ethylene reaction, and residual ammonia from the ammonia reaction, were trapped in liquid nitrogen, while liquid nitrogen under reduced pressure (−210°) was found necessary to trap quantitatively the NO from the nitrogen oxide reactions. A small coil of silver wire was placed ahead of the trap to remove oxygen atoms and prevent formation of small amounts of ozone that tended to cause explosions if trapped.

To obtain maximum precision in the experiments, the power supply to the discharge tube was voltage-controlled, and the flash-rate in the discharge tube was controlled at either 12 or 20 flashes per second, as indicated by an oscilloscope or by a 929 phototube recording on a Brush oscillograph.

The extent of decomposition of NO was obtained by analysis of residual reactant. No attempt was made to distinguish NO from NO_2 in the products, since excess NO was partially oxidized to NO_2 by reactions with atomic and molecular oxygen. An excess of oxygen was added to the trapped products of reaction, after which the mixture was allowed to warm to room temperature to ensure complete oxidation of unreacted NO. The NO_2 was then frozen out, excess oxygen pumped off, and the amount of NO_2 finally measured by pressure measurements in a known volume at constant temperature.[15] It might be noted perhaps that generally accepted methods of analysis based on oxidation of NO_2 to nitric acid were not found to yield satisfactorily reproducible results.

(1) With financial assistance from Imperial Oil Ltd., Sarnia, and the National Research Council, Ottawa.

(2) Holder of a National Research Council bursary, 1954–1955, studentship, 1955–1956, and a Province of Quebec Scholarship, 1956–1957.

(3) (a) P. Gartaganis and C. A. Winkler, *Can. J. Chem.*, **34**, 1457 (1956); (b) B. Dunford, H. G. V. Evans and C. A. Winkler, *ibid.*, **34**, 1074 (1956); (c) D. Wiles and C. A. Winkler, *ibid.*, **35**, 1298 (1957).

(4) N. V. Klassen, M. Onyszchuk, J. McCabe and C. A. Winkler, *ibid.*, **36**, 1217 (1958).

(5) R. J. Strutt, *Proc. Roy. Soc. (London)*, **A86**, 56 (1912).

(6) E. J. B. Willey and E. K. Rideal, *J. Chem. Soc.*, 1804 (1926).

(7) M. L. Spealman and W. H. Rodebush, *J. Am. Chem. Soc.*, **57**, 1474 (1935).

(8) P. Harteck and S. Dondes, *J. Chem. Phys.* **22**, 953 (1954).

(9) P. Harteck and S. Dondes, *ibid.*, **24**, 619 (1956).

(10) P. Harteck and S. Dondes, *ibid.*, **27**, 546 (1957).

(11) G. B. Kistiakowsky and G. G. Volpi, *ibid.*, **27**, 1149 (1957).

(12) J. T. Herron, J. L. Franklin, P. Bradt and V. H. Dibeler, *ibid.*, **29**, 230 (1958).

(13) J. T. Herron, J. L. Franklin, P. Bradt and V. H. Dibeler, *ibid.*, **30**, 879 (1959).

(14) P. Harteck, R. R. Reeves and G. Manella, *ibid.*, **29**, 608 (1958).

(15) F. H. Verhoek and F. Daniels, *J. Am. Chem. Soc.*, **53**, 1250 (1931).

The products of the NO_2 reaction were analyzed by adding a known pressure p_1 of oxygen to oxidize all the NO, and the total pressure p_2, was measured. Unreacted oxygen was then pumped off while the other gases were frozen with liquid nitrogen, after which they were allowed to warm to room temperature and their pressure, p_3, determined. The partial pressure of NO then was given by

$$p_{NO} = 2(p_1 + p_3 - p_2)$$

Finally, the gases were surrounded with a Dry Ice–acetone bath and N_2O pumped off to permit the pressure p_4 of residual NO_2 to be obtained when it was again restored to room temperature. The partial pressure of N_2O was given, of course, by $p_3 - p_4$, while p_4 gave the sum of NO and unreacted NO_2.

Hydrogen cyanide and cyanogen in the ethylene reaction were analyzed by titration methods, as in previous investigations, and ammonia was estimated by absorption in standard acid, followed by back titration with standard alkali. Experiments with known amounts of the various gases showed that the analytical methods gave results within ±2%.

Results

Nitric Oxide Reaction. Products of Reaction and Reaction Flame.—The amount of NO destroyed increased linearly with flow rate until it reached a rather critical value. This behavior is characteristic of a rapid reaction in which the reactant present in smaller amount is completely consumed. The plateau of NO destruction at higher flow rates was found to be essentially independent of temperature up to 400°, the maximum temperature studied.

No N_2O was produced at any flow rate in the range studied. Ozone was the only product condensed at flow rates below the critical value, where a blue reaction flame (β- and γ-bands of NO) was observed.[16] On the other hand, both NO and NO_2, but no ozone, were found at flow rates above the critical, under which conditions the blue glow contracted to a layer of few millimeters thick just below the reactant inlet and was largely (*though not completely*) replaced by a yellowish-green glow (NO_2 continuum).

Effect of Active Nitrogen Concentration.—The amount of NO destroyed by active nitrogen was compared with the amount of HCN produced in the reaction of active nitrogen with ethylene when the concentration of active nitrogen was changed by alteration of the capacitance in the electrical circuit over a 16-fold range. Experiments were made with excess of NO or C_2H_4 and with the reaction vessel heated to 300 and to 400°, over which interval it was found that the extent of reaction with both reactants was independent of temperature. Analysis of products showed that cyanogen production from ethylene did not exceed 1% of the hydrogen cyanide production and was therefore neglected in drawing the comparison. The results for a range of capacitance values are shown in Fig. 1A. The ordinates represent maximal values for NO destroyed or HCN produced, read from plots of NO destroyed or HCN produced against the corresponding reactant flow rates. Within the error of the experiments, the ratio of NO destroyed to HCN produced appeared to be constant, as indicated by the data

Capacitance (μfd.):	0.25	0.50	1.0	2.0	4.0
Ratio $\frac{\text{NO destroyed:}}{\text{HCN produced}}$	1.52	1.71	1.49	1.41	1.51

(16) F. Kaufman and J. Kelso, *J. Chem. Phys.*, **27**, 1209 (1957).

Comparison of the Reaction of Active Nitrogen with NO, NH_3 and C_2H_4.—Figure 1B shows the amounts of NO and NH_3 destroyed, and of HCN formed from C_2H_4, when excesses of these different reactants were introduced into the tubular reaction vessel at different positions. The molecular nitrogen flow was 170 micromoles/sec., at a pressure of 1.90 mm., with a discharge rate of 20 flashes per second. No difference was observed in the amount of NO destroyed at the top reactant inlet over the temperature range 100 to 300°. The reaction tube was not heated during any of the experiments with NH_3, but was heated to 300° or higher for all the experiments with C_2H_4. The ratio of NO destroyed to HCN formed from ethylene appeared to increase slightly, though the increase was of the same order as the experimental error, as decay of active nitrogen progressed down the tube.

Distance below first inlet (cm.):	0	20	40	60	80	120
Ratio $\frac{\text{NO destroyed:}}{\text{HCN produced}}$	1.35	1.39	1.36	1.37	1.40	1.50

An increase was observed in the ratio of NO destroyed to HCN produced, when the total pressure was increased,[17] as shown by

N_2 pressure (mm.):	1	2	4	8	16
Ratio $\frac{\text{NO destroyed:}}{\text{HCN produced}}$	1.4	1.6	1.9	2.3	2.4

Nitrogen Dioxide Reaction.—In Fig. 2 (A, B and C) are shown the results of experiments with NO_2 at the top reactant inlet, in an unheated reaction tube and with the tube heated to 300°. The blue glow indicative of oxygen atoms again was observed, and increased in intensity as the flow rate of NO_2 was increased up to a critical flow rate where a sharp transition to the yellow-green glow occurred. Nitrous oxide was the only condensable product at flow rates where only the blue glow could be seen. The green glow was gradually reduced in extent and finally disappeared, as the flow rate of NO_2 was further increased. The ratio of NO_2 flow at which the green flow disappeared to the flow at which it first appeared was found to be 1.8 ± 0.1 for three different values of energy input to the discharge tube. For flow rates of NO_2 in excess of that where the green glow appeared, both NO and NO_2, as well as N_2O, were recovered in the products.

Rate Constants for the Nitric Oxide and Nitrogen Dioxide Reactions.—Rate constants for the reactions of NO and NO_2 with active nitrogen were determined by a gas "titration" for active nitrogen analogous to that proposed for oxygen atoms by Kaufman.[18] The analysis was based on the observation, established experimentally, that the green glow appeared simultaneously with the first analytically detectable excess of either reactant in the effluent gases from the reaction vessel. Apparently the process responsible for the green

(17) A microwave generator was used to produce the active nitrogen, owing to difficulties in maintaining a condensed discharge at the higher pressures.

(18) F. A. Kaufman, *J. Chem. Phys.*, **28**, 352 (1958).

glow ($NO + O \rightarrow NO_2^* \rightarrow NO_2 + h\nu$) is slower than the reactions of active nitrogen with either NO or NO_2, and does not occur in the presence of active nitrogen. Hence, essentially all the active nitrogen reaction occurs in the region where the blue glow is visible. A measure of reaction time should therefore be possible from the length of the (contracted) blue region and the linear velocity of the gas in the reaction tube. The length of the blue region (generally a few millimeters) was easily measured in a darkened room. The linear velocity was calculated from the cross-section of the reaction tube and the volume of flow, without attempting a correction for a possible velocity gradient between the center of the tube and the wall. For the calculations, the reaction was assumed to be 90% complete in the reaction time, hence the values obtained for the rate constants must be regarded as lower limits. The integrated rate expression, assuming a bimolecular rate-controlling step with complete lateral mixing, takes the form

$$k = \frac{1}{t(N_i - R_i)} \ln \frac{R_i N_f}{N_i R_f}$$

where

k = second-order rate constant
t = reaction time
N_i and R_i = initial concn. of active nitrogen and reactant
N_f and R_f = concn. of active nitrogen and reactant after time t

From thermocouple measurements with comparable flow conditions in the spherical reaction vessel, the temperature was estimated to be approximately 500°K. Collision numbers were calculated from kinetic theory in the usual way, assuming collision diameters to be: N atom, 2.98 Å.; NO, 3.4 Å.; NO_2, 5 Å. The data used in the calculations and the values of the second-order rate constants were

Active N_2 flow rate, moles/sec.	Reactant flow rate, moles/sec.	Length of blue zone, mm.	Reaction time, sec.	k_2, cc./mole sec.
		A. Nitric oxide		
18.7×10^{-6}	20×10^{-6}	4	2.5×10^{-4}	4.0×10^{12}
18.7×10^{-6}	40×10^{-6}	3	1.9×10^{-4}	1.2×10^{12}
Collision no. = 2.0×10^{14} cc./mole sec.				
		B. Nitrogen dioxide		
14.0×10^{-6}	18×10^{-6}	2	1.2×10^{-4}	5.3×10^{12}
14.0×10^{-6}	28×10^{-6}	1.5	1.0×10^{-4}	4.5×10^{12}
Collision no. = 2.6×10^{14} cc./mole sec.				
Total flow rate = 200×10^{-6} mole/sec.				
Total pressure = 2.2 mm.				
Temperature = 500°K.				
Linear velocity = 16 m./sec.				

Discussion

Nitric Oxide Reaction.—The most striking observation of the present study was that nitric oxide was destroyed by active nitrogen in significantly larger amounts than hydrogen cyanide was formed from ethylene for conditions of maximal hydrogen cyanide production. In previous studies from this Laboratory, the maximal production of hydrogen cyanide from ethylene (together with a small amount of cyanogen) has been taken to be a measure of the concentration of nitrogen

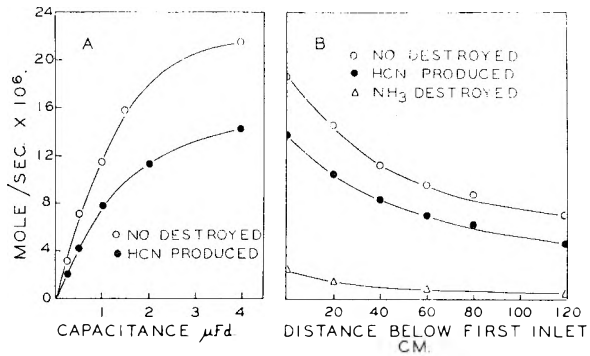

Fig. 1.—(A) effect of active nitrogen concentration on the rate of destruction of NO and on the rate of formation of HCN from C_2H_4; (B) amounts of NO and NH_3 destroyed, and HCN produced from C_2H_4, after different times of decay of active nitrogen.

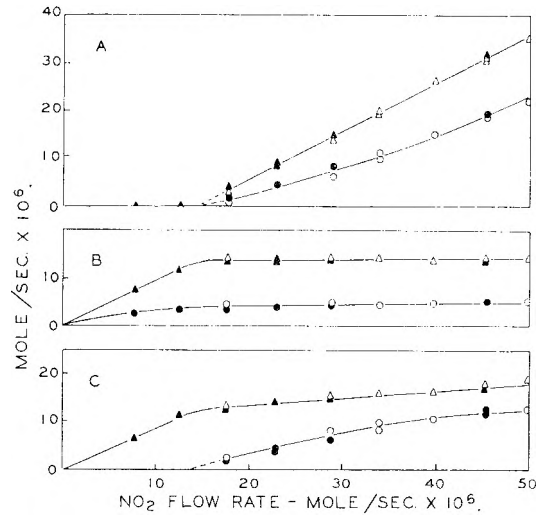

Fig. 2.—Rates of formation of products in the reaction of NO_2 with active nitrogen: A, ○ NO_2 (unheated), ● NO_2 (300°); △ NO + NO_2 (unheated), ▲ NO + NO_2 (300°). B. ○ N_2O (unheated), ● N_2O (300°); △ N_2O produced + nitrogen oxides lost (unheated), ▲ N_2O produced + nitrogen oxides lost (300°). C. ○ NO (unheated), ● NO (300°); △ O_2 (unheated) ▲ O_2 (300°).

atoms, and a good deal of evidence supports this view. In particular, when hydrogen cyanide formation is plotted against flow rate of ethylene, a plateau value for hydrogen cyanide production is reached which is independent of ethylene flow rate at high flow rates, and independent of temperature in the range of about 250 to 450°. Moreover, this maximal hydrogen cyanide formation is found to be essentially the same as that from such diverse reactants as propane,[19] isobutane,[20] cyclopentane,[4] methyl- and dimethylacetylene,[21] and methyl chloride[2,22] under comparable conditions.

The lower concentration of active nitrogen indicated by the yield of hydrogen cyanide from ethylene, compared with that inferred from the decomposition of nitric oxide, is not likely to be due to loss of nitrogen atoms by recombination catalyzed by ethylene or one of the reaction products[23]

(19) M. Onyszchuk, L. Breitman and C. A. Winkler, *Can. J. Chem.*, **32**, 351 (1954).
(20) R. A. Back and C. A. Winkler, *ibid.*, **32**, 718 (1954).
(21) A. Schavo and C. A. Winkler, *ibid.*, in press.
(22) S. Sobering and C. A. Winkler, *ibid.*, **36**, 1223 (1958).
(23) W. Forst, H. G. V. Evans and C. A. Winkler, THIS JOURNAL, **61**, 320 (1957).

since the plateau from which the active nitrogen concentration is inferred in the ethylene reaction is not dependent on either flow rate of reactant or temperature. If it is accepted that the nitrogen atom flow rate in the present study is given by the hydrogen cyanide plateau value (11 ± 0.2 μ-mole/sec. for a condenser capacitance of 2 fd.) the difference between this value and the corresponding plateau value for decomposition of nitric oxide (16 ± 0.2 μmole/sec.) is presumably due to destruction of nitric oxide by some reaction other than direct attack by nitrogen atoms. The extent of the NO reaction might therefore be a quite unsatisfactory measure of the *nitrogen atom* concentration in active nitrogen.

There is little doubt that the main reaction of active nitrogen with NO is

$$N + NO \longrightarrow N_2 + O + 75 \text{ kcal.}^{24} \qquad (1)$$

The spin forbidden reaction

$$N(^4S) + NO(^2\pi) \longrightarrow N_2O(^1\Sigma) + 114.5 \text{ kcal.} \qquad (2)$$

apparently did not occur since no N_2O was found as a product at any flow rate of NO, yet it is known that N_2O is stable to active nitrogen at temperatures up to 200°,[11,18] and was observed to react to less than 5% in some experiments at 300° in the present study.

A possible chain reaction for the decomposition of NO by nitrogen atoms is

$$N + NO \longrightarrow N{\cdot}NO \qquad (3)$$
$$NO + N{\cdot}NO \longrightarrow N_2 + O_2 + N \qquad (4)$$
$$N{\cdot}NO \longrightarrow N_2 + O \qquad (5)$$

However, the complex, N·NO, should be comparable with a highly excited N_2O molecule, and should not have significant life-time. However, if this lifetime were sufficient to allow further reaction of the complexes with NO, some of them would presumably be stabilized to N_2O by collision with nitrogen molecules.

A scheme involving excited oxygen atoms seems even less attractive since there is only enough energy available from reaction 1 to produce the low lying ^1D state.

A difference between the maximal amount of HCN produced from C_2H_4 and the amount of NO decomposed is explained readily if it is assumed that, in addition to atomic nitrogen, with which both C_2H_4 and NO react, there is a second species in active nitrogen that is capable of decomposing NO but is not capable of reacting with C_2H_4 to produce HCN. If, as suggested previously,[25] this second species were an excited molecule, destruction of NO might occur by

$$NO + N_2^* \longrightarrow N_2 + N + O \qquad (9)$$

Decomposition of NO by electronically excited N_2 seems plausible, especially since the $A^3\Sigma_u^+$ state lies particularly close to the dissociation energy of NO (6.49 e.v.) which would favor collisions of the second kind. The A state is the end product of the radiative recombination of nitrogen atoms and is also one of the states into which two ^4S atoms can recombine directly. The radioactive half-life of the A state is now recognized to be of the order of 0.1 sec., which is approximately equal to the time required for the active nitrogen to travel the length of the long reaction tube used in the present experiments, and considerably longer than the 0.02 sec. required for it to reach the spherical reaction vessel from the discharge tube. Rigorous treatment is not possible without knowing the initial extent of dissociation in the discharge tube. However, approximate calculations show that the rate constant for the homogeneous recombination of N atoms to form excited molecules[26] is of the right order to permit a concentration of molecules in the A state sufficient to account for the excess of NO destroyed over HCN formed from C_2H_4 under conditions of complete reaction.

Ground state vibrationally excited molecules ($\nu \geq 27$) might also be effective in causing dissociation of NO.[25] If the half-life of a vibrational level of ground state nitrogen is of the order of 10^6 collisions,[27] the half-life for the experimental conditions used would have been about 0.1 sec., *i.e.*, about the same as the probable half-life of the A state. It does not seem possible, from the present study, to come to any conclusion about the relative importance of electronically and vibrationally excited molecules in promoting the dissociation of NO.

Nitrogen Dioxide Reaction.—The reaction of active nitrogen with NO_2 was found to yield considerable N_2O. The relative amount of this product was larger than that found by Kistiakowsky and Volpi[11] in their mass spectrometric investigation.[28] These differences are almost certainly due to the difficulty, mentioned by these authors, in obtaining reliable mass spectrometer data in the presence of NO_2.

There seems little doubt that N_2O was formed from NO_2 by the reaction

$$N + NO_2 \longrightarrow N_2O + O + 42 \text{ kcal.} \qquad (10)$$

Since N_2O is not significantly attacked by active nitrogen, the amount of N_2O formed may safely be taken as a measure of the extent to which this reaction occurs.

Since the N_2O yield was never more than a fraction of the NO_2 that was not recovered as either NO or NO_2, some NO_2 must have been converted to non-condensable products. This would suggest an additional reaction such as

$$N + NO_2 \longrightarrow N_2 + O_2 + 122 \text{ kcal.} \qquad (11)$$

which, however, might have occurred by a more complex mechanism, *e.g.*

$$NO_2 + O \longrightarrow NO + O_2 + 47 \text{ kcal.} \qquad (12)$$

followed by reaction 1.

The data for the production of atomic oxygen in the system reveal that reactions 10 and 11 are not adequate to explain all the experimental results

(24) Values for the heats of formation, used to calculate the heats of reaction, were taken from Circular 500, National Bureau of Standards, Washington, 1952.

(25) H. G. V. Evans, G. R. Freeman and C. A. Winkler, *Can. J. Chem.*, **34**, 1217 (1956).

(26) (a) J. Berkowitz, W. A. Chupka and G. B. Kistiakowsky, *J. Chem. Phys.*, **27**, 1417 (1957); (b) R. Kelly and C. A. Winkler, *Can. J. Chem.*, **37**, 62 (1959).

(27) S. J. Lukasik and J. E. Young, *J. Chem. Phys.*, **27**, 1149 (1957).

(28) The rate of formation was a smooth function of NO_2 flow rate with neither maxima nor minima.

with NO_2*. The green afterglow due to NO + O → NO_2 became visible when the flow rate of NO_2 exceeded 14 μmoles/sec., and disappeared rather suddenly when the flow rate was increased to 25 μmoles/sec., at which point it may be assumed[11] that all the oxygen atoms were consumed by reaction 12. Since no NO or NO_2 was recovered at flow rates of NO_2 smaller than 14 μmoles/sec., it may be concluded that the minimum flow rate of atomic oxygen was 11 μmoles/sec. Obviously, this cannot be explained by only reactions 10 and 11, since the maximum production of atomic oxygen from these reactions cannot exceed the flow rate of N_2O, which was never greater than 4.9 μmoles/sec.

The most plausible reaction to produce additional atomic oxygen is probably

$$NO_2 + N \longrightarrow N_2 + 2O + 4 \text{ kcal.} \qquad (13)$$

If this reaction were responsible for all the destruction of NO_2 by active nitrogen (14.0 μmoles/sec.), apart from that converted to N_2O (4.9 μmoles/sec.), an atomic oxygen flow of at least 18 μmoles/sec. would result. Since this is considerably in excess of 11 μmoles/sec. indicated by "titration" to the disappearance of the green glow, it would be necessary for reaction 13 to occur to a limited extent of about 3 μmoles/sec. destruction of NO_2.

The recovery of NO + NO_2 was linear in NO_2 flow rate, with a slope of unity, and extrapolated to 14.0 μmoles/sec. of NO_2 for zero recovery of the oxides. This suggests that, up to a flow rate of 14.0 μmoles/sec., all the NO_2 reacts with active nitrogen while, at higher flow rates, some of the excess is converted to NO, presumably by reaction of oxygen atoms formed in the active nitrogen reaction, *i.e.*, reaction 12.

It seems likely that the reaction

$$2NO + O_2 \longrightarrow 2NO_2 \qquad (14)$$

occurred in competition with the reaction of NO with NO_2 to form N_2O_3, which was evident in the trap from its blue color.

If, as indicated above, the amount of NO_2 destroyed by active nitrogen may be taken as 14.0 μmoles/sec., it is necessary to account for the discrepancy between this value and the 18.7 μmoles/sec. of NO destroyed under identical conditions. It could be explained if the reaction

$$N + NO_2 \longrightarrow 2NO \qquad (15)$$

consumed 2.35 μmoles/sec. of NO_2, to form 4.7 μmoles/sec. of NO, which also was destroyed by active nitrogen. The total destruction of (NO + NO_2), in μmoles/sec., would then be (14–2.35) by reactions other than reaction 15, plus 7.05 by reaction 15 followed by reactions of NO with atomic nitrogen. However, this would require the rather remarkable coincidence that reaction 15 occur to just the extent necessary to make the total amount of NO_2 destroyed correspond almost exactly with the amount (13.9 μmoles/sec.) of HCN produced from C_2H_4 under optimal conditions. It might be preferable to assume that part of the NO_2 suffers destructive collisions with excited molecules present in the active nitrogen

$$NO_2 + N_2^* \longrightarrow N_2 + NO + O \qquad (16)$$

A study of the reaction of NO_2 with active nitrogen over a range of operating pressures might help to assess the reality of reaction 16, although the rather obvious complexity of the reactions that occur in the NO_2–active nitrogen system is not particularly encouraging to a detailed study of it.

INTRAMOLECULAR PROCESSES IN UNIMOLECULAR REACTIONS[1]

By David J. Wilson

Department of Chemistry, University of Rochester, Rochester, New York

Received August 18, 1959

A general method is developed for handling intra- and intermolecular energy transfer and chemical decomposition in unimolecular reactions. The method is applied to two simple models and it is shown that weak intramolecular coupling between the oscillators representing the reactant molecule leads to a transition region between the high and low pressure limits of the rate constant of a unimolecular reaction that is broader than that predicted by Kassel theory.

It is well established that unimolecular reactions take place *via* a mechanism involving collisional activation and deactivation of the reactant molecule, redistribution of internal energy within the reactant molecule, and reaction of activated reactant molecules. Most previous theories of unimolecular reactions have assumed that the redistribution of internal energy in, and the reaction of, an activated molecule are characterized by a single half-life or relaxation time dependent only on the total vibrational energy of the molecule. We shall here consider a model in which redistribution of internal energy may take place either by processes leading to a single, energy-dependent relaxation time, or by single-quantum-transfer processes leading to several energy-dependent relaxation times, or by any type of process intermediate between these two extremes. It will be assumed that the rate of formation by intramolecular energy transfer of one state $A_{\{i\}}$ of the reactant molecule from another state $A_{\{m\}}$ having the same internal energy is equal to $\alpha(\{m\};\{i\})A_{\{m\}}$, where {i} is a set of quantum numbers specifying $A_{\{i\}}$ and $\alpha(\{m\};\{i\})$ is proportional to the transition probability for the indicated transition. The nature of the collision mechanism and the microscopic decomposition rate will be left general for the time being. This theory will include (in a

(1) This work was supported by the National Science Foundation under Grant 9460.

formal way) the previous theories as special cases, and will also allow us to investigate the effects on the first-order rate constant of Markoff-like intramolecular energy transfer processes.

It was remarked by Zwolinski and Eyring[2] that the rate constant for a unimolecular reaction could be viewed as an eigenvalue of a certain matrix, and these authors carried out calculations for a simple model. Montroll, Rubin and Shuler, *et al.*,[3] Kim,[4] Nikitin[5] and others have developed mathematical techniques for handling unimolecular reactions of diatomic molecules at the low-pressure limit in connection with studies of vibrational relaxation processes and atom recombinations. Hirschfelder[6] has considered a simple model involving stepwise activation. Mahan[7] has presented a thermodynamic formulation of stepwise activation. Buff and Wilson[8] have considered the case of a polyatomic molecule at any pressure whose collisional transition probabilities and microscopic decomposition rates are functions only of the total vibrational energy and which can be represented by a system of s coupled harmonic oscillators.

It is proposed here to generalize the results of Kassel[9] and Buff and Wilson to permit the inclusion of more detailed information about the nature of the collisional transition probabilities, the intramolecular energy transfer parameters, and the microscopic decomposition rate. In Slater's[10] theory of unimolecular rates very careful attention is paid to the reaction coördinate, but mathematical difficulties prevent a precise treatment of anharmonicities and a perhaps questionable assumption about collisional transition probabilities is made. (The occurrence of deactivation upon every collision of an activated molecule has been shown unlikely.[11]) In Kassel's theory the same assumption about the collisional transition probabilities is made, and a crude (although strikingly successful) assumption is made about the nature of the reaction event and the effects of anharmonicities. Rice[12] has qualitatively discussed the effect of restricting energy transfer between some of the oscillators representing the reactant molecule. Buff and Wilson used Kassel's assumptions about anharmonicities and the reaction event, but used what is hoped (although certainly not known) to be a better assumption about the nature of the collisional transition probabilities.

Let us consider a reactant with three vibrational degrees of freedom; the extension to more complex molecules is trivial. Equations 1 describe the variation with time of the concentrations of reactant molecules in the various quantum states if reactant concentration A is much less than inert gas concentration M. The first pair of summations takes into account intramolecular energy transfer processes, so that $\epsilon_{lmn} = \epsilon_{ijk}$ (ϵ_{fgh} is the internal energy of A_{fgh}). The second pair of summations takes into account collisional transfer of energy between reactant and heat bath molecules, and the last term is due to chemical reaction.

$$\frac{dA_{ijk}}{dt} = \sum_{lmn} \alpha(l,m,n;i,j,k)A_{lmn} - \sum_{lmn} \alpha(i,j,k;l,m,n)A_{ijk} + \sum_{pqr} a(p,q,r;i,j,k)MA_{pqr} - \sum_{pqr} a(i,j,k;p,q,r)MA_{ijk} - c(i,j,k)A_{ijk} \quad (1)$$

Here $\alpha(l,m,n;i,j,k)$ is the rate constant for the intramolecular process $A_{lmn} \rightarrow A_{ijk}$, $a(p,q,r;i,j,k)$ is the rate constant for the process $A_{pqr} + M \rightarrow A_{ijk} + M$, $c(i,j,k)$ is the rate constant for the process $A_{ijk} \rightarrow$ Products, M is the concentration of chemically inert heat bath molecules, and A_{ijk} is the concentration of reactant molecules in the state specified by the quantum numbers i,j,k. Two assumptions implicit in equations 1 are that the reaction events of A_{ijk} are randomly distributed,[13] and that the intramolecular processes involved can be described by a linear operator of the type used. The detailed nature of the reaction event determines the functional form of $c(i,j,k)$, the nature of the anharmonic interactions between the oscillators determines the quantities α, and the collisional transition probabilities determine the quantities a.

In order to formulate this problem in matrix notation, one need merely decide on some convention for ordering the A_{ijk} in a one-dimensional array. One way of doing this is to place them in dictionary order according to increasing $i+j+k$, increasing i, and increasing j. If one then makes the substitution

$$A_{lmn} = \exp(-\lambda t) \exp(-\epsilon_{lmn}/kT) B_{lmn}$$

where t is time, λ a parameter, and B_{lmn} the new dependent variable, the resulting matrix is symmetric, by virtue of the principle of microscopic reversibility, so its eigenvalues are all real if the a's, α's and c's are real. In the situation usually encountered, where $c(i,j,k)$ is zero unless ϵ_{ijk}/kT is fairly large, the smallest eigenvalue of this matrix is, as shown in reference 8, the observed first-order rate constant.

It is apparent that, for molecules of any complexity and with realistically spaced vibrational energy levels, the problem of finding the lowest eigenvalue of equations 1 becomes quite formidable. If, however, one is willing to wash out some of the detail, the problem can be simplified somewhat in the following way.

Following Kassel, we shall assume that the reactant molecule consists of s degenerate, weakly

(2) B. J. Zwolinski and H. Eyring, *J. Am. Chem. Soc.*, **69**, 2702 (1947).

(3) R. J. Rubin and K. E. Shuler, *J. Chem. Phys.*, **25**, 59 (1956); **25**, 68 (1956); **26**, 137 (1957); K. E. Shuler, THIS JOURNAL, **61**, 849 (1957); E. W. Montroll and K. E. Shuler, *J. Chem. Phys.*, **26**, 454 (1957); N. W. Bazley, E. W. Montroll, R. J. Rubin and K. E. Shuler, *ibid.*, **28**, 700 (1958); R. Herman and K. E. Shuler, *ibid.*, **29**, 366 (1958).

(4) Shoon Kyung Kim, *ibid.*, **28**, 1057 (1958).

(5) E. E. Nikitin, *Doklady Akad. Nauk SSSR*, **116**, 584 (1957); **119**, 526 (1958).

(6) J. O. Hirschfelder, *J. Chem. Phys.*, **16**, 22 (1948).

(7) B. H. Mahan, *ibid.*, **31**, 270 (1959).

(8) F. P. Buff and D. J. Wilson, *J. Chem. Phys.*, in press; D. J. Wilson, Thesis, pp. 54–62, California Institute of Technology, Pasadena, 1958.

(9) L. S. Kassel, "Kinetics of Homogeneous Gas Reactions," Chemical Catalog Co., New York, N. Y., 1932.

(10) N. B. Slater, *Phil. Trans.*, **A246**, 57 (1953).

(11) D. J. Wilson and H. S. Johnston, *J. Am. Chem. Soc.*, **75**, 5763 (1953).

(12) O. K. Rice, *Z. physik. Chem.*, **7B**, 226 (1930); see also reference 9, p. 107.

(13) N. B. Slater, *J. Chem. Phys.*, **24**, 1256 (1956).

coupled oscillators. Further, let us assume that one of these oscillators (the reactive oscillator) is the site of chemical reaction—that when its quantum number k equals or exceeds some critical value n^*, reaction occurs with a rate constant $c(k,n)$, where n is the total number of quanta in the molecule. Let A_{kn} be the concentration of molecules having a total of n quanta, k of which are in the reactive oscillator. The system of equations analogous to (1) is then

$$\frac{dA_{kn}}{dt} = \sum_{l=0}^{n} a(l,n;\ k,n)A_{ln} - \sum_{l=0}^{n} a(k,n;\ l,n)A_{kn} + \sum_{m}\sum_{l=0}^{m} a(l,n;\ k,n)A_{l,m}M - \sum_{m}\sum_{l=0}^{m} a(k,n;\ l,m)A_{kn}M - c(k,n)A_{kn} \quad (2)$$

If one makes the substitution

$$A_{kn} = \exp(-\lambda t)\exp(-\epsilon_n/kT)\, g_{s-1}(n-k)B_{kn}$$

where

$$g_{s-1}(m) = (m+s-2)!/[m!\,(s-2)!]$$

the matrix of coefficients of equations 2 becomes symmetric. As in the earlier case, the lowest eigenvalue of (2) is the observed first-order rate constant.

If we delete the anharmonic coupling terms in (1), select the $c(i,j,k)$ as the frequency of bond-breaking as analyzed by Slater, and assume that only collisional transition probabilities involving large amounts of energy transfer contribute to the collision mechanism, we obtain something formally similar to Slater theory. In a similar way, the results of Kassel and of Buff and Wilson can be considered as special limiting cases of this formulation.

Of particular interest is the effect of the intramolecular coupling parameters α on the rate constant. It has been remarked earlier[8,12,14] that the transition region between the high and low pressure limits could be broadened by the effect of various types of anharmonic coupling. Let us consider the simplest model which exhibits this feature; the reactant A is assumed to have only two degrees of freedom and three states (A_{00}, A_{01}, A_{10}), of which only the last is capable of undergoing reaction. The equations analogous to equations 1 are

$$\frac{dA_{00}}{dt} = a(1,0;\ 0,0)MA_{10} + a(0,1;\ 0,0)MA_{01} - [a(0,0;\ 1,0)M + a(0,0;\ 0,1)M]A_{00}$$

$$\frac{dA_{01}}{dt} = a(0,0;\ 0,1)MA_{00} + \alpha A_{10} - [a(0,1;0,0)M + \alpha]A_{01} \quad (3)$$

$$\frac{dA_{10}}{dt} = a(0,0;1,0)MA_{00} + \alpha A_{01} - [a(1,0;0,0)M + \alpha + c]A_{10}$$

The lowest eigenvalue of this set of equations could be computed, and its dependence on α and M investigated. However, Buff has shown[8] that, if $\epsilon_{10}/kT >> 1$ (where ϵ_{10} is the activation energy of the reaction), then the formulation of the problem by this method leads to results which are the same, to a very good approximation, as those obtained by the much simpler steady-state formulation. We shall therefore utilize the latter approach.

Setting

$$\dot{A}_{01} = \dot{A}_{10} = 0, A_{00} = A$$

in equations 3 gives two linear equations which can be solved for A_{10}. The observed unimolecular rate constant then is given by

$$k = -\frac{1}{A}\frac{dA}{dt} = \frac{c\exp(-\epsilon_{10}/kT)}{1 + \dfrac{\left(1+\dfrac{\alpha}{bM}\right)c}{bM + 2\alpha}} \quad (4)$$

where $b = a(1,0;\ 0,0) = a(0,1;\ 0,0)$. It readily is apparent that $k_0M = 2bM\exp(-\epsilon_{10}/kT)$ and that $k_\infty = c\exp(-\epsilon_{10}/kT)$, where k_0M and k_∞ are the limiting forms of k as $M \to 0$ and ∞, respectively.

Letting $y = k_0M/k_\infty = 2bM\exp(-\epsilon_{10}/kT)$ gives

$$\frac{k}{k_\infty} = \frac{1}{1 + \dfrac{(1+2\gamma/y)}{(2\gamma - y/2)}},\ \gamma = \frac{\alpha}{c} \quad (5)$$

If $\gamma \to \infty$, $k/k_\infty = 1/(1+1/y)$. If $\gamma \to 0$, $k/k_\infty = 1/(1+2/y)$. In Fig. 1, k/k_∞ is plotted against k_0M/k_∞ on a log-log scale. The effect of finite values of γ in broadening the transition region between the high and low pressure limits is quite apparent. A value of γ equal to ∞ is analogous to Kassel theory, in which a microcanonical distribution of energy among the oscillators representing the molecule is assumed.[8]

It can be shown quite generally that, given a collision mechanism in which reactant molecules are activated by the transfer of a large quantity of energy on a single collision, a weak coupling mechanism of intramolecular energy transfer leads to a broadened transition region between the high and low pressure limits. If we express equation 1 as

$$\frac{dA_n}{dt} = \left(\frac{\partial A_n}{\partial t}\right)_{\text{collisional}} - c_nA_n \quad (6)$$

where the subscript n represents total internal energy and the term c_nA_n represents the occurrence of chemical reaction in the nth state, the quantities c_n depend, in general, on pressure. This is associated with the fact that, in general, mechanisms of intramolecular energy transfer do not lead to a random occurrence of reaction events.[13]

To illustrate this last point, let us consider a weak coupling intramolecular mechanism of the type mentioned above. Kassel theory[9] calculates c_n by assuming that a random redistribution of quanta among the s degenerate oscillators representing the molecule takes place every $(1/\nu_K)$ seconds, on the average, where ν_K is the high pressure limit of the pre-exponential factor of the rate constant. Reaction is said to occur when the number of quanta in one oscillator exceeds some critical value, n^*. This redistribution is such that the distribution of quanta among the oscillators at a given instant is completely independent of the previous distributions; that is, intramolecular energy transfer is assumed to be, in a certain sense, a strongly coupled process. The alternative extreme is that in which only one quantum is transferred randomly from one oscillator to another every τ seconds. The probability of finding a

(14) E. K. Gill and K. J. Laidler, *Can. J. Chem.*, **36**, 1570 (1958).

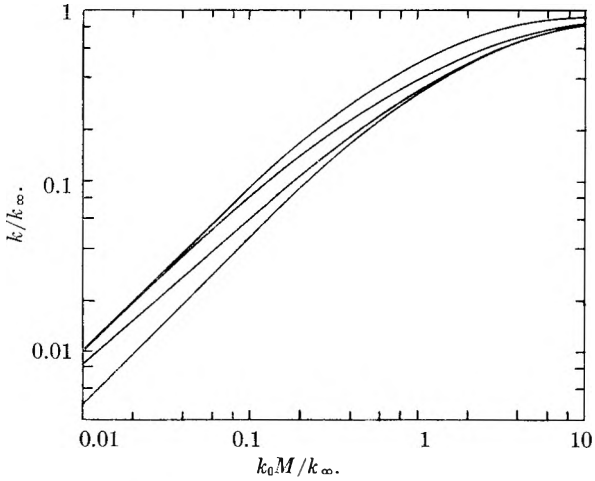

Fig. 1.—k/k_∞ *versus* k_0M/k_∞; from top to bottom: $\gamma = \infty$, 0.2, 0.01, $\rightarrow$ 0. These curves apply to the three-level model discussed in the text.

certain number of quanta in a given oscillator at a given time is, in this case, strongly dependent on the distribution of quanta that was present during the preceding instant. This Markov process leads to a set of equations by which the evolution of the energy distribution with time may be followed in isolated molecules.

We shall consider the differential equations describing the time-evolution of the internal energy distribution in the absence of collision processes. The results of this calculation will enable us to calculate the unimolecular rate associated with this model at any pressure.[13] Let us assume that (1) reaction occurs with a rate constant $c(k,n)$ when k, the quantum number of the reactive oscillator, is equal to or greater than n^*, (2) the total number of quanta distributed among the s degenerate oscillators representing the molecule is n, and (3) the distribution of quanta among the $s-1$ nonreactive oscillators is random. Then

$$\frac{dA_{k,n}}{dt} = \alpha(k-1,n;k,n)A_{k-1,n} + \alpha(k+1,n;k,n)A_{k+1,n} - [\alpha(k,n;k+1,n) + \alpha(k,n;k-1,n) + c(k,n)]A_{k,n} \quad (7)$$

in the absence of collision processes.

At equilibrium

$$A_{kn} = N \exp(-\epsilon_n/kT) g_{s-1}(n-k)A$$

where N is a normalizing constant, $g_s(m)$ is the degeneracy of the mth state of an s-fold degenerate oscillator, and A is the total reactant concentration. From microscopic reversibility one gets the relations

$$\alpha(k-1,n;k,n) = \alpha(k,n;k-1,n)\frac{g_{s-1}(n-k)}{g_{s-1}(n-k+1)} \quad (8)$$

and

$$\alpha(k,n;k+1,n) = \alpha(k+1,n;k,n)\frac{g_{s-1}(n-k-1)}{g_{s-1}(n-k)}$$

Let us choose $\alpha(k+1,n;k,n)$ proportional to the number of ways by which one can go from the state $(k+1,n)$ to the state (k,n) divided by the total number of ways by which the state $(k+1,n)$ can transfer one quantum. There is, admittedly, a certain arbitrariness in this choice, but it is not unreasonable in the absence of more detailed information about intramolecular processes.

Then

$$\alpha(k+1,n;k,n) = \frac{\alpha(s-1)g_1(k)}{(s-1)[g_1(k) + \sum_{j=2}^{s} g_1(k_j - 1)]} \quad (9)$$

where k_j is the quantum number of the jth (nonreactive) oscillator before the transition takes place. If $s = 2$, this formula may be used as is; if $s > 2$, it is necessary to average over a random distribution of the quantum numbers k_j. $\langle g_1(k_j - 1)\rangle$ is the probability that k_j is non-zero. This is one minus the probability that k_j is zero, so

$$\langle g_1(k_j - 1)\rangle = 1 - \frac{g_{s-2}(n-k_j-1)}{g_{s-1}(n-k_j-1)} = \frac{n-k_j-1}{n+s-k_j-3} \quad (10)$$

where $g_s(m)$ has been set equal to $(m+s-1)!/m!(s-1)!$. One then replaces the sum in equation 9 by $(s-1)\langle g_1(k_j-1)\rangle$ and uses this result with equation 8 in equation 7 to obtain explicitly the differential equations governing internal energy transfer. A plausible value for $c(k,n)$ is simply $\nu S(k-n^*)$, $S(x) = 0, x<0$; $S(x) = 1, x \geq 0$.

By setting $A_{kn}(t) = \exp(-\lambda t)g_{s-1}(n-k)B_{kn}$, equations 7 are converted into a set of ordinary linear equations with a symmetric matrix of coefficients and with eigenvalues $\lambda_{1n},\lambda_{2n},\ldots\lambda_{n+1,n}$. It is therefore possible, by use of the eigenvectors of this system, to write $A_{kn}(t)$ as $\sum_{j=1}^{n+1} h_{jkn}\exp(-\lambda_{jn}t)$, where the quantities h_{jkn} are constants. The fraction $P(n,t)$ of reactant molecules in the nth energy state at time t then is given by

$$P(n,t) = \frac{A_n(t)}{A_n(0)} = \frac{\sum_{k=0}^{n} A_{n,k}(t)}{\sum_{k=0}^{n} A_{n,k}(0)} = \sum_{j=1}^{n+1} d_{nj}\exp(-\lambda_{nj}t), \quad \sum_{j=1}^{n+1} d_{nj} = 1 \quad (11)$$

The probability that a molecule A_n will react (in the absence of collisions) in the time interval t, $t + dt$ is

$$-\frac{\partial P}{dt}(n,t)\,dt = \sum_{j=1}^{n+1} d_{nj}\lambda_{nj}\exp(-\lambda_{nj}t)dt$$

The fraction of molecules A_n which react before suffering a collision is therefore given by[13]

$$\int_0^\infty \sum_{j=1}^{n+1} d_{nj}\lambda_{nj}e^{-\lambda_{nj}t}e^{-bMt}\,dt = \sum_{j=1}^{n+1}\frac{d_{nj}\lambda_{nj}}{\lambda_{nj}+bM} \quad (12)$$

where we have assumed that deactivation occurs upon every collision of an activated molecule and that reactant is present in only trace quantities. b is the kinetic collision constant for A–M collisions. Next, let us multiply this fraction by the rate at which molecules A_n are produced by collisional activation and then sum over all reactive states $n \geq n^*$ to obtain

$$-\frac{dA}{dt} = AbM\sum_{n=n^*}^{\infty} P(n)\left[\sum_{j=1}^{n+1}\frac{d_{nj}\lambda_{nj}}{\lambda_{nj}+bM}\right] \quad (13)$$

where $P(n)$ is the equilibrium probability of the

state n. The first-order rate constant is therefore given by

$$k = bM \sum_{n=n^*}^{\infty} P(n) \left[\sum_{j=1}^{n+1} \frac{d_{nj}\lambda_{nj}}{\lambda_{nj} + bM} \right] \quad (14)$$

If the inner sum in equation 14 contains only one term, (14) is just the Lindemann theory expression. In any case, equation 14 can be cast into the form of the Lindemann expression by allowing the function c_n to depend on M. We set

$$\frac{c_n(M)}{bM + c_n(M)} = \sum_{j=1}^{n+1} \frac{d_{nj}\lambda_{nj}}{bM + \lambda_{nj}}$$

which yields

$$c_n(M) = \frac{\sum_{j=1}^{n+1} \frac{d_{nj}\lambda_{nj}}{1 + \lambda_{nj}/bM}}{1 - \sum_{j=1}^{n+1} \frac{d_{nj}\lambda_{nj}}{bM + \lambda_{nj}}} \quad (15)$$

As $M \to 0$

$$c_n(M) \to \left(\sum_{j=1}^{n+1} \frac{d_{nj}}{\lambda_{nj}} \right)^{-1} \quad (16)$$

and as $M \to \infty$

$$c_n(M) \to \sum_{j=1}^{n+1} d_{nj}\lambda_{nj} \quad (17)$$

Therefore it is immediately apparent that $c_n(0) \leqslant c_n(\infty)$, where the equality holds only if all the λ_{nj} are equal for a given n.

Furthermore, it can be shown that $\partial c_n/\partial M \geqslant 0$ for all M. Differentiating equation 15 yields

$$\frac{\partial c_n}{\partial M} = \frac{bf}{1 - f} \left[1 - \frac{bM}{f(1 - f)} \cdot \sum_{j=1}^{n+1} \frac{d_{nj}\lambda_{nj}}{(bM + \lambda_{nj})^2} \right] \quad (18)$$

where

$$f = \sum_{j=1}^{n+1} \frac{d_{nj}\lambda_{nj}}{bM + \lambda_{nj}}$$

The first factor of equation 18 is certainly positive for finite M. The inequality

$$\sum_{j=1}^{n+1} d_{nj} \left(\frac{\lambda_{nj}}{bM + \lambda_{nj}} \right)^2 \geqslant \left(\sum_{j=1}^{n+1} \frac{d_{nj}\lambda_{nj}}{bM + \lambda_{nj}} \right)^2$$

readily can be shown to imply that the factor in brackets in equation 18 is greater than or equal to zero. Therefore $c_n(M)$ is a monotonically increasing function of M.

The M dependence of the c_n affects the rate constant as shown by (19)

$$k = \sum_{n=n^*}^{\infty} \frac{p(n)c_r(M)bM}{bM + c_n(M)} \quad (19)$$

Since all the $c_n(M)$ monotonically decrease with decreasing M

$$\frac{c_n(M)}{bM + c_n(M)} < \frac{c_n(\infty)}{bM + c_n(\infty)}$$

so that

$$k(M) < \sum_{n=n^*}^{\infty} \frac{P(n)c_n(\infty)bM}{bM + c_n(\infty)}$$

In particular, if $c_n(\infty)$ is set equal to the expression used by Kassel for this quantity, it is apparent that $k(M) < k_{\text{Kassel}}(M)$ for finite M. At the low pressure limit the two theories give identical results, $k = P(n)bM$, as they do (for this choice of $c_n(\infty)$) at the high pressure limit. One readily can show from equation 14 that all of the remarks made by Johnston and White[15] as to the nature of k *vs.* M curves are applicable to this expression for the rate constant. Therefore one concludes that, as found for the simpler model considered earlier in this paper, the transition region between the low pressure and high pressure limits is broader (for given s and given spacing of energy levels) for the model discussed here than it is for that of Kassel. This may possibly explain Powell's finding[16] that the data on nitrous oxide require that s be equal to five, which would appear to be unreasonably large.

Rabinovitch and co-workers[17] have found that k_∞ for the *trans-cis* isomerization of cyclopropane-d_2 is about six times *greater* than k_∞ for the structural isomerization to propylene. It is very difficult to see how this can be explained in terms of Slater's theory. If hydrogen motions are dominant in the reaction coördinates of both isomerizations, one would expect the ratio of K_∞ (*trans-cis*) to K_∞ (structural) to be about one sixth, due to the fact that the degeneracy of the reaction coördinate in the geometrical isomerization is two, while the degeneracy of the reaction coördinate in the structural isomerization is 12. On the other hand, Slater[18] has shown that his theory does not give satisfactory results when a carbon–carbon bond scission is taken as the reaction coördinate for the structural isomerization of cyclopropane. This suggests that it may be necessary to appeal to some type of anharmonic interactions to account for these data.

It was suggested to the author by Professor N. B. Slater that an investigation of somewhat more general expressions for $P(n,t)$ than the one given in equation 11 might be of interest. If one assumes the "strong collision" mechanism used by Slater and Kassel, the general expression for the unimolecular rate constant is (by the same method used in reference 13)

$$k = bM \sum_{n=n^*}^{\infty} P(n) \int_0^{\infty} \left[-\frac{\partial P(n,t)}{\partial t} e^{-bMt} \right] dt \quad (20)$$

This implies that if $\partial P/\partial t(n,0) = 0$, the high pressure limit of the rate constant is zero—that a plot of k *vs.* M should go through a maximum and then diminish. The pyrolysis of cyclobutane in the presence of high pressures of inert gas might therefore be of interest, since cyclobutane attains what appears to be a high pressure limit at pressures less than 100 mm. and would therefore be convenient to investigate at pressures well above that required to attain the high pressure limit.

Acknowledgment.—The author has enjoyed profitable discussions with Professors Frank P. Buff and W. D. Walters and with Dr. R. Srinivasan on the theory of unimolecular rates.

(15) H. S. Johnston and J. R. White, *J. Chem. Phys.*, **22**, 1969 (1954).

(16) R. E. Powell, *ibid.*, **30**, 724 (1959).

(17) B. S. Rabinovitch, E. W. Schlag and K. B. Wiberg, *ibid.*, **28**, 504 (1958).

(18) N. B. Slater, *Proc. Roy. Soc. (London)*, **A218**, 224 (1953).

HYDROTHERMAL REACTIONS OF CALCIUM HYDROXIDE-QUARTZ AT 120–220°

BY GUNNAR O. ASSARSSON

Chemical Laboratory, Geological Survey, Stockholm 50, Sweden

Received August 21, 1959

The phases formed at the reaction between calcium hydroxide and quartz depend on the amount of calcium hydroxide per unit area of grain surface, on the reaction temperature and on the period of reaction time. There are two principally different reaction ranges; within the one a monocalcium silicate hydrate (the tobermorite phase) is formed; the second one has the α-dicalcium silicate monohydrate as initial product. The concentration boundary between these ranges lies at about 200 mg. CaO/m.^{2}. On extension of the reaction time the mono- and dicalcium silicates behave as sources of calcium ions; the reactions when continued lead to a formation of new compounds poorer in lime (the 2:3-calcium silicate, the gyrolite phase), the silica ions necessary for this reaction reaching the reaction layer by diffusion from the underlying quartz surface. Secondary, accessory phases also occur (the Z-phase, the xonotlite compound). All these reactions must be referred to the slowness of the transformation reactions, rendering an observation of the reaction stages possible.

In some earlier papers the author already has given the results of some investigations on the hydrothermal reactions between calcium hydroxide and amorphous silica between 120 and 220°.[1] The formation of calcium silicate hydrates takes place rapidly with the production of different phases depending on the reaction time, the temperature and the vapor pressure within the autoclave. It was shown that there are distinct stages in the formation of the phases and that these stages depend on the reaction temperatures. At lower temperatures (about <150°) and with saturated vapor there are two stages. The first involves the formation of a substance, in the author's papers designated as phase B, which probably can not be distinguished as a pure chemical compound in the true sense. During the second stage compounds are formed which probably are stable phases at the temperatures in question, and which have a composition depending upon the molar ratio of the autoclaved mixture. These phases are: phase Z (composition unknown), the tobermorite compound (monocalcium silicate monohydrate) and α-dicalcium silicate monohydrate. At higher temperatures (about 150–220°) new phases are formed by recrystallization of the second stage phases which are metastable at these temperatures. The phases of this third stage are: the gyrolite compound (dicalcium trisilicate dihydrate), the xonotlite compound (tricalcium trisilicate monohydrate) and the hillebrandite compound (β-dicalcium silicate monohydrate). These reaction stages suggest that similar reactions would take place when calcium hydroxide reacts with silicate or quartz at corresponding temperatures. It is evident that the nature of the compounds formed in these cases must depend largely on the nature of the surface of the silica-containing compound. The reactions might therefore be elucidating in connection with the formation of calcium silicate minerals and their paragenesis in hydrothermal deposits and also with the products of some technical autoclave processes.

Very few investigations have been published on the systematically performed hydrothermal reaction calcium hydroxide–quartz and, as far as is known to the author, none on the reaction calcium hydroxide–silicates, although these reactions must be of a certain interest. Some results concerning the hydrothermal reaction between calcium hydroxide and quartz, tridymite and cristobalite are given by Nagai, Jander and Franke, Kalousek and others.[2] The important experimental condition, however, the amount of calcium hydroxide available per unit area of the surface of the grains, does not seem to have been taken into consideration. A discussion of phases formed must be based upon the reactions that can be expected to occur in the diffusion layers at the phase boundaries. The results of the investigations on amorphous silica–calcium hydroxide may therefore only be applied to the reaction quartz–calcium hydroxide when all possible reaction conditions are taken into account.

This report presents some facts which are related to two aspects of the problem in question, namely: the character of the phases formed on autoclaving mixtures of calcium hydroxide and quartz at 120–220° for varying periods of time 2 hr.–24 days, and in special cases longer, the dependence of the reactions on the relative grain surface area.

Material. Quartz.—A piece of well-crystallized quartz, shown to be free from other minerals, was ground in a steel mill to about 1 mm. maximum particle size, the powder was sieved and the fraction smaller than about 0.2 mm. particle size was removed. The powder was washed, the small iron filings from the mill were removed with a magnet and with hydrogen chloride, and the quartz powder was carefully washed. It was ground in an agate mortar to the required grain size, with the exercise of usual precautions. A control analysis of the final product showed a residue of 0.05% after removal of the silica with hydrogen fluoride and sulfuric acid. The sample of quartz used for the experiments had a grain surface area of 0.85 m.^{2}/g. determined with nitrogen adsorption according to the BET-method.[3]

Experimental and the Identification of the Phases.—The autoclaving experiments were performed in the stainless steel autoclaves earlier described, equipped with valves to allow evacuation before the experiments and with manometers for pressure control.

The phases were identified by means of X-ray diffraction measurements and by the quantitative extraction of the uncombined lime, both methods having been described in earlier papers. The former method is semi-quantitative and a certain minimum amount of the phase in question is required. Because of the presence of the mineral in the reaction mixtures efforts were made to obtain the reaction products free

(1) G. Assarsson, THIS JOURNAL, **62**, 223 (1958).

(2) S. Nagai, *Z. anorg. Chem.*, **206**, 177 (1932); W. Jander and B. Franke, *Z. anorg. allgem. Chem.*, **241**, 161 (1941); G. L. Kalousek, *J. Am. Ceram. Soc.*, **40**, 74 (1957).

(3) S. T. Brunauer, P. H. Emmett and E. Teller, *J. Am. Chem. Soc.*, **60**, 309 (1938); P. H. Emmett and I. Dewitt, *Ind. Eng. Chem., Anal. Ed.*, **13**, 28 (1941); H. K. Livingstone, *J. Colloid Sc.*, **4**, 447 (1949).

TABLE I

MIXTURES QUARTZ-CALCIUM HYDROXIDE AUTOCLAVED

Symbol for the phases: O = poorly crystallized product, spacings chiefly according to Table II; T, G, X = compounds resembling the minerals tobermorite (T), gyrolite (G) and xonotlite (X), 2A = α-dicalcium silicate monohydrate.

	130 mg. CaO/m.²			300 mg. CaO/m.²			400 mg. CaO/m.²		
Autoclave temp., °C.	Time, hr.	CaO combined, mg./m.²	Phase	Time, hr.	CaO combined, mg./m.²	Phase	Time, hr.	CaO combined, mg./m.²	Phase
120	24	90	O	24	160	O	24	100	(2A)
	72	130	O	72	220	O,2A	72	150	2A
	500	130	O,T	500	300	2A	500	300	2A
140	12	120	O	12	160	O	12	120	(2A)
	24	130	O	24	270	2A	24	260	2A
	170	130	T,O	170	300	T,O	170	400	2A,T
160	2	100	O	2	130	2A	2	150	(2A)
	4	110	O	4	200	2A	4	160	2A
	8	130	O,T	8	300	2A	..	..	..
	24	130	T,O	24	300	2A,T	24	280	2A
180	2	130	O	2	210	2A	2	190	(2A)
	4	130	O,T	4	300	2A	4	270	2A
	..	..	..	6	300	T,2A	..	..	..
	..	..	..	12	300	2A,T	..	..	..
	24	130	T,O	24	300	T (X)	24	400	2A
	..	..	..	..	..	..	48	400	2A,T
200	2	130	T,O	2	240	2A	2	270	2A
	..	..	..	4	300	2A	..	..	..
	..	..	..	10	300	T,2A	..	..	..
	..	..	..	..	..	..	16	300	2A
	24	150	T	24	300	T (X)	24	320	2A
	..	..	..	48	300	T,X	48	400	T,G,X
220	24	130	T,G (X)	24	300	T,G (X)	..	..	..
	48	130	T,G	48	300	T,G	48	400	G,T,X

from the mother substances; in some cases most of the quartz was removed by sieving and the autoclave products then were examined a little more easily. A microscope also was used with varying success.

The Formation of the Ca-Compounds.—From the first experiments it was evident that the reactions between the calcium hydroxide and the silica in the layers between the lime solution and the quartz grain were of two principal types, depending on the available amount of calcium hydroxide at the surface of the quartz grains, and also on the temperature and time of autoclaving. In this report two groups of experimental series will be described: namely, one with mixtures poor in lime with the lime proportion 130 mg. CaO/m.² and one with two mixtures rich in lime with the lime proportion 300 and 400 mg. CaO/m.².

Mixtures Poor in Lime (130 mg. CaO/m.²).—At low temperature (120–140°) the calcium silicate hydrate is formed rather slowly, a complete combination of the lime requiring 10–20 days at 120° and about 5–7 days at 140°. The compounds formed are discerned in the X-ray photographs only as shadows, although most of the calcium hydroxide has been combined as silicate hydrates (Table I). After further autoclave treatment the crystallites reach dimensions facilitating an establishment of their identity. The mixtures poor in lime yield autoclave products that contain the tobermorite compound as a principal phase, as shown by its characteristic spacings 11.3, 5.47 Å. It must be emphasized, however, that the X-ray photographs of the initial hydrated products do not show the spacing 11.3 Å. Other diffraction lines, about 3.05, 2.97, 2.80 Å., usually discerned in the first products as lines of weak intensity do not necessarily indicate the tobermorite phase. The spacing 11.3 Å. appears slowly with the more intensive treatment and in relation to the increasing growth of the crystallites.

An autoclave treatment at somewhat higher temperature and reasonably extended time (160–180°, 24 hr.) does not vary the products (Table I). More intensive treatment (24–48 hr., 180–220°) introduces new reactions. The tobermorite compound earlier formed is transformed slowly into the gyrolite-phase, identified by its spacings (22, 4.76 Å.). The spacing 22 Å. is also characteristic for the compound okenite, but other spacings characteristic for this compound (8.8 Å.) are missing. The products formed by treatment at 200–220° contain in addition some amount of the xonotlite compound, shown by its spacings 7.03 and 3.65 Å. A few other diffraction lines that have not yet been identified also occur; they are listed in Table II. These lines seem to be found in the products after treatment for sufficiently extended periods of time at all the temperatures used here. A few of them coincide with some lines of the α-dicalcium monosilicate monohydrate, some others with the lines of the afwillite compound, but others, probably connected with some special phases, with neither.

TABLE II

DIFFRACTION LINES UNIDENTIFIED IN THE AUTOCLAVED PRODUCTS

130 mg. CaO/m.² quartz surface, 120–220°

I	*d* (Å.)	*I*	*d* (Å.)
w	6.60[a]	ww	2.58
w	4.94[a]	ww	2.42
w	4.46[a]	w	2.31[a]
ww	3.26	w	1.88
w	3.14[a]	w	1.80
ww	2.83		

[a] Occurring only in preparations at 180–220°.

Mixtures Rich in Lime (300 mg. and 400 mg. CaO/m.² of the quartz surface).—During an autoclave treatment at 120–140° for 1–3 days the calcium hydroxide is combined, at first to form of crystallites too small to be identified by X-rays. Later, however, the spacings of the α-dicalcium silicate monohydrate become successively more easily discernible (Table I). Further treatment of the mixture 300 mg./m.² (7–21 days) causes a transformation of this silicate into the tobermorite phase. The mixtures richer in lime (400 mg. CaO/m.²), on the other hand, contain after this period of time well crystallized α-dicalcium silicate; the X-ray photographs indicate no presence of the tobermorite phase (11.3 Å.).

On autoclaving at 160–220° for 2–48 hr. the mixtures at first yield the α-dicalcium silicate which is later successively transformed into the monocalcium silicate tobermorite, the

rate of this transformation depending on the amount of calcium hydroxide available at the beginning of the autoclaving (Table I). The more intensive treatment (200°, 24–48 hr.) causes formation of further phases in addition to the tobermorite: the gyrolite and the xonotlite compounds. Besides the diffraction lines 22 and 11.3 Å. belonging to the spacings of the gyrolite and tobermorite compounds, a shadow corresponding in about 15 Å., possibly deriving from the Z-phase earlier described, is often discernible between these two lines. No distinct diffraction line of the Z-phase has, however, been established in the present investigation.

Some comments may be made concerning two of the phases. Attempts to prepare samples of the Z-phase sufficiently pure for an estimation of its probable composition so far have been unsuccessful. The X-ray spacings of an obviously rather well-crystallized preparation, however, are listed in Table III, which contains some new lines. It also seems possible that the composition of the Z-phase could correspond to the proportion lime:silica = 1:2. Its stability in the sytem may be questioned; it is probable that this compound is also a transition phase observed in some reaction products of low lime content because of its slow rate of transformation.

TABLE III

NEW X-RAY DATA FOR THE SYNTHETIC PHASE Z

Preparation: CaO:amorphous SiO_2 = 0.40:1 and 0.50:1, autoclaved, 140°, 7 days.

I	*d* (Å.)	*I*	*d* (Å.)
s	15.1	ww	3.142
m	8.35	m-s	3.033
m	5.070	Band	3.14–3.03
w	4.390	br.,w	2.778
ww	4.165	w	2.410
w	3.786	w	1.911
w-m	3.357	s	1.817
Band	3.80–3.36	br.,w	1.336
		w	1.192

The other compound that plays an important role in the hydrothermal reactions in the present investigation is the α-dicalcium silicate monohydrate. The preparations are commonly well crystallized. The photographs of the best determinations are compared and listed in Table IV together with the observations by Heller.[4] Some discrepancies occur; the measurements of the present investigation may be relevant in the study of the hydrothermal products.

TABLE IV

X-RAY DATA OF THE α-DICALCIUM SILICATE MONOHYDRATE

A: autoclave product of 300 mg. CaO/m.² quartz surface, B: according to Heller.[4]

A		B		A		B		A		B	
I	*d* (Å.)	*d* (Å.)	*I*	*d* (Å.)	*d* (Å.)	*I*	*d* (Å.)	*d* (Å.)			
w-m	5.32	5.35	m	2.662	2.65	w	1.965	1.982			
ww	5.635	4.63	s	2.605	2.60	m	1.959	1.956			
ww	4.453	..	m	2.572	2.56	m	...	1.926			
m	4.208	4.22	ww	2.561	..	m	1.896	1.890			
w	4.139	..	s	2.528	2.52	w-m	1.875	1.872			
m	3.915	3.90	w	2.501	..	ww	1.864	...			
w-m	3.860	..	w	2.462	2.47	m	1.816	1.842			
m-s	3.540	3.54	s	2.417	2.41	m	...	1.820			
m	3.305	..	m	2.339	..	w	1.778	1.778			
s	3.271	3.27	m	2.316	2.31	w	1.772	...			
br., ww	3.128	..	m	2.302	2.27	w	1.745	...			
w	3.042	3.04	m	2.163	2.18	w	1.736	1.737			
m	2.875	2.87	w	...	2.16	w	1.714	1.712			
m	2.813	2.80	w-m	2.102	2.10	ww	1.696	1.687			
w	...	2.77	m	2.085	2.08	w	1.663	1.662			
m	2.714	2.71	s-m	2.06	2.06	m	...	1.654			
m	2.695	2.69	w	...	2.02	w	1.642	1.645			

Discussion

In the following discussion of the results it should be borne in mind that the experimental conditions during the autoclaving of a heterogeneous material such as that involved here, are such that it will always be difficult to perform experiments with the accuracy desirable for a good treatment of all the details of the problems. The results of the present investigation, however, give a sufficiently clear representation of most of the details.

The Reactions at the Phase Boundary Quartz–Lime Solution.—At the temperatures 120–220° a liquid phase of calcium hydroxide solution is necessary for a formation of calcium silicate hydrates. Lowering of the vapor pressure in the autoclave to somewhat below that of saturated steam causes a complete cessation of the reactions lime–quartz within a reasonable period of time. At the boundary, therefore, there are calcium and hydroxyl ions that will attack the silica valences at the quartz surface. The number of these ions available for the reactions will define the type of the primary products formed at that moment. It was established above that during the first moments there are two types of reactions resulting in the formation either of the monocalcium silicate tobermorite or of the α-dicalcium silicate monohydrate. The concentration limit between these two types of reactions involved is shown experimentally to lie between 130 and 300 mg. CaO/m.² quartz surface.

The reactions described above agree in some cases well, in others not, with those shown by the system amorphous silica–calcium hydroxide. The tobermorite compound and the α-dicalcium silicate hydrate are the compounds first formed when the molar proportion of amorphous silica:calcium hydroxide exceeds 1:>1. In the system quartz–calcium hydroxide this is always the case. It may be concluded from this fact, that these two types are the fundamental ones. A certain deficiency of lime favors the formation of the monocalcium silicate, *i.e.*, the tobermorite phase, an excess of lime causes the formation of the α-dicalcium silicate.

Some silicates with less lime, the gyrolite compound and the Z-phase, are reported in the system amorphous silica–calcium hydroxide. The gyrolite compound also occurs among the reaction products in the system quartz–calcium hydroxide but it always appears as a distinct secondary compound formed by an attack of the tobermorite compound on the quartz. From this it may be concluded that in the mixtures amorphous silica–calcium hydroxide silica exceeding the monocalcium proportion rapidly reacts with the monocalcium silicate first formed resulting in the formation of the gyrolite phase. The Z-phase, which is obviously an unstable compound, would possibly react as a transition phase in the presence of a substantial excess of amorphous silica.

Amorphous silica–calcium hydroxide mixtures rich in lime yield products consisting mainly of dicalcium silicates. As no essential change in molar proportions can occur in these mixtures the compound most stable at the reaction conditions will appear, *i.e.*, the hillebrandite compound mixed with the xonotlite compound when the mixture contains silica–lime in proportion 1:1–2. In the

(4) L. Heller, *Acta Cryst.*, **5**, 724 (1952).

system quartz–calcium hydroxide, on the other hand, the α-dicalcium silicate is not transformed into the β-dicalcium silicate, the hillebrandite phase, since silicon ions diffusing from the quartz surface form silicates less rich in lime. The gyrolite compound may therefore be considered as a final product of this reaction. The appearance of the monocalcium silicate, the xonotlite phase, must be referred to the slowness of the reactions which permits an indication of the metastable phases of the system. It is, however, probable that the initial reaction silica–calcium hydroxide occurs according to both the types. The mixtures calcium hydroxide–quartz can never correspond to an equal distribution of the lime along the quartz surface, there are always pores and cavities in which some lime remains. When the reaction leading to the formation of calcium silicate hydrates takes place the lime in the cavities will move toward the quartz surface and reach it by diffusion after a certain period of time.

When all calcium hydroxide has been consumed other reactions occur. The dicalcium silicate hydrate behaves as a compound producing calcium ions. Thus, the quartz surface gives off silica ions, forming the monosilicate tobermorite until all the dicalcium compound is transformed into the monosilicate. As there are no further possibilities for the formation of silicates, a subsequent phase change is dependent upon the stability of the tobermorite compound under the reaction conditions. It was shown that the monocalcium silicate tobermorite is transformed slowly into the gyrolite compound. The tobermorite phase reacts with the silica ions at the quartz surface in the same way as the dicalcium silicate does, but obviously more slowly. The gyrolite compound never appears as an initial product. It must therefore be considered as a product originating from the compound richer in lime, the tobermorite compound.

The reactions discussed above may be summarized: compound rich in lime (dicalcium silicate) → monocalcium silicate → 2:3 calcium silicate.

In addition to this it must be emphasized that the first product formed on autoclaving is always a product of nearly sub-X-ray dimensions which does not show any diffraction line.

According to a recent report by O'Connor and Greenberg[5] the attack of alkali on silica is ruled by a formation of monosilicic ions $(SiO_4)^{4-}$. From this it may be concluded here that the primary ions will be saturated immediately, partially or completely depending on the available amount of positive ions. In the mixture quartz–calcium hydroxide it may be considered that the silicic ions are released from the quartz surface as monosilicic ones, and afterwards react with the amount of calcium hydroxide available at any given moment.

Other compounds occurring in the reaction products are the xonotlite compound and the Z-phase. The xonotlite phase occurs only in products autoclaved at rather high temperature. As it is a monocalcium silicate, formed by recrystallization of the tobermorite phase by expulsion of some water, it should occur in the masses autoclaved at high temperature; it is formed at the same time or before the tobermorite compound reacts with the silica ions originating from the quartz surface. This obviously is possible when the tobermorite compound is formed at such a high temperature that the rate of the transformation tobermorite–xonotlite exceeds the rate of exchange of the silica–calcium ions through the diffusion layers. As a consequence, the xonotlite compound does occur only in products formed at the highest temperature here used (200–220°). The rather weak indication of the occurrence of the phase Z appears only in connection with a formation of the gyrolite compound; the Z-phase may also be considered as a short lived transition compound.

Another question of some importance concerns the equilibria of the system. The results above indicate a consistent, successive formation of compounds of low lime content. The compound of lowest lime content hitherto shown in the system between 160–220° is the gyrolite phase. Consequently it could be suggested that at the final equilibrium the gyrolite compound should be the stable phase. However, some minerals of lower lime content do exist, their formation conditions being unknown. For the present, however, the gyrolite phase may be considered as the final compound in the system between 160 and 220°. At lower temperature the gyrolite phase was not established but only the tobermorite phase; for the present, the latter may be considered the stable phase.

(5) T. L. O'Connor and S. A. Greenberg, THIS JOURNAL, **62**, 1195 (1958).

DOUBLE LAYER STRUCTURE AND RELAXATION METHODS FOR FAST ELECTRODE PROCESSES—THE DOUBLE PULSE GALVANOSTATIC METHOD

BY HIROAKI MATSUDA[1] AND PAUL DELAHAY

Coates Chemical Laboratory, Louisiana State University, Baton Rouge, Louisiana

Received September 21, 1959

An equation is derived for the overvoltage–time characteristic in the double pulse galvanostatic method, the structure of the double layer being considered in the boundary value problem. It is shown that a previous treatment without consideration of the double layer structure can be applied with simple modifications in the expression of the measured exchange current density. The measured transfer coefficient α_{ms}, is seriously in error in case of strong repulsion and, especially, attraction of the discharged species in the diffuse double layer. Abnormally high transfer coefficients recently reported by other investigators are interpreted. A detailed mathematical analysis is given.

The structure of the double layer at electrode–electrolyte interfaces is neglected in the solutions of boundary value problems which have been given for relaxation methods[2] in electrochemical kinetics. Such a simplification is entirely justified for not too rapid electrode processes for which the thickness of the diffusion layer is so much larger than the diffuse double layer thickness. Under such conditions kinetic parameters can be corrected[3] very simply for the double layer structure without change in the boundary value problem, *i.e.*, the original ideas of Frumkin[4] on the effect of the double layer structure on electrochemical kinetics then can be applied without further mathematical analysis. However, as will be shown below, boundary value problems must be reconsidered for rapid processes, that is, for processes having a standard rate constant larger than perhaps 0.01–0.1 cm. sec.$^{-1}$. Such fast processes can be studied quite easily thanks to the recent development of the faradaic rectification[5] and the double pulse galvanostatic[6] methods. The latter method, which is the simpler to apply, is analyzed here in detail for the double layer effect. It will be seen that correction of kinetic parameters can be very significant and that the abnormally high transfer coefficients reported by Barker,[5] and confirmed by Randles,[7] for certain processes can be interpreted. Such double layer effects cannot be dismissed even in rather concentrated electrolytes (≥ 1 M).

Boundary Value Problem

Consider the electrode reaction

$$O^{z_O} + ne = R^{z_R} \qquad (1)$$

where O and R are soluble species having the ionic valencies z_O and $z_R (z_O = z_R + n)$. R is soluble either in solution or in the electrode (amalgam; $z_R = 0$). The solution contains a large excess of z-z indifferent electrolytes which are assumed to determine entirely the double layer structure. In the absence of specific adsorption the gradient of potential in the diffuse double layer is, according to the Gouy–Chapman theory

$$d\varphi/dx = -(2RT/|z|F)\kappa \sinh (|z|F\varphi/2RT) \qquad (2)$$

with

$$1/\kappa = (RT\epsilon/8\pi z^2F^2C_t)^{1/2} \qquad (3)$$

where ρ is the electrical potential referred to the potential in the bulk of solution, ϵ is the dielectric constant, and C_t is the sum of the concentrations of z-z indifferent electrolytes.

The concentration of species i (O or R) involved in the electrode reaction at a plane electrode is a solution of[8]

$$\partial C_i/\partial t = D_i\partial/\partial x[\partial C_i/\partial x + (z_iF/RT)C_i\partial\varphi/\partial x] \qquad (4)$$

where z_i and D_i are the ionic valence and diffusion coefficient of species i, respectively. The origin of the coördinate x is taken as the plane of closest approach (Helmholtz plane). At equilibrium, *i.e.*, at $t = 0$, one has the Boltzmann distribution

$$C_i = C_i^0 \exp(-z_iF\varphi/RT) \qquad (5)$$

where C_i^0 is the bulk concentration of species i outside the double layer region. Furthermore, one has the boundary conditions

$$x \longrightarrow \infty: \; C_i \longrightarrow C_i^0 \qquad (6)$$

$$x = 0: \; D_i[\partial C_i/\partial x + (z_iF/RT)C_i\partial\varphi/\partial x] = \pm I_f/nF \qquad (7)$$

where I_f is the faradaic current density. The plus sign in front of I_f holds for species O, the minus sign for species R.

General Solution in the Form of Laplace Transform

We shall first obtain a general solution of eq. 4 in the form of a Laplace transform and then derive the inverse transform for the particular case of the double pulse galvanostatic method. We set $u_i = \mathcal{L}C_i$ as the Laplace transform[9] of the function C_i. Equations 4, 6 and 7 become after transformation

$$su_i - C_i^0 \exp(-z_iF\varphi/RT) = D_i d/dx[du_i/dx + (z_iF/RT)u_i d\varphi/dx] \qquad (8)$$

(1) Research Associate, 1958–1959; on leave from the Government Chemical Industrial Research Institute, Tokyo.

(2) For reviews see for instance, P. Delahay, "New Instrumental Methods in Electrochemistry," Interscience Publ., Inc., New York, N. Y., 1954; P. Delahay, *Ann. Rev. Phys. Chem.*, **8**, 229 (1957).

(3) M. Breiter, M. Kleinerman and P. Delahay, *J. Am. Chem. Soc.*, **80**, 5111 (1958).

(4) For a recent review, see A. N. Frumkin, *Z. Elektrochem.*, **59**, 807 (1955). See also ref. 3.

(5) G. C. Barker, R. L. Faircloth and J. A. W. Gardner, *Nature*, **181**, 247 (1958); G. C. Barker, *Anal. Chim. Acta*, **18**, 118 (1958); G. C. Barker, "Proceedings of the Symposium on Electrode Processes," Philadelphia, May, 1959, E. Yeager ed., John Wiley and Sons, Inc., New York, N. Y., in course of publication.

(6) (a) H. Gerischer and M. Krause, *Z. physik. Chem. (Frankfurt)*, **10**, 264 (1957); **14**, 184 (1958). (b) H. Matsuda, S. Oka and P. Delahay, *J. Am. Chem. Soc.*, **81**, 5077 (1959).

(7) J. E. B. Randles, "Proceedings of the Symposium on Electrode Processes," Philadelphia, May, 1959, E. Yeager ed., John Wiley and Sons, Inc., New York, N. Y., in course of publication.

(8) See for instance, B. Levich, *Dokl. Acad. Nauk*, **67**, 309 (1949).

(9) See for instance, R. V. Churchill, "Modern Operational Mathematics in Engineering," McGraw-Hill Book Co., New York, N. Y., 1944.

$$x \longrightarrow \infty: \; u_i \longrightarrow C_i^0/s \tag{9}$$

$$x = 0: \; D_i[\mathrm{d}u_i/\mathrm{d}x + (z_iF/RT)u_i\mathrm{d}\varphi/\mathrm{d}x] = \mathfrak{L}(\pm I_f/nF) \tag{10}$$

s being the parameter for transformation

The general solution, derived in the Appendix, is at $x = 0$, *i.e*, in the Helmholtz plane ($u_i = u_i^*$ at $x = 0$)

$$u_i^* = \exp(-z_iF\varphi_0/RT)\{(C_i^0/s) - [\mathfrak{L}(\pm I_f/nF)](1/D_is)^{1/2}\,G_i\} \tag{11}$$

with

$$G_i = \xi_0^{2p+2}\,\frac{\begin{matrix}K_{p+1/2}[(2/\kappa)(s/D_i)^{1/2}\,\xi_0^{-1}]\{I_{p+3/2}[(2/\kappa)(s/D_i)^{1/2}] + I_{p+1/2}[(2/\kappa)(s/D_i)^{1/2}]\} + \\ I_{p+1/2}[(2/\kappa)(s/D_i)^{1/2}\,\xi_0^{-1}]\{K_{p+3/2}[(2/\kappa)(s/D_i)^{1/2}] - K_{p+1/2}[(2/\kappa)(s/D_i)^{1/2}]\}\end{matrix}}{\begin{matrix}K_{p+3/2}[(2/\kappa)(s/D_i)^{1/2}\,\xi_0^{-1}]\{I_{p+3/2}[(2/\kappa)(s/D_i)^{1/2}] + I_{p+1/2}[(2/\kappa)(s/D_i)^{1/2}]\} - \\ I_{p+3/2}[(2/\kappa)(s/D_i)^{1/2}\,\xi_0^{-1}]\{K_{p+3/2}[(2/\kappa)(s/D_i)^{1/2}] - K_{p+1/2}[(2/\kappa)(s/D_i)^{1/2}]\}\end{matrix}} \tag{12}$$

$$p = \pm(|z_i|/|z|) - 1 \tag{13}$$

$$\xi_0 = \exp(|z|F|\varphi_0|/2RT) \tag{14}$$

Further notations: φ_0 is the potential in the Helmholtz plane; and the I_ν's and the K_ν's are modified Bessel functions of the ν-th order and of the first and second kind, respectively. *The upper and lower signs in eq. 13 correspond to the cases $z_i\varphi > 0$ and $z_i\varphi < 0$, respectively.*

General Current–Overvoltage Relationship in the Form of Laplace Transform

The faradaic current density I_f for processes corresponding to eq. 1 is for a rate-determining step involving n electrons[2]

$$I_f = (I_0)_{app}\left\{\begin{matrix}(C_O^*/C_O^0)\exp(z_OF\varphi_0/RT)\exp[(-\alpha nF/RT)(E - E_e)] - \\ (C_R^*/C_R^0)\exp(z_R\,F\varphi_0/RT)\exp[\{(1-\alpha)nF/RT\}\,(E - E_e)]\end{matrix}\right\} \tag{15}$$

with

$$(I_0)_{app} = I_0\exp[(\alpha n - z_O)F\varphi_0/RT] \tag{16}$$

$$I_0 = nFk_sC_O^{0(1-\alpha)}C_R^{0\alpha} \tag{17}$$

where I_0 is the exchange current density, $(I_0)_{app}$ the apparent exchange current density, k_s the standard rate constant, α the transfer coefficient, E the electrode potential, E_e the equilibrium electrode potential corresponding to the bulk concentrations, φ_0 the potential in the Helmholtz plane, the C^*'s the concentrations in the Helmholtz plane, and the C^0's the bulk concentrations. When $(E-E_e) << \alpha nF/RT$ (or $(1-\alpha)nF/RT$), *i.e.*, for overvoltages not exceeding a few millivolts, eq. 15 can be linearized and φ_0 can be regarded as constant in the interval $E-E_e$ (but φ_0 varies with E_e). Thus

$$I_f = (I_0)_{app}\left\{\begin{matrix}(C_O^*/C_O^0)\exp(z_OF\varphi_0/RT) - \\ (C_R^*/C_R^0)\exp(z_RF\varphi_0/RT) - \\ (nF/RT)(E - E_e)\end{matrix}\right\} \tag{18}$$

The Laplace transform of eq. 18 is

$$\mathfrak{L}I_f = (I_0)_{app}\left\{\begin{matrix}(u_O^*/C_O^0)\exp(z_OF\varphi_0/RT) - \\ (u_R^*/C_R^0)\exp(z_RF\varphi_0/RT) - \\ (nF/RT)\,\mathfrak{L}(E - E_e)\end{matrix}\right\} \tag{19}$$

or, in view of eq. 11

$$\mathfrak{L}I_f = -\frac{nF}{RT}\,\frac{(I_0)_{app}}{1 + \dfrac{(I_0)_{app}}{nF}\left(\dfrac{G_O}{C_O^0D_O^{1/2}} + \dfrac{G_R}{C_R^0D_R^{1/2}}\right)\dfrac{1}{s^{1/2}}}\,\mathfrak{L}(E - E_e) \tag{20}$$

where the functions G_O and G_R are defined by eq. 12.

The cell current density in electrolysis also includes a capacity current density component I_c due to the charging or discharging of the double layer. One has

$$I_c = c_1\,\mathrm{d}(E - E_e)/\mathrm{d}t \tag{21}$$

where c_1 is the differential capacity of the double layer per unit area (assumed to be constant in the interval $E - E_e$ of a few millivolts). By noting that

$$\mathfrak{L}I_c = -c_1\,s\mathfrak{L}(E - E_e) \tag{22}$$

and that the cell current density $I_t = I_f + I_c$, one obtains the general current–overvoltage characteristic in the form of Laplace transform

$$\mathfrak{L}(E - E_e) = -\frac{\mathfrak{L}I_t}{c_1}\,\frac{s^{1/2} + \dfrac{(I_0)_{app}}{nF}\left(\dfrac{G_O}{C_O^0D_O^{1/2}} - \dfrac{G_R}{C_R^0D_R^{1/2}}\right)}{s^{1/2}\left[s + \dfrac{(I_0)_{app}}{nF}\left(\dfrac{G_O}{C_O^0D_O^{1/2}} + \dfrac{G_R}{C_R^0D_R^{1/2}}\right)s^{1/2} + \dfrac{nF}{RT}\,\dfrac{(I_0)_{app}}{c_1}\right]} \tag{23}$$

Overvoltage–Time Relationship for the Double Pulse Galvanostatic Method

The inverse Laplace transform of eq. 23 gives the overvoltage–time characteristic for current-controlled method. In the double pulse method the current density I_t varies in steps from 0 to I_1 for $0 \leqslant t \leqslant t_1$, and from I_1 to I_2 for $t \geqslant t_1$. Inverse transformation, however, is very involved in view of the nature of the functions G_O and G_R ,and we shall only consider a limiting case which, at any rate, corresponds to practical conditions.

The thickness of the diffuse double layer $1/\kappa$ is smaller than 10^{-7} cm. for fairly concentrated electrolytes (the value 10^{-7} cm. corresponds to a 0.1 M solution of a 1-1 electrolyte). Conversely the thickness of the diffusion layer, which is of the order of $(\pi D_it)^{1/2}$, may exceed 5×10^{-6} cm. (this value corresponds to $t = 1$ microsec.). Since t is the order of a few microseconds in the double pulse galvanostatic method, one has $1/\kappa(D_it)^{1/2} << 1$. The functions G_O and G_R defined by eq. 12 can be expanded according to a procedure not too uncommon in the application of Laplace transforms[10]

$$G_i = 1 + a_i(1/\kappa D_i^{1/2})s^{1/2} + \ldots\ldots \tag{24}$$

with

$$a_i = \frac{\exp[F(\pm|z_i| - |z|/2)|\varphi_0|/RT] - 1}{\pm|z_i/z| - 1/2} - \frac{\exp[F(\mp|z_i| - |z|/2)|\varphi_0|/RT] - 1}{\mp|z_i/z| - 1/2} \tag{25}$$

where the upper and lower signs in front of $|z_i/z$ correspond to $z_i\varphi_0 > 0$ and $z_i\varphi_0 < 0$, respectively. By retaining only two terms in eq. 24, one obtains after introduction in eq. 23

(10) H. S. Carslaw and J. C. Jaeger, "Conduction of Heat in Solids," Oxford University Press, London, 1947, p. 264.

$$\mathfrak{F}(E - E_e) = -(\mathfrak{F}I_t/c_1)(s^{1/2} + B_1)/s^{1/2}(s + B_1 s^{1/2} + B_2) \quad (26)$$

with

$$B_1 = \frac{[(I_0)_{app}/nF][(1/C_O{}^0 D_O{}^{1/2}) + (1/C_R{}^0 D_R{}^{1/2})]}{1 + [(I_0)_{app}/nF][a_O/\kappa C_O{}^0 D_O) + (a_R/\kappa C_R{}^0 D_R)]} \quad (27)$$

$$B_2 = \frac{(nF/RT)[(I_0)_{app}/c_1]}{1 + [(I_0)_{app}/nF][(a_O/\kappa C_O{}^0 D_O) + (a_R/\kappa C_R{}^0 D_R)]} \quad (28)$$

Equation 26 is the same as the result obtained by ignoring the effect of the double layer structure, except that in previous results[11] the denominators in the constants B_1 and B_2 are equal to unity. In view of our previous result,[6] the overvoltage–time characteristic is

$$E - E_e = \frac{I_1}{c_1}\frac{1}{\beta - \gamma}\left\{\begin{array}{l}(\gamma/\beta^2)[\exp(\beta^2 t)\,\mathrm{erfc}(\beta t^{1/2}) + 2\beta(t/\pi)^{1/2} - 1] - \\ (\beta/\gamma^2)[\exp(\gamma^2 t)\,\mathrm{erfc}(\gamma t^{1/2}) + 2\gamma(t/\pi)^{1/2} - 1]\end{array}\right\} - \frac{I_1 - I_2}{c_1}\frac{1}{\beta - \gamma}\left\{\begin{array}{l}(\gamma/\beta^2)\{\exp[\beta^2(t - t_1)]\mathrm{erfc}[\beta(t - t_1)^{1/2}] + 2\beta[(t - t_1)/\pi]^{1/2} - 1\} - \\ (\beta\gamma^2)\{\exp[\gamma^2(t - t_1)]\mathrm{erfc}[\gamma(t - t_1)^{1/2} + 2\gamma[(t - t_1)/\pi]^{1/2} - 1\}\end{array}\right\} \quad (29)$$

with

$$\beta, \gamma = (1/2)[B_1 \pm (B_1{}^2 - 4B_2)^{1/2}] \quad (30)$$

Equation 29 holds for $t > t_1$, and this equation with only the first term on the right-hand side holds for $0 < t < t_1$.

By transposition of a previous result,[6b] one deduces that the overvoltage, $E_h - E_e$, at time t_1 for the overvoltage–time curve with a horizontal tangent at t_1 is, for sufficiently small values of t_1

$$E_h - E_e = -\frac{RT}{nF} I_2 \left\{\begin{array}{l}[1/(I_0)_{app}] + (1/nF)[(a_O/\kappa C_O{}^0 D_O) + (a_R/\kappa C_R{}^0 D_R)] + \\ (4/3\pi^{1/2})(1/nF)[(1/C_O{}^0 D_O{}^{1/2}) + 1/C_R{}^0 D_R{}^{1/2})]t_1{}^{1/2} + \ldots\end{array}\right\} \quad (31)$$

A plot of $E_h - E_e$ against $t_1{}^{1/2}$ for sufficiently small values of t_1 yields a straight line whose intercept is

$$-(RT/nF)I_2\{[1/(I_0)_{app}] + (1/nF')[(a_O/\kappa C_O{}^0 D_O) + (a_R/\kappa C_R{}^0 D_R)]\}$$

or $-(RT/nF)I_2[1/(I_0)_{ms}]$, where the measured exchange current density $(I_0)_{ms}$ that is obtained by neglecting the double layer structure is

$$(I_0)_{ms} = \frac{(I_0)_{app}}{1 + [(I_0)_{app}/nF][(a_O/\kappa C_O{}^0 D_O) + (a_R/\kappa C_R{}^0 D_R)]} \quad (32)$$

It turns out that eq. 32 is identical, in the case of repulsion of the discharged species (not for attraction), with a result previously derived[21] for steady-state electrolysis by the solving of eq. 4 for $\partial C_i/\partial t = 0$. The approximation on the G_i function in eq. 24 thus amounts (a) to neglecting the time variation of the concentrations in the derivation of the double layer correction, and (b) to considering the effect of migration in the double layer as embodied in eq. 4.

(11) Compare with eq. 35 for the single pulse galvanostatic method, T. Berzins and P. Delahay, *J. Am. Chem. Soc.*, **77**, 6448 (1955); compare also with eq. 9 in ref. 6 for the double pulse method.

(12) H. Matsuda and P. Delahay, discussion of a paper by L. Gierst in "Proceedings of the Symposium on Electrode Processes," Philadelphia, May 1959, E. Yeager ed., John Wiley and Sons, Inc., New York, N. Y., in course of publication. See also Gierst's paper in the same volume. *Cf.* also Levich.[8]

Dependence of the Measured Exchange Current Density and Transfer Coefficient on the Double Layer Structure

The following discussion of eq. 32 will be limited to the important case of metal deposition ($a_R = 0$; see eq. 25), but transposition to other cases is immediate.

It follows from eq. 32 that $(I_0)_{ms} \rightarrow (I_0)_{app}$ when $a_O \rightarrow 0$, *i.e.*, when the potential φ_0 in the Helmholtz plane approaches zero (see eq. 25). One has $(I_0)_{ms} < (I_0)_{app}$ when $z_O\varphi_0 > 0$ and $|z_O/z| > 1/2$, *i.e.*, when z_O and φ_0 have the same sign and there is repulsion of the species being discharged. Conversely, $(I_0)_{ms} > (I_0)_{app}$ when $z_O\varphi_0 < 0$ and $|z_O/z| > 1/2$, *i.e.*, for attraction of the discharged species. The effect is quite pronounced (Fig. 1), especially in the case of attraction, even when the φ_0 is quite small (1 *M* solution of a 1-1 electrolyte).

It is seen in Fig. 1 that $(I_0)_{app}/(I_0)_{ms}$ can become negative when the discharged ion is sufficiently attracted in the diffuse double layer. This implies that $(I_0)_{ms}$ is negative or that one has for the extrapolated overvoltage at $t_1 = 0$, $E - E_e > 0$ in a reduction or $E - E_e < 0$ in an oxidation. Under these conditions, the overvoltage deduced from the plot of $E_h - E_e$ against $t_1{}^{1/2}$ according to eq. 31 has the opposite sign of the one to be expected. Proper correction for the double layer eliminates this abnormality. One also should not overlook that eq. 32 is approximate.

The transfer coefficient α_{ms} which one deduces from $(I_0)_{ms}$ also can be seriously in error. Thus, one has, by definition, for the true transfer coefficient α (see eq. 17)

$$\alpha = 1 - \partial \log I_0/\partial \log C_O{}^0 \quad (33)$$

at constant $C_R{}^0$. By analogy one can define

$$\alpha_{app} = 1 - \partial \log (I_0)_{app}/\partial \log C_O{}^0 \quad (34)$$

$$\alpha_{ms} = 1 - \partial \log (I_0)_{ms}/\partial \log C_O{}^0 \quad (35)$$

In view of eq. 16 and of the Nernst equation one has

$$\alpha_{app} = \alpha - [\alpha - (z_O/n)](\partial|\varphi_0|/\partial E)_{e=E_e} \quad (36)$$

One deduces from eq. 32, as written for $a_R = 0$ (metal deposition), and eq. 35

$$\alpha_{ms} = \alpha_{app}\left\{1 - \frac{[(I_0)_{app}/nF](a_O/\kappa C_O{}^0 D_O)}{1 + [(I_0)_{app}/nF](a_O/\kappa C_O{}^0 D_O)}\left[1 - \frac{1}{\alpha_{app}}\frac{d \log |a_O|}{d \log C_O{}^0}\right]\right\} \quad (37)$$

or by noting that

$$d \log |a_O|/d \log C_O{}^0 = (d \log |a_O|/d |\varphi_0|) \times (d |\varphi_0|/dE_e)(dE_e/d \log C_O{}^0) \quad (38)$$

$$d \log |a_O|/d \log |\varphi_0| \approx (|z_O| - |z|/2)F/2.3RT \quad (39)$$

one transforms the term $[1 - (1/\alpha_{app})(d \log|a_O|/d \log C_O{}^0)]$ in eq. 37 into $\{1 - [\partial|\varphi_0|/\partial E]_{EE=e} - [|z_O| - |z|/2]/\alpha_{app}n\}$. If one neglects the term in $[\partial|\varphi_0|/\partial E]_{E=E_e}$ one can write, as a first approximation

$$\alpha_{app}/\alpha_{ms} = (I_0)_{app}/(I_0)_{ms} \quad (40)$$

Abnormally low values of α_{ms} are obtained for repulsion, and abnormally high α_{ms} are measured for attraction (*cf.* Fig. 1).

Abnormally high transfer coefficients were reported recently by Barker[5] and Randles[7] for fast electrode processes involving species that were specifically adsorbed on the electrode or at least strongly attracted in the diffuse double layer. These transfer coefficients were not obtained by the double pulse method but it seems likely, in view of the foregoing analysis, that the rather puzzling results of Barker and Randles can be accounted for by the double layer effect discussed above.

Experimental study of fast processes by the double pulse method is now in progress in this Laboratory for cases of repulsion (discharge of mercurous ion on mercury) and attraction (discharge of alkali metals on their amalgams) under conditions in which specific adsorption is minimized.

Conclusion

The structure of the double layer must be considered in the solution of boundary value problems in relaxation methods for fast electrode processes. Otherwise, erroneous exchange current densities and abnormally low or high transfer coefficients are obtained. Extension of these ideas to alternating current methods for fast processes is now being considered.

Appendix

Derivation of the General Solution of Equation II

The problem stated in eq. 8–10 will be solved by the use of a mathematical device, namely, the division of the electrolyte solution into two regions inside ($0 \leq x \leq \delta$) and outside ($\delta \leq x$) the diffuse double layer. This approach is quite justified since the potential according to Gouy and Chapman decreases exponentially with x at sufficient distances from the electrode.

Region $0 \leq x \leq \delta$.—A new variable and function are introduced according to

$$u_i = \exp(-z_i F\varphi/RT)(C_i^0/s - v_i) \quad (41)$$

$$\xi = \exp(|z|F|\varphi|/2RT) \quad (42)$$

In view of eq. 2 one has

$$d/dx = (d\xi/dx)(d/d\xi) = -(\kappa/2)[\exp(|z|F|\varphi|/RT) - 1] \times (d/d\xi) = (\kappa/2)(1 - \xi^2)(d/d\xi) \quad (43)$$

or for $\exp(F|z\varphi_0|/RT) >> 1$ (φ_0 the potential in the Helmholtz plane, *i.e.*, the largest possible value of φ)

$$d/dx \approx -(\kappa/2)\xi^2(d/d\xi) \quad (44)$$

Equation 8 now becomes

$$(d/d\xi)[\xi^{-2p}(dv_i/d\xi)] - (2/\kappa)^2(s/D_i)\xi^{-2p-4}v_i = 0 \quad (45)$$

p being defined by eq. 13. Equation 45 is equivalent to a modified Bessel equation of $(p + 1/2)$-th order of the form[13]

$$d^2w_i/d\eta^2 + (1/\eta)(dw_i/d\eta) - [1 + (p + 1/2)^2/\eta^2]w_i = 0 \quad (46)$$

as one can show by setting

$$\eta = (2/\kappa)(s/D_i)^{1/2}\xi^{-1} \text{ and } v_i = \xi^{p+1/2}w_i \quad (47)$$

in eq. 45. The general solution of eq. 45 is

$$v_i = \{[z(\pm I_f/nF)]/(D_i s)^{1/2}\}\xi^{p+3/2}\xi^{p+1/2} \times \{A_1 I_{p+1/2}[(2/\kappa)(s/D_i)^{1/2}\xi^{-1}] + A_2 K_{p+1/2}[(2/\kappa)(s/D_i)^{1/2}\xi^{-1}]\} \quad (48)$$

(13) T. v. Karman and M. A. Biot, "Mathematical Methods in Engineering," McGraw-Hill Book Co., New York, N. Y., 1940, p. 66.

where I_ν and K_ν are modified Bessel functions of ν-th order and of the first and second kind, respectively, and A_1 and A_2 are integration constants to be determined for the boundary conditions at $x = 0$ and $x = \delta$.

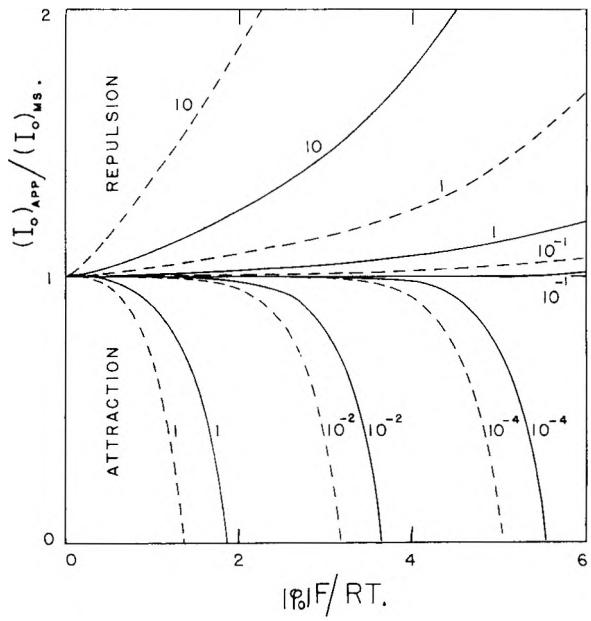

Fig. 1.—Variations of $(I_0)_{app}/(I_0)_{ms}$ with the potential φ_0 in the Helmholtz plane for different exchange current densities I_0 (in amp. cm.$^{-2}$; see eq. 17). Solid and dashed curves correspond to $1/\kappa = 3 \times 10^{-8}$ cm. and $1/\kappa = 10^{-7}$ cm., respectively, *i.e.*, to approximately 1 and 0.1 M solution of a 1-1 electrolyte, respectively. Note that $|\varphi_0|F/RT = 1$ corresponds approximately to $|\varphi_0| = 0.025$ volt at 25°. Data used in calculations: $\alpha = 0.5$, $z_O = n = 2$, $z_R = 0$, $C_O = 10^{-6}$ mole cm.$^{-3}$, $D_O = 10^{-5}$ cm.^{2} sec.$^{-1}$.

Equation 10 holds at $x = 0$ while at $x = \delta$ one has

$$D_i(\partial u_i/\partial x) = h\xi_0 p + 3/2 z(\pm I_f/nF) \quad (49)$$

where h is a constant to be determined below from the continuity for mass transfer. By noting further that $\xi = \xi_0$ at $x = 0$ and $\xi = 1$ at $x = \delta$ one obtains systems of linear equations in A_1 and A_2

$$-A_1 I_{p+3/2}[(2/\kappa)(s/D_i)^{1/2}\xi_0^{-1}] + A_2 K_{p+3/2}[(2/\kappa)(s/D_i)^{1/2}\xi_0^{-1}] = 1 \quad (50)$$

$$-A_1 I_{p+3/2}[(2/\kappa)(s/D_i)^{1/2}] + A_2 K_{p+3/2}[(2/\kappa)(s/D_i)^{1/2}] = h \quad (51)$$

Thus

$$A_1 = \frac{K_{p+3/2}[(2/\kappa)(s/D_i)^{1/2}] - hK_{p+3/2}[(2/\kappa)(s/D_i)^{1/2}\xi_0^{-1}]}{\{K_{p+3/2}[(2/\kappa)(s/D_i)^{1/2}\xi_0^{-1}]I_{p+3/2}[(2/\kappa)(s/D_i)^{1/2}] - \{I_{p+3/2}[(2/\kappa)(s/D_i)^{1/2}\xi_0^{-1}]K_{p+3/2}[(2/\kappa)(s/D_i)^{1/2}]\}} \quad (52)$$

and A_2 is given by the same equation but with the numerator

$$I_{p+3/2}[(2/\kappa)(s/D_i)^{1/2}\xi_0^{-1}] - hI_{p+3/2}[(2/\kappa)(s/D_i)^{1/2}]$$

Region $x \geq \delta$.—One has $\varphi = 0$ outside the double layer and the solution of eq. 8 for $\varphi = 0$ and for the boundary conditions of eqs. 9 and 49 for $\varphi = 0$ is

$$u_i = (C_i^0/s) - \{[z(\pm I_f/nF)]/(D_i s)^{1/2}\}h\xi_0 p + 3/2 \times \exp[-(s/D_i)^{1/2}(x - \delta)] \quad (53)$$

At $x = \delta$ this value of u_i should be identical to the value given by eq. 48, and consequently one must have

$$h = A_1 I_{p+1/2}[(2/\kappa)(s/D_i)^{1/2}] + A_2 K_{p+1/2}[(2/\kappa)(s/D_i)^{1/2}] \quad (54)$$

The solution of this linear equation in h is

$$h = \frac{K_{p+3/2}[(2/\kappa)(s/D_i)^{1/2}]I_{p+1/2}[(2/\kappa)(s/D_i)^{1/2}] + I_{p+3/2}[(2/\kappa)(s/D_i)^{1/2}]K_{p+1/2}[(2/\kappa)(s/D_i)^{1/2}]}{K_{p+3/2}[(2/\kappa)(s/D_i)^{1/2}\xi_0^{-1}]\{I_{p+3/2}[(2/\kappa)(s/D_i)^{1/2}] + I_{p+1/2}[(2/\kappa)(s/D_i)^{1/2}]\} - I_{p+3/2}[(2/\kappa)(s/D_i)^{1/2}\xi_0^{-1}]\{K_{p+3/2}[(2/\kappa)(s/D_i)^{1/2}] - K_{p+1/2}[(2/\kappa)(s/D_i)^{1/2}]\}}$$

After introduction of this value of h in eq. 48 and setting $x = 0$ one obtains eq. 11 and 12.

Acknowledgment.—The support of the Office of Naval Research is gladly acknowledged.

DOUBLE LAYER STRUCTURE AND ELECTRODE PROCESSES WITH A PRECEDING CHEMICAL REACTION

BY HIROAKI MATSUDA[1]

Coates Chemical Laboratory, Louisiana State University, Baton Rouge, Louisiana

Received September 21, 1959

An analysis is made of the influence of the double layer structure on electrode processes with a pseudo-first order preceding chemical reaction in which a non-reducible (non-oxidizable) substance (Y) is transformed into a reducible (oxidizable) one (O) in presence of a large excess of another reactant (X). The concentration of O in the Helmholtz plane is derived, and several particular forms of the resulting equation are reported. It is shown that the magnitude of the double layer effect depends, among several factor, on the ratio of the diffuse double layer thickness ($1/\kappa$) to the reaction layer thickness (μ). When $(1/\kappa) \ll \mu$ there is hardly any double layer effect; when $(1/\kappa) \gg \mu$ the double layer effect can be analyzed in terms of a simple Boltzmann distribution. The general equation is applied to the derivation of the transition time in chronopotentiometry and the limiting current in polarography.

The influence of the double layer structure on electrode processes with a preceding chemical reaction (so-called kinetic processes) was recently discussed in a paper from this Laboratory[2] and by Gierst.[3] It was shown in these investigations that the polarographic and galvanostatic characteristics of kinetic processes are accounted for by a simple Boltzmann correction for the concentrations of reactants in the plane of closest approach (Helmholtz plane). A more rigorous approach[4] in which the double layer structure is considered in the solution of the boundary value problem was announced by Gierst.[3b] The same problem is considered here but for conditions somewhat more general than those mentioned by Gierst.[3b] Equations are derived by the limiting current in polarography and the transition time in chronopotentiometry (galvanostatic method) for the reactions

$$Y^{(z_Y)} \rightleftarrows O^{(z_O)} + \nu X^{(z_X)} \quad (z_Y = z_O + \nu z_X) \quad \text{(I)}$$

$$Y^{(z_Y)} + \nu X^{(z_X)} \rightleftarrows O^{(z_O)} \quad (z_Y + \nu z_X = z_O) \quad \text{(II)}$$

where Y and X are not reduced or oxidized at the potential at which substance O is reduced.

General Assumptions

For the sake of simplicity, we introduce the assumptions:

(i) The solution contains a large excess of indifferent z–z electrolytes, which essentially determine the double layer structure. According to the Gouy–Chapman theory of the diffuse double layer one has

$$d\varphi/dx = -2(RT/|z|F)\kappa \sinh(|z|F\varphi/2RT) \quad (1)$$

with

$$(1/\kappa) = (RT\epsilon/8\pi z^2F^2C_t)^{1/2} \quad (2)$$

where φ is the electrical potential, ϵ the dielectric constant and C_t the sum of the bulk concentrations of indifferent electrolytes.

(ii) The thickness of the diffuse double layer δ and the reaction layer μ are very small in comparison with the diffusion layer thickness δ', and consequently the time-variation of the concentrations of substances O and Y within the former two layers can be neglected.

(iii) The solution contains a large excess of substances X in comparison with the concentrations of O and Y. The concentration distribution of X thus is independent of time during electrolysis and is not influenced by current flowing. One has

$$C_X = C_X^0 \exp(-z_XF\varphi/RT) \quad (3)$$

where C_X^0 is the bulk concentration of X.

(iv) The equilibrium between the substances O and Y is greatly in favor of Y, *i.e.*

$$(C_O^0/C_Y^0) \ll 1 \quad (4)$$

where the C^0's are the bulk concentrations.

Since the flux of Y at the Helmholtz plane is zero and the thicknesses δ and μ are assumed to be very small, one can assume on the basis of condition (4), that the concentration of Y in the diffuse double layer and reaction layer is much larger than that of O. Hence, the concentration distribution of Y in these two layers is given by the Boltzmann distribution

$$C_Y = C_Y^S \exp(-z_YF\varphi/RT) \text{ for } x < \delta, \mu \quad (5)$$

where $C_Y^{S'}$, the concentration of Y outside the diffuse double and reaction layers, is a function of time.

Formulation of Problem

Region within the Reaction and Diffuse Double Layers.—The differential equation for the concentration distribution of O is

(1) Research associate, 1958–1959; on leave from the Government Chemical Industrial Research Institute, Tokyo.

(2) M. Breiter, M. Kleinerman and P. Delahay, *J. Am. Chem. Soc.*, **80**, 5111 (1958).

(3) (a) L. Gierst, "Cinetique d'approche et reactions d'electrodes irreversibles," these d'agregation, University of Brussels, 1958; (b) L. Gierst, "Proceedings of the Symposium on Electrode Processes," Philadelphia, May, 1959. E. Yeager, editor, John Wiley and Sons, Inc., New York, N. Y., in course of publication.

(4) L. Gierst and H. Hurwitz, *Z. Elektrochem.*, in press.

For the reaction (I)

$$D_0(\partial/\partial x)\{\partial C_0/\partial x + (z_0F/RT)C_0\,\partial\varphi/\partial x\} + \{k_fC_Y^S \exp(-z_YF\varphi/RT) - k_b(C_X^0)^\nu \exp(-\nu z_XF\varphi/RT)C_0\} = 0 \quad (6)$$

and for the reaction (II)

$$D_0(\partial/\partial x)\{\partial C_0/\partial x + (z_0F/RT)C_0\partial\varphi/\partial x\} + k_fC_X^S(C_X^0)^\nu \exp[-(z_Y + \nu z_X)F\varphi/RT] - k_B\,C_0\} = 0 \quad (7)$$

where C_Y is expressed on the basis of eq. 5 and the k's are rate constants for the reaction (I) and (II). The boundary condition at $x = 0$ is

$$(I/nF) = D_0\{\partial C_0/\partial x + (z_0F/RT)C_0\partial\varphi/\partial x\}_{x=0} \quad (8)$$

where I is the current density, D_0 the diffusion coefficient of substance O, and n the number of electrons involved in the charge transfer process.

Region outside the Reaction and Diffuse Double Layers.—The differential equation for the concentration distribution of Y is

$$\partial C_Y/\partial t = D_Y\partial^2C_Y/\partial x^2 \quad (9)$$

for a plane stationary electrode, and

$$\partial C_Y/\partial t = D_Y\partial^2C_Y/\partial x^2 + (2x/3t)\,\partial C_Y/\partial x \quad (10)$$

for the dropping mercury electrode. The initial and boundary conditions are

$$t = 0:\ C_Y = C_Y^0 \quad (11)$$

$$\left.\begin{aligned} x &\longrightarrow \infty:\ C_Y \longrightarrow C_Y^0 \\ x &= \delta \text{ or } \mu:\ D_Y(\partial C_Y/\partial x) = (I/nF) \end{aligned}\right\} \quad (12)$$

Since the thicknesses δ and μ are both very small in comparison with δ', the last condition is equivalent to

$$x = 0:\ D_Y(\partial C_Y/\partial x) = (I/nF)$$

General Solution

The solution of eq. 6 for reaction I and the above conditions is (see Appendix)

$$C_0^* = \exp(-z_0F\varphi_0/RT)K_d(C_X^0)^{-\nu} \times \left\{C_Y^S - \frac{(I/nFD_0^{1/2})}{K_d[k_b/(C_X^0)^\nu]^{1/2}}\,G_I\right\} \quad (13)$$

with

$$G_I = \xi_0^{2p+q}\,\frac{K_{p/q}[(2/\kappa\mu|q|)\xi_0^{-q}]\{(q/|q|)I_{(p/q)+1}(2/\kappa\mu|q|) + I_{p/q}(2/\kappa\mu|q|)\} + I_{p/q}[(2/\kappa\mu|q|)\xi_0^{-q}]\{(q/|q|)K_{(p/q)+1}(2/\kappa\mu|q|) - K_{p/q}(2/\kappa\mu|q|)\}}{K_{(p/q)+1}[(2/\kappa\mu|q|)\xi_0^{-q}]\{I_{(p/q)+1}(2/\kappa\mu|q|) + (q/|q|)I_{p/q}(2/\kappa\mu|q|)\} - I_{(p/q)+1}[(2/\kappa\mu|q|)\xi_0^{-q}]\{K_{(p/q)+1}(2/\kappa\mu|q|) - (q/|q|)K_{p/q}(2/\kappa\mu|q|)\}} \quad (14)$$

$$\xi_0 = \exp(|z|F|\varphi_0|/2RT) \quad (15)$$

$$p = [\pm|z_0| - (|z|/2)]/|z| \quad (16)$$

$$q = [\pm|z_Y| \mp |z_0| + |z|]/|z| \quad (17)$$

$$\mu = [D_0/k_b(C_X^0)^\nu]^{1/2} \quad (18)$$

There, C_0^* is the concentration of O in the Helmholtz plane, C_X^0 is the bulk concentration of X, φ_0 is the potential in this plane with respect to the bulk of the solution, K_d is the dissociation constant of substance Y, and $I_{p/q}$ and $K_{p/q}$ are modified Bessel functions of the first and second kinds, respectively. The upper and lower sign in eq. 16 and 17 correspond to the case of $Z_0\varphi_0 > 0$ and $z_0\varphi_0 < 0$, respectively, or the case $z_Y\varphi_0 > 0$ and $z_Y\varphi_0 < 0$.

For reaction II, the solution of the corresponding eq. 7 for the above conditions is (see appendix)

$$C_0^* = \exp[-z_0F\varphi_0/RT)K_a(C_X^3)^\nu \times \left\{C_Y^S - \frac{(I/nFD_0^{1/2})}{K_a(C_X^0)^\nu k_b^{1/2}}\,G_{II}\right\} \quad (19)$$

with

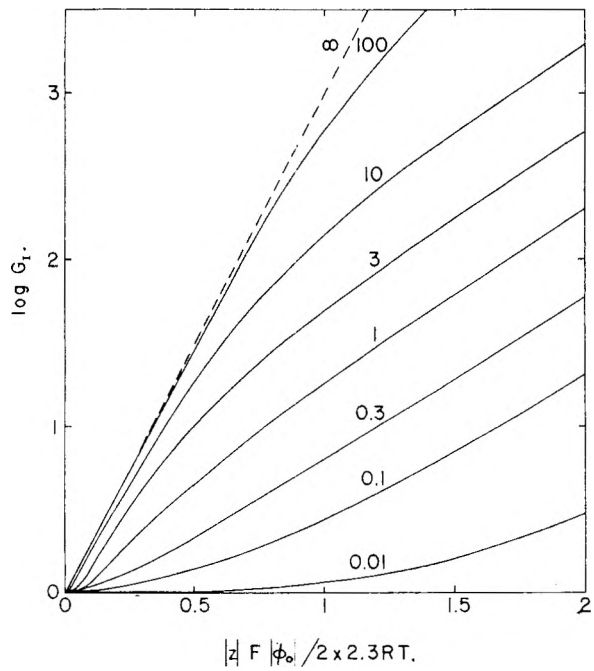

Fig. 1.—Variations of G_I (eq. 14) with the potential φ_0 in the Helmholtz plane for $p = 1/2$ and $q = 2$. Number on each curve is the value of $1/\kappa\mu$.

$$G_{II} = \xi_0^{2p+1}\,\frac{K_p[(2/\kappa\mu')\xi_0^{-1}]\{I_{p+1}(2/\kappa\mu') + I_p(2/\kappa\mu')\} + I_p[(2/\kappa\mu')\xi_0^{-1}]\{K_{p+1}(2/\kappa\mu') - K_p(2/\kappa\mu')\}}{K_{p+1}(2/\kappa\mu')\xi_0^{-1}]\{I_{p+1}(2/\kappa\mu') + I_p(2/\kappa\mu')\} - I_{p+1}[(2/\kappa\mu')\xi_0^{-1}]\{K_{p+1}(2/\kappa\mu') - K_p(2/\kappa\mu')\}} \quad (20)$$

$$\mu' = (D_0/k_b)^{1/2} \quad (21)$$

where $K_a = k_f/k_b$, and $q = 1$.

If one replaces $k_bG_I^{-2}$ in eq. 13 and $k_bG_{II}^{-2}$ in eq. 19 by an apparent rate constant k_b' one obtains the usual expressions for the concentration of O at the electrode surface which are derived without consideration of the double layer structure. The effect of the double layer structure thus can be determined from the properties of the functions G_I and G_{II}.

Some of these properties are apparent from Figs. 1 and 2 which were constructed[5] for $z = 1$ and for the values of p and q corresponding to the often studied[1,2] discharge of $Cd(CN)_4^{--}$ with the intermediate formation of $Cd(CN)_3^-$. Note that when $1/\kappa\mu < 0.01$, *i.e.*, when the diffuse double layer thickness $1/\kappa$ is much smaller than the reaction layer thickness μ, one has $G_I \approx 1$, and there is hardly an effect of the double layer structure. Conversely, when $1/\kappa\mu > 100$, *i.e.*, when the diffuse double layer is much thicker than the reaction layer, the function G_I varies exponentially with the potential φ_0, and a simple Boltzmann cor-

(5) Values of Bessel functions from "Tables of Bessel Functions of Fractional Order," Vol. II, prepared by National Bureau of Standards, Columbia University Press, New York, N. Y., 1949.

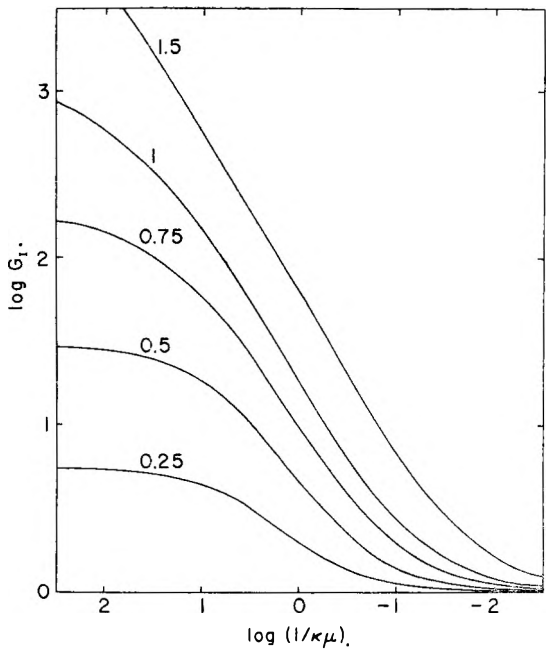

Fig. 2.—Variations of G_I (eq. 14) with $1/\kappa\mu$ for different potential φ_0 and for $p = 1/2$ and $q = 2$. Number on each curve is the value of $|z|F|\varphi_0|/2 \times 2.3\ RT$.

rection can be applied for the correction of concentrations. The latter correction was used by Gierst[3a] and by Delahay and co-workers[2] in their interpretation of the cadmium cyanide discharge.

Evaluation of G_I and G_{II} for Different Limiting Cases

By noting that for large or small values of the argument the modified Bessel functions can be expanded, these approximate expressions of G_I and G_{II} are obtained. Thus, for $\zeta \gg 1$

$$I_r(\zeta) \longrightarrow \exp \zeta/(2\pi\zeta)^{1/2}$$
$$K_r(\zeta) \longrightarrow \exp(-\zeta) \times (\pi/2\zeta)^{1/2}$$

and, for $\zeta \ll 1$

$$I_r(\zeta) \longrightarrow \begin{cases} (\zeta/2)^r/\Gamma(1+r) & (r \neq \text{integer}) \\ (\zeta/2)^{|r|}/|r|! & (r = \text{integer}) \end{cases}$$

$$K_r(\zeta) \longrightarrow \begin{cases} \dfrac{(\pi/2)}{\sin|r|\,\pi} \dfrac{(\zeta/2)^{-|r|}}{\Gamma(1-|r|)} & (r \neq \text{integer}) \\ 1/2\,(|r|-1)!\,(\zeta/2)^{-|r|} & (r = \text{integer}) \\ -\ln(\zeta/2) & (r = 0) \end{cases}$$

Function G_I (for the usual case of $q > 0$)

(1) For $(2/\kappa\mu q) \gg 1$

$$G_I = \xi_0^{2p+q} \frac{K_{p/q}[(2/\kappa\mu q)\xi_0^{-q}]}{K_{(p/q)+1}[(2/\kappa\mu q)\xi_0^{-q}]} \qquad (22)$$

Furthermore, if $(2/\kappa\mu q)\xi_0^{-q} \gg 1$, one has

$$G_I = \xi_0^{2p+q} \qquad (23)$$

If $(2/\kappa\mu q)\xi_0^{-q} \ll 1$, one has in view of eq. 22

$$G_I = \begin{cases} (1/\kappa\mu p)\xi_0^{2p} & (p > 0) \\ (1/\kappa\mu q)\ln(\kappa\mu q\xi_0^q) & (p = 0) \\ [\Gamma(|p/q|)/\Gamma(1-|p/q|)](1/\kappa\mu q)^{2(p/q)+1} & (0 > p > -q) \\ (\kappa\mu q/2)/\ln(\kappa\mu q\xi_0^q) & (p = -q) \\ (|p| = q)\kappa\mu\xi_0^{-2(|p|-q)} & (-q > p) \end{cases} \qquad (24)$$

(2) $(2/\kappa\mu q) \ll 1$

$$G_I = \begin{cases} \dfrac{1 + (1/\kappa\mu p)(\xi_0^{2p} - 1)}{1 - (1/\kappa\mu[p+q])[\xi_0^{-2(p+q)} - 1)} & (p \neq 0 \text{ or } -q) \\ 1 + (2/\kappa\mu)\ln\xi_0 & (p = 0) \\ [1 + (2/\kappa\mu)\ln\xi_0]^{-1} & (p = -q) \end{cases} \qquad (25)$$

Furthermore, if $(1/\kappa\mu p)\xi_0^{2p} \ll 1$ and $(1/\kappa\mu[p+q])\xi_0^{-2(p+q)} \ll 1$, one obtains

$$G_I = 1$$

Function G_{II}.—The same considerations as for G_I give the approximate expressions

(1) $(2/\kappa\mu') \gg 1$

$$G_{II} = \xi_0^{2p+1} \frac{K_p[(2/\kappa\mu')\xi_0^{-1}]}{K_{p+1}[(2/\kappa\mu')\xi_0^{-1}]} \qquad (27)$$

$(2/\kappa\mu') \gg 1$ and $(2/\kappa\mu')\xi_0^{-1} \gg 1$

$$G_{II} = \xi_0^{2p+1} \qquad (28)$$

$(2/\kappa\mu') \gg 1$ and $(2/\kappa\mu')\xi_0^{-1} \ll 1$

$$G_{II} = \begin{cases} (1/\kappa\mu' p)\xi_0^{2p} & (p > 0) \\ (2/\kappa\mu')\ln(\kappa\mu'\xi_0) & (p = 0) \\ [\Gamma(|p|)/\Gamma(1-|p|)](1/\kappa\mu')^{2p+1} & (0 > p > -1) \\ (\kappa\mu'/2)/\ln(\kappa\mu'\xi_0) & (p = -1) \\ (p-1)\kappa\mu'\xi_0^{-2(|p|-1)} & (-1 > p) \end{cases} \qquad (29)$$

(2) $(2/\kappa\mu') \ll 1$

$$G_{II} = \begin{cases} \dfrac{1 + (1/\kappa\mu' p)(\xi_0^{2p} - 1)}{1 - (1/\kappa\mu'[p+1])(\xi_0^{-2(p+1)} - 1)} & (p \neq 0 \text{ or } -1) \\ 1 + (2/\kappa\mu')\ln\xi_0 & (p = 0) \\ [1 + (2/\kappa\mu')\ln\xi_0]^{-1} & (p = -1) \end{cases} \qquad (30)$$

$(2/\kappa\mu') \ll 1$, $(1/\kappa\mu' p)\xi_0^{2p} \ll 1$ and $(1/\kappa\mu'[p+1])\xi_0^{-2(p+1)} \ll 1$

$$G_{II} = 1 \qquad (31)$$

Transition Time in Chronopotentiometry

In chronopotentiometry, the current density is held constant during electrolysis, and the concentration C_Y^S in eq. 13 is given by the Sand equation[6,7]

$$C_Y^S = C_Y^0 - (2It^{1/2})/\pi^{1/2}nFD_Y^{1/2} \qquad (32)$$

where C_Y^0 is the bulk concentration of Y. The transition time τ_k is defined by the condition $C_O^* = 0$ for $t = \tau_k$, *i.e.*, in view of eq. 13 and 32, one has for reaction I

$$I\tau_k^{1/2} = \frac{\pi^{1/2}nFD_Y^{1/2}C_Y^0}{2} - \frac{\pi^{1/2}(D_Y/D_O)^{1/2}I}{2K_d[k_b/(C_X^0)]^{\nu 1/2}} G_I \qquad (33)$$

Equation 33 is identical, except for the function G_I, to the result that Delahay and Berzins[8] ($D_Y = D_O$) derived without consideration of the double layer structure.

For reaction II one has

$$I\tau_k^{1/2} = \frac{\pi^{1/2}nFD_Y^{1/2}C_Y^0}{2} - \frac{\pi^{1/2}(D_Y/D_O)^{1/2}I}{2K_a(C_X^0)^{\nu}(k_b)^{1/2}} G_{II} \qquad (34)$$

Limiting Current in Polarography

The condition for a limiting current in polarography can be stated as $C_O^* = 0$. In view of eq. 12 and 13 one has for reaction I

$$I_l/nF = D_O^{1/2}K_d\{k_b/(C_X^0)^{\nu}\}^{1/2}C_Y^S G_I^{-1} \qquad (35)$$

where I_l is the limiting current density. Thus, the boundary value problem is stated by the system of eq. 10, 11, 12 and 35. This problem was already solved by Koutecky,[9] and the following approximate expression for the average limiting current $\bar{i}_l$ holds

(6) H. J. S. Sand, *Phil. Mag.*, **1**, 45 (1901).

(7) P. Delahay, "New Instrumental Methods in Electrochemistry," Interscience Publ., Inc., New York, N. Y., 1954, p. 180.

(8) P. Delahay and T. Berzins, *J. Am. Chem. Soc.*, **75**, 2486 (1953).

(9) J. Koutecky, *Collection Czechoslov. Chem. Communs.*, **18**, 311 (1953).

$$\frac{\bar{i}_d - \bar{i}_l}{\bar{i}_l} = \left(\frac{D_Y}{D_O}\right)^{1/2} \frac{G_I}{0.89\tau^{1/2}K_d\{k_b/(C_X^0)^\nu\}^{1/2}} \quad (36)$$

Here, $\bar{i}_d$ is the average diffusion current given by the Ilkovic equation, *i.e.*

$$\bar{i}_d = (24/7)(7\pi/3)^{1/2}(3/4\pi d)^{2/3}nFD_O^{1/2}m^{2/3}C_Y^0\tau^{1/6}$$

where τ is the drop time, d the specific gravity of mercury and m the rate of flow of mercury.

By the same procedure as above, one derives for reaction II

$$\frac{\bar{i}_d - \bar{i}_l}{\bar{i}_l} = \left(\frac{D_Y}{D_O}\right)^{1/2} \frac{G_{II}}{0.89\tau^{1/2}K_a(C_X^0)^\nu(k_b)^{1/2}} \quad (37)$$

The validity of eq. 36 was verified by Kleinerman[10] in this Laboratory for the discharge of cadmium cyanide in connection with a study of thallium-amalgam electrodes.

Appendix

Derivation of Equations 13 and 19

The new functions u and ξ

$$C_O = \exp(-z_O F\varphi/RT)\{K_d(C_X^0)^{-\nu}C_Y^S - u\} \quad (38)$$

$$\xi = \exp(|z|F|\varphi_0|/2RT) - (\kappa/2)\int_0^x \exp(|z|F|\varphi|/RT)dx \quad (39)$$

are introduced and eq. 6 and 8 are transformed into

$$\frac{d}{d\xi}\left\{\exp\left[\frac{F}{RT}(|z\varphi| - z_0\varphi)\right]\frac{d\mu}{d\xi}\right\} - \left(\frac{2}{\kappa\mu}\right)^2 \exp\left[-\frac{F}{RT}(|z\varphi| - z_Y\varphi)\right]u = 0 \quad (40)$$

(10) P. Delahay and M. Kleinerman, *J. Am. Chem. Soc.*, in course of publication.

$$(I/nF) = (\kappa D_O/2)\exp[F(|z\varphi_0| - z_O\varphi_0)/RT](du/d\xi)_{\xi=\xi_0} \quad (41)$$

where ξ_0 and μ are defined by eq. 15 and 18, respectively.

The integral in eq. 39 is evaluated by the use of eq. 1 and there results

$$\xi = \exp(|z|F|\varphi_0|/2RT) - (\kappa/2)\left\{\int_{\varphi_0}^{\varphi} \frac{\exp(|z|F|\varphi|/RT) - 1}{(d\varphi/dx)}d\varphi + x\right. \quad (42)$$

Since x is very small in the diffuse double layer the last term in eq. 42 can be dropped and

$$\xi \sim \exp(|z|F|\varphi|/2RT) \quad (0 < x < \delta) \quad (43)$$

By combination of eq. 40, 41 and 43 one obtains

$$(d/d\xi)\{\xi^{(F2|z_0/z|+2)}du/d\xi\} - (2/\kappa\mu)^2\xi^{(F'2|zY/z|-2)}u = 0 \quad (44)$$

$$(I/nF) = (\kappa D_0/2)\xi_0^{(F2|z_0/z|+2)}(du/d\xi)_{\xi=\xi_0} \quad (45)$$

where the significance of the upper and lower signs is the same as for p and q of eq. 16 and 17.

Equation 44 is a modified Bessel equation similar to the one recently solved in connection with another double layer problem. Details of the calculation are given in this previous paper.[11]

Equation 19 for reaction II is derived by the same method, the function u', defined by

$$C_O = \exp(-z_O F\varphi/RT)[K_a(C_X^0)^\nu C_X^S - u'] \quad (46)$$

being now introduced.

Acknowledgment.—This work was supported by the Office of Naval Research. The author expresses his thanks to Professor Paul Delahay for his interest and discussions of this work.

(11) H. Matsuda and P. Delahay, THIS JOURNAL, **64**, 332 (1960).

DOUBLE LAYER STRUCTURE AND RELAXATION METHODS FOR FAST ELECTRODE PROCESSES. II. FARADAIC IMPEDANCE MEASUREMENTS

BY HIROAKI MATSUDA[1]

Contribution from the Coates Chemical Laboratory, Louisiana State University, Baton Rouge, La.

Received October 21, 1959

The elements of the equivalent circuit for the faradaic impedance are derived, due consideration being given to the structure of the double layer in the solution of the boundary value problem. It is shown that the classical theory is applicable but that measured exchange current densities and transfer coefficients must be corrected. The phase angle which is also affected can exceed $\pi/4$ when the reactants are strongly attracted in the diffuse double layer. Comparison is made with a similar treatment for the galvanostatic double pulse method.

It was pointed out in a previous paper[2] that the structure of the double layer must be considered in the solution of the boundary value problems for the analysis of relaxation methods for very fast electrode processes. A detailed treatment was given for the double pulse galvanostatic method *in the absence of specific adsorption at the electrode.* These ideas are now extended to faradaic impedance measurements.

Concentrations of Reactants in the Helmholtz Plane

The problem is stated as previously for the particular case in which the faradaic current density is $I_f = I\exp(i\omega t)$, where $i = (-1)^{1/2}$, $\omega = 2\pi f$ (f, frequency), and I is the amplitude of the sinusoidal current. The concentration of reactant at a distance x from the plane of closest approach, under steady conditions, is in a general form

$$C_j = \exp[-(z_jF/RT)\varphi]\{C_j^0 - \exp(i\omega t)u_j(x)\} \quad (1)$$

where j corresponds to species O or R for the electrode reaction $O + ne = R$, z_j is the valence of species j, φ the difference of potential in the diffuse double layer between the point at x and the bulk of the solution, C_j^0 is the bulk concentration of species j outside the diffuse double layer and diffusion layer, and $u_j(x)$ is a function to be determined.

The solution, as derived by a method analogous to the one previously applied,[2] is for the plane of closest approach

$$C_j^* = \exp[-(z_jF/RT)\varphi_0]\{C_j^0 - (\pm I_f/nF)(1/\omega D_j)^{1/2}i^{-1/2}G_j \quad (2)$$

(1) Research Associate, 1958–1959; on leave from the Government Chemical Industrial Research Institute, Tokyo.

(2) H. Matsuda and P. Delahay, THIS JOURNAL, **64**, 332 (1960).

where D_j is the diffusion coefficient of species j, and the function G_j depends on the double layer structure.[3] In the actual case in which $f < 10^6$ cycles, one can write by analogy with a previous result[2]

$$G_j = \frac{1 + i^{1/2}(\omega^{1/2}/\kappa D_j^{1/2})g_j(\pm|z_j/z|)}{1 + i^{1/2}(\omega^{1/2}/\kappa D_j^{1/2})g_j(\mp|z_j/z|)} \quad (3)$$

with

$$g_j(y) = \frac{\exp[(y - 1/2)|z|F|\varphi_0|/RT] - 1}{y - 1/2} \quad (4)$$

where φ_0 is the potential difference across the diffuse double layer, $1/\kappa$ characterizes the diffuse double layer "thickness" (Gouy-Chapman theory) and the upper and lower signs in front of $|z_j/z|$ correspond to $z_j\varphi_0 > 0$ and $z_j\varphi_0 < 0$, respectively. By noting that $i^{\pm 1/2} = (1 \pm i)/2^{1/2}$, one has

$$i^{-1/2}G_j = 2^{-1/2}\{(h_j)_{re} - i(h_j)_{im}\} \quad (5)$$

with

$$(h_j)_{re} = \frac{1 + 2^{1/2}(\omega^{1/2}/\kappa D_j^{1/2})g_j(\pm|z_j/z|) + (\omega^{1/2}/\kappa D_j^{1/2})^2 g_j(\pm|z_j/z|)g_j(\mp|z_j/z|)}{1 + 2^{1/2}(\omega^{1/2}/\kappa D_j^{1/2})g_j(\mp|z_j/z|) + (\omega^{1/2}/\kappa D_j^{1/2})^2[g_j(\mp|z_j/z|)]^2} \quad (6)$$

$$(h_j)_{im} = \frac{1 + 2^{1/2}(\omega^{1/2}/\kappa D_j^{1/2})g_j(\mp|z_j/z|) + (\omega^{1/2}/\kappa D_j^{1/2})^2 g_j(\mp|z_j/z|)g_j(\pm|z_j/z|)}{1 + 2^{1/2}(\omega^{1/2}/\kappa D_j^{1/2})g_j(\mp|z_j/z|) + (\omega^{1/2}/\kappa D_j^{1/2})^2[g_j(\mp|z_j/z|)]^2} \quad (7)$$

By combination of eq. 2, 5, 6 and 7 there follows

$$C_j^* = \exp(-z_jF\varphi_0/RT) \times \{C_j^0 \mp (I/nF)(1/2\omega D_j)^{1/2}\exp(i\omega t)[(h_j)_{re} - i(h_j)_{im}]\} \quad (8)$$

where the minus and plus signs in front of (I/nF) correspond to j = O and j = R, respectively. One can transform this expression into real form by noting that $I_f = I \sin \omega t$ and by retaining the imaginary part of the second term between brackets in eq. 8. Thus

$$C_j^* = \exp(-z_jF\varphi_0/RT)\{C_j^0 \mp \Delta C_j \sin(\omega t - \theta_j)\} \quad (9)$$

with

$$\Delta C_j = (I/nF)(1/\omega D_j)^{1/2}\{[(h_j)_{re}^2 + (h_j)_{im}^2]/2\}^{1/2} \quad (10)$$

$$\cot\theta_j = (h_j)_{re}/(h_j)_{im} \quad (11)$$

Faradaic Impedance

The faradaic impedance is derived by introduction of the concentrations (eq. 9) in the current–potential characteristic for the electrode process (see, for example, eq. 15 in ref. 2). After expansion of the exponentials in this characteristic (limited to the first order terms) one obtains for the overvoltage V

$$-V = \left(\frac{RT}{nF}\right) I \left\{\left[\frac{1}{(I_0)_{app}} + \frac{1}{2^{1/2}nF\omega^{1/2}}\left(\frac{(h_0)_{re}}{C_0^0 D_0^{1/2}} + \frac{(h_R)_{re}}{C_R^0 D_R^{1/2}}\right)\right]\sin\omega t - \left[\frac{1}{2^{1/2}nF\omega^{1/2}}\left(\frac{(h_0)_{im}}{C_0^0 D_0^{1/2}} + \frac{(h_R)_{im}}{C_R^0 D_R^{1/2}}\right)\right]\cos\omega t\right\} \quad (12)$$

where $(I_0)_{app}$ is the *apparent* exchange current density, *i.e.*, the exchange current density corrected for double layer effects on the basis of Frumkin's ideas.[4] One has

$$(I_0)_{app} = I_0 \exp[(\alpha n - z_O)F\varphi_0/RT] \quad (13)$$

$$I_0 = nFk_s(C_O^0)^{1-\alpha}(C_R^0)^{\alpha} \quad (14)$$

where I_0 is the exchange current density, α the transfer coefficient, and k_s the standard rate constant.

For the series equivalent circuit $R_s - C_s$ of the faradaic impedance, one has

$$-V = I\{R_s \sin\omega t - (1/\omega C_s)\cos\omega t\} \quad (15)$$

i.e., after comparison of eqs. 12 and 15

$$R_s = \frac{RT}{nF}\left\{\frac{1}{(I_0)_{app}} + \frac{1}{2^{1/2}nF\omega^{1/2}}\left[\frac{(h_O)_{re}}{C_O^0 D_O^{1/2}} + \frac{(h_R)_{re}}{C_R^0 D_R^{1/2}}\right]\right\} \quad (16)$$

$$(1/\omega C_s) = \frac{RT}{nF}\left\{\frac{1}{2^{1/2}nF\omega^{1/2}}\left[\frac{(h_O)_{im}}{C_O^0 D_O^{1/2}} + \frac{(h_R)_{im}}{C_R^0 D_R^{1/2}}\right]\right\} \quad (17)$$

These expressions, which are fairly involved in view of the nature of the functions $(h_j)_{re}$ and $(h_j)_{im}$, can be simplified if the frequency of the applied alternating current is so small that the condition

$$(\omega^{1/2}/\kappa D_j^{1/2})g_j(\pm|z_j/z|) < 0.1 \quad (18)$$

holds. Then, by expanding eq. 6 and 7 into power series of $(\omega^{1/2}/\kappa D_j^{1/2})$ and neglecting the second and higher order terms, one has

$$(h_j)_{re} = 1 + 2^{1/2}(\omega^{1/2}/\kappa D_j^{1/2})a_j \quad (19)$$

$$(h_j)_{im} = 1 \quad (20)$$

with

$$a_j = g_j(\pm|z_j/z|) - g_j(\mp|z_j/z|) \quad (21)$$

Hence, eq. 16 and 17 can be simplified into

$$R_s = \frac{RT}{nF}\left\{\frac{1}{(I_0)_{app}} + \frac{1}{nF}\left(\frac{a_O}{\kappa C_O^0 D_O} + \frac{a_R}{\kappa C_R^0 D_R}\right) + \frac{1}{2^{1/2}nF\omega^{1/2}}\left(\frac{1}{C_O^0 D_O^{1/2}} + \frac{1}{C_R^0 D_R^{1/2}}\right)\right\} \quad (22)$$

$$(1/\omega C_s) = \frac{RT}{nF}\frac{1}{2^{1/2}nF\omega^{1/2}}\left(\frac{1}{C_O^0 D_O^{1/2}} + \frac{1}{C_R^0 D_R^{1/2}}\right) \quad (23)$$

It follows from eq. 22 and 23 that plots of the quantities R_s and $(1/\omega C_s)$ against $\omega^{-1/2}$ yield two parallel straight lines which are such

$$R_s - (1/\omega C_s) = \frac{RT}{nF}\left\{\frac{1}{(I_0)_{app}} + \frac{1}{nF}\left(\frac{a_O}{\kappa C_O^0 D_O} + \frac{a_R}{\kappa C_R^0 D_R}\right)\right\} \quad (24)$$

On the other hand, the classical theory of faradaic impedance leads to

$$R_s - (1/\omega C_s) = (RT/nF)[1/(I_0)_{ms}] \quad (25)$$

where $(I_0)_{ms}$ is the measured exchange current density that is obtained by neglecting the double layer structure. By comparing of eq. 24 and 25 one deduces

$$(I_0)_{ms} = \frac{(I_0)_{app}}{1 + [(I_0)_{app}/nF][(a_O/\kappa C_O^0 D_O) + (a_R/\kappa C_R^0 D_R)]} \quad (26)$$

This result is identical with the one derived for the galvanostatic double pulse method,[2] and the previous discussion of measured exchange current densities and transfer coefficient can be transposed to faradaic impedance measurements.

Phase Angle

The measured phase angle ϕ_{ms} is such that $\cot(\phi_{ms}) = \omega R_s C_s$, *i.e.*, in view of eq. 22 and 23

$$\cot(\phi_{ms}) = 1 + 2^{1/2}nF\omega^{1/2} \times \left\{\frac{1}{(I_0)_{app}} + \frac{1}{nF}\left(\frac{a_O}{\kappa C_O^0 D_O} + \frac{a_R}{\kappa C_R^0 D_R}\right)\right\} \Big/ \left(\frac{1}{C_O^0 D_O^{1/2}} + \frac{1}{C_R^0 D_R^{1/2}}\right) \quad (27)$$

(3) The complete form of G_j is the same as before except that s in eq. 12 of ref. 2 is now replaced by $i\omega$.

(4) For a review, see for instance, M. Breiter, M. Kleinerman and P. Delahay, *J. Am. Chem. Soc.*, **80**, 5111 (1958).

Since the apparent phase angle ϕ_{app}, that is related to the apparent exchange current density, is given by

$$\cot(\phi_{app}) = 1 + 2^{1/2}nF\omega^{1/2}/(I_0)_{app}\left(\frac{1}{C_O^0 D_O^{1/2}} + \frac{1}{C_R^0 D_R^{1/2}}\right) \quad (28)$$

one obtains

$$\cot(\phi_{ms}) - \cot(\phi_{app}) = 2^{1/2}\omega^{1/2} \times \left(\frac{a_O}{\kappa C_O^0 D_O} + \frac{a_R}{\kappa C_R^0 D_R}\right)\Big/\left(\frac{1}{C_O^0 D_O^{1/2}} + \frac{1}{C_R^0 D_R^{1/2}}\right) \quad (29)$$

It is easily seen in view of the nature of the functions a_O and a_R that $\cot(\phi_{ms}) > \cot(\phi_{app})$ when $z_j\phi_0 < 0$ (*i.e.*, repulsion case), and conversely $\cot(\phi_{ms}) > \cot(\varphi_{app})$ when $z_j\varphi_0 < 0$ (*i.e.*, attraction case). Especially, when the discharged ions are sufficiently attracted in the diffuse double layer, $\cot(\phi_{ms})$ can become smaller than unity, *i.e.*, the measured phase angle ϕ_{ms} can exceed 45°. This observation was reported by Laitinen and Randles[5,6] for fast electrode processes involving species that were specifically adsorbed on the electrode surface or at least attracted in the diffuse double layer.

Acknowledgment.—This work was supported by the Office of Naval Research. The author is indebted to Professor Paul Delahay for his interest and discussions of this problem.

(5) H. A. Laitinen and J. E. B. Randles, *Trans. Faraday Soc.*, **51**, 54 (1955).

(6) J. E. B. Randles, "Transactions of the Symposium on Electrode Processes," Philadelphia, 1959, E. Yeager ed., John Wiley and Sons, Inc., New York, N. Y., in course of publication.

VAPOR PRESSURE OF THORIUM[1]

BY A. J. DARNELL, W. A. MCCOLLUM AND T. A. MILNE

Atomics International, A Division of North American Aviation, Inc., Canoga Park, California

Received September 24, 1959

The vapor pressure of solid thorium was determined over the temperature interval 1757 to 1956°K. by the vacuum evaporation method of Langmuir. Special purification of the thorium was necessary since traces of ThO_2 react with thorium to give ThO(g). Thorium also reacts with residual gaseous oxygen in the vacuum system to form ThO(g). The latter effect was found to be negligible at residual oxygen pressures of less than 2×10^{-8} mm. The vapor pressure equation for Th(s) → Th(g) is $\log P_{atm} = -28{,}780 \pm 620/T°K. + 5.991 \pm 0.333$. These results yield values of $\Delta H^0_{298(Sub)}$ of 137.3 ± 2.8 kcal./mole and 136.6 ± 0.5 kcal./mole from a slope and third law determination, respectively. From an estimate of the pressure of ThO(g) over Th(s) containing ThO_2(s), D_0^0(ThO) = 196 kcal./mole.

Introduction

There is only a meager amount of data reported in the literature for the vapor pressure of thorium. Dushman,[2] Brewer[3] and Loftness[4] give data which are based on the work of Zwikker.[5] However, Zwikker did not publish the original data from which his reported vapor pressure curve was obtained; therefore, no evaluation of Zwikker's results can be made. Andrews[6] reports thorium vaporization rate data, which are actually for thorium dioxide. In view of the above, a redetermination of the vapor pressure of thorium seemed desirable.

The vapor pressure measurements were carried out using the vacuum evaporation method of Langmuir.[7] Measurements were limited to the solid because the reactivity of liquid thorium presents a formidable container problem. The vaporization rate study of thorium metal was complicated by reaction of thorium with oxide impurity initially in the metal and also with residual gaseous oxygen in the vacuum system. These reactions with oxide and oxygen were examined in order to determine their effect on the thorium vaporization rates.

Experimental

Apparatus and Procedure.—The Langmuir[7] vaporization method has been described in detail elsewhere.[2] Basically, the rate of vaporization of a substance of known area and at a known temperature is determined under high vacuum conditions and the vapor pressure is calculated by applying the kinetic theory of gases with the assumption that the evaporation coefficient is unity. Vaporization rate experiments were carried out on solid right cylinders of thorium metal ranging in diameter from $^5/_8$'' to 1'' and from $^1/_2$'' to 1'' long. These cylinders were mounted in a vacuum system on a tungsten rod and were heated by a radio-frequency induction coil placed around the vacuum manifold. The vaporization experiments were carried out at residual pressures of less than 1×10^{-7} mm. as measured by an ionization gauge placed near the heated specimen. The temperature of the cylinder was measured with a disappearing filament type optical pyrometer, which was calibrated with a tungsten ribbon lamp, which in turn was calibrated by the U. S. Bureau of Standards. Three sight holes with a depth to diameter ratio of 4:1 or greater were drilled in the top surface of the cylinder in order to determine the temperature at different positions on the disk. The peripheral hole consistently gave temperature readings 7 to 10° higher than the center hole. This was attributed to uneven heating of the cylinder by the induction field. The peripheral hole readings were weighted in averaging the temperature readings of the sight holes since most of the surface of the disk is nearer the temperature of this sight hole. A correction was made for the absorption of light by the optical window in the vacuum system.

The amount of material vaporizing from the cylinder was determined by weight loss of the cylinder, and by analysis for thorium deposited on a cylindrical quartz collector tube. In the latter method, the sublimate was dissolved from the collector with nitric acid containing a trace of fluoride ion and then analyzed for thorium by the colorimetric method of Thomason,[8] *et al.* The weight loss method was used when

(1) This work was supported by the Atomic Energy Commission. This paper has been presented in part before the Division of Physical Chemistry at the 135th National Meeting of the American Chemical Society in April, 1959.

(2) S. Dushman, "Scientific Foundations of Vacuum Technique," John Wiley and Sons, Inc., New York, N. Y., 1949.

(3) L. Brewer, "The Thermodynamic and Physical Properties of the Elements," Paper 3 in "Chemistry and Metallurgy of Miscellaneous Materials: Thermodynamics," Ed. by L. Quill, McGraw-Hill Book Co., New York, N. Y., 1950.

(4) R. L. Loftness, "A Vapor Pressure Chart for Metals," U.S.A.-E.C. Report No. NAA-SR-132, 1952.

(5) C. Zwikker, *Physica*, **8**, 240 (1928).

(6) M. R. Andrews, *Phys. Rev.*, **33**, 454 (1929).

(7) I. Langmuir, *ibid.*, **2**, 329 (1913).

(8) P. Thomason, M. Perry and W. Byerly, U.S.A.E.C. Report Mon-C-83, 1946.

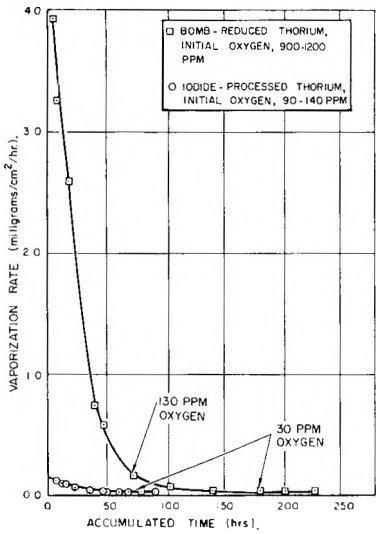

Fig. 1.—Vaporization rate *vs.* time for thorium samples showing decrease in vaporization rate as oxygen is removed from samples: temperature 1610°.

the quantity of sublimate was above 15 mg.; the colorimetric method was used for quantities below 5 mg. Both methods were employed between these limits The results from the two methods agreed to within ± 5%.

Materials.—Samples for the vaporization rate measurements were prepared from two different sources of thorium: (1) Modified Kroll process[9] thorium made by the reduction of $ThCl_4$ with calcium in a bomb, and (2) van Arkel–deBoer iodide-processed[10] thorium made by the thermal decomposition of ThI_4. The former, which will be referred to as "bomb-reduced" thorium, was obtained from the National Lead Company; the latter which will be referred to as "iodide-processed" thorium was obtained from Metal Hydrides, Inc. The initial impurities in the thorium from sources (1) and (2) are shown in Table I. The most significant difference was the greater oxygen, Fe, Ni and Cu content of the bomb-reduced thorium.

TABLE I

IMPURITIES IN THORIUM (P.P.M. BY WEIGHT)[a]

Sample	Fe	Si	Ni	Cu	Al	N	O
Bomb-reduced (initial)	200	20	100	70	10	110	900–1200
Iodide-processed (initial)	20	35	10	1	3	60	90–140
Bomb-reduced (after purification)	<10	<10	<10	1	3	<30	<30
Iodide-processed (after purification)	<10	<10	<10	1	3	<30	<30

[a] Nitrogen and oxygen determined by vacuum fusion analysis, metals determined by spectrographic analysis.

Samples from the bomb-reduced material were prepared by machining cylinders from the ingots. However, since the iodide thorium was in the form of small crystals, it was necessary to cast this material in order to prepare samples for the Langmuir vaporization experiments. This was done by melting briefly the thorium crystals in a tungsten or tantalum crucible in high vacuum.

Purification of Samples.—The data in Table II show the initial vaporization rates of the bomb-reduced and iodide-processed samples prepared by different methods. These rates were calculated from the weight loss of the samples, after a short initial heating during which the bulk of the volatile metal impurities vaporized. Except for the case of iodide-processed thorium cast in a thoria crucible, the vaporization rate of the bomb-reduced thorium was approximately 25 times greater than that yielded by the iodide-processed thorium. This was found to be the case even after the more volatile metallic impurities in the bomb-reduced thorium had been reduced to a level comparable to the level present in the iodide-processed thorium. The lower rate of the iodide-processed thorium was not likely to be due to impurities introduced in the casting process since casting bomb-reduced thorium in a tantalum crucible reduced the vaporization by only a small amount. Since casting the iodide-processed thorium in a thoria crucible increased both the vaporization rate and the oxygen content of this sample, this suggested that the greater amount of thorium dioxide impurity in the bomb-reduced sample caused the higher vaporization rate.

The higher vaporization rate of the samples containing thorium dioxide impurity indicated that this impurity could be selectively removed from the thorium by distillation at high temperatures and under high vacuum.

Figure 1 shows the vaporization rates at 1610° obtained from a series of experiments made on a sample of bomb-reduced thorium initially containing approximately 1000 p.p.m. oxygen. The vaporization rate of the bomb-reduced sample continued to decrease with each successive run, until finally the vaporization rate became constant at 0.030 mg./cm.²/hr. The oxygen content at this time was less than 30 p.p.m. Figure 1 also shows the vaporization rates from a similar series of runs made with iodide-processed thorium. The initial weight loss rate yielded by this thorium which contained less oxygen, was lower than that from the bomb-reduced disk. However, both samples ultimately attained the same constant vaporization rate. This constant rate was attributed principally to the vaporization of thorium as thorium gas. Table I shows that this purification procedure also lowered the metallic impurities in the samples, thus yielding very high purity thorium for the vapor pressure measurements.

TABLE II

INITIAL VAPORIZATION RATES OF VARIOUS THORIUM SAMPLES AT 1610°

Sample type	Vaporization rate[a] (mg./cm.²/hr.)
Bomb-reduced thorium	
(a) Machined	5
(b) Cast in tantalum crucible	4
Iodide-processed thorium	
(a) Cast in tantalum crucible	0.2
(b) Cast in tungsten crucible	0.2
(c) Cast in ThO_2 crucible	3

[a] Calculated from weight loss of sample.

Discussion and Results

A. Reaction of Thorium with ThO_2.—As stated above, the vaporization rate from thorium was significantly higher when it contained ThO_2 as an impurity. Figure 1 shows that the initial vaporization rate from a sample which contained 1000 p.p.m. oxygen (~0.8% ThO_2), was approximately 100 times greater than the rate yielded by the purified samples. However, the vapor pressure reported for ThO_2[11–13] was too low by a factor of 10^4 to account for this high initial rate, based on the most recent data.[13] However, the decrease in oxygen content of the thorium sample during the purification process suggested that the vaporizing species was a thorium oxide.

The explanation offered, therefore, for the high vaporization rate observed with thorium containing ThO_2 is that ThO_2(s) reacts with Th(s) at elevated temperatures to form ThO(g), *i.e.*

(9) Annual Summary Report on Thorium Research for the Period Oct. 1, 1954 to June 30, 1955, U.S.A.E.C. Report NLCO-578, National Lead Co. of Ohio, 1955.

(10) N.D. Veigel, E. M. Sherwood and I. E. Campbell, "The Preparation of High Purity Thorium by the Iodide Process," U.S.A.E.C. Report BMI-777, Battelle Memorial Institute, 1953.

(11) E. Shapiro, *J. Am. Chem. Soc.*, **74**, 5233 (1952).

(12) M. Hoch and H. L. Johnston, *ibid.*, **76**, 4833 (1954).

(13) R. J. Ackermann, private communication.

$$Th(s) + ThO_2(s) \rightleftarrows 2ThO(g) \qquad (1)$$

Langmuir vaporization rate experiments on a thorium sample containing ThO_2 showed that the gaseous product from this reaction has a thorium to oxygen atom ratio of 1:1. This ratio was determined by introducing a known amount of oxygen into a pure thorium sample, then determining the thorium to oxygen atom ratio of the material which was vaporized at a rate in excess of the vaporization rate yielded by pure thorium. To illustrate, Fig. 2 shows the vaporization rate at 1610° of a thorium sample which contained 30 p.p.m. or less oxygen. The sample was then partially oxidized at 500° in pure oxygen. The amount of oxygen introduced, as determined by weight gain, is given in Table III, and represents about 200 p.p.m. Figure 2 shows that the vaporization rate was markedly increased after the oxidation. However, the vaporization rate decreased with time and after 68 hours it was equal to the rate before oxidation. The oxygen content also had been reduced to the initial value.

TABLE III

STOICHIOMETRY OF GASEOUS THORIUM OXIDE FROM THE REACTION OF Th(s) + ThO_2(s)

(a)	Total wt. of material vaporized in time interval $t_0 - t_i$, Th(g) + gaseous thorium oxide, mg.	= 447
(b)	Wt. of Th(g) vaporized during this interval (from rate before oxidn.), mg.	= 71
(c)	Wt. attributed to gaseous thorium oxide, mg.	= 376
(d)	Wt. of oxygen introduced during oxidn. process, mg.	= 24
(e)	Wt. of thorium vaporized as oxide, mg.	= 352
(f)	Atom ratio of gaseous oxide, Th/O, *i.e.*, ThO	= 1/0.98

The total quantity vaporized during the interval t_0 to t_i was assumed to be principally from two species, Th(g) and a gaseous thorium oxide. Also, the vaporization rate of Th(g) was assumed to be unaffected by the oxide. A layer was formed on the metal during the oxidation process; however, this surface layer disappeared after the sample was heated for 30 minutes at 1610°. Since this oxide layer did not vaporize in this short time interval, presumably it dissolved or diffused into the metal. The reduction of the vapor pressure of thorium due to the solution of this oxide would be expected to be small since the sample was 99.8 mole % thorium.

The total weight of material vaporized from the sample during the interval $t_0 - t_i$ was 447 mg. The quantity attributed to Th(g) is represented by the shaded area in Fig. 2 and amounted to 71 mg. The remainder, 376 mg., is represented approximately by the area ABC in Fig. 2. This is attributed to ThO (g) since the atom ratio of thorium to oxygen is essentially unity, as shown in Table III.

Inghram, Chupka and Berkowitz,[14] in a mass spectrometric study, report ion currents which they attribute to ThO(g) when ThO_2(s) is heated in a tantalum cell. Thus, Th as well as Ta reduces ThO_2 at high temperatures to give ThO(g).

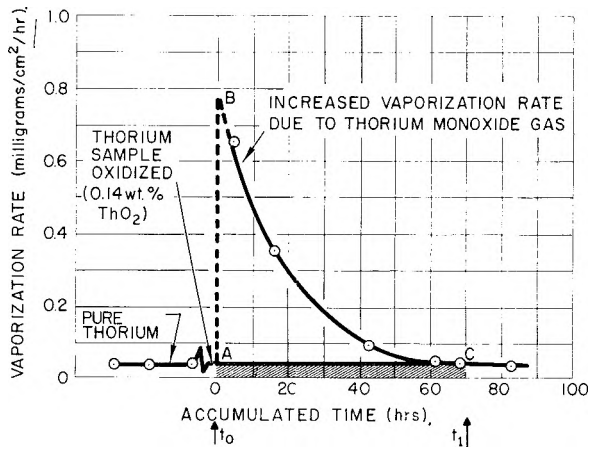

Fig. 2.—Vaporization rate *vs.* time for partially oxidized thorium illustrating increase in vaporization rate due to ThO(g); temperature 1610°.

B. Reaction of Thorium with Gaseous Oxygen.—The residual pressure of oxygen in the vacuum system also has an effect on the over-all vaporization rate of thorium. Contrary to the behavior observed under similar conditions with uranium[15] and zirconium,[16] in this case the volatility is enhanced. At high temperatures and low oxygen pressures, thorium reacts to form gaseous ThO. The over-all reaction can be expressed by

$$Th(s) + {}^1/_2O_2(g) = ThO(g) \qquad (2)$$

Oxide and/or oxygen also dissolved in the thorium sample and, at oxygen pressures greater than 1×10^{-3} mm. and at 1610°, sufficient oxide was present to form a second phase on the surface of the thorium as observed visually by the appearance of bright areas on the thorium disk. However, it has been been established[17] that, at 1610° and $P_{O_2} < 1 \times 10^{-3}$ mm., the rate of formation of ThO(g) can be expressed by

$$W = (1.26 \times 10^{-3})(P_{O_2}) \qquad (3)$$

when $P_{O_2} < 1 \times 10^{-3}$ mm., where W = grams of ThO(g) formed per sec. per cm.^{2} of thorium surface and P_{O_2} = pressure of oxygen in mm.

The contribution of reaction 2 to the total vaporization rate can be determined from (3). As stated earlier, the thorium vapor pressure measurements were carried out at residual pressures of less than 1×10^{-7} mm. Assuming that 1/5 of this residual pressure is oxygen, then at 1610° the rate due to reaction 2 is calculated to be 2.52×10^{-11} g. cm.$^{-2}$ sec.$^{-1}$. The measured vaporization rate [Th(g) + ThO(g)] at this oxygen pressure and temperature was 1.25×10^{-8} g. cm.$^{-2}$ sec.$^{-1}$. Thus, the contribution from reaction 2 at 1610° was only 0.1% of the total rate. At 1484°, the lowest temperature at which thorium vaporization rate measurements were made, the

(14) M. Inghram, W. Chupka and J. Berkowitz, Proceedings of the 1956 International Conference of Astrophysics.

(15) E. G. Rauh and R. J. Thorn, *J. Chem. Phys.*, **22**, 1414 (1954).

(16) G. B. Skinner, J. W. Edwards and H. L. Johnston, *J. Am. Chem. Soc.*, **73**, 174 (1951).

(17) A. J. Darnell, *et al.*, to be published.

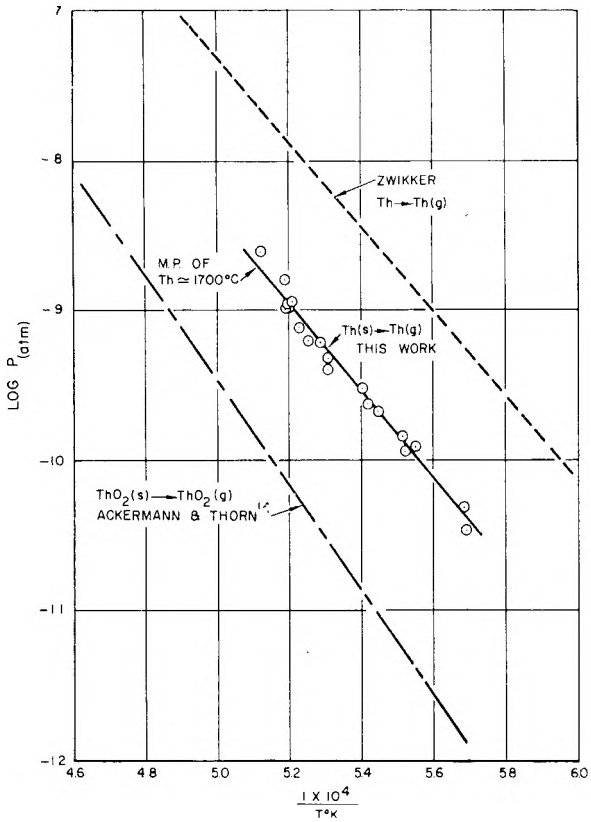

Fig. 3.—Log P *vs.* $1/T$ for thorium and thorium dioxide.

contribution from reaction 2 was less than 4% of the measured vaporization rate.

C. Vapor Pressure of Thorium.—Table IV gives the vaporization rates obtained for purified thorium metal where the residual gas pressure was less than 1×10^{-7} mm. The area of the thorium was calculated assuming the disk was a solid right cylinder. A correction was made to account for a change in the surface area due to thermal expansion[18] of thorium from 25° to the operating temperature.

Thorium vapor pressures were calculated from these vaporization rates by use of the Langmuir[7] equation

$$p = \frac{m}{\alpha}\left(\frac{2\pi RT}{M}\right)^{1/2} \qquad (4)$$

where

m = vaporization rate
α = evaporation coefficient
M = molecular weight of thorium gas

In these calculations, it was assumed that thorium vaporizes as a monatomic gas. The evaporation coefficient α was also assumed to be unity. The value of the evaporation coefficient can be checked by vapor pressure measurements with a Knudsen cell. However, the vapor pressure of solid thorium was too low for the utilization of this technique. A less sensitive test of α, similar to that used by Holden, Speiser and Johnston,[19] was used to determine whether α was greatly different from unity. The vaporization rates of a solid cylinder and a cylinder in which a large number of holes had been drilled were compared, assuming the area of the drilled cylinder to be the same as though the holes had not been drilled. The vaporization rates were the same within the experimental precision of our measurements, thus indicating $\alpha = 1$. However the variation introduced in this experiment was such that only a relatively large deviation in α from unity, *i.e.*, below 0.5, would have been observed.

TABLE IV

RATE OF EVAPORATION, VAPOR PRESSURE, AND HEAT OF SUBLIMATION OF THORIUM METAL

Temp. (°K.)	Vaporization rate mg./cm.²/hr.	Pressure, Th (atm.)	$\Delta\left(\frac{F^0_T - H^0_{298}}{T}\right)$ gas→solid	ΔH^0_{298} (kcal./mole)
1956	0.1355	2.43×10^{-9}	29.90	135.60
1930	.08832	1.60×10^{-9}	29.93	135.46
1927	.05585	1.01×10^{-9}	29.94	137.03
1926	.05606	1.01×10^{-9}	29.94	136.96
1926	.05663	1.09×10^{-9}	29.94	136.67
1925	.06172	1.11×10^{-9}	29.94	136.53
1921	.06412	1.16×10^{-9}	29.95	136.09
1910	.04353	7.81×10^{-10}	29.97	136.86
1905	.03529	6.33×10^{-10}	29.97	137.29
1892	.03368	6.03×10^{-10}	29.99	136.58
1884	.02669	4.76×10^{-10}	30.01	136.93
1884	.02271	4.05×10^{-10}	30.01	137.53
1852	.01711	3.03×10^{-10}	30.06	136.36
1847	.01350	2.39×10^{-10}	30.06	136.86
1837	.01216	2.14×10^{-10}	30.08	136.56
1815	.008213	1.44×10^{-10}	30.12	136.43
1811	.006636	1.16×10^{-10}	30.12	136.92
1803	.006915	1.21×10^{-10}	30.14	136.18
1760	.003398	5.86×10^{-11}	30.21	135.59
1757	.001918	3.31×10^{-11}	30.21	137.36
			Av.	136.59 ± 0.45

Thorium vapor pressures calculated from equation 4 are given in Table IV. Figure 3 shows a plot of thorium vapor pressure data *vs.* $1/T$. The vapor pressure of ThO_2 reported by Ackermann and Thorn[13] and the vapor pressure for Th given by Zwikker[5] are shown for comparison.

The data in Table IV can be used in two ways to obtain the heat of sublimation. First, the ordinary plot of log P *vs* $1/T$ yields ΔH_T from the slope. A least squares analysis of the data gives

$$\log P_{(atm)} = -\frac{28{,}780 \pm 620}{T(°K.)} + 5.991 \pm 0.333$$

This yields a heat of sublimation at the mid-temperature of the experiments (1856°K.) of 131.7 ± 2.8 kcal./mole.

The second method requires a knowledge of the free energy functions for both the solid and the gas and yields a ΔH^0_{298} of sublimation for each measured pressure of thorium.

Stull and Sinke[20] tabulate the necessary thermodynamic functions for solid thorium based on heat capacity measurements to 1500°K. For gaseous thorium a knowledge of the low lying term values

(18) J. R. Murray, "The Preparation, Properties, and Alloying Behavior of Thorium," Report AERE-M/TN-12, Great Britain Atomic Energy Research Establishment, 1952.

(19) R. B. Holden, R. Speiser and H. L. Johnston, *J. Am. Chem. Soc.*, **70**, 3897 (1948).

(20) D. R. Stull and G. C. Sinke, "Thermodynamic Properties of the Elements," American Chemical Society, Washington 6, D. C., 1956.

and of the multiplicity of the ground state is required. Zalubas,[21] at the National Bureau of Standards, in the course of the analysis of the spectrum of neutral thorium, has established a number of the low lying levels. The ground state is $^3F_2$. Although the analysis is as yet incomplete it is expected that all of the even levels below 10,000 cm.$^{-1}$ have been identified (13 levels). Of the odd levels found, none are below 10,000 cm.$^{-1}$, although such levels are probably to be expected.[21]

Considering that the effect of the 16 lowest levels above the ground state, considered here, is such as to raise the free energy function at 2000°K. by only 0.7 cal./deg. mole it is unlikely that the neglect of any as yet unidentified levels could produce any significant change in the present calculations.

In Table V are listed the calculated values of $(F^0_T - H^0_{298})/T$, $(H^0_T - H^0_{298})$ and S^0_T over the temperature range of interest in the present experiments. The equations and constants listed by Gilles, *et al.*,[22] were used. It would appear desirable to wait for the completed analysis of the spectrum of thorium before reporting a more extensive calculation of these functions.

The heat of sublimation can now be determined from

$$\Delta H^0_{298} = -\Delta\left[T\left(\frac{F^0_T - H^0_{298}}{T}\right)\right] - RT \ln P_{Th}$$

The values of $\Delta[(F^0_T - H^0_{298})/T]$, obtained by interpolation, and of ΔH^0_{298} are listed in Table IV. The values of ΔH^0_{298} so obtained show no temperature dependence and yield an average value of 136.6 kcal./mole. The slope value when corrected to 298°K. gives the value 137.3 ± 2.8 kcal./mole. This agreement furnishes strong confirmation of the interpretation of the vaporization behavior presented earlier.

TABLE V

CALCULATED THERMODYNAMIC FUNCTIONS FOR IDEAL MONATOMIC THORIUM GAS

T, °K.	$-\left(\frac{F^0_T - H^0_{298}}{T}\right)$, cal./deg./mole	$(H^0_T - H^0_{298})$, cal.	S^0_F, e.u.
1500	49.80	7429	54.76
1600	50.13	8236	55.28
1700	50.45	9062	55.78
1800	50.76	9901	56.26
1900	51.06	10750	56.72
2000	51.35	11610	57.16
2500	52.71	15900	59.07
3000	53.91	20070	60.60

The entropy of sublimation at 1856°K. as determined from the slope heat is 27.4 ± 1.5 e.u. while the value determined from the spectroscopic entropy of the gas and from heat capacity measurements on the solid[20] is 27.1 e.u. This value may appear anomalously low when compared to the entropies of sublimation of many of the refractory metals, but is explained by the unusually high value of the entropy of thorium solid.

The initial vaporization rate data given in Fig. 1 may be used to calculate the free energy change associated with reaction 1, and thus to obtain a lower limit for the stability of ThO(g). To make such a calculation it now becomes necessary to make some assumption about the activity of ThO_2(s) in thorium metal containing about 1000 p.p.m. oxygen. There are indications from other experiments[23] that the solubility of oxygen in thorium is quite low. In addition Hoch and Johnston's[12,24] work indicates that ThO(s) is not stable under our experimental conditions. Finally it was noticed by visual observations during the vaporization runs corresponding to the upper portions of Fig. 1 that there were present on the surface of the disk areas of two quite different emmissivities, presumably corresponding to Th(s) and ThO_2(s).

Assuming the activities of Th(s) and ThO_2(s) to be unity, the free energy of reaction 1 can be calculated from the vaporization rate data assuming the only gaseous species is ThO. Combining this result with the free energy of formation of ThO_2(s), from Coughlin,[25] yields a free energy of formation of ThO(g) of −41.5 kcal./mole at 1883°K. If the initial vaporization rate from this Langmuir experiment did not yield the equilibrium pressure of ThO(g) or if the activity of ThO_2(s) or Th(s) was not unity then ThO(g) would be more stable than the value given above.

In order to obtain the corresponding heat of formation of ThO(g) one must estimate the entropy of ThO(g) since reliable molecular parameters are not available. Following Brewer,[26] the electronic partition function for ThO(g) is estimated on the basis of the low lying states of Th(III) as reported by Charles.[27] The vibrational frequency is taken to be 740 cm.$^{-1}$ as reported by Krishnamurty[28] on the basis of an extrapolation from the measured frequencies of other oxides. The internuclear distance was obtained from this frequency by the application of Badger's rule,[29] and gave r_e = 1.93 ± 0.04 Å. The resulting contributions to S^0_{1883} ThO(g) are

$$S^0_{trans} = 51.56 \text{ e.u.}$$
$$S^0_{rot} = 18.66 \pm 0.08 \text{ e.u.}$$
$$S^0_{elect} = 5.91 \text{ e.u.}$$
$$S^0_{vib} = 3.15 \text{ e.u.}$$

so that

$$S^0_{1883} \text{ ThO(g)} = 79.3 \text{ e.u.}$$

Using this value together with the entropies of $^1/_2O_2$(g) and Th(g) from Stull and Sinke[20] gives,

(21) R. Zalubas, private communication.

(22) H. G. Kolsky, R. M. Gilmer and P. W. Gilles, "The Thermodynamic Properties of 54 Elements Considered as Ideal Monatomic Gases," Los Alamos Scientific Laboratory of the University of California, U. S. Atomic Energy Report LA-2110, 1957.

(23) A. F. Gerds and M. W. Mallett, *J. Electrochem. Soc.*, **101**, 171 (1954).

(24) R. J. Ackermann, R. J. Thorn and P. W. Gilles, *J. Am. Chem. Soc.*, **78**, 1767 (1956).

(25) J. P. Coughlin, "Contributions to the Data on Theoretical Metallurgy," U. S. Bureau of Mines Bulletin 542, 1954.

(26) L. Brewer and M. S. Chandrasekaraiah, "Free Energy Functions for Gaseous Monoxides," University of California Radiation Laboratory, U. S. Atomic Energy Report UCRL-8713, 1959.

(27) G. W. Charles, "A Compilation of Data on Some Spectra of Thorium," Oak Ridge National Laboratory, U. S. Atomic Energy Report ORNL-2319, 1958.

(28) S. Krishnamurty, *Proc. Phys. Soc.* (*London*), **64A**, 852 (1951).

(29) R. M. Badger, *J. Chem. Phys.*, **3**, 710 (1935).

for the heat of formation of ThO(g), ΔH^0_{1883} (form) = −8.0 kcal./mole. Combining this value with the dissociation energy of oxygen and our heat of sublimation of thorium metal yields a dissociation heat at 1883°K. for ThO(g) of +200.0 kcal./mole corresponding to D_0^0(ThO) = 196.1 kcal./mole. This is to be compared with Brewer's[30] estimated value of 200 ± 20 kcal./mole.

Further work on the reaction of thorium with thorium dioxide and with oxygen is in progress.

Acknowledgment.—The authors wish to thank Dr. S. J. Yosim and Dr. D. E. McKenzie for many enlightening discussions and Romuald Zalubas of the National Bureau of Standards for providing us with his preliminary data on the spectra of thorium.

(30) L. Brewer, "Dissociation Energies of Gaseous Oxides," University of California Radiation Laboratory, U. S. Atomic Energy Report UCRL-8356, 1958.

SUBSTITUTION REACTIONS OF OXALATO COMPLEX IONS. II. KINETICS OF AQUATION OF TRISOXALATOCHROMIUM(III) ION—SOLVENT DEUTERIUM ISOTOPE EFFECT

BY KOTRA V. KRISHNAMURTY AND GORDON M. HARRIS

Department of Chemistry, University of Buffalo, Buffalo, N. Y.

Received September 30, 1959

The kinetics of aquation of the ion $Cr(C_2O_4)_3^{-3}$ have been studied as a function of complex ion concentration, acidity, added oxalic acid, temperature and heavy water solvent composition, using a spectrophotometric method. The total reaction in strongly acid solution is $Cr(C_2O_4)_3^{-3} + 2H_3O^+ \rightarrow Cr(C_2O_4)_2(H_2O)_2^- + H_2C_2O_4$. The following rate law is consistent with the observed kinetic data $-d(Cr(C_2O_4)_3^{-3})/dt = k'(H_3O^+)(Cr(C_2O_4)_3^{-3}) + k''(H_3O^+)^2(Cr(C_2O_4)_3^{-3})$. The mixed order with respect to (H^+) is interpreted in terms of a rapid pre-equilibration of complex with one proton, followed by parallel rate-determining reaction paths involving either non-catalyzed or acid-catalyzed displacement of oxalate. Experiments in H_2O/D_2O solvent mixtures show that the rate of aquation increases as a function of deuterium atom fraction in agreement with the Gross–Butler equation. This finding is consistent with the proton pre-equilibration postulate made here, and in an earlier study of the oxalate exchange reaction of $Cr(C_2O_4)_3^{-3}$ ion. Some exchange experiments using carbon-14 labelled free oxalate–$Cr(C_2O_4)_2(H_2O)_2^-$ ion mixtures indicate that oxalate exchange with the latter ion occurs at a negligible rate, even under conditions where exchange with $Cr(C_2O_4)_3^{-3}$ ion is quite rapid.

In the first communication in this series[1] a study of the kinetics of oxalate exchange of the tris-oxalato chromium(III) ion was reported. A mechanism was proposed which was consistent with the rate data, and part of which consisted of the acid-catalyzed aquation of the tris-oxalato ion to produce a small equilibrium concentration of bis-oxalatodiaquochromium(III) ion. It was thus deemed worthwhile to supplement this exchange investigation with cognate work along two lines—firstly, an attempt to study the rate of the oxalate exchange reaction of the bis-oxalatodiaquo ion, and secondly, an attempt to determine the kinetics of the acid-catalyzed aquation of the tris-oxalato ion. The first of these aims has been only partially accomplished, due to complications discussed below. The aquation reaction has proved amenable to detailed study, and a report on it forms the major part of this paper.

Four previous studies involving the $Cr(C_2O_4)_2(H_2O)_2^-$ ion are of significance to the present work. Hamm and Perkins[2] investigated the kinetics of the reaction

$$Cr(Ch)_2(H_2O)_2^- + Ch^= \longrightarrow Cr(Ch)_3^{-3} + 2H_2O$$

where Ch = oxalate or malonate. The rates were first order in the diaquo-chromium species and independent of added anion concentration. They were also independent of *p*H over the range on each side of the neutral point within which acidic or basic decomposition reactions of $Cr(Ch)_3^{-3}$ are negligibly slow. For the oxalate, this range was from 4.0 to 9.3, and within these limits the association appeared to be completely unidirectional as written, with a half-time of 26 minutes at 50°. Dutt and Sur[3] attempted to determine the stepwise instability constants of $Cr(C_2O_4)_3^{-3}$, and found that only the first step is observable even with acid concentration as high as 0.16 *M*, clearly indicating the great stability of the diaquo ion. Studies of the *trans–cis* isomerization of $Cr(C_2O_4)_2(H_2O)_2^-$ ion have been made independently by Hamm[4] and by Cunningham, Burley and Friend.[5] The *trans* to *cis* reaction goes essentially to completion in aqueous solution, is first order in complex, independent of *p*H, and only slightly affected by ionic strength. The reaction half-time is less than 3 minutes at 50°.

Experimental

a. Materials.—Crystalline $K_3Cr(C_2O_4)_3 \cdot 3H_2O$ and *cis*-$KCr(C_2O_4)_2(H_2O)_2 \cdot 2H_2O$ were prepared according to published procedures[6,7] using reagent grade chemicals. The purity of each salt was checked by analysis. Oxalate was determined permanganometrically after decomposing the complex with hot KOH, filtering off the $Cr(OH)_3$, and acidifying the filtrate with H_2SO_4. The $Cr(OH)_3$ precipitate, after washing free of alkali, was ignited to Cr_2O_3 and weighed to determine the chromium. The found oxalate–chromium ratios were 2.96 and 1.99, respectively, for the tris and bis complexes.

(1) F. D. Graziano and G. M. Harris, THIS JOURNAL, **63**, 330 (1959).

(2) R. E. Hamm and R. H. Perkins, *J. Am. Chem. Soc.*, **77**, 2083 (1955).

(3) N. K. Dutt and B. Sur, *Z. anorg. allgem. Chem.*, **293**, 195 (1957).

(4) R. E. Hamm, *J. Am. Chem. Soc.*, **75**, 609 (1953).

(5) G. E. Cunningham, R. W. Burley and M. T. Friend, *Nature*, **166**, 1103 (1952).

(6) H. Croft, *Phil. Mag.*, **21**, 197 (1842).

(7) A. Werner, *Ann.*, **406**, 261 (1914).

Absorption spectra of the two oxalato complexes were run in 1-cm. Corex cells in a Beckman Model DK-2 Spectrophotometer. The observed peak wave lengths and corresponding molar absorption coefficients were: tris-oxalato, 420 and 573 mμ, 87.5 and 68.9, respectively; *cis*-bis-oxalato, 416 and 562 mμ, 67.3 and 52.0, respectively.

Baker C.P. perchloric acid and G. F. Smith anhydrous sodium perchlorate were used without further purification. All other standard chemicals were of reagent grade. Commercial carbon-14 labelled oxalic acid solution of high specific activity was diluted with inactive potassium oxalate to give a stock solution such that when precipitated as $CaC_2O_4 \cdot H_2O$ the counting rate by conventional thin solid-sample counting technique was about 600 counts/mg./min. CO_2-free water from an ion-exchange purifier was used in making all solutions. 99.5% heavy water was obtained from the Stuart Oxygen Company.

b. **Exchange Studies.**—Calculated volumes of 0.05 *M* $KCr(C_2O_4)_2(H_2O)_2$ and of standardized solutions of $HClO_4$ and/or $NaClO_4$ were mixed in 40-ml. glass-stoppered centrifuge tubes and thermostated, as also was the stock solution of labelled oxalate. Reaction was commenced by pipetting aliquots together with rapid mixing. Three-ml. samples were withdrawn at intervals and quenched by adding 4 ml. of solution 0.25 *M* in each of $CaCl_2$, NH_4Cl and HOAc. The precipitated $CaC_2O_4 \cdot H_2O$ was separated immediately by centrifugation, washed and counted according to established procedure.[1] A check of the separation method showed that recovery of the free oxalate was not quantitative at higher acidities due to the solubility of the precipitate in acid. However, specific activity determinations of the samples were generally reproducible within ±1%. At the lower acidities, oxalate recovery was complete, but the experiments were complicated by the rapid reaction between $Cr(C_2H_4)_2(H_2O)_2^-$ and free oxalate ion already mentioned.

c. **Aquation Studies.**—Kinetic runs were made in a Beckman Model DU Spectrophotometer, using a thermostated cell compartment capable of temperature control ±0.2°. Calculated volumes of standardized solutions of $HClO_4$ and $NaClO_4$, diluted with the necessary amount of water, were mixed in a 25-ml. volumetric flask and brought to temperature equilibrium in the bath used to thermostat the cell compartment. The required volume of 0.05 *M* $K_3Cr(C_2O_4)_3$ stock solution, similarly thermostated, was pipetted into the reaction flask with thorough mixing. A portion of the reaction mixture was immediately transferred to the spectrophotometer cell and the run commenced. These preliminary operations were completed within 45 seconds. The optical density of the reaction mixture at 420 mμ was determined at frequent intervals. Since the zero time optical density D_0 is entirely due to the pure tris complex, and that at infinite time, D_∞, that of pure *cis*-bis complex,[8] the fraction of reaction F in any given run where D_t is the optical density at time t is given by the equation

$$F = (D_0 - D_t)/(D_0 - D_\infty)$$

Series of experiments were carried out to determine the effects of variation of the concentration of complex ion, hydrogen ion and oxalate ion, and of temperature and ionic strength, all in normal water solvent. Deuterium solvent effect experiments were done using a 0.05 *M* stock solution of complex made by dissolving the required quantity of solid $K_3Cr(C_2O_4)_3 \cdot 3H_2O$ in pure D_2O, and a stock solution of deuterated perchloric acid made by diluting 11.6 *M* $HClO_4$ with pure D_2O. Reaction mixtures containing as much as 91% D could be prepared in this way, and runs were made with several such mixtures in the manner already described.

Results and Discussion

a. Exchange Studies.—Several experiments were carried out in which the specific activity of the free oxalate was determined as a function of duration of mingling with the bis-oxalato complex compound. At 25°, with *p*H 6, (complex) = 0.01 *M*, (free oxalate) = 0.02 *M*, there was no significant change in free oxalate activity during 26 hours, although nearly half of the free oxalate was used up by the association reaction to form $Cr(C_2O_4)_3^{-3}$ under these conditions.[2] At 50°, with *p*H 1.0, ionic strength = 0.5, (complex) = (free oxalate) = 0.05 *M*, no exchange was detected during a 6 hour period. Finally, a more detailed experiment was carried out under conditions closely comparable to those of the $Cr(C_2O_4)_3^{-3}$-oxalate exchange study,[1] yielding the results recorded in Table I.

TABLE I

EXCHANGE OF FREE OXALATE WITH BOUND OXALATE OF THE $Cr(C_2O_4)_2(H_2O)_2^-$ ION

Temp., 75°; (complex) = 0.05 *M*; (free oxalate) = 0.02 *M*, *p*H 3

Time, min.	Wt. of $CaC_2O_4 \cdot H_2O$, mg.	Specific activity,[a] counts/min./mg.
1.5	9.2	303[b]
15	6.4	322
30	5.1	325
120	2.8	276
360	2.2	128
720	2.2	108

[a] Corrected for self-absorption and self-scattering.[1] [b] Large sample, subject to greater counting errors than the others.

It is obvious that oxalate exchange of the $Cr(C_2O_4)_2(H_2O)_2^-$ ion is a negligibly slow process both under conditions where addition of $C_2O_4^=$ ion to the complex goes essentially to completion (at 25° and *p*H 6, half-time for association reaction is 9 hours[2]), and under conditions where the reverse process, aquation of $Cr(C_2O_4)_3^{-3}$ ion, is completely predominant (at 50° and *p*H 1, half-time for aquation is also 9 hours—see Table III). The data of Table I enable three significant qualitative deductions: (i) as shown by the second column, the association reaction

$$Cr(C_2O_4)_2(H_2O)_2^- + C_2O_4^= = Cr(C_2O_4)_3^{-3} + 2H_2O \quad (1)$$

proceeds rapidly at 75° and *p*H 3 to an equilibrium, with a half-time of the order of magnitude of 25 minutes. An extrapolation of the data of Hamm and Perkins[2] leads to a value of 1.6 minutes for this quantity at the same temperature and *p*H 6. The reaction clearly becomes *p*H-dependent outside the range studied by these authors. Further work is necessary to determine the exact nature of this dependence.

(ii) The equilibrium constant for the dissociation of $Cr(C_2O_4)_3^{-3}$ (reverse of reaction 1) at 75° may be estimated[9] to be K = (bis-oxalato)$(C_2O_4^=)$/(tris-oxalato) = 3.5×10^{-4}. The only comparable figure in the literature[3] is $K = 3.4 \times 10^{-6}$ at 32°. Our value is consistent with this if the heat of the reaction has the reasonable magnitude of 20 kcal./mole.

(iii) The half-time of exchange obtained from the conventional linear plot of the ln(1 − fraction exchange) *vs.* time is close to 4 hours. It is unlikely

(8) Proven by the fact that the spectra of the reaction mixtures became indistinguishable after several reaction half-times from those of pure *cis*-$KCr(C_2O_4)_2(H_2O)_2$ solutions of the same concentration. No *trans*-isomer appears among the products, as is expected from the instability of the latter form under the present conditions (see also ref. 4).

(9) The precipitate weight figures show that about 3/4 of the free oxalate is used up by reaction with bis-oxalato ion. Thus the equilibrium concentrations of bis-oxalato, tris-oxalato and total free oxalate ions are estimated to be 0.035 *M*, 0.015 *M* and 0.005 *M*, respectively. The actual $(C_2O_4^=)$ is obtained from the total oxalate figure by use of the value of 3×10^{-5} for the second ionization constant of oxalic acid, extrapolated from the data of Harned and Fallon.[10]

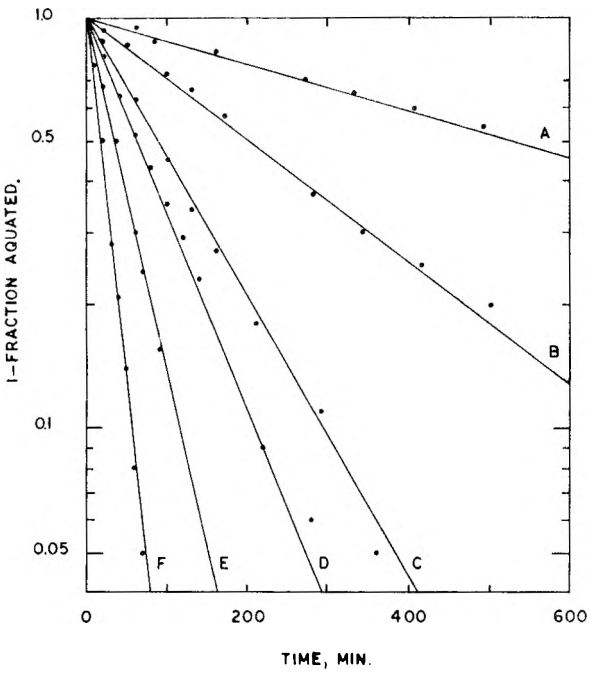

Fig. 1.—Typical aquation runs—conditions: 50.0°, 5.0×10^{-3} *M* $Cr(C_2O_4)_3^{-3}$, 15×10^{-3} *M* K^+, 0.97 *M* ClO_4^-, ionic strength adjusted to 1.00 by addition of $NaClO_4$ except in run F: curve A, 0.10 *M* H^+, $t^1/_2$ 530 min.; B, 0.20 *M* H^+, $t^1/_2$ 202 min.; C, 0.40 *M* H^+, $t^1/_2$ 88 min.; D, 0.50 *M* H^+, $t^1/_2$ 63 min.; E, 0.65 *M* H^+, $t^1/_2$ 35 min.; F, 0.97 *M* H^+, $t^1/_2$ 17 min.

to be sheer coincidence that this figure agrees well with the expected value of 3.9 hours calculated from the data of Graziano and Harris for $Cr(C_2O_4)_3^{-3}$ oxalate exchange under the same conditions. The logical conclusion is that only the $Cr(C_2O_4)_3^{-3}$ formed in the system provides a path for oxalate exchange. The $Cr(C_2O_4)_2(H_2O)_2^-$ species is so stable that direct oxalate substitution is negligibly slow under the present conditions. Similar behavior previously has been inferred for the corresponding cobalt(II) complex ion.[11]

b. Aquation Studies.—For individual runs, plots of $\ln(1 - F)$ against time give good straight lines, as seen in Fig. 1. This seeming first-order dependence on tris-oxalato complex ion concentration was confirmed by a series of runs where all factors were fixed except the initial (complex ion), as shown in Table II.

TABLE II

DEPENDENCE OF AQUATION RATE OF CONCENTRATION OF $Cr(C_2O_4)_3^{-3}$ ION

Temp., 50.0°; (H^+) = 0.97 *M*; ionic strength = 1.00 (adjusted with $NaClO_4$)

(Complex), $M \times 10^3$	$t_{1/2}$, min.	$0.693/t_{1/2}$, sec.$^{-1} \times 10^4$
2.5	17.0 ± 0.3	6.80
4.0	17.5 ± .3	6.60
5.0	17.0 ± .3	6.80
6.0	19.0 ± 1.0	5.99
7.5	22.0 ± 2.0	5.26[a]
25.0	18.0 ± 0.7	6.41[b]
	Mean	6.48 ± 0.26[c]

[a] Optical density data inaccurate due to high absorption in 1 cm. cell. [b] 1 mm. path-length cell used. [c] Excluding 5th run in series.

The dependence of the rate on the concentration of hydrogen ion is shown in Table III. The values for $k_{exp} = 0.693/t_{1/2}$ were obtained from straight line plots such as illustrated in Fig. 1. The calculated over-all rate constants were determined by the assumption that $k_{calcd} = k'(H_3O^+) + k''(H_3O^+)^2$, where k' and k'' have the values 1.7×10^{-4} l.mole^{-1} sec.$^{-1}$ and 5.0×10^{-4} l.^{2}mole^{-2}. sec.$^{-1}$, respectively, at 50°.

TABLE III

DEPENDENCE OF AQUATION RATE ON CONCENTRATION OF HYDROGEN ION

Temp., 50.0°; (complex) = 5.0×10^{-3} *M*; ionic strength = 1.00 (adjusted with $NaClO_4$)

(H^+), *M*	k_{exp}, sec.$^{-1} \times 10^4$	$k_{calcd.}$ sec.$^{-1} \times 10^4$
0.01	0.03	0.02
.02	.04	.03
.05	.11	.09
.10	.22	.22
.20	.57	.54
.40	1.31	1.48
.50	1.83	2.10
.65	3.30	3.22
.80	4.45	4.56
.97	6.48[a]	6.35

[a] Mean value from Table II.

Some other experiments were done at 50°, with (complex) = 0.005 *M* and (H_3O^+) = 0.97 *M*, and other conditions set as follows: (i) solution also 0.005 *M* in oxalic acid, ionic strength adjusted to 1.00 with $NaClO_4$; (ii) ionic strength made up to 1.50; (iii) ionic strength made up to 2.00. In none of these experiments was the rate of aquation significantly different from the mean value of Table II. The temperature dependence of the rate was as shown in Fig. 2, which presents the results of experiments at two acidities carried out at temperatures of 40, 50, 60 and 75, respectively. The lines have the same slopes within experimental error, and the over-all activation energy calculated from this slope is 22.1 ± 0.2 kcal./mole.

The rate of aquation data can be interpreted by the reaction mechanism

$$Cr(C_2O_4)_3^{-3} + H_3O^+ \rightleftharpoons Cr(C_2O_4)_2OC_2O_3H\cdot H_2O^- \quad K_2 \quad (2)$$

$$Cr(C_2O_4)_2OC_2O_3H\cdot H_2O^- + H_2O \longrightarrow Cr(C_2O_4)_2(H_2O)_2^- + HC_2O_4^- \quad k_4 \quad (3)$$

$$Cr(C_2O_4)_2OC_2O_3H\cdot H_2O^- + H_3O^+ \longrightarrow Cr(C_2O_4)_2(H_2O)^- + H_2C_2O_4 \quad k_7 \quad (4)$$

This leads to the rate law

$$-d(Cr(C_2O_4)_3^{-3})/dt = K_2k_4(H_2O)(H_3O^+)(Cr(C_2O_4)_3^{-3}) + K_2k_7(H_3O^+)^2(Cr(C_2O_4)_3^{-3})$$

where the symbols K_2, k_4 and k_7 are consistent with those used in the first paper of this series,[1] and the same assumptions concerning equilibrium reaction 2 are made as before. The last column of Table III illustrates that this law fits the data well with previously defined constants k' and k'' equated to $K_2k_4(H_2O)$ and k_2k_7, respectively. The absence of ionic strength effects in the present study is probably without real significance, since the values used were so high as to be outside the range of

applicability of the Debye–Hückel theory in any case. Also, added oxalate should have no effect on the rate if reactions 3 and 4 are essentially unidirectional, as is the case under present conditions.[8]

The experimental activation energy is apparently independent of (H_3O^+), indicating that the activation energies for reactions 4 and 3, (E_7 and E_4), are equal. Assuming that ΔH for reaction 2 is not very different from that for protonation of a free oxalate ($C_2O_4^=$) ion (calculated to be 2.8 kcal./mole from data in the literature[10]), it follows that $E_4 = E_7 = 19.3$ kcal./mole. This value for E_4 is in reasonable agreement with an approximate figure of 20 kcal./mole derivable from the exchange data.[11] Other comparable data are those of Schläfer and co-workers[12] who report values of 24.6 and 19.5 kcal./mole for the activation energies of hydrolytic displacement of en from $Cr(en)_3^{+3}$ and $Cr(C_2O_4)_2en^-$, respectively. It is also of interest that the activation energy for the process

$$Co(tn)_2Co_3^+ + 2H_2O = Co(tn)_2(H_2O)_2^{+3} + CO_3^=$$

is 24.8 kcal./mole.[13] Finally, one notes that the value for $K_2k_4(H_2O)$ at 75° deduced from the data of this paper is 1.7×10^{-3} l. mole^{-1} sec.$^{-1}$, in good agreement with the figure 1.8×10^{-3} obtained for the same constant in the oxalate exchange study.[1]

The runs made in H_2O–D_2O solvent mixtures of several compositions resulted in the data shown in Table IV. Also tabulated are the various k_n/k_H values calculated according to Purlee's recapitulation of the Gross–Butler equation,[14] utilizing the k_D/k_H value obtained by graphical extrapolation from our data. The good agreement between the observed and calculated values for k_n/k_H can be taken as strong support for the general acid catalysis mechanism: $S + H^+ \rightleftarrows SH^+$; $SH^+ \rightarrow$ products, with the second step rate-determining but not subject to isotope effect.[15] This is exactly the type

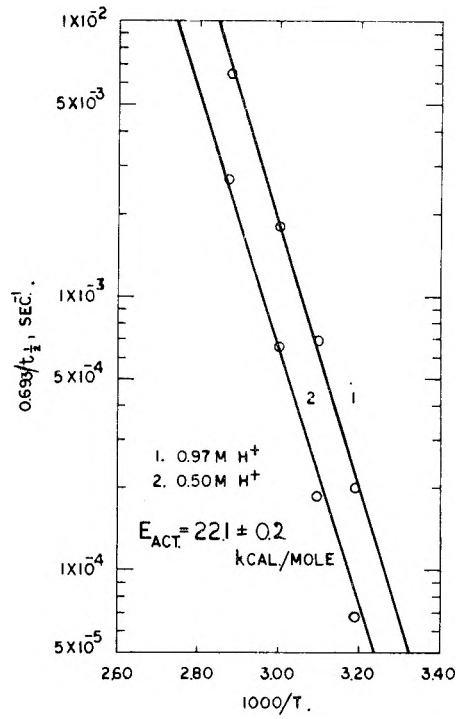

Fig. 2.—Temperature dependence of rate—conditions: 5.0×10^{-3} M $Cr(C_2O_4)_3^{-3}$, 15×10^{-3} M K^+, 0.97 M ClO_4^-, ionic strength adjusted to 1.00 by addition of $NaClO_4$.

TABLE IV

SOLVENT DEUTERIUM ISOTOPE EFFECT ON THE AQUATION RATE OF $Cr(C_2O_4)_3^{-3}$

Temp., 50.0°, (complex) = 0.005 M; (acid) = 0.97 M; ionic strength = 1.00

n = (D)/(H + D)	k_{exp}, sec.$^{-1}$ × 10^4	k_n/k_H (obsd.)	k_n/k_H (calcd.)
0.00	6.8	1.00	1.00
.26	7.7	1.13	1.24
.49	10.1	1.49	1.52
.91	16.0	2.35	2.38
1.00	17.8[a]	2.62	(2.62)

[a] Graphically extrapolated value.

of mechanism proposed in the present study, with our k_D/k_H ratio of the same order of magnitude as observed in reactions of this type involving organic compounds.[14,15] Absence of hydrogen isotope effect in either reaction 3 or 4 is to be expected, since the rate-determining process in these reactions is almost certain to be either Cr–O or C–O bond breakage, as appears to be the case for acid-catalyzed aquation of the $Co(NH_3)_4CO_3^+$ ion.[16,17]

(10) H. S. Harned and L. D. Fallon, *J. Am. Chem. Soc.*, **61**, 3111 (1939).

(11) See ref. 1, p. 332.

(12) H. L. Schläfer and O. Kling, *Z. physik. Chem. (Frankfurt)*, **16**, 14 (1958); H. L. Schläfer, Abstracts of Papers, Int. Conf. Co-ord. Chem., London, April, 1959.

(13) J. E. Boyle and G. M. Harris, *J. Am. Chem. Soc.*, **80**, 782 (1958).

(14) E. L. Purlee, *ibid.*, **81**, 263 (1959). A modified Gross–Butler equation was used in obtaining the k_n/k_H calculated value

$$\frac{k_n}{k_H} = \frac{1}{Q'(n)}\left[(a_{H_2O})_n^{1/2} + \frac{k_D}{k_H}\frac{(a_{D_2O})_n^{1/2}}{L^{1/2}}\right]$$

where k_H, k_n, and k_D are the rate constants in pure H_2O, H_2O–D_2O and D_2O. a_{H_2O} and a_{D_2O} are the activities of H_2O and D_2O, and are given, in terms of mole fractions, by $(1 - n)^2$ and n^2, respectively. Values for the $Q'(n)$ function and the equilibrium constant L at 50° were taken from Purlee's tabulated data.

(15) K. B. Wiberg, *Chem. Revs.*, **55**, 713 (1955).

(16) F. A. Posey and H. Taube, *J. Am. Chem. Soc.*, **75**, 4099 (1953).

(17) D. R. Stranks and G. M. Harris, THIS JOURNAL, **56**, 906 (1952).

FREE ENERGIES OF FORMATION OF GASEOUS URANIUM, MOLYBDENUM, AND TUNGSTEN TRIOXIDES[1]

BY R. J. ACKERMANN, R. J. THORN,
Argonne National Laboratory, Lemont, Illinois

CARL ALEXANDER AND
Battelle Memorial Institute, Columbus, Ohio

MARVIN TETENBAUM[1a]
General Electric Co., Aircraft Nuclear Propulsion Department, Cincinnati, Ohio

Received October 3, 1959

Measurements of the vapor density in equilibrium with molybdenum trioxide and uranium oxide (U_3O_8) have been performed by means of the transpiration method with oxygen employed as a carrier gas. The standard free energy of sublimation in calories per mole of gas for molybdenum trioxide is given over the temperature range 980 to 1060°K. by the equation $\Delta F^0_s = (87.8 \pm 1.0)\,10^3 - (73.0 \pm 1.0)\,T$ cal. mole^{-1}, in which the polymeric species in the vapor are recognized. In the case of uranium oxide variation of the oxygen pressure in the carrier gas establishes the oxygen-to-uranium ratio equal to three for the volatile uranium oxide molecule. By a comparison with the entropies of sublimation of molybdenum and tungsten trioxides it is inferred that gaseous monomeric uranium trioxide is the principal species produced by the reaction of U_3O_8 with oxygen. Although the vapor may not consist entirely of monomer, the standard free energy of formation in calories per mole of this gas over the temperature range 1230–1700°K. can be expressed by the equation $\Delta F^0_f = -198{,}500 + 19.0T$ cal. mole^{-1}.

Introduction

Certain aspects of the chemical behavior of solid and gaseous compounds of uranium can be understood better by considering it as a member of the group containing chromium, molybdenum and tungsten rather than as a member of the actinide elements, so it is significant to study the stability and complexity of gaseous uranium oxides in relation to those of molybdenum and tungsten. It has been shown[2,3] that there is a gaseous uranium oxide of oxidation state higher than four which can be observed at temperatures above 1000° over the higher oxides in the condensed state. The identification with a mass spectrometer[4] of gaseous uranium trioxide in an effusion study with uranium dioxide at temperatures near 1800° suggests that the volatile oxide observed at the lower temperature and higher pressure of oxygen is the trioxide. However, principally because of the difficulty of maintaining the condensed phase sufficiently oxidized during measurements *in vacuo* the partial pressure and the free energy of formation of this gas have not been measured. In addition to the interest already cited the latter quantity is also needed to ascertain the contribution of the trioxide to the vapor pressure of uranium dioxide.[5]

Previous measurements of the vapor pressure and/or density of molybdenum trioxide have been effected, but some rather serious discrepancies exist. Using the effusion method in a mass spectrometer, Berkowitz, Chupka and Inghram[6] identified gaseous trimer, tetramer and pentamer, and obtained the free energies of sublimation of molybdenum trioxide to these species. Blackburn, Hoch and Johnston[7] determined the total effusion rates of molybdenum and tungsten trioxides. Employing the transpiration method with air as the transporting gas, Ariya, Shchukarev and Glushkova[8] measured the vapor density of molybdenum trioxide. The last cited study yields a vapor pressure 1.14 times the second and 3.0 times the first. The transpiration and boiling point measurements of Zelikman, Gorovitz and Prosenkova[9] yield an average molecular weight of 3.2 times the monomer whereas the measurements of Berkowitz, Chupka and Inghram yield an extrapolated value of 3.6. In the case of tungsten trioxide Berkowitz, *et al.*,[10] reported an entropy of sublimation to the trimer of 69.5 e.u. cal./mole whereas Blackburn, *et al.*,[7] reported a value of 54.1 e.u. Since it is known that tungsten trioxide *in vacuo* loses significant amounts of oxygen at elevated temperatures[11] one suspects that molybdenum trioxide behaves similarly and, since some of the earlier investigations were carried out *in vacuo*, it is desirable to measure the vaporization rates under conditions that maintain the solid in the highest possible oxidation state by maintaining as large as feasible an oxygen pressure in the system. This is especially true in the case of the uranium oxide.

Experimental

The vapor densities of the gases were determined by the use of the transpiration method in which oxygen flowed through the powdered solid and carried the saturated vapor into a condenser. In using this method one must design the apparatus so as to eliminate two possible errors. First, the rate of gas flow must not be greater than the rate at

(1) Based on work performed under the auspices of the U. S. Atomic Energy Commission. Presented at 135th Meeting of the American Chemical Society, Boston, 1959.

(2) (a) W. Biltz and H. Mueller, *Z. anorg. allgem. Chem.*, **163**, 257 (1927); (b) L. Brewer, *Chem. Revs.*, **52**, 1 (1953).

(3) R. J. Ackermann and R. J. Thorn, "Reactions Yielding Volatile Oxides at High Temperatures," XVI International Congress of Pure and Applied Chemistry, Paris, 1957. See also Argonne National Laboratory Report, ANL-5824, Jan., 1958.

(4) W. A. Chupka, Argonne National Laboratory Report, ANL-5786, July, 1957.

(5) R. J. Ackermann, P. W. Gilles and R. J. Thorn, *J. Chem. Phys.*, **25**, 1089 (1956).

(6) J. Berkowitz, W. A. Chupka and M. Inghram, *ibid.*, **26**, 842 (1957).

(7) P. E. Blackburn, M. Hoch and H. L. Johnston, THIS JOURNAL, **62**, 769 (1958).

(8) S. M. Ariya, S. A. Shchukarev and V. B. Glushkova, *J. General Chem.* (*U.S.S.R.*), **23**, 2063 (1953).

(9) A. N. Zelikman, N. N. Gorovitz and T. E. Prosenkova, *J. Inorg. Chem.* (*U.S.S.R.*), **1**, 332 (1956).

(10) J. Berkowitz, W. A. Chupka and M. Inghram, *J. Chem. Phys.*, **27**, 85 (1957).

(11) R. J. Ackermann, E. G. Rauh and R. J. Thorn, unpublished data, Argonne National Laboratory.

which evaporation can occur at the solid surface. Second, the rate of gas flow must be sufficiently rapid so as to minimize diffusion effects. Optimum conditions to circumvent the first difficulty were achieved by having the carrier gas pass directly through the powdered oxide which rested on either a fused silica disk or a column of aluminum oxide powder. Optimum conditions to eliminate significant diffusion were attained by having the saturated carrier gas pass through four small holes (0.05 inch in diameter) in the condenser so that the flow velocity was large at these points. A sketch of the essential features of the apparatus is shown in Fig. 1. A thermocouple of platinum and platinum with 10% rhodium, standardized by means of samples of copper, aluminum and zinc obtained from the National Bureau of Standards, was located just beneath the top surface of the oxide sample. In order to eliminate entrainment of solid particles in the flow gas, a plug of fused silica wool was inserted between the sample and the condenser. The volume of gas flowed was measured by a Model S-39466 Precision wet test meter.

To find the optimum flow rates measurement of the weight of molybdenum trioxide collected per liter of gas flowed was carried out at various flow rates. A typical result as shown in Fig. 2 confirms the behavior discussed by Lepore and Van Wazer[12] and by Merten.[13] The plateau indicates the region in which the carrying gas is essentially saturated with the trioxide. Because all transpirations reported herein were measured in this region of flow rates, no extrapolations to zero flow rate were necessary. With the apparatus described the increase in apparent vapor density caused by diffusion was not observed definitely although the curve drawn suggests the onset of it.

The procedure employed with the uranium oxide, U_3O_8, was similar to that employed with molybdenum oxide except that in the former case the amount of gaseous uranium oxide transported was determined by specifically assaying the amount of uranium in a sample prepared from the collection after its removal from the inside of the condenser by dissolution with hot concentrated nitric acid.

Discussion of Results

The experimental results for molybdenum trioxide are shown in Fig. 3. Assuming the measurements of Berkowitz, Chupka and Inghram[6] to yield the relative amounts of trimer, tetramer and pentamer in the vapor phase, one obtains the average molecular weights necessary for the calculation of pressures. The ratios of the mole fractions of trimer–to–tetramer, N_3/N_4, calculated from the data of these authors and given in Fig. 3 show that both species are important. From the weight of oxide transported, w, and the average molecular weight, $\bar{M}$, the vapor pressures were calculated according to the ideal gas equation

$$p = \frac{w}{V_r}\frac{R}{\bar{M}}T_r \qquad (1)$$

in which V_r is the volume of carrier gas measured at a temperature T_r. From these pressures one finds for the standard free energy of sublimation of molybdenum trioxide the equation

$$\Delta F^0_s(MoO_3) = (87.8 \pm 1.0)10^3 - (73.0 \pm 1.0)T \text{ cal. mole}^{-1} \qquad (2)$$

The errors given are standard deviations. The results obtained with helium and nitrogen as carrier gases do not differ within the experimental errors from those obtained with oxygen. Hence, the slight loss of oxygen from the solid molybdenum trioxide under these conditions does not detectably affect its vapor pressure. Also in Fig. 3 are

(12) J. V. Lepore and J. R. Van Wazer, "A Discussion of the Transpiration Method for Determining Vapor Pressure," MDDC-1188, U. S. Atomic Energy Commission.

(13) U. Merten, THIS JOURNAL, **63**, 443 (1959).

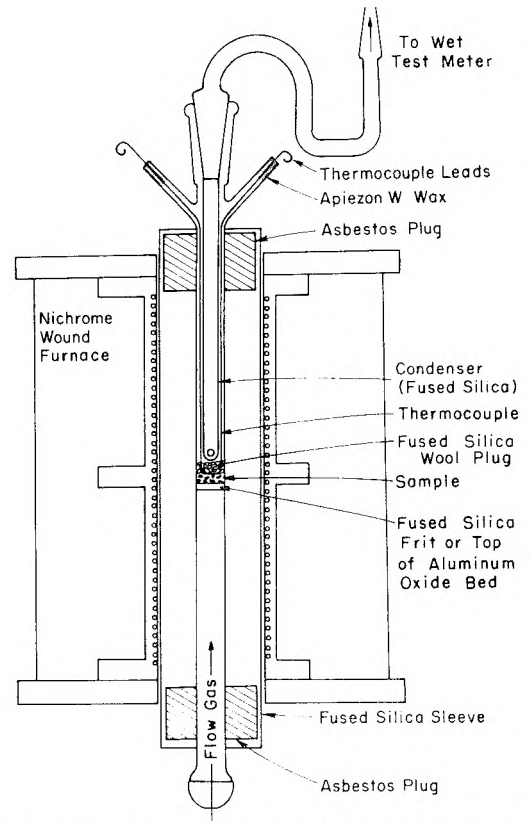

Fig. 1.—Schematic sketch of apparatus used to transpire gaseous molybdenum and uranium trioxides.

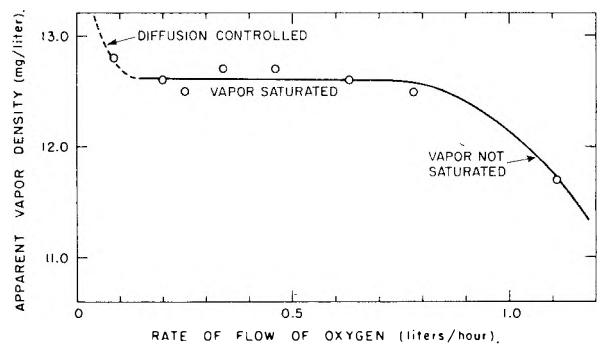

Fig. 2.—Variation of the amount of molybdenum trioxide transpired with flow rate at 1000°K.

given the heats and entropies of sublimation of molybdenum trioxide to the trimer, tetramer and pentamer, respectively. These quantities were calculated from the vapor density determinations reported herein and from the ratios of mole fractions of vapor species obtained from the investigation of Berkowitz, *et al.*[6] According to previously presented discussions[14] one predicts both from theoretical and experimental considerations that the entropies of sublimation to polymers will be

(14) The standard entropy and free energy of formation of $WO_3(g)$ were obtained[3] from measurements over the temperature range 1920–2020°K. of the reaction

$$3MgO(s) + W(s) \longrightarrow 3Mg(g) + WO_3(g) \qquad (3)$$

from which the equation

$$\Delta F^0_f\,[WO_3(g)] = -75{,}700 + 15.54T \text{ cal. mole}^{-1} \qquad (4)$$

was derived for the standard free energy of formation of gaseous, monomeric tungsten trioxide. The entropy of vaporization of molybdenum trioxide to the monomer was estimated.[15]

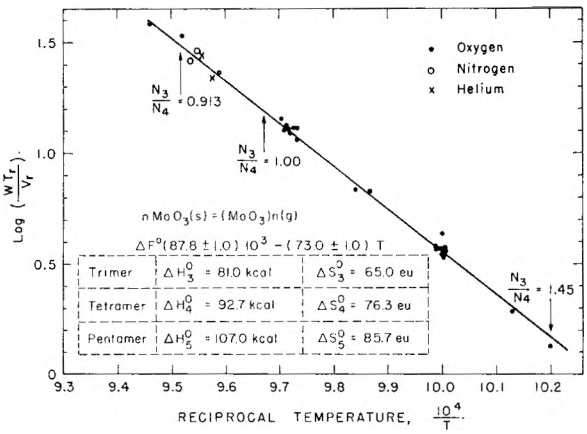

Fig. 3.—Plot of logarithm of vapor density of molybdenum trioxide as a function of the reciprocal of the absolute temperature. The quantity N_3/N_4 is the ratio of the mole fraction of trimer to tetramer in the vapor.

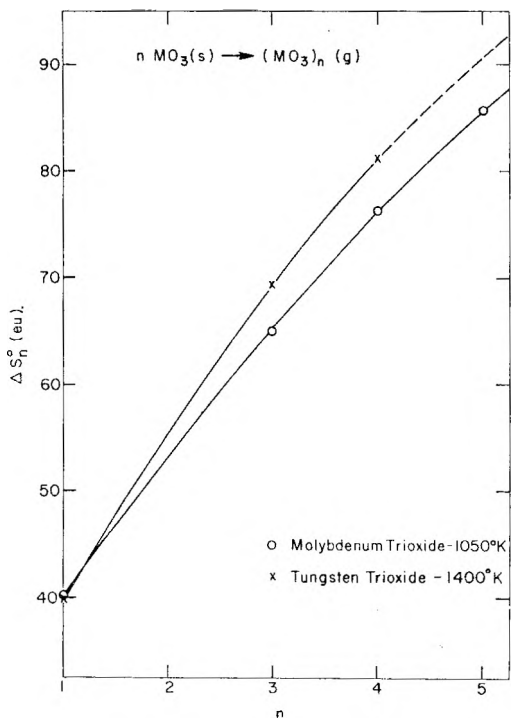

Fig. 4.—The entropy of sublimation of the n-mer as a function of n.

larger than that to monomers, so that the entropy change of 73.0 for a mixture of trimer, tetramer and pentamer is expected to be considerably larger than the estimated value of 40 e.u. for sublimation to the monomer.

In Fig. 4 is plotted the change in entropy that results from the sublimation of molybdenum and tungsten trioxides to yield one mole of gaseous polymer. The values of the quantity ΔS^0_n for the trimer and tetramer of tungsten trioxide have been taken from the work of Berkowitz, *et al.*,[10] while in the case of both monomeric tungsten and molybdenum trioxide ($n = 1$) the values of ΔS^0_1 were taken from the work of Ackermann and Thorn.[3] A comparison of the results presented here with those of previous investigations is given in Table I and Fig. 5. The lack of agreement is quite impressive even though all the investigations have been corrected to the same molecular weights obtained from the work of Berkowitz, *et al.*[6] There appears to be no single error large enough to account for this wide divergence of results. The present study agrees with that of Berkowitz, *et al.*,[6] within the respectively quoted errors. From both boiling point determinations and transpiration measurements of liquid molybdenum trioxide Zelikman, *et al.*,[9] concluded that trimeric molybdenum trioxide is predominant in the vapor phase whereas the results of Berkowitz, *et al.*,[6] when extrapolated to the liquid region by means of the measured heat of fusion for $MoO_3(s)$,[17] predict that tetrameric molybdenum trioxide predominates in the vapor phase.

TABLE I

HEATS AND ENTROPIES OF SUBLIMATION AND VAPORIZATION OF MOLYBDENUM TRIOXIDE

Investigators	T, °K.	ΔH^0_T (kcal. mole^{-1} of vapor)	ΔS^0_T (e.u. mole^{-1} of vapor)
Ueno[16]	908– 948	62.5	42.8
Ariya, *et al.*[8]	941– 987	67.0	53.3
Zelikman, *et al.*[9]	1178–1373[a]	35.6	24.9
Berkowitz, *et al.*[6]	810–1000	85.4	71.7
Blackburn, *et al.*[7]	808– 958	78.8	66.6
Ackermann, *et al.*	980–1060	87.8	73.0

[a] Measurements made above melting point.

With uranium oxide (U_3O_8) measurements were obtained in the temperature ranges 1200 to 1370°K. (at Argonne National Laboratory), 1425 to 1790°K. (at General Electric, Aircraft Nuclear Propulsion Department), and 1400 to 1800°K. (at Battelle Memorial Institute). In the last case the oxide was contained in a platinum dish over which oxygen flowed. In all cases the calculated pressure is independent of the ratio of uranium-to-oxygen in the molecule because the number of moles of uranium was assayed, by α-counting in the first two Laboratories, and by colorimetric[18] and fluorophotometric[19] methods in the last, but it does depend upon whether the gaseous species is monomeric or polymeric. The dependence of the pressure of the gaseous uranium oxide molecule on the pressure of oxygen in the carrier gas establishes a value nearly equal to three for the oxygen-to-uranium ratio of this molecule. The use of a mass spectrometer[20] to identify the vapor arising from a condensed phase which initially was $U_3O_8(s)$ shows an appreciable ion current due to UO_3^+. These observations suggest the possibility that monomeric uranium trioxide gas is the principal species in equilibrium with $U_3O_8(s)$ under the experimental conditions of this investigation The like-

(15) R. J. Ackermann and R. J. Thorn, "High Temperature Vaporization of Inorganic Substances: Entropy Considerations," XVI International Congress of Pure and Applied Chemistry, Paris, 1957.

(16) K. Ueno, *J. Chem. Soc. Japan*, **62**, 990 (1941).

(17) L. A. Cosgrove and P. E. Snyder, *J. Am. Chem. Soc.*, **75**, 1227 (1953).

(18) H. J. Seim, R. J. Morris and D. W. Frew, *Anal. Chem.*, **29**, 443 (1957).

(19) E. J. Center, "Topical Report on the Direct Micro Determination of Uranium Using a Modified Fluorophotometer," AECD-3006, June, 1948.

(20) Measurements performed at General Electric Co., Aircraft Nuclear Propulsion Department, Cincinnati, Ohio, by D. K. Conley and R. Kupel.

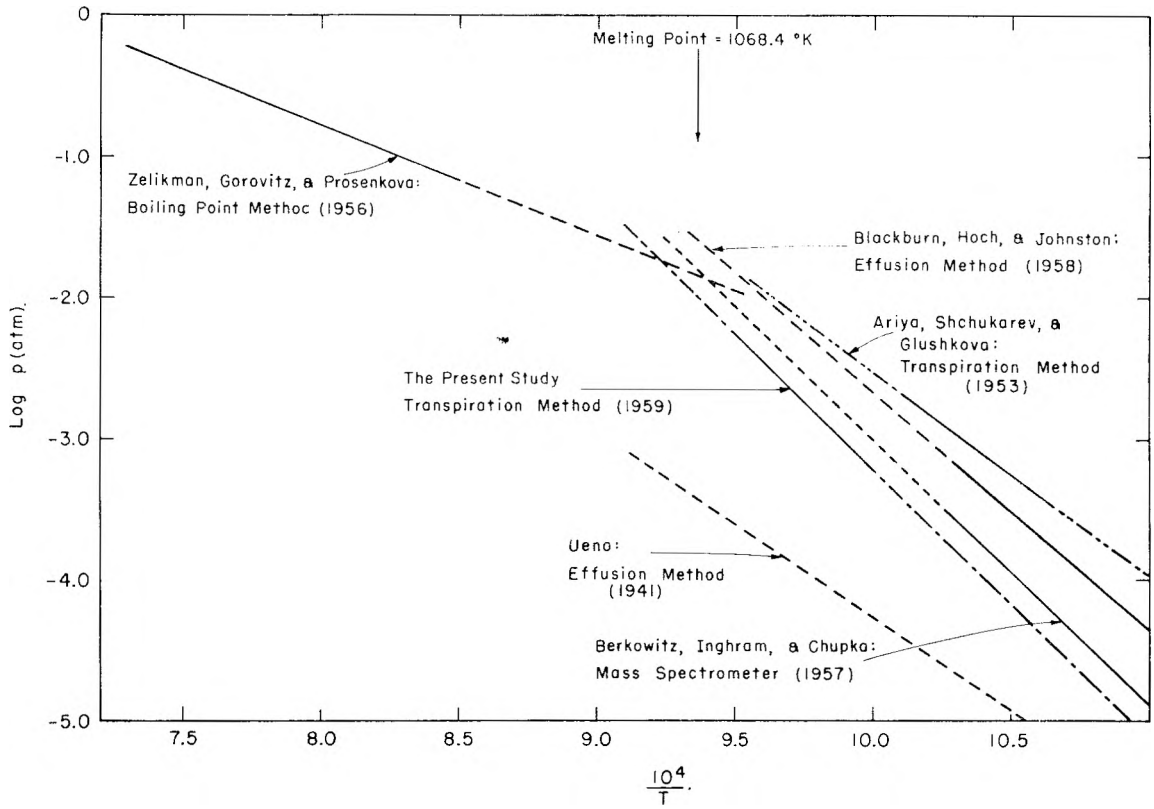

Fig. 5.—Plots of logarithm of vapor pressure of molybdenum trioxide *vs.* the reciprocal of the temperature derived from various measurements.

lihood of this possibility and of the presence of polymeric species is analyzed further by the entropy arguments given below.

For the reaction

$$\frac{n}{3}\,U_3O_8(s) + \frac{n}{6}\,O_2(g) \longrightarrow (UO_3)_n(g) \qquad (5)$$

the data derived from measurements in the lower temperature range (1200 to 1370°K.) yield 31, 30 and 29 e.u. for n equal to 1, 2 and 3, respectively. Deriving the entropies of sublimation of uranium trioxide [$nUO_3(s) \rightarrow (UO_3)_n(g)$] from these values and the entropies of formation of $UO_3(s)$,[21] and U_3O_8[22-24] one finds 41, 49 and 58 e.u. for n equal to 1, 2 and 3, respectively. The values 49 and 58 are about 5 and 10 e.u. smaller than one would expect for predominant amounts of dimers and trimers, respectively, by analogy with molybdenum and tungsten trioxides, whereas the value of 41 e.u. agrees with the values near 40 e.u. cited by Ackermann and Thorn[3,15] for the entropies of sublimation to gaseous monomers of molybdenum and tungsten trioxides, respectively. Therefore, one surmises that gaseous monomeric trioxide is the principal species in equilibrium with $U_3O_8(s)$ at the temperatures and pressures of this investigation.

With $n = 1$ in eq. 5 one then can use the data at the lower temperatures to derive the equation for the partial pressure of uranium trioxide

$$-R'T \log p_{UO_3}(\text{atm.}) = (83.3 \pm 3.4)\,10^3 - (31.3 \pm 2.6)\,T \text{ cal. mole}^{-1} \qquad (6)$$

in which the quantity R' is 4.576. The standard free energy of formation of U_3O_8, which is necessary for the evaluation of the standard free energy of formation of gaseous uranium trioxide in accordance with eq. 5, has been tabulated at various temperatures by Coughlin.[21] However, Blackburn[25] has pointed out that these free energies lead to thermodynamic inconsistencies, and consequently has reported the stardard heat and entropy of formation of U_3O_8 based on measurements of dissociation pressures of oxygen for univariant uranium oxide systems. Recently, Westrum and Grønvold[22], and Popov, *et al.*,[23] have reported heat capacity data for U_3O_8 from 0 to 300°K. and 380 to 900°K., respectively. These heat capacity data when extrapolated to 1300°K. and combined with the thermodynamic functions for uranium metal and oxygen[24] and the heat of formation of U_3O_8,[26] yield for the standard free energy of formation of U_3O_8 the equation

$$\Delta F^0_f(U_3O_8) = 230.8T - 856{,}070 - 23.20T \log T \text{ cal. mole}^{-1} \qquad (7)$$

The agreement between the value obtained from this equation at 1300°K. is within approximately 0.5 kcal. mole^{-1} with that reported by Blackburn at the same temperature. For practical purposes, however, eq. 7 can be expressed in linear form over the temperature range of stability of the γ-phase of uranium metal such that when it is combined

(21) J. P. Coughlin, U. S. Bureau of Mines Bulletin 542, 1954.

(22) E. F. Westrum, Jr., and F. Grønvold, *J. Am. Chem. Soc.*, **81**, 1777 (1959).

(23) M. M. Popov, G. L. Galchenko and M. D. Senin, *J. Inorg. Chem.* (*U.S.S.R.*), **3**, 1734 (1958).

(24) D. R. Stull and G. C. Sinke, "Thermodynamic Properties of the Elements." American Chemical Society, Washington, D. C., 1956.

(25) P. E. Blackburn, THIS JOURNAL, **62**, 897 (1958).

(26) E. J. Huber, Jr., C. E. Holley, Jr. and E. H. Meierkord, *J. Am. Chem. Soc.*, **74**, 3406 (1952).

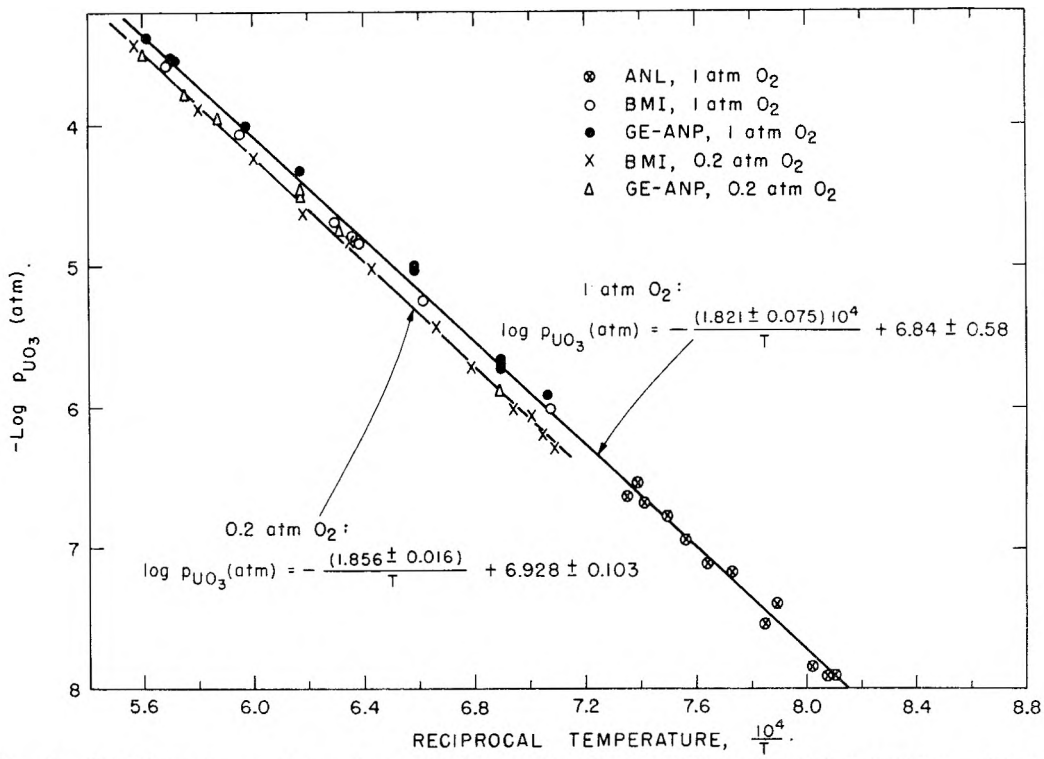

Fig. 6.—Partial pressures of uranium trioxide resulting from reaction $^1/_3U_3O_8(s) + {}^1/_6O_2(g) \rightarrow UO_3(g)$.

with eq. 6 one obtains for the standard free energy of formation of gaseous uranium trioxide the equation

$$\Delta F^0_f\,[UO_3(g)] = -198{,}500 + 19.0T \text{ cal. mole}^{-1} \quad (8)$$

The absolute entropy of gaseous uranium trioxide is 91 e.u. at 1000°K. compared with values of 83 and 87 e.u. obtained for monomeric molybdenum and tungsten trioxides.

In Fig. 6 are given the results obtained at temperatures in the range from 1400 to 1800°K. as well as that for the lower temperatures. These results comprise separate experiments carried out in three different laboratories by different investigators with somewhat different equipment. In agreement with the discussion given above these results are reported in terms of partial pressure of monomeric uranium trioxide. The equations for the partial pressure of UO_3 in the higher temperature range for 1 and 0.2 atm. oxygen, respectively, are

$$-R'T \log p_{UO_3}(\text{atm.}) = (80.9 \pm 1.4)\,10^3 - (29.9 \pm 0.9)T \text{ cal. mole}^{-1} \quad (9)$$

and

$$-R'T \log p_{UO_3}(\text{atm.}) = (84.9 \pm 0.5)\,10^3 - (31.7 \pm 0.5)T \text{ cal. mole}^{-1} \quad (10)$$

The errors quoted are standard deviations. No doubt the composition of the condensed phase at the temperatures near 1700°K. was different from that near 1300°K. It is for this reason that eq. 8 was derived from the data at the lower temperatures at which both the condensed phase composition and free energy of formation are more precisely known. However, provided both measurements were effected with the same condensed phase the difference between the free energies of the different compositions will be small and the difference between the two curves at different oxygen pressures will be essentially $-{}^1/_6$ log 0.2 or 0.12. The fact that the two measurements differ by only 0.16 suggests that the single condensed phase U_3O_{8-x} was present in both experiments. This suggestion is substantiated by the measurements of oxygen decomposition pressures by Blackburn[25] and Ackermann and Thorn,[27] which indicate that lower oxygen pressures are necessary at these temperatures to form the U_4O_9–U_3O_{8-x} system.

By means of eq. 8, the free energy of formation of solid uranium dioxide,[21] and the necessary thermochemical quantities for UO(g),[3,4] it is possible to calculate that the pressure of $UO_3(g)$ is only a few per cent. of the total pressure in equilibrium with solid $UO_{2.00}$ at 2500°K. Hence, this species is of little consequence in explaining the high temperature (2300 to 2500°K.) sublimation behavior of uranium dioxide studied by Ackermann, Gilles and Thorn.[5] In view of this calculation and also the lack of identification of a more complex species in the vapor phase of this system,[4] the sublimation behavior in this range of temperature remains at present unexplained.

In Table II is compiled an intercomparison of the experimental conditions and the gaseous species observed from the evaporation of molybdenum, tungsten and uranium oxides. For the solid trioxides one observes less polymers with increasing atomic number. This trend is intimately connected with the fact that at a given temperature the total gas pressure decreases from molybdenum to tungsten to uranium. The principal cause of this decrease in total pressure can be traced to the

(27) R. J. Ackermann and R. J. Thorn, "Partial Pressure of Oxygen in Equilibrium with Uranium Oxides," 133rd National Meeting of the American Chemical Society, San Francisco, April, 1958.

TABLE II

GASEOUS OXIDES OF MOLYBDENUM, TUNGSTEN AND URANIUM

Evaporation process	Pressure range of investigation (atm.)	Mean temp., °K.	Gaseous species	Ref.
$nMoO_3(s) \rightarrow (MoO_3)_n(g)$	10^{-6}–10^{-4}	900	Trimer, tetramer, pentamer	6, this work
$\frac{n}{3} Mo_4O_{11} \rightarrow (MoO_3)_n(g) + \frac{n}{3} MoO_2(s)$	10^{-6}–10^{-4}	900	Trimer	7
$MoO_2(s) \rightarrow (1 - 3y)MoO_2(g) + 2yMoO_3(g) + yMo(s)$	10^{-4}–10^{-3}	1900	Monomers	7
$nWO_3(s) \rightarrow (WO_3)_n(g)$	10^{-5}	1400	Trimers, tetramers, very small pentamer, monomer, and dimer ions obsd.	10
$\frac{3}{2}WO_2(s) \rightarrow WO_3(g) + \frac{1}{2}W(s)$	10^{-6}–10^{-3}	1500	Trimer	7
$UO_3(s) \rightarrow UO_3(g)$	3×10^{-7}	1300	Monomer inferred	This work
$\frac{1}{3}U_3O_8(s) + \frac{1}{6}O_2 \rightarrow UO_3(g)$	10^{-8}–10^{-7}	1300	Monomer inferred	This work
$UO_2(s) \rightarrow UO_2(g)$ Small amount UO(g), $UO_3(g)$	10^{-11}–10^{-3}	2206	Monomer	4, 5

increasing stability (ΔF^0_f becomes more negative) of the respective solid trioxides. Hence, the trioxide monomer in the uranium oxide measurements is consistent with the properties of molybdenum and tungsten trioxides. It will be important to attempt to identify the gaseous species in equilibrium with solid uranium oxide ($O/U > 2$) at temperatures such that the gas pressure is of the order of 10^{-4} atm. because higher pressures should favor the formation of polymeric gaseous uranium trioxide.

In the case of the solid dioxides, one does not observe a trend similar to that observed in the case of the trioxides principally because the free energy of formation of molybdenum dioxide[7] is appreciably more negative than that of tungsten dioxide. Therefore, the total pressure at a given temperature above molybdenum dioxide is several orders of magnitude less than above tungsten dioxide, and under these conditions of temperature and pressure only the monomeric species $MoO_2(g)$ and $MoO_3(g)$ are important in the vapor phase.

Acknowledgments.—The authors wish to acknowledge the assistance of Bert Ercoli of Argonne National Laboratory, Richard W. Stone of Battelle Memorial Institute and Paul Richardson of General Electric, Aircraft Nuclear Propulsion Department in carrying out the measurements.

HEATS OF IMMERSION. III. THE INFLUENCE OF SUBSTRATE STRUCTURE IN THE SiO_2–H_2O SYSTEM

BY W. H. WADE, R. L. EVERY AND NORMAN HACKERMAN

Department of Chemistry, The University of Texas, Austin, Texas

Received October 5, 1959

Previous microcalorimetric measurements at this Laboratory yielded somewhat unexpected results in that the heats of immersion per square centimeter of silica in water increased with increased particle size. This effect has been reinvestigated in the present work, and the changes in surface structure as a function of outgassing temperature are noted. This work is supplemented with weight loss and water adsorption studies.

Introduction

There is satisfactory evidence[1] showing that surface hydration of SiO_2 particles produces a silanol structure. This surface structure undoubtedly plays an important role in hydrogen bonding interactions between the SiO_2 substrate and adsorbed molecular H_2O. The surface dehydration of SiO_2 at elevated temperatures is an endothermic conversion to a strained Si–O–Si bridge structure (siloxane modification).

Heats of immersion measurements do not permit an absolute evaluation of surface energies of solids but they do measure any relative variations between surfaces of different structures. A variation of immersion heat with particle size clearly introduces another parameter in the expression of the surface energy of SiO_2. In a previous paper from this Laboratory[2] evidence was offered that the heat of immersion of SiO_2 in water is a function of the SiO_2 particle size. In addition, measurements showed a variation of immersional heats with pretreatment temperature which was interpreted in terms of changes of surface structure of the SiO_2. The present paper amplifies on these earlier results.

(1) R. K. Iler, "The Colloid Chemistry of Silica and Silicates," Cornell University Press, Ithaca, N. Y., Chapter VIII.

(2) A. C. Makrides and N. Hackerman, THIS JOURNAL, **63**, 594 (1959).

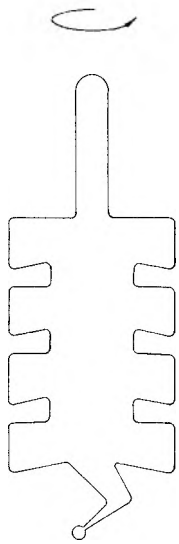

Fig. 1.—Immersion calorimeter sample bulb.

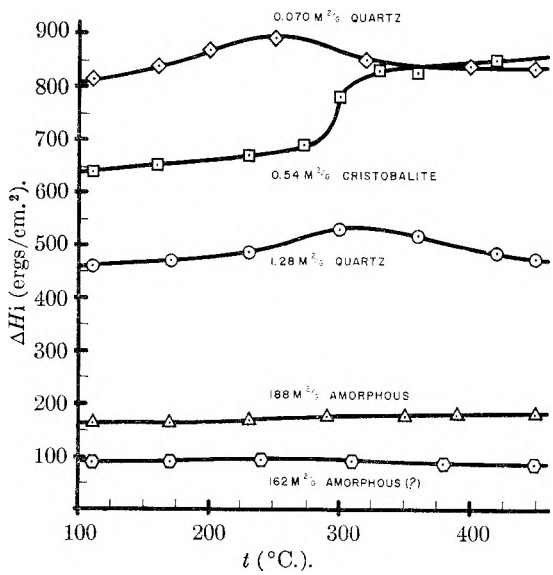

Fig. 2.—Heats of immersion *vs.* outgassing temperature.

Experimental

Samples.—The five samples of SiO_2 investigated are listed in Table I. Sample B was prepared from sample C by heating to 1500° and quenching rapidly in water. The resulting material is approximately 90% cristobalite and 10% quartz as measured by X-ray diffraction. Sample E was prepared from the material D by heating for 8 hours at 800° and subsequently subjecting to saturated water vapor for two weeks. The particle size was too small to determine by X-ray analysis whether or not crystallization of the originally amorphous material had occurred.

Calorimeter.—The calorimeter was described previously.[2] It is of the twin adiabatic type with thermistor temperature sensing elements. All measurements were at 25 ± 0.1°. The only difference in experimental technique from that used before concerns the low area sample A. For these, a new technique for exposure of the outgassed sample to water was needed since the experimental limits of error for heat evolution due just to bulb breaking (±0.2 joule) is approximately ±30% of the heat of immersion. It was impossible to reduce this uncertainty appreciably by trying for more careful control in the sample bulb manufacture. The solution finally arrived at was to mount the outgassed sample bulb (see Fig. 1) on the rotating stirrer shaft. For immersion, the thin "break-off" seal at the bottom is fractured and solution under atmospheric pressure enters and wets the sample. Heat exchange through the convoluted glass walls is quite rapid and equilibration with the excess water takes no longer than when the whole sample bulb is broken and the sample is in direct contact with the calorimeter fluid. There is no measurable heat evolution due to breaking the glass tip, and thus there was a ten-fold gain in the reproducibility for the A samples.

There were four electrical calibration runs for each immersion measurement. The average deviation for these runs was less than ±1%. All points shown in Fig. 2 and Table II are the average of two determinations. The usual agreement for immersion measurements was ±1% for all samples studied. Sample weights of A, B and C were approximately 10 grams, and of D and E, 0.3 gram. The temperature changes during immersion varied from 3×10^{-4} to 3×10^{-3} degree with the needed variations in sensitivity being accomplished by attenuation of the DC amplifier gain. During experiments requiring the highest gain (sample A) base line temperature excursions were less than $\pm 2 \times 10^{-6}$ degree over the 15-minute periods required for a run. The outgassing temperatures are ±5° and the ultimate outgassing pressures attained were 5×10^{-6} mm.

TABLE I

Sample	SiO_2, %	Surface area ($m.^2/g.$)[d]	Crystalline modification
A[a]	99.96	0.070	β-quartz
B	99.92	0.54	β-cristobalite
C[b]	99.92	1.28	β-quartz
D[c]	99.6	188	amorphous
E	99.6	162	amorphous (?)

[a] Supplied by Cleveland Quartz Works, General Electric Company. [b] Supplied by C. A. Wagner, Inc. [c] Supplied by Godfrey L. Cabot, Inc. (Cab-O-Sil). [d] Surface areas were measured by Kr adsorption with the exception of samples D and E which were measured by Dr. J. W. Whaley of the Magnolia Petroleum Company Field Research Laboratory using N_2 adsorption.

TABLE II

HEAT OF IMMERSION IN ERGS/CM.² AT 25° AS A FUNCTION OF OUTGASSING TEMPERATURE

	Sample				
t (°C.)	A	B	C	D	E
110	811	638	457	162	88.4
150	843	..	..	..	..
170	..	652	468	162	89.7
200	871	..	..	..	..
230	..	670	488	168	93.6
260	892	..	..	..	..
300	..	781	535	174	..
310	..	..	..	..	92.1
320	845	..	..	..	..
330	..	828	..	..	..
360	..	825	521	175	..
380	..	..	..	..	89.0
400	839	842	..	177	..
420	..	..	486	..	..
450	836	..	477	182	88.8

Weight Loss Measurements.—The various samples studied after equilibration at 25 ± 1° were heated in air to the temperatures noted in Fig. 3 for 24 hours, allowed to cool in a desiccator, and weighed on a standard analytical balance (readability of 0.1 mg.). The temperature control was ±2°.

Adsorption Measurements.—The volumetric adsorption apparatus and the experimental techniques used are the same as previously described.[3] Adsorption isotherms (Fig. 4) were obtained only for samples B, C and D, outgassed at 160, 260 and 115°, respectively. These temperatures were chosen to give surfaces with a minimum amount of physically adsorbed water and a maximum concentration of silanol groups. Each of the three isotherms is constructed from about twenty experimental values with the values having an average deviation of less than 1% from the line as drawn.

(3) N. Hackerman and A. C. Hall, *ibid.*, **62**, 1212 (1958).

Results and Discussion

It should be noted that the present data in part reproduce earlier work[2] in that the same variation of heat of immersion, ΔH_i, with particle size has been noted. The previous value of 160 ergs/cm.^{2} (sample outgassed at 115°) noted for Cab-O-Sil, sample D, with a surface area of 190 m.^{2}/g. agrees to within 0.3 erg/cm.^{2} of the present value of 162 ergs/cm.^{2} at 110° (Fig. 2) when the slightly more refined surface area of 188 m.^{2}/g. is applied. The present sample C of surface area 1.28 m.^{2}/g. can be compared with the previously studied samples of 0.91 m.^{2}/g. specific area, the respective heats of immersion being 457 and 450 ergs/cm.^{2}, respectively (outgassed 110 and 115°). The present study on sample A is not in agreement with the earlier measurements of 1450 ergs/cm.^{2} for quartz of surface area of 0.082 m.^{2}/g. The original value was based on duplicate measurements and apparently the heat of bulb breaking was consistently larger than average for the two measurements. The present values for the same material, but of specific area 0.070 m.^{2}/g. (decrease in area due to more extensive removal of the fines), consistently fall between 800–900 ergs/cm.^{2} and were quite reproducible utilizing the new immersion technique.

The heats of immersion of samples A and C (Fig. 2) vary with outgassing temperature in the manner previously noted: as the temperature is increased the heats rise, pass through a maximum, and then decrease. This variation is considered to be due to the interplay of two processes: (1) reversible loss and gain of physically adsorbed water during the outgassing and subsequent immersion processes, and (2) irreversible—on the time scale of the calorimeter measurements—loss of surface hydroxyl groups with simultaneous formation of a metastable Si–O–Si bridge structure during the outgassing process. Lattice parameters set an upper limit of 8 OH groups per 100 Å.^{2} and any additional surface water must be physically adsorbed. Presence of physically adsorbed water 100 to 200° above the boiling point is open to question, and a relatively large bonding energy would be required. Weight loss experiments were run to check the existence of water still adsorbed at these temperatures. The quartz sample, C (Fig. 3), shows loss of copious quantities of water above 100°: namely, three times the value of 8 OH's/100 Å.^{2}. The fine structure in the 220–260° region should not be taken too seriously because the weight losses shown for C have nominal limits of error of ±5%. The loss of approximately 8 OH's/100 Å.^{2} at a temperature corresponding to the maximum in the ΔH_i for sample C may be fortuitous. However, this weight loss study does bolster the previous suggestion concerning the initial increase in ΔH_i data with increased outgassing temperature.

The low area sample A shows the same features for ΔH_i as sample C, but there is a shift of the maximum to lower outgassing temperatures and a general elevation of the absolute heat values by a factor of two (Fig. 2, Table II). The peak shift and enhanced heats have been noted previously[2] for samples similar to C which were annealed at 700 and 1100°; however, no ΔH_i's for the previously annealed samples were as high as those for sample A. This annealing process undoubtedly removed strains introduced in the surface layers during the grinding operations. Obviously there is no guarantee that the 0.070 m.^{2}/g. material presents a perfect crystalline surface to the aqueous phase. Probably a quartz sample of still larger particle size, which had undergone a less extensive grind-

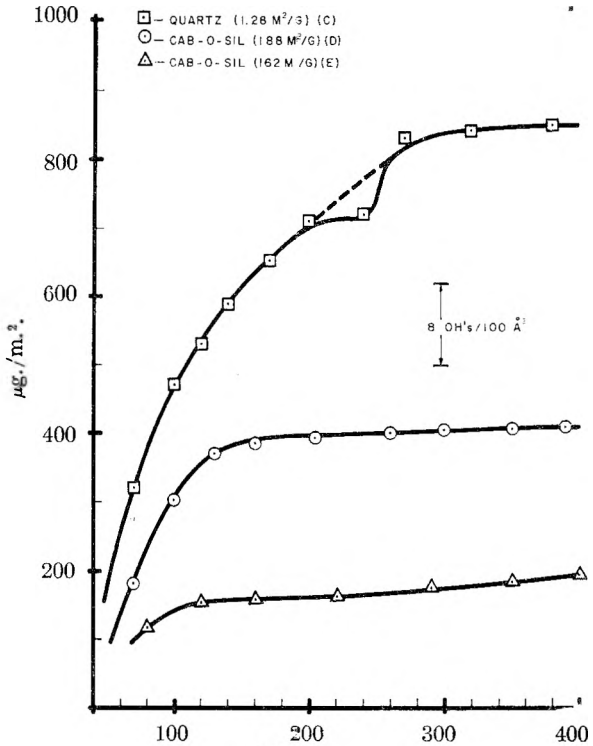

Fig 3.

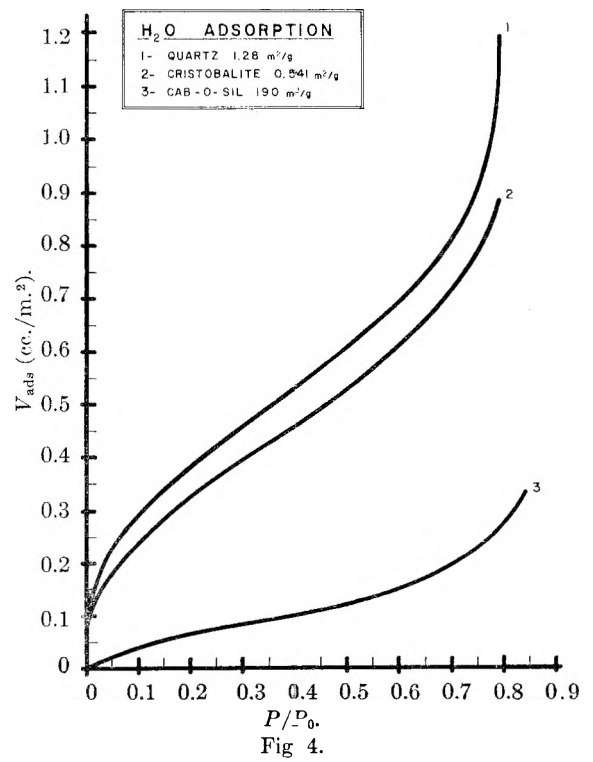

Fig 4.

ing operation, would exhibit larger immersional heats. At the present time such studies are outside the limits of sensitivity of the calorimeter used in these studies. The specific area of sample A was too low to permit a weight loss study.

Sample B was derived from C. Originally the purpose was to convert to β-cristobalite to ensure complete recrystallization of an amorphous surface using X-ray diffraction to note changes in crystalline modification. The supposition that the extent of the amorphous character of the surface affects the ΔH_i obviously can explain the results obtained for the cristobalite sample since the recrystallized surface does show an enhanced ΔH_i. Nevertheless, it might as well be argued that these ΔH_i's are characteristic of β-cristobalite whereas the values for sample C are characteristic for quartz. There is an additional point of interest in that, differing from samples A and C (Fig. 2), the ΔH_i's for β-cristobalite do not pass through a maximum value but exhibit a step at an outgassing temperature of 270–300°—approximately at the temperature of the maximum of sample C. If lattice parameters at the surface are related to those of the bulk lattice, then the lower density of cristobalite (2.3 as compared to 2.65 for quartz) dictates a diminished stability of the siloxane bridge structure and hence a rapid rehydration rate upon immersion. At outgassing temperatures above 300° the measured heats arise from two processes: (a) the immersion process, and (b) an exothermic conversion from a siloxane to a silanol surface. The step height of 150 ergs/cm.^{2} agrees well with the value of 130 ergs/cm.^{2} by Brunauer, *et al.*,[4] as the energy difference between the silanol and siloxane structures.

The ΔH_i's for the amorphous sample D are similar to those of commercially available silica gels.[5,6] There is only a slight variation of the heat of immersion with outgassing temperature indicating an absence of both physically adsorbed water and removable surface hydroxyl groups. The weight loss studies for D show this to be true. The equivalent of only 1 OH/100 Å.^{2} is removed over the temperature range of 160–400°, and in addition the extent of physical adsorption of water is much lower than for sample C. Since the weight loss measurements for D compared to C level off at lower temperatures, the heat of adsorption of water must be lower for D than for C, and this is reflected in the immersion heats.

The adsorption isotherms (Fig. 4) measured at 25° bear out the previous conclusions for sample D. The three isotherms of Fig. 4 all show Type II behavior. Possibly the isotherms for samples B and C would be coincident if the B.E.T. method afforded more accurate surface area measurements, but adsorption on sample D is much too small to be within experimental error of agreeing with samples B and C. These results concur with the weight loss studies. The water molecule areas for samples B, C and D are 12.5, 11.3, and a "nominal" 50.5 Å.^{2}, respectively. A more exhaustive series of investigations is in progress for evaluation of the free energy of immersion from adsorption isotherms with specific emphasis on variations due to particle size.

The ΔH_i values for sample E fall uniformly below those of D. It can be seen from Table II that E shows a slight maximum. The weight loss at temperatures greater than 160° is more extensive for E than for D, even though physical adsorption of water is much lower for E than for D (as is the average ΔH_i). The annealing process used for E probably generates a surface structure with a maximum of 2–3 OH's/100 Å.^{2} which are irreversibly removed at elevated temperatures as for samples A and C which undoubtedly have a more complete hydroxyl covering. The gradual slight increase of ΔH_i with temperature can be due either to a process similar to that of sample B or to the gradual removal of the last traces of physically adsorbed water.

Conclusions

The present and previous work[2] clearly demonstrate the inadvisability of trying to characterize the SiO_2 surface on the basis of present knowledge. It is possible to observe changes in surface structure induced by various thermal treatments. These tend to confirm the assumption that increased amorphous character in the substrate structure drastically reduces the heats of immersion. At the present time only one explanation is offered for this variation of ΔH_i with varying amorphous character. Consider one extreme case where a surface presents a uniform sheet of Si^{+4} ions or a uniform sheet of what may be formally called hydroxide or oxide ions (depending on whether the silanol or siloxane surface is in question), and the other extreme where there is a random distribution of positive and negative ions in the surface layers. Simply put, the ordering effects will be of longer range in the former than in the latter case. Put another way, the interaction energies between adsorbate and adsorbent can be expressed by

$$\sum_n = A_n r^{-n}$$

where r is the interaction distance, A_n is a constant, and n usually can assume several discrete values. In general, n values will be higher for an amorphous substrate due to the random distribution of ions in the surface layer. To put this argument on a quantitative basis would require a lattice summation procedure and still would not be too applicable since it neglects hydrogen bonding effects.

Acknowledgment.—This work is a contribution from Project 47D of the American Petroleum Institute at the Department of Chemistry, The University of Texas. The authors wish to take this opportunity to express their appreciation to the American Petroleum Institute for their continued support and interest in this project.

(4) S. Brunauer, D. L. Kantro and C. H. Weiss, *Can. J. Chem.*, **34**, 1483 (1956).

(5) W. A. Patrick, quoted by (I), pp. 240–242.

(6) M. M. Egorov, K. G. Krasil'nikov and E. A. Sysoev, *Doklady Akad. Nauk S.S.S.R.*, **108**, 103 (1956).

EFFECTS OF ETHYLENE, HYDROGEN AND RADIATION DOSAGE ON THE TRITIATED PRODUCTS RESULTING FROM THE $He^3(n,p)H^3$ REACTION IN GASEOUS HYDROCARBONS

BY MYRAN C. SAUER, JR., AND JOHN E. WILLARD

Contribution from the Department of Chemistry, University of Wisconsin, Madison, Wisconsin

Received October 16, 1959

The yields of HT, and of the tritiated hydrocarbons through C_8 produced by the neutron irradiation of mixtures of He^3 with methane, ethane and propane have been determined in the presence and absence of added ethylene and of hydrogen, and under different intensities of ionizing radiation. The results indicate that the thermal tritium atoms are effectively scavenged by ethylene with a resultant increase in the yield of tritiated butane and other products which may be formed by combination of C_2H_4T radicals with other radicals. Added H_2 increases the yield of HT and decreases that of tritiated chain lengthened products. Tests have been made of the effects of radiation intensity and dose.

Introduction

Recoiling tritium atoms produced with 0.2 Mev. kinetic energy by the $He^3(n,p)H^3$ reaction in the presence of gaseous hydrocarbons form HT, the tritiated parent hydrocarbon and other hydrocarbons.[1-5] The atom is either charged as a result of internal conversion at birth or acquires a positive charge as a result of one of its first collisions with surrounding molecules, loses energy by ionization and excitation of other molecules in its path and is neutralized when its energy has been reduced to about 1 kev. Since it is improbable that it can enter stable combination with energy greater than 1 kev. the observed tritiated products are believed to result from reactions of neutral tritium atoms[3,4] or from secondary reactions of HT or radicals formed from these atoms. Halogen scavenger techniques have indicated that somewhat over half of the atoms abstract hydrogen to form HT or react with the parent hydrocarbon in a hot displacement reaction of the type $T + RH \rightarrow TR + H$. The remainder of the atoms become thermalized and are available for competitive thermal reactions with the molecules, ions and radicals in the system. Further incorporation of tritium into organic combinations may take place by reaction of radicals or ions with HT which has been formed. This paper summarizes the results of experiments we have made to investigate further the competitive reactions in the system by using ethylene and hydrogen as scavengers and by varying the total dose and dose rate of the ionizing radiation.

Experimental[6]

All samples were prepared by vacuum line techniques, and were contained in thin-walled quartz bulbs of about 5 ml. volume. Hydrocarbons were Phillips Research Grade and the hydrogen Airco. The tritium content of the He^3 used was shown to be negligible compared to the activities of tritiated products from a typical irradiation.

Details of sample composition and irradiation conditions are given in the Tables. Samples were irradiated in the CP-5 reactor at Argonne National Laboratory. The flux of $2\text{–}3 \times 10^{12}$n cm.$^{-2}$ sec.$^{-1}$ was obtained in the isotope tube facility, and the flux of $2\text{–}3 \times 10^{13}$n cm.$^{-2}$ sec.$^{-1}$ in the vertical thimble facility.

For analysis of the tritiated products the sample bulbs were broken in the flow stream of a gas chromatography apparatus. The column was a 12 foot spiral of 6 mm. o.d. Pyrex packed with 40–60 mesh silica gel. Activated alumina also was found to be satisfactory as a column packing. When the sample was introduced the column was at room temperature to permit separation of HT and CH_3T. The temperature was increased gradually to about 230° to obtain the higher products. Methane flowing at about 30 ml./min. was used as the carrier gas. The effluent gases were passed through a flow proportional counter,[7,8] the output of which was amplified by a ratemeter and recorded by a recording potentiometer. Characterization of the tritiated products through the butanes was accomplished by running a known mixture of untritiated hydrocarbons through the column under the same conditions as used for the tritiated samples and observing the retention times by thermal conductivity detection. The other products (designated as C_5–C_8) were not characterized.

Results and Discussion

Effect of Ethylene Scavenger.—In Table I the tritiated products of the $He^3(n,p)H^3$ reaction in methane, ethane and propane are compared with and without about 8 mole % of ethylene present in the reaction mixture. In these hydrocarbons it would be expected that the reaction, for thermal T atoms, $C_2H_4 + T \rightarrow C_2H_4T$ would compete effectively with abstraction of hydrogen ($T + CH_4 \rightarrow CH_3 + HT$).[9,10] This expectation is confirmed by the fact that the yields of HT from methane, ethane and propane, which are 51, 60 and 61%, respectively, without added ethylene, are reduced to 28, 36 and 41% in the presence of ethylene. The reduction in the HT yield is in agreement with the previously observed effect of halogen scavengers.[1-3] The fact that the yields of tritiated ethane from ethane and of tritiated propane from propane are unaffected (within the experimental error) by the presence of ethylene suggests that these products are formed entirely by hot displacement reactions of tritium with the parent hydrocarbon. It would be expected, however, that the 8 mole % of ethylene would compete somewhat for the hot tritium atoms forming tri-

(1) M. F. A. El-Sayed and R. Wolfgang, *J. Am. Chem. Soc.*, **79**, 3286 (1957).

(2) A. A. Gordus, M. C. Sauer, Jr., and J. E. Willard, *ibid.*, **79**, 3284 (1957).

(3) M. F. A. El-Sayed, P. J. Estrup and R. Wolfgang, THIS JOURNAL, **62**, 1356 (1958).

(4) J. B. Evans, J. E. Quinlan, M. C. Sauer, Jr., and J. E. Willard, *ibid.*, **62**, 1351 (1958).

(5) P. J. Estrup and R. Wolfgang, *ibid.*, **64**, in press (1960).

(6) Further details of experimental procedure are given in the Ph.D. thesis of M. C. Sauer, Jr., filed with the University of Wisconsin Library in December, 1958, and available from University Microfilms, Ann Arbor, Michigan.

(7) A. A. Gordus, Ph.D. thesis, University of Wisconsin, 1956, available from University Microfilms, Ann Arbor, Michigan.

(8) R. Wolfgang and F. S. Rowland, *Anal. Chem.*, **30**, 903 (1958).

(9) M. R. Berlie and D. J. Leroy, *Can. J. Chem.*, **32**, 650 (1954).

(10) E. W. R. Steacie, "Atomic and Free Radical Reactions," 2nd edition, Reinhold Publ. Corp., New York, N. Y., 1954, pp. 438–439.

tiated ethylene (as indicated by the last column of Table I and discussion to follow), thus lowering the ethane and propane yields. It seems probable therefore that part of the tritiated ethane and propane formed in the presence of ethylene results from reactions of C_2H_4 radicals formed when thermal T atoms are scavenged by C_2H_4. There may be reactions such as $C_2H_4T + C_2H_5 \rightarrow C_2H_5T + C_2H_4$, $C_2H_4T + C_2H_6 \rightarrow C_2H_5T + C_2H_5$, and $C_2H_4T + CH_3 \rightarrow C_3H_7T$. There are no reactions in which C_2H_4T can yield CH_3T. Consequently it is not surprising that the yield of CH_3T from methane is reduced by added ethylene.

TABLE I

TRITIATED PRODUCTS OF THE $He^3(n,p)H^3$ REACTION IN METHANE, ETHANE, PROPANE AND ETHYLENE[a]

System / Product	Methane[b]	Methane + 4.5 cm. ethylene	Ethane	Ethane + 5.0 cm. ethylene	Propane	Propane + 5.0 cm. ethylene	Ethylene
Hydrogen	51	28	60	36	61	41	16
Methane	33	24	3.2	2.4	2.5	3.0	0.2
Ethane	7.4	6.3	25	26	2.4	5.2	2.3
Ethylene	0.0	3.2	0.0	3.7	0.0	2.5	53
Propane	3.1	14	5.1	7.7	26	25	1.8
Isobutane	1.0	0	0.2	0	2.0	Trace	0
Butane	1.1	19	3.6	20	1.1	11	16
C_5	1.5	1.1	1.0	0.6	2.5	4.4	1.2
C_6	0.5	0.3	0.1	0.1	2.0	3.0	0.2
C_6	0.7	1.6	1.1	1.3			6.4
C_7	1.0	0.9	0.5	0.4	0.3	3.6	0.4
C_8	..	1.2	0.6	0.7	0.3	1.6	2.1

[a] All samples contained 60 to 70 cm. of hydrocarbon, 6 mm. of He^3 and were irradiated for one hour at 2–3 $\times 10^{12}$ neutrons cm.$^{-2}$ sec.$^{-1}$. The numbers reported are percentages of the total observed activity. [b] Average of first two columns of Table II.

In contrast to the halogen scavengers which convert the tritium atoms to the tritium halide, which is not observable in the gas chromatographic analysis, ethylene produces C_2H_4T which reacts to generate observable organic products. The fact that the ethane yields of Table I for the runs with ethylene present are not significantly greater than for the runs without ethylene shows that the reaction $C_2H_4T + RH \rightarrow C_2H_5T + R$ is improbable in this system relative to reactions of the radical with other radicals. It is probable that reaction of C_2H_4T with methyl radicals accounts for the increase in the propane yield from methane and that reaction of C_2H_4T with ethyl radicals accounts for the increased yield of butane from each of the three target compounds. The preponderance of tritiated butane over tritiated ethane and ethylene indicates that two ethyl radicals combine much more frequently than they disproportionate which is in qualitative agreement with the low disproportionation–combination ratios which have been reported in the literature.[11] Generally speaking the yields of the higher hydrocarbons are not greatly altered by the presence of ethylene, although there are some changes which suggest two-carbon units of the ethylene may be uniting with radicals formed from the hydrocarbon. By contrast halogen scavengers have been reported to eliminate chain lengthening.[1-3] The system is so complex as to forbid an intelligent selection from the various possible explanations of this difference.

Of particular interest is the 53% yield of tritiated ethylene from mixtures of He^3 and pure ethylene. This seems to indicate a high probability for the hot reaction $T + C_2H_4 \rightarrow C_2H_3T + H$. The probability for thermal T atoms to undergo this type of exchange must be low. This is shown by the fact that 8 mole % scavenger ethylene reduces the yields of CH_3T, C_2H_5T and C_3H_7T from CH_4, C_2H_6 and C_3H_8, respectively, by 20% while the yield of C_2H_3T is only 3%. Yang and Gant[12] have found that irradiation of T_2 or HT in C_2H_4 produced C_2H_3T with a G-value of about 0.007, which is too low to explain the 53% yield of tritium in ethylene.

The cause of the large difference between the 60% HT yield from ethane observed in this work and the 44% yield reported by El Sayed, Estrup and Wolfgang,[3] is not apparent.

Effect of Hydrogen.—Because hydrogen is known to react readily in certain ion–molecule reactions and might therefore serve as a scavenger for chain carrying ions, and because hydrogen is always present as a product in irradiated hydrocarbons, tests were made to determine the effect of added hydrogen on the tritiated product yields from the $He^3(n,p)H^3$ reaction in CH_4. The results shown in Table II indicate that there is no dramatic change caused by as much as 12 cm. of added hydrogen. The total average concentration of hydrogen in these runs, including that produced by the radiolysis of the CH_4 (3 mm.) is given in the parentheses at the head of the table. In the run with an average hydrogen pressure of 12.3 cm. the mole fraction of H_2 was about 20%. The reduction in the CH_3T yield may be accounted for by formation of some HT by hot reaction of T with H_2, by the greater effectiveness of H_2 than CH_4 as a moderator for energetic T atoms with high kinetic energy, and by some thermal exchange of T with H_2, with the first and last of these effects accounting for the increase in HT. The decrease of over 50% in the yield of most of the chain lengthened products may be accounted for by the decrease in the specific activity of the HT if these products occur as a result of the reaction of chain lengthened intermediates with HT.

Effect of Dose Rate.—El Sayed and Wolfgang[1] have reported an increase from 51 to 62% in the yield of HT, accompanied by a decrease by a factor of about two in the yield of hydrocarbons higher than CH_3T, when samples of He^3 in CH_4 were irradiated at a neutron flux of $10^{9.3}$ rather than $10^{12.6}$. As we have discussed earlier[4] it is difficult to explain these observations. To explore this intensity effect further we have irradiated methane, ethane and propane containing He^3 at two different neutron fluxes and at two different He^3 pressures as indicated in Table III. Comparison of columns A with columns B indicates that no appreciable change in product spectrum occurred when samples irradiated for 1 hour at 2×10^{12}n cm.$^{-2}$ sec.$^{-1}$

(11) A. F. Trotman-Dickenson, "Gas Kinetics," Butterworths Scientific Publications, London, 1955, p. 236.

(12) K. Yang and P. L. Gant, private communication.

TABLE II

EFFECT OF HYDROGEN ON THE YIELDS OF THE TRITIATED PRODUCTS OF THE $He^3(n,p)H^3$ REACTION IN METHANE[a]

Product	P_{H_2} (cm.) added → 0[b] Av. P_{H_2} present → (0.3)	0.6[b] (0.9)	5.0 (5.3)	9.0 (9.3)	12.0 (12.3)
Hydrogen	50	52	65	75	74
Methane	34	32	26	20	20
Ethane	7.5	7.4	4.1	3.0	2.8
Propane	3.3	3.0	1.7	1.0	0.9
Isobutane	1.0	1.0	0.5	0.4	.3
Butane	1.0	1.1	.7	.4	.4
C_5	0.3	0.5	.2	.2	.2
C_5	1.0	1.1	.6	.3	.4
C_6	..	0.5	.2	..	.2
C_6	..	0.7	.2	..	.3
C_7	..	1.0	1.1	..	.3

[a] All samples contained 50–60 cm. of methane and about 6 mm. of He^3, and were irradiated for one hour at 2–3 × 10^{12}n m.$^{-2}$ sec.$^{-1}$. The numbers listed in the table are percentages of the total observed activity. [b] Average of two runs. These columns were averaged to obtain the first column of Table I.

As we have discussed,[4] it is not possible to explain the earlier results[1] on the basis of a competition between intensity dependent second-order reactions and intensity independent first-order reactions such as one might expect to be occurring in the system. The present results on CH_4 show a reduction in chain lengthened products by factors of the order of 3–10 which are in the range of the square root of the decrease in radiation intensity as might be expected if tritium incorporation occurred by reaction of a tritium atom or tritiated radical or ion with another radical or atom, but this appears to be fortuitous in view of the absence of intensity effect for increasing the intensity from 2 × 10^{12} to 2 × 10^{13}n cm.$^{-2}$ sec.$^{-1}$ in the present work and the rather small effect observed for a 2000-fold change in intensity in the earlier work.[1]

Other features of interest in the data of Table III include the following: (1) the HT yields from

TABLE III

EFFECTS OF INTENSITY OF DOSE AND TOTAL ENERGY FROM RECOIL PARTICLES AND γ-RAYS ON THE YIELDS OF TRITIATED PRODUCTS OF THE $He^3(n,p)H^3$ REACTION IN METHANE, ETHANE AND PROPANE[a]

A—neutron flux 2–3 × 10^{12}, He^3 pressure 6 mm., irrad. time 1 hour (from Table I). B—neutron flux 2–3 × 10^{13}, He^3 pressure 6 mm., irrad. time 10 min. C—neutron flux 2–3 × 10^{12}, He^3 pressure 0.1 mm., irrad. time 60 hours. D—neutron flux 2–3 × 10^{12}, He^3 pressure 6 mm., irrad. time 3 min.

	Methane				Ethane				Propane		
Product	A	B	C	D	A	B	C	D	A	C	D
Hydrogen	51	51	61	65	60	57	63	70	61	62	75
Methane	33	32	36	29	3.2	3.9	3.7	3.5	2.5	3.0	2.0
Ethane	7.4	6.9	2.3	5.5	25	26	25	19	2.4	2.9	2.0
Propane	3.1	3.2	0.3	0.7	5.1	5.3	4.9	3.0	26	25	18
Isobutane	1.0	0.9	.1	0.3	0.2	0.3	0.2	2.0	2.0	1.7	1.6
Butane	1.1	1.2	.2		3.6	4.2	2.2		1.1	1.0	
C_5	0.4	0.3	.3		1.0	1.1	0.3	0.7	2.5	2.3	0.6
C_5	1.1	1.3									
C_6	0.5	0.3	.3		0.1	0.1	0.3		2.0	1.4	
C_6	0.7	0.8			1.1	1.3					
C_7	1.0	1.1	..		0.5	0.5	0.2		0.3	0.0	
C_8	..	0.7	..		0.6	0.8			0.3	..	

[a] Pressure of alkane in all samples was 60 to 70 cm.

were compared with similar samples irradiated for 10 min. at 2 × 10^{13}n cm.$^{-2}$ sec.$^{-1}$, giving approximately the same total dose at a 10-fold difference in intensity. For the experiments of columns C in Table III the He^3 pressure (0.1 mm.) was 1/60 of that for the experiments of column A and the irradiation time was 60 times greater at the same position in the reactor. It may be estimated that the energy dissipated per unit time in the reaction vessels by the H^3 and H^1 recoil fragments at the He^3 pressure of the A experiments was 30 times greater than the energy dissipated by the gamma radiation, whereas in the C experiments the gamma contribution was double that of the recoil fragments. Thus the dosage rate of ionizing radiation for the C experiments was 1/20 that of the A experiments and the total estimated dose in the C experiments was three times that of the A experiments. Under these conditions the yield of HT in CH_4 was increased from 51 to 61% and the yields of chain lengthened products were decreased by a factor of 3 or more. These changes are very similar to those observed by El Sayed and Wolfgang[1] for a 2000-fold change in radiation flux. ethane and propane are not significantly changed by the change in radiation intensity between experiments C and A; (2) for each of the three gases tested (methane, ethane and propane) a three minute irradiation at a flux 2 × 10^{12} (D) gave a much higher HT yield than a 60 min. irradiation.

Mechanism of Chain Lengthening.—It now appears probable that at least part of the yields of tritiated products incorporated in compounds of longer chain length than the hydrocarbon initially present in the irradiation vessel are the result of reactions of radiation-produced radicals or ions with tritium atoms, tritiated radicals, or HT, and are not the result of a step propagated solely as a result of the species formed by the initial interaction of the recoil tritium atom with the hydrocarbon.[13] The number of chain lengthened products which remain nearly constant in yield in the presence of

(13) It does not appear that the tritiated chain-lengthened products formed in CH_4 can be explained on the basis of reactions of CH_3T induced by ionizing radiation. Lampe's[14] G-value of 7.6 for the disappearance of CH_4 leads to the prediction that only about 1% of the CH_4 would be decomposed during a typical irradiation of the type used in the present work (column A, Table III).

(14) F. W. Lampe, *J. Am. Chem. Soc.*, **79**, 1055 (1957).

8 mole % of added ethylene however seems improbably high if they are formed by a different mechanism in the presence of ethylene than in its absence. If their formation does not involve the ethylene then it would appear that the tritium incorporation step must be a hot reaction on CH_4 (or C_2H_6 or C_3H_8) followed by a rapid series of chain lengthening and termination steps not interfered with by the ethylene. (By contrast to the insensitive yields it may be noted that the yield of isobutane is completely eliminated by ethylene). The reduction in chain lengthened yields by added H_2 strongly suggests that part of these yields is due to reaction of chain carriers with HT. From a knowledge of the average amount of H_2 in the system (calculated from the G-value of 5.7 for H_2 formation in CH_4), and from the fraction of the tritium found as chain lengthened hydrocarbons compared to that as HT, it may be estimated that if all incorporation of chain lengthened products occurred by R or R^+ + HT the G for chain lengthening is about unity. This is a reasonable value and therefore does not exclude this mechanism. The observed effects of intensity of radiation indicate that chain lengthened products may possibly be formed by both intensity dependent and intensity independent reactions. Results on the radiolysis of mixtures of HT and CH_4 indicate that a mechanism involving reactions of chain-lengthened species with HT may be important in the systems reported here.[15,16] A systematic and extensive study of the radiation chemistry of HT-hydrocarbon mixtures with varying amounts of H_2 at varying radiation intensities will be required to understand the observed effects.

In considering the observed chain lengthening it should be noted that chain lengthening has been observed in systems which do not contain ions. I_2 molecules activated by 1849 Å. radiation in methane lead to the production of C_2H_6, C_3H_8, C_2H_5I, C_3H_9I, etc., as well as CH_3I and HI,[17] and chain lengthening has been observed in various other photochemically activated systems where CH_2 radicals may be produced.[18-19]

Halogen atoms activated by the (n,γ) nuclear reaction undergo hot replacement reactions[20-22] similar to those observed for recoil tritium atoms and also initiate chain lengthening.[23]

Acknowledgment.—This work has been supported in part by the United States Atomic Energy Commission and in part by the University Research Committee with funds made available by the Wisconsin Alumni Research Foundation.

(15) R. W. Ahrens, M. C. Sauer, Jr., and J. E. Willard, *J. Am. Chem. Soc.*, **79**, 3285 (1957).

(16) R. W. Ahrens, Ph.D. thesis, University of Wisconsin, 1959, available from University Microfilms, Ann Arbor, Michigan.

(17) T. A. Gover and J. E. Willard, *J. Am. Chem. Soc.*, in press.

(18) (a) W. E. Doering, R. G. Battery, R. G. Laughlin and N. Chaudhuri, *J. Am. Chem. Soc.*, **78**, 3224 (1956); (b) H. M. Frey and G. B. Kistiakowsky, *ibid.*, **79**, 6373 (1957).

(19) W. H. Urry and J. R. Eiszner, *ibid.*, **73**, 2977 (1951).

(20) J. F. Hornig, G. Levey and J. E. Willard, *J. Chem. Phys.*, **20**, 1556 (1952).

(21) G. Levey and J. E. Willard, *ibid.*, **25**, 904 (1956).

(22) A. Gordus and J. E. Willard, *J. Am. Chem. Soc.*, **79**, 4609 (1957).

(23) J. E. Quinlan, Ph.D. thesis, University of Wisconsin, 1958, available from University Microfilms, Ann Arbor, Michigan.

DISTRIBUTION OF SILVER BETWEEN LIQUID LEAD AND ZINC[1a,b]

BY DAVID T. PETERSON AND R. KONTRIMAS

Institute for Atomic Research and Department of Chemistry, Iowa State University, Ames, Iowa

Received October 22, 1959

The distribution coefficient of silver between liquid zinc and lead was determined over a wide concentration range at three temperatures. The coefficient did not change with concentration. The enthalpy of transfer of silver from lead to zinc was −10.9 kcal. This agrees with the value calculated from the partial molar enthalpy of silver in liquid zinc and lead.

Introduction

Silver has been known for many years to alloy more strongly with zinc than with lead. This is the basis of the Parks process for the separation of silver from lead by precipitation of a solid silver–zinc alloy. The distribution of silver between lead and zinc in the liquid state was studied by Naish[2] who found that K_d, expressed as wt. % silver in zinc over wt. silver in lead, increased with temperature. This indicated that the partial molar enthalpy of silver in zinc was more positive than that of silver in lead which does not agree with the thermodynamic data which are available. The distribution coefficient of silver between liquid lead and zinc was measured over a considerable concentration range and at several temperatures.

Experimental

The distribution coefficients were determined by measuring the ratio of the concentrations of silver in samples pipetted from equilibrated liquid zinc and lead layers. The concentration ratio was measured by using an Ag^{110} tracer and counting the activity of the silver precipitate from each sample. A tracer technique was chosen so that the coefficient could be determined at very low silver concentrations where the amount of silver in the lead sample would be too small to weigh.

Materials.—The zinc was cast zinc, 99.99+% pure. Granular lead was melted and cast into cylinders which could be cleaned by scraping the oxidized surface. The lead was 99.98% pure and contained 0.0001% Ag, 0.0003% Cu, 0.0003% Fe, 0.01% total foreign metals and 0.0001% As. Granular electrolytic silver, which by spectrographic analysis contained 0.0005% Cu and 0.002% Fe as the principal impurities, was used. The silver tracer was obtained as a nitrate solution and was plated onto small zinc cathodes from an alkaline 3 N NaCN bath at 40°. The current density

(1) (a) Contribution No. 797. Work was performed in the Ames Laboratory of the U. S. Atomic Energy Commission. (b) Based in part on a dissertation by R. Kontrimas to the Graduate School, Iowa State University, in partial fulfillment of the requirements for the degree of Master of Science, 1959.

(2) W. A. Naish, *Trans. Faraday Soc.*, **21**, 102 (1925).

was 30 mamp. per sq. cm. The silver deposit was adherent and the plated cathodes could be handled without loss of radioactive silver.

Equilibration and Sampling.—The lead, zinc and silver were melted together under argon in a 28 mm. diameter vertical quartz tube which was sealed off at the lower end. The temperature of the melt was measured with a chromel-alumel thermocouple in a 5 mm. diameter Pyrex protection tube immersed in the melt. This tube also was used to stir the melt to hasten equilibration. The temperature of the melt was uniform from top to bottom within 1° and was constant during a run within 2°. The system was held at temperature for 24 hours to allow equilibration before sampling was begun.

The two liquid metal phases were sampled with a pipet fabricated from a 5 mm. diameter Pyrex tube with an enlarged end to which a coarse sintered glass filter disc was sealed. The major difficulty in sampling was the adherence of small amounts of zinc as the pipet was inserted into the lead phase. As the zinc was much richer in silver than the lead, the inclusion of small amounts of zinc caused erroneous distribution coefficients. The adherence of zinc was minimized by preheating the pipets to the temperature of the melt and applying a slight positive pressure to the pipets as they were inserted. The filter surface was inclined at 45° to the pipet to prevent entrapment of zinc on the filter surface. One hour was allowed for phase separation after insertion of the pipets before they were filled. That this was adequate was verified by samples which were withdrawn ten hours after insertion and which gave the same distribution coefficient as samples withdrawn after one hour. After a pair of samples was taken, lead and zinc were added to replace the amounts withdrawn and silver was added to give the desired silver concentration. After 10–12 hours, the next samples were taken.

Analysis.—The outside of the pipet was cleaned to remove adhering metal, the glass broken away and the sample weighed. The zinc samples were 10–15 g. and the lead samples 20–30 g. Each sample was dissolved in dilute nitric acid and the solution evaporated to dryness by a stream of warm air to remove excess nitric acid. The crystals were dissolved in water and the solution was filtered into a volumetric flask and diluted to volume. Appropriate aliquots were taken, silver nitrate added to bring the total silver content to 10 mg., and the *p*H adjusted to 2.0–2.5 with nitric acid or sodium hydroxide.

The silver was precipitated by adding an excess of rhodanine and allowing the solution to stand at room temperature for 10 hours. Rhodanine was used to precipitate silver as Feigl[3] reports that no elements except mercury and silver are precipitated by this reagent from acid solutions. Rhodanine was chosen rather than the more commonly used dimethylaminobenzylidenerhodanate to keep self adsorption by the sample to a minimum. The silver rhodanate was filtered by a standard procedure[4] into filter paper discs, washed with water and alcohol, and dried at 110° for 15–20 minutes. The precipitate was weighed to check the recovery, mounted in a planchet, covered with a thin Mylar tape, and the activity of the precipitate measured with a G-M counter. The recovery of silver as determined by weighing the precipitate was 100 ± 0.3%, and a second precipitation of silver from solutions containing Ag^{110} gave a precipitate with less than 0.1% of the counting rate of the original. Three aliquots were taken of each sample and the standard deviation of the counting rate for the three precipitates was usually 0.4% and always less than 1%.

Results and Discussion

The distribution coefficient K_d is the atom fraction silver in zinc over the atom fraction silver in liquid lead. The concentration of silver in the zinc phase was known from the amounts of material charged into the melt and was checked by analysis at concentrations above 0.5 wt. %. The concentration of silver in the lead phase was calculated from the concentration in the zinc phase and the ratio of the counting rates per gram of each phase.

(3) F. Feigl, *Z. anal. Chem.*, **74**, 380 (1928).

(4) G. Friedlander and J. W. Kennedy, "Introduction to Radiochemistry," John Wiley and Sons, Inc., New York, N. Y., 1949.

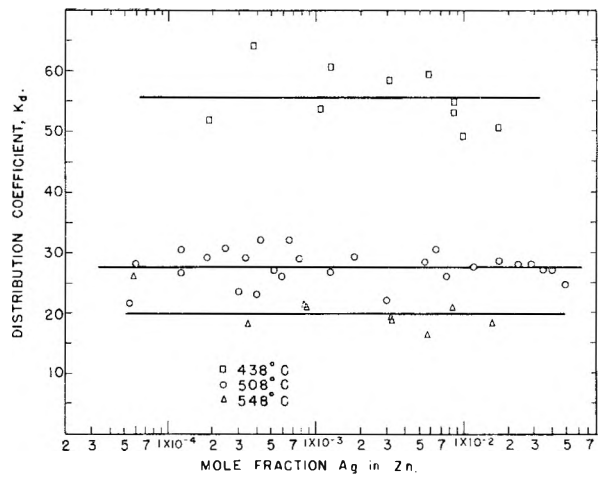

Fig. 1.—Distribution coefficients of several temperatures and concentrations.

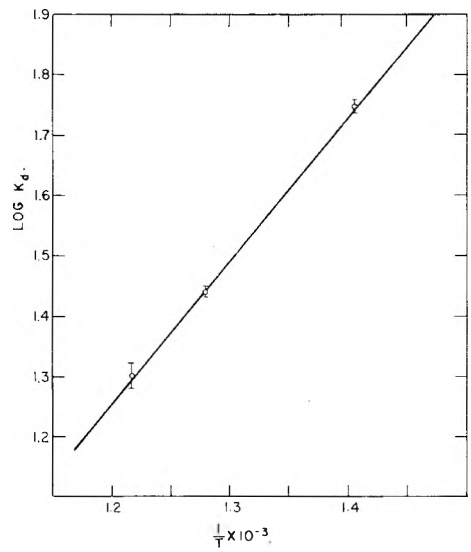

Fig. 2.—Variation of log K_d with reciprocal temperature.

The solubilities of lead in zinc and of zinc in lead, which were needed to calculate the atom fractions, were assumed to be the same as the binary solubilities. These were estimated from the data reported by Rosenthal, Mills and Dunkerley.[5] The values used are given in Table I.

TABLE I

COMPOSITION OF EQUILIBRIUM PHASES IN THE LEAD–ZINC SYSTEM

Temp., °C.	N_{Pb} in Zn	N_{Zn} in Pb	N_{Zn} in Pb[a]
438	0.0052	0.055	0.056
508	.0082	.090	.093
548	.010	.120	...

[a] Solubility of zinc in liquid lead which was found in the present investigation.

The distribution coefficient at a given temperature did not change as the silver concentration in the zinc phase was increased from 5.5×10^{-5} to 4.8×10^{-2} atom fraction. The values at each temperature were fitted to an equation of the form $K_d = A + BN_{Ag}$ by a least squares treatment. The largest number of determinations was made

(5) F. D. Rosenthal, G. J. Mills and F. J. Dunkerley, *Trans. AIME*, **212**, 153 (1958).

at 508°, and for these points the value of B was so small that the indicated concentration dependence was much smaller than the standard deviation. The concentration dependence at 548° was also less than the standard deviation. The values of K_d are plotted in Fig. 1 against the logarithm of the silver concentration. The logarithmic ordinate was used to expand the concentration scale so that the coefficients at low concentrations could be shown more clearly. The coefficients at 438° indicate a small concentration dependence of K_d, but this resulted largely from two low values at the highest concentrations. The larger scatter and small number of determinations at this temperature reduce the significance of this variation.

The mean distribution coefficient and the standard deviation of the mean were calculated at each temperature. The values are given in Table II and the logarithm of K_d plotted against reciprocal temperature in Fig. 2. The mean values at each temperature were weighted as the reciprocal of the square of the standard deviation of the mean, and a least squares method was used to calculate the slope and intercept. The enthalpy of transfer of silver from liquid lead to liquid zinc, calculated from the slope, was −10.9 kcal. with a standard deviation of 0.13 kcal.

TABLE II

DISTRIBUTION COEFFICIENTS OF SILVER BETWEEN LIQUID LEAD AND ZINC

Temp., °C.	K_d
438	55.7 ± 2.1
508	27.5 ± 0.5
548	20.1 ± 1.1

If the partial molar enthalpy of silver in each liquid phase were unaffected by the small amount of the other component dissolved when the liquid phases were equilibrated, the enthalpy of transfer of silver would be equal to the partial molar heat of silver in zinc minus the partial molar heat of silver in lead. The partial molar heat of silver in dilute solutions in lead (reference state pure solid silver) is given by Kleppa[6] as +5.74 kcal. per mole. The partial molar enthalpy of silver in zinc was estimated from data compiled by Kubaschewski and Evans[7] to be between −3.2 and −6.0 kcal. per mole. A lack of data at low silver concentrations prevented a closer determination of this value. The calculated enthalpy of transfer is −8.9 to 11.7 kcal. per mole of silver.

The agreement between the calculated and observed enthalpies indicates that the partial molar enthalpy of silver in liquid lead and zinc is either not changed by saturation with the other liquid phase, or is changed in the same direction in both phases. This agreement also indicates that the enthalpy of transfer of +2.06 kcal. which was observed by Naish[2] must be in error. The constancy of the distribution coefficient at each temperature over a wide range of silver concentration shows that Henry's law is obeyed by silver in both liquid phases or that the deviations from Henry's law in each phase are so similar as to compensate. Considering the wide concentration range over which the distribution coefficient was constant, the considerable difference between the concentration in the zinc and lead phases, and the difference between Ag–Zn and Ag–Pb interactions, compensating deviations from Henry's law are very unlikely. The distribution in this system is governed by the interaction of silver with each liquid phase, and these seem to be identical to the interactions in the Ag–Zn and Ag–Pb binary systems.

(6) O. J. Kleppa, THIS JOURNAL, 60, 440 (1956).

(7) O. Kubaschewski and E. L. Evans, "Metallurgical Thermochemistry," 3rd ed., Pergamon Press, New York, N. Y., 1958.

LOW ANGLE X-RAY SCATTERING FROM SYNTHETIC ZEOLITES: ZEOLITES A, X AND Y

BY P. A. HOWELL

Contribution from the Research Laboratory of Linde Company, Division of Union Carbide Corporation, Tonawanda, N. Y.

Received October 22, 1959

X-Ray scattering has been observed at low diffraction angles for several synthetic crystalline zeolites. For hydrous and anhydrous sodium and calcium exchanged forms of zeolite type A, the observed intensity in the range $2\theta = 1$ to 5° depends on the cation content of the zeolite and the degree of hydration. For hydrous and anhydrous sodium zeolites types X and Y, the scattering curves are characteristic of a material possessing a distribution of scattering objects of different sizes. The observed scattering probably arises because of the disorder of the cations within these crystal structures.

Introduction

The small angle X-ray scattering technique has found use in recent years for the characterization of inhomogeneities in various systems usually of an amorphous nature.[1] In this technique where the X-ray scattering given by a substance at angles near the main beam is measured and interpreted, the magnitude of the scattered intensity and the angular dependence of this intensity is determined. The angular dependence can be interpreted in terms of the size and shape of the inhomogeneities of the material while the intensity depends on the difference of electronic density between the inhomogeneity and its surroundings. In this paper we will show that certain crystalline zeolite minerals scatter X-radiation at low to moderate angles and that this scattering probably is due to cation disorder in their structures.

(1) A. Guinier and G. Fournet, "Small-Angle Scattering of X-Rays," John Wiley and Sons, Inc., New York, N. Y., Chapter 6, p. 167.

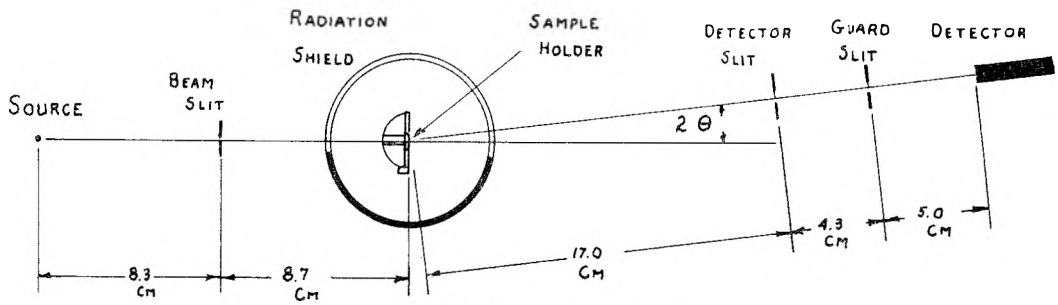

FIG. 1.—The experimental geometry.

Experimental

A commercial type spectrometer was modified to give the geometry of Fig. 1. Copper Kα radiation filtered with Ni foil was the X-ray source. Several combinations of slit sizes were employed; the combination of beam slit = 0.010″ detector slit = 0.010″, and guard slit = 0.015″ was found to give a reasonable compromise between small beam width and high scattered intensity. Three types of detector were used: a Geiger counter; a scintillation counter using pulse height analysis, and a flow proportional counter using pulse height analysis. The results were essentially the same with each mode of detection. The sample was pressed between dies into a 1/4 inch hole drilled through the sample holder. The resulting wafer was about 0.3 mm. thick. Sample weights ranged from 9–15 mg. The volume within the radiation shield was kept under a positive pressure of dry or wet helium.

The following materials were studied: Sodium zeolite type A[2] (Linde Company, Lot 4541), a selected commercial material that has the X-ray, adsorption and chemical analysis of pure zeolite type A; Calcium exchanged type A zeolites (Linde Company, Lot 5478 and Lot 80–47) which have the X-ray, adsorption and chemical analyses expected for 38 and 76% exchanged materials; Sodium zeolite type X (Linde Company Lot 7324–43A) and sodium zeolite type Y[3] (Linde Company Lot 7823–70A).

The general procedure followed was to place a sample in the holder and activate it by heating to 350° for 16 hours. The activated sample then was placed in the spectrometer and with a dry helium atmosphere the scattering was measured by counting at predetermined angles (2θ in the range 0.4–5.0°). After securing the activated data, the sample was hydrated in place using wet helium and the scattering measurements repeated. Blank runs without the sample were used to determine the background. Typical scattering curves are given in Figs 2 and 3.

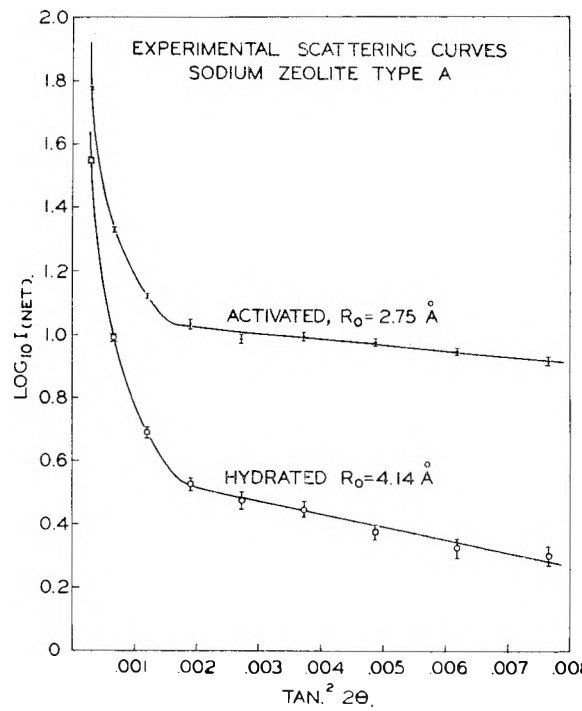

Fig. 2.

Interpretation

Zeolite Type A.—As illustrated by Fig. 2, the experimental scattering curves for zeolite type A divide themselves naturally into two sections: the scattering above and below $2\theta \sim 2°$. The scattering below $2\theta \sim 2°$ depended on such variables as sample weight and degree of compaction. This intensity undoubtedly is due to scattering from the voids between the zeolite particles and the zeolite particles themselves (cubes ~ 1–5μ in size). This portion of the scattering curve will not be discussed further.

The portion of the scattering curve in the range $2\theta = 2$ to 5°, fits the empirical relation

$$\log I_{net} = -p \tan^2 2\theta + C$$

where p and C are constants and $I_{net} = I_{obs} - I_{background}$. Using the expression of Guinier[4] the radius of gyration of the scattering system R_0 was related to p by the expression (valid for copper radiation)

$$R_0 = 0.645\sqrt{p}$$

Values of R_0 and p derived from the experimental curves for various forms of zeolite type A by fitting the experimental points in the range 1–5° 2θ by the method of least squares are given in Table I. The structure of zeolite type A has been determined[5,6] and unit cell formulas (based on pseudo cell $a_0 = 12.28$ Å., activated, and chemical analyses of the materials used) are given in Table I.

As zeolite type A contains spherical cavities 11.4 and 6.6 Å. in diameter, it is tempting to ascribe the observed scattering to these baskets but this is incorrect as single crystals of greater than 1μ size would not scatter in this angular range. Further consideration indicates that the observed scattering is due to the random occupancy of sites within the structure by the cations. A disordering of the cations has been shown to improve the fit with conventional X-ray data.[7] The relationship between number of cations in the unit cell and R_0 is given

(2) D. W. Breck, W. G. Eversole, R. M. Milton, T. B. Reed and T. L. Thomas, *J. Am. Chem. Soc.*, **78**, 5963 (1956).

(3) D. W. Breck and E. M. Flanigen, in preparation.

(4) A. Guinier and G. Fournet, ref. 1, p. 127.

(5) T. B. Reed and D. W. Breck, *J. Am. Chem. Soc.*, **78**, 5972 (1956).

(6) P. A. Howell, Paper B-3 American Crystallographic Association Annual Meeting, July 19–24, 1959.

(7) P. A. Howell, Paper B-3 American Crystallographic Association Annual Meeting, July 19–24, 1959.

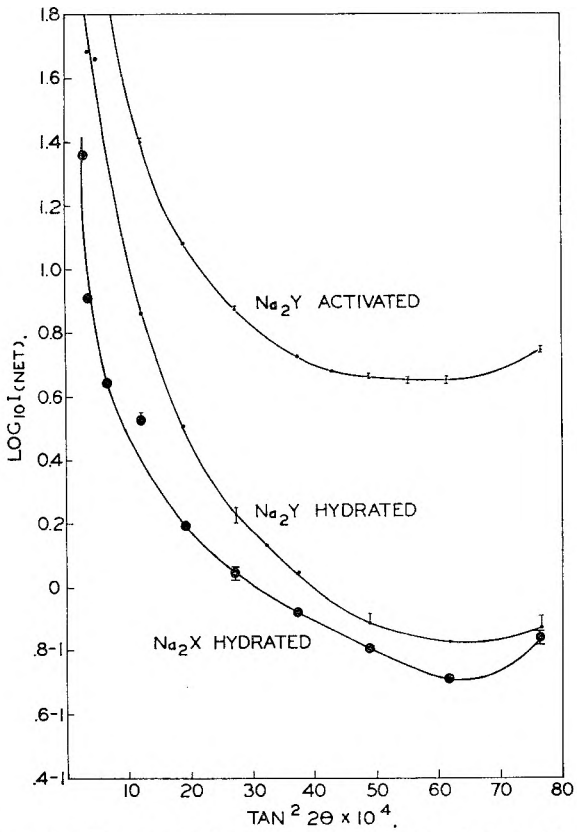

Fig. 3.—Experimental scattering curves of sodium zeolites types X and Y.

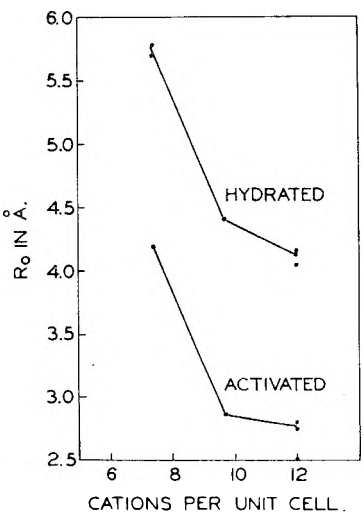

Fig. 4.—Radius of gyration R_0 *vs.* cations per unit cell of zeolite type A.

in Fig. 4. As the number of cations in the structure decreases, the distances between cations must increase, hence R_0 increases. The increase in R_0 upon hydration is caused by the cations on the average moving further apart in the hydrated materials, *e.g.*, they tend to "float" into the zeolite cavities away from the SiO_2·AlO_2 framework.

Upon hydration the observed intensity falls by a factor of 2 to 3. This could be due to the cations taking up more ordered positions and/or the scattering from the cations and water molecules destructively interfering. As the cation and water

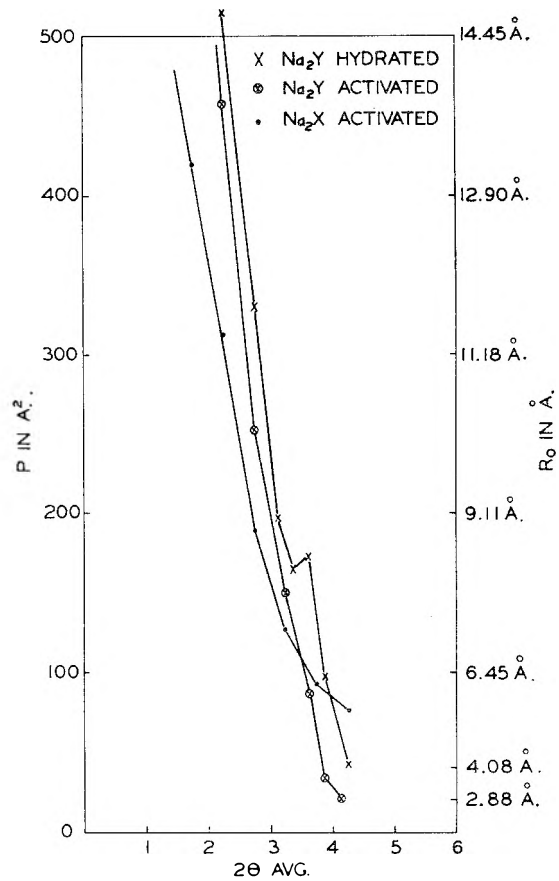

Fig. 5.—Slope of the scattering curve *vs.* angle for zeolites types X and Y.

positions have not been determined for the hydrated materials one cannot choose at this time between the two possibilities.

Zeolites Types X and Y.—The scattering curves given in Fig. 3 show a continuous change of slope as indicated in Fig. 5 where the slope over various ranges of 2θ of the log $I_{(net)}$ *vs.* $\tan^2 2\theta$ curve is plotted as a function of the average 2θ for the range. These changes in slope imply a distribution of sizes for the scattering entities (radii of gyration R_0, varying from 2.8 Å. upwards).

The structures of zeolites types X and Y are not yet properly determined; however, a postulated framework for the 192 Si, AlO_2 tetrahedra in a cubic unit cell (a_0 = 24.64 Å. (Na_2Y), a_0 = 24.97 Å. (Na_2X) has been suggested.[8] Only some of the cation positions are known.

Analyses of samples of the two zeolites studied can be represented by the unit cell formulas

Sodium zeolite type X

$$Na_{82}H_7[(AlO_2)_{89}(SiO_2)_{103}]\cdot 275H_2O$$

Sodium zeolite type Y

$$Na_{45}H_6[(AlO_2)_{55}(SiO_2)_{137}]\cdot 252H_2O$$

The major difference between the two zeolites is

(8) These zeolites have a framework structure similar to that of Faujasite. For the framework structure of Faujasite, see: G. Bergerhoff, H. Kogana and W. Nowacki, *Experientia*, **12**, 418 (1956); W. Nowacki and G. Bergerhoff, *Acta Cryst.*, **10**, 761 (1957). For the structure of hydrated sodium X zeolite see: L. Broussard and D. P. Shoemaker, Paper B-5 American Crystallographic Association Annual Meeting, July 19–24, 1959.

TABLE I

EXPERIMENTAL RESULTS FOR SODIUM AND CALCIUM EXCHANGED FORMS OF ZEOLITE TYPE A

Material and activated unit cell formula	Run no.	Activated		Hydrated	
		p in Å.^{2}	R_0 in Å.	p in Å.^{2}	R_0 in Å.
Sodium A $Na_{12}[(AlO_2)_{12}(SiO_2)_{12}]$	1	15.3	2.52	72.4	5.49
	2	18.2	2.75	41.3	4.14
	3	18.7	2.79	..	..
	4	..	..	39.4	4.05
	5	..	2.6–3.5[a]	41.4	4.15
Calcium A, 38% exchanged $Na_{7.4}Ca_{2.3}[(AlO_2)_{12}(SiO_2)_{12}]$	1	19.7	2.86	47.2	4.4
Calcium A, 76% exchanged $Na_{2.9}Ca_{4.6}[(AlO_2)_{12}(SiO)_{12}]$	1	42.1	4.19	80.4	5.78
	2	63.9	5.15[a]	78.0	5.7

[a] Moisture pickup during the experiment.

the SiO_2/Al_2O_3 ratio and consequently the number of cations within the unit cell. As in the case of zeolite type A, it is most likely that the scattering observed arises from the cations in the structure being in disorder. As zeolite Y has fewer cations per unit cell than zeolite X, the average distance between cations must be larger in Y than X and hence the slope of the scattering curve should be increased relative to X as is shown by Fig. 5. Upon hydration the cations would be expected to assume positions farther from each other as they "float" into the zeolite channels thus increasing the slope of the scattering curve. This is observed, Fig. 5, for zeolite type Y. The loss of intensity upon hydration comes about either because the cations take up more ordered positions or because the scattering from the cations and water molecules interferes destructively.

Acknowledgments.—The author is indebted to Mr. L. G. Dowell who supervised the modification of the spectrometer and recorded many of the data; to Mr. L. J. Dobmier who aided in the experimental work; to Dr. D. W. Breck who suggested that zeolites might scatter X-rays at low angles; and to Dr. V. Schomaker for his assistance in clarifying the interpretation of the experimental data.

NOTES

THE ULTRAVIOLET ABSORPTION SPECTRUM OF CHLORANIL[1]

BY KARL H. HAUSSER AND R. S. MULLIKEN

Laboratory of Molecular Structure and Spectra, Department of Physics, University of Chicago, Chicago 37, Illinois

Received September 23, 1959

Chloranil is known to be a strong electron acceptor and to form complexes with various electron donating molecules.[2] Its absorption spectrum in chloroform down to about 2300 Å. has been recorded by Pummerer and co-workers.[3] More recently, Smith[4] has investigated the interaction of chloranil with various electron donors. In the course of this work it was noted that chloranil in *n*-heptane shows a weak absorption band at 27,500 cm.$^{-1}$, in addition to the much stronger absorption with peak at 34,600 cm.$^{-1}$. (The same bands were recorded by Pummerer, *et al.*, in chloroform; their curve indicates peaks at about 26,600 and 35,000 cm.$^{-1}$ with log ϵ 2.48 and 4.02, respectively.) Because chloranil is a strong electron acceptor, it was thought that the weak band at longer wave lengths might be analogous to the strong ultraviolet absorption observed at longer wave lengths than that of I_2 itself in iodine solutions in *n*-heptane and other paraffin hydrocarbons, and thus be identified as a contact charge-transfer spectrum.[5]

In order to distinguish between this and the possibility that the band in question is characteristic of chloranil itself, we have measured the absorption spectrum of chloranil in ethanol, *n*-heptane, perfluoroheptane, and in the vapor phase (see Fig. 1). The absorption band at 27,500 cm.$^{-1}$ appears in all three solvents at nearly the same frequency and with the same intensity within the experimental error. Since perfluoroheptane is known to be an extremely inert solvent, having no detectable interaction with dissolved molecules and giving rise for the latter to spectra very similar to their vapor spectra,[6] this indicates that the band at 27,500 cm.$^{-1}$ is an intrinsic transition of the molecule itself. We have not been able to find in the region above 42,000 cm.$^{-1}$ any absorption attributable to an interaction between chloranil and *n*-heptane or ethanol.

Since the long wave length absorption band is only a rather weak band (extinction coefficient ϵ

(1) This work was assisted by the Office of Ordnance Research under Project TB2-0001(505) of Contract DA-11-022-ORD-1002 with the University of Chicago.

(2) E. Weitz, *Z. Elektrochem.*, **34**, 538 (1928); *Angew. Chem.*, **66**, 658 (1954).

(3) Pummerer, Schmidutz and Seifert, *Chem. Ber.*, **85**, 545 (1952).

(4) N. S. Smith with W. G. Brown, to be published.

(5) D. F. Evans, *J. Chem. Phys.*, **23**, 1424 (1955); *J. Chem. Soc.*, 4229 (1957); L. E. Orgel and R. S. Mulliken, *J. Am. Chem. Soc.*, **79**, 48 (1957).

(6) *Cf.* D. F. Evans, *J. Chem. Phys.*, **23**, 1424, 1426, 1429 (1955).

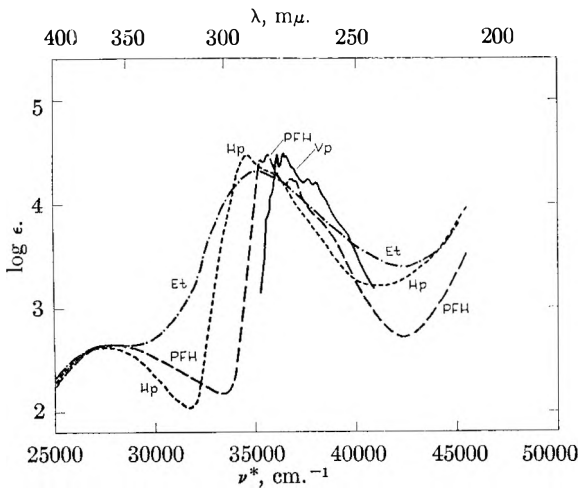

Fig. 1.—Absorption spectrum of chloranil, molar extinction coefficient ϵ as function of wave number, Vp——, vapor; PFH——, perfluoroheptane solution; Hp...., *n*-heptane solution; Et-·-·-, ethanol solution. In the case of the vapor only *relative* ϵ values were determined; the curve plotted in Fig. 1 is based on the assumption that ϵ_{max} for the peak at 36,500 is the same as for the highest peak in perfluoroheptane solution.

about 300), and since the solubility of chloranil in perfluoroheptane is very poor (about 10^{-5} mol./l.), it was necessary to use absorption cells of 10 cm. light path length. With regard to the vapor, unfortunately at the highest temperature obtainable with our equipment (about 120°) the vapor pressure of chloranil is so small that with the same 10 cm. light path length the maximum extinction of the strong band near 35,000 cm.$^{-1}$ was about 0.3; consequently the extinction expected for the weak band would be of the order of 0.004 and therewith below the limit of detectability.

The center of gravity of the strong absorption band near 35,000 cm.$^{-1}$ is nearly the same in *n*-heptane and ethanol. However, whereas in *n*-heptane one can still clearly recognize the doublet structure of the band, it is broadened to one single somewhat asymmetric band by the stronger interaction with the polar solvent ethanol.

As one would expect, the vapor spectrum is shifted toward shorter wave lengths (by nearly two thousand wave numbers) as compared with the *n*-heptane solution spectrum, and shows a resolved fine structure. In perfluoroheptane, the center of gravity of the absorption band is closer to the vapor spectrum than to the *n*-heptane solution spectrum. Further, it has almost the same fine structure as the vapor spectrum, only slightly less resolved. This shows again that in perfluorinated solvents the interaction between the solvent and the dissolved molecule, and consequently the influence of the solvent on the absorption spectrum, is much smaller than in hydrocarbons.

THE STANDARD FREE ENERGY OF FORMATION OF SILICON CARBIDE

BY J. SMILTENS

Air Force Cambridge Research Center, Bedford, Mass.

Received August 24, 1959

Silicon carbide has considerable practical importance as an abrasive and also as a refractory material. In addition to this, it recently has found application as a high-temperature semi-conductor. This should warrant the determination of the thermodynamic properties of silicon carbide. Unfortunately, presumably on account of the refractory nature of this compound, the literature data on the heat of formation of silicon carbide do not agree. Mixter[1] finds 1.3 kcal., Ruff and Grieger[2] 26.8 kcal. and Humphrey, *et al.*,[3] 12.3 kcal. In this note the original literature values have been adjusted for a graphite with heat of combustion 94.0 kcal./fwt. The three different free energy of formation functions arising from these heats of formation are plotted in Fig. 1. These free energy functions have been calculated by means of the equation

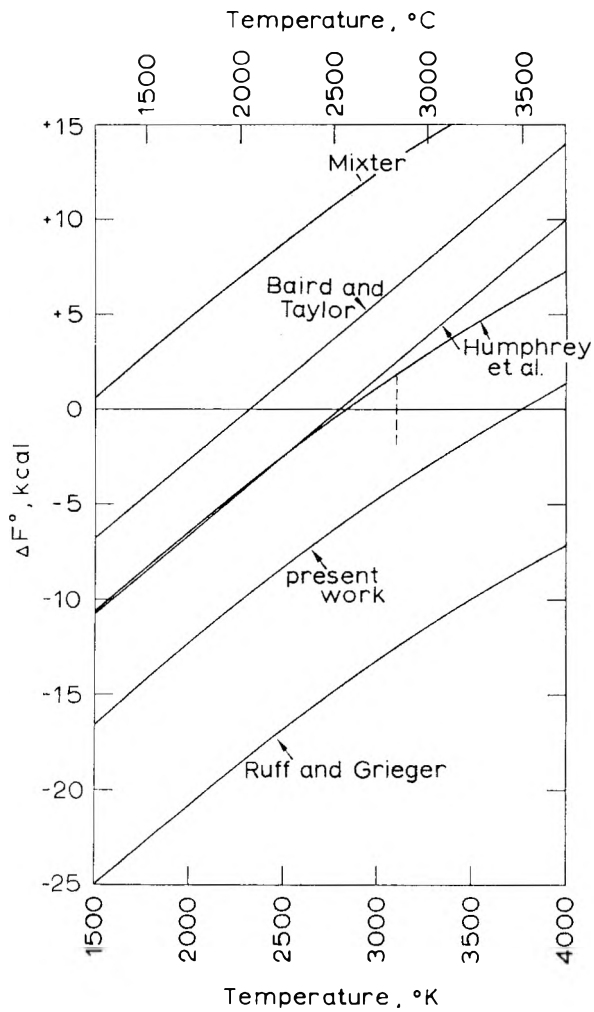

Fig. 1.—The standard free energy of formation of silicon carbide (from graphite and liquid silicon) according to data of various investigators. The short dashed line across the $\Delta F^0 = 0$ line indicates the temperature, 2830°, at which silicon carbide decomposes into graphite and a solution of carbon in liquid silicon, at 35 atmospheres (Scace and Slack[11]).

(1) W. G. Mixter, *Am.J. Sci.*, [4] **24**, 130 (1907).

(2) O. Ruff and P. Grieger, *Z. anorg. allgem. Chem.*, **211**, 145 (1933).

(3) G. L. Humphrey, S. S. Todd, J. P. Coughlin and E. G. King, "Some Thermodynamic Properties of Silicon Carbide," U. S. Department of Interior, Bureau of Mines Report of Investigations 4888, Berkeley, Calif., 1952.

TABLE I

HEAT CAPACITY DATA USED FOR DERIVING EQ. 1

Substance	$S^0_{298.16}$, cal./fwt. deg.	Ref.	$C_p = a + b \times 10^{-3} T + c \times 10^5 T^{-2}$, cal./fwt. deg. a	b	c	Range of validity, °K.	Ref.
Graphite, fwt. = 12.01	1.3609	4	4.10	1.02	−2.10	298–2300	5
Silicon, fwt. = 28.06, solid	4.47	4	5.79	0.56	−1.09	298-1200	5
Silicon, fwt. = 28.06, liquid	..		6.12	0	0	<1823	6
SiC, fwt. = 40.07, solid	3.935	4	8.93	3.00	−3.07	298-1700	5

Melting point of silicon: 1685°K. (ref. 6). Heat of fusion of silicon: 12095 cal./fwt. (ref. 6).

$$\Delta F^0 \text{ (cal.)} = \Delta H^0_{298.16} - 12135 - 0.485 \times 10^5 T^{-1} + 1.1811T + 2.97T \log T - 0.99 \times 10^{-3} T^2 \quad (1)$$

which was derived from the heat capacity data listed in Table I. The increment $\Delta H^0_{298.16}$ refers to a change with all substances in the solid state; the increment ΔF^0 refers to a change involving silicon in the liquid state. Two functions, which differ but little at temperatures below 2500°, have been plotted for the ΔF^0 function derived from the Humphrey, *et al.*, heat of formation data. The straight line is given by these investigators themselves. The curved function was obtained by using eq. 1. It may be said regarding the discrepancy of these two functions that: (1) Humphrey, *et al.*, have used somewhat different heat capacity data, (2) having found that the function is not much curved they have replaced it by a straight line. This is justifiable, because the big discrepancy occurs at temperatures which are higher than the limiting temperatures for validity of the heat capacity functions (*cf.* Table I).

Recently Baird and Taylor,[7] from the pressure of carbon monoxide at the equilibrium

$$SiO_2 + 3C = SiC + 2CO$$

have determined another ΔF^0 function, which is also plotted in Fig. 1. Lastly, the ΔF^0 function proposed by this note has been shown. The method for obtaining it will be described.

Let us consider two three-phase equilibria. The first equilibrium, which we henceforth shall denote by a single prime, is: vapor, silicon carbide and graphite. The second equilibrium, which we shall denote by two primes, is: vapor, silicon carbide and liquid silicon. Since the number of components is 2, both equilibria are univariant. Further, let us denote by C_iSi_j a general molecular species present in the binary vapor. Let the partial pressure of this species at equilibrium′ be P_{ij}' and at equilibrium ″ be P_{ij}''. We have shown elsewhere[8] that

$$P_{ij}'/P_{ij}'' = e^{(j-i)\Delta F^0/RT} \quad (2)$$

Drowart, De Maria and Inghram[9] have determined by a mass spectroscope technique the partial pressures of several molecular species in vapor effusing from a graphite crucible containing silicon carbide (equilibrium′). On learning of this investigation we suggested that they also determine the corresponding pressures at equilibrium″ (silicon carbide crucible containing liquid silicon). Drs. Drowart and De Maria[10] also have performed this series of experiments and thus ΔF^0 can be determined.

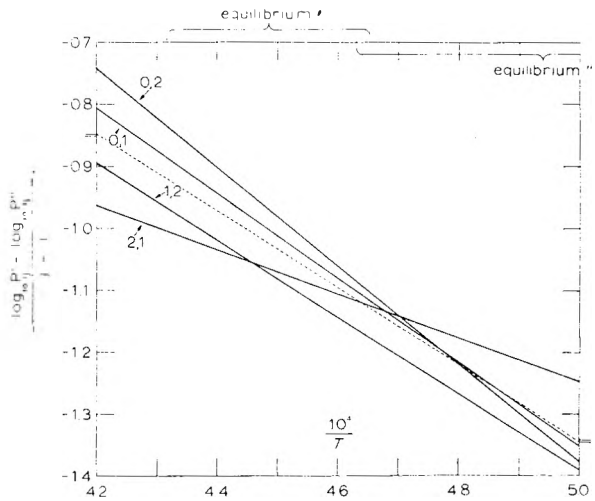

Fig. 2.—Determination of ΔF^0 by means of mass spectroscopic data of Drowart, De Maria and Inghram[9] and Drowart and De Maria.[10]

Equation 2 was derived for a case when the condensed phases participating in the two equilibria are: pure liquid silicon, stoichiometric silicon carbide and pure graphite. In Drowart's and De Maria's experiments on equilibrium″ the highest temperature was 1887°, at which temperature the solubility of carbon in liquid silicon is 0.2 atom % (upper limit) according to Scace and Slack.[11] We shall consider it negligibly small for the present purposes. According to Lely[12] silicon carbide is stoichiometric. There are no data on the solubility of silicon in graphite. We have assumed it also to be negligibly small.

In Fig. 2 $(\log P_{ij}' - \log P_{ij}'')/(j - i) = 0.4343\Delta F^0/RT$ has been plotted *vs.* $10^4/T$. Since the original investigators have plotted their data as the best straight lines through the experimental points, we also obtain only straight lines here. The temperature ranges covered in both series of experiments are indicated by the brackets at the top of the figure. The pair of numerals at each line are the i, j values. The four lines (0,1), (0,2), (1,2)

(4) F. D. Rossini, *et al.*, "Selected Values of Chemical Thermodynamic Properties," Circular 500, National Bureau of Standards, Washington, D. C., 1952.

(5) K. K. Kelley, "Contributions to the Data on Theoretical Metallurgy," Bureau of Mines Bull. 476, Washington, D. C., 1949.

(6) M. Olette, *Compt. rend.*, **244**, 1033 (1957).

(7) J. D. Baird and J. Taylor, *Trans. Faraday Soc.*, **54**, 526 (1958).

(8) "Silicon Carbide—A High Temperature Semiconductor." Proceedings of the Conference on Silicon Carbide, Boston, Mass., April 2-3, 1959, Pergamon Press, New York, N. Y., p. 3.

(9) J. Drowart, G. De Maria and Mark G. Inghram, *J. Chem. Phys.*, **29**, 1015 (1958).

(10) Reference (8), p. 16.

(11) R. I. Scace and G. A. Slack, *J. Chem. Phys.*, **30**, 1551 (1959).

(12) J. A. Lely, *Ber. deut. keram. Ges.*, **32**, 229 (1955).

and (2,1) are closest together near the overlap of the two temperature ranges, the smallest width of the bundle, measured vertically, being about 0.07 ordinate unit. This uncertainty is not larger than the uncertainty expected by mass spectroscopists.[13] At $10^4/T = 4.7$ (1855°) we obtain an average value -11.3 kcal. for ΔF^0. The corresponding 0.4343 $\Delta F^0/RT$ function through this pair of values of T and ΔF^0, as calculated by means of eq. 1 ($\Delta H^0_{298.16} = -18223$ cal.), is shown in Fig. 2 by the dashed line. It is remarkable that this line almost coincides with the average straight line of lines (0,1), (0,2), (1,2) and (2,1). This average line is indicated only by its intercepts on the $10^4/T = 4.2$ and $10^4/T = 5.0$ axes. The plot of the $0.4343\Delta F^0/RT$ function obtained from the Humphrey, *et al.*, ΔF^0 function would lie almost entirely above the $(\log P_{ij}' - \log P_{ij}'')/(j - i) = -0.7$ line in Fig. 2.

In their experiments with a pressure furnace at 35 atmospheres Scace and Slack[11] have found that at 2830° silicon carbide decomposes into graphite and a solution of carbon (19 atom %) in liquid silicon. Let us consider these changes, all taking place at 35 atmospheres and 2830°

$$SiC_x(\text{liquid}) + (1 - x)C\ (\text{graphite}) + \Delta F_a = SiC\ (\text{solid}) \quad (3)$$

$$Si(\text{liquid}) + xC(\text{graphite}) + \Delta F_b = SiC_x(\text{liquid}) \quad (4)$$

$$Si(\text{liquid}) + C(\text{graphite}) + \Delta F_c = SiC(\text{solid}) \quad (5)$$

In eq. 3 and 4 the formula SiC_x denotes a solution of carbon in liquid silicon; let us assume that $x = 19/(100 - 19) = 0.235$. Addition of eq. 3 and 4 gives eq. 5, whence

$$\Delta F_a + \Delta F_b = \Delta F_c \quad (6)$$

Now, ΔF_a is zero, because all three phases shown in eq. 3 are in equilibrium. We also know that ΔF_b is negative because carbon dissolves in liquid silicon. Therefore $\Delta F_c = \Delta F_b$ must also be negative. From the densities of graphite, liquid silicon and silicon carbide, and by assuming zero compressibilities, one finds $\Delta F_c - \Delta F^0 = -3.24$ cal. The difference being so small, for the present purposes ΔF_c can be taken as equal to ΔF^0. Hence it can be concluded that at 2830° the ΔF^0 function must be negative. The ΔF^0 function proposed in this note satisfies this requirement. However, since the right-hand side of Fig. 1 was obtained by an extrapolation beyond the limits of validity of the heat capacity functions, it is not possible to elaborate here.

(13) W. A. Chupka, private communication.

THE ENTROPY OF SOLUTION OF IODINE AT CONSTANT VOLUME

By J. H. Hildebrand

Department of Chemistry, University of California, Berkeley 4, California

Received October 10, 1959

Recent studies[1] of solutions of iodine and of gases have revealed large partial molal volumes with correspondingly large contributions to the entropy of solution. We now have data on the partial molal volume of iodine[2] and the entropy of expansion of solvents[3] sufficient to enable us to evaluate the relation between the entropy of adding dN_2 moles of solute to a solution of $N_1 + N_2$ moles of solvent and solute (a) at constant pressure, with volume increasing by v_2, the partial molal volume of the solute, and (b) to the solution at a pressure sufficiently higher to restrict the increase in volume to the molal volume of the pure liquid solute, v_2^0.

We may write the identity

$$\left(\frac{\partial S}{\partial N_2}\right)_P = \left(\frac{\partial S}{\partial N_2}\right)_V + \left(\frac{\partial S}{\partial V}\right)_{N_2}\left(\frac{\partial V}{\partial N_2}\right)_P$$

which yields

$$(\bar{S}_2 - S_2^S)_P = (\bar{S}_2 - S_2^S)_V + \left(\frac{\partial S}{\partial V}\right)_{N_2}(\bar{v}_2 - v_2^0) \quad (1)$$

The entropy of solution of solid iodine at constant pressure is obtained from the temperature dependence of solubility

$$(\bar{S}_2 - S_2^S)_P = R(\partial \ln a_2/\partial \ln x_2)_T\,(\partial \ln x_2)/\partial \ln T)_{sat}$$

where a_i is activity. The term $(\partial S/\partial V)_{N_2}$ refers to the solution, but we are dealing with solutions so dilute that there is negligible error in using values for the pure solvents. For v_2^0 we can do no better than use the value 59 cc. for liquid iodine extrapolated from the melting point to 25°. A different value would affect all the calculated values of $(\bar{S}_2 - S_2)_V$ equally.

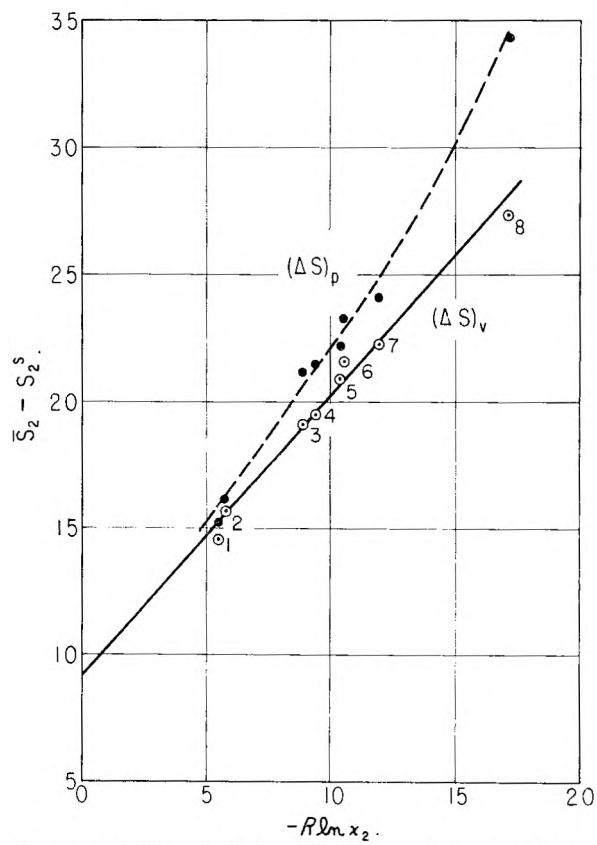

Fig. 1.—1, $CHBr_3$; 2, CS_2; 3, CCl_4; 4, c-C_6H_{12}; 5, *i*-C_8H_{18}; 6, $SiCl_4$; 7, CCl_2FCClF_2; 8, C_7F_{16}.

(1) Kōzō Shinoda and J. H. Hildebrand, This Journal, **62**, 292 (1958); (b) J. E. Jolley and J. H. Hildebrand, *ibid.*, **60**, 1050 (1958).

(2) D. N. Glew and J. H. Hildebrand, *ibid.*, **60**, 616 (1956). Kōzō Shinoda, *ibid.*, **62**, 295 (1958).

(3) E. Brian Smith and J. H. Hildebrand, *J. Chem. Phys.*, **31**, 145 (1959).

The entropy of solution at constant pressure is

$$(\bar{S}_2 - S_2^S)_P = R(\partial \ln a_2/\partial \ln x_2)_T (\partial \ln x_2/\partial \ln T)_{sat}$$

Although the "Henry's law correction," $\partial \ln a_2/\partial \ln x_2$ is nearly unity in the poorer solvents, it is distinctly less in the better solvents. For solutions in CS_2 and CCl_4, Walkley and Hildebrand[4] determined directly the variation of the partial vapor pressure of iodine with composition. For the other solutions we have evaluated this factor from the solubility data by the method described by Shinoda and Hildebrand.[5]

Figure 1 shows values of $-R \ln x_2$ at 25° plotted against the entropy of solution of solid iodine at both constant pressure and constant volume for representative solutions relatively free from complicating factors, such as polarity, donor–acceptor interaction (slight in the case of $CHBr_3$) and geometrical asymmetry. The slope of the line for the entropy of solution at constant volume is 1.10, only slightly greater than 1.00, which it would be if my original definition of a regular solution, as one in which the entropy of solution at constant volume is $-R \ln x_2$, were strictly valid.

The line extrapolates to 9.0 e.u. for the entropy of fusion of iodine, at 25°, not far from the value, 8.0, extrapolated from the heat of fusion at the melting point and the heat capacities of the solid and liquid phases.

I wish to acknowledge the support of the Atomic Energy Commission in obtaining many of the data upon which these findings are based.

(4) J. Walkley and J. H. Hildebrand, THIS JOURNAL, **63**, 1174 (1959).

(5) K. Shinoda and J. H. Hildebrand, *ibid.*, **61**, 789 (1957).

DIFFUSION WITH RAPID IRREVERSIBLE IMMOBILIZATION

BY BERTIL OLOFSSON

The Swedish Institute for Textile Research, Gothenburg, Sweden

Received October 12, 1959

A critical discussion of methods for calculating diffusion coupled with rapid irreversible immobilization has been given by Crank.[1] By a convenient numerical procedure he calculated and tabulated values of diffusion constants for some combinations of "input" parameter values. He also examined incidentally the conditions under which the "steady-state approximation" method is useful for practical evaluations of such problems.

Another approximation method has been worked out by the present author.[2] Crank has referred to this method but not discussed its applicability. We have found that this method is more useful than the steady-state method in some cases, as will be demonstrated here.

We consider diffusion coupled with immobilization by absorption or rapid reaction into a circular cylinder (fiber) from a limited bath. This process is governed by the parameters Dt/a^2 (reduced diffusion constant), $A/\pi a^2$ (bath volume/fiber volume) and s/c_B (relative concentration immobilized), the symbols in ref. 1 everywhere used. By the "steady-state approximation" (method I) we get the relationships (eq. 15 and 14 in ref. 1)

$$\frac{Dt}{a^2} = \frac{s}{c_B}\int_1^{r_0/a} \frac{(r_0'/a)\ln(r_0'/a)\,d(r_0'/a)}{1 + (\pi a^2 s/A c_B)[(r_0'/a)^2 - 1]} \quad (1)$$

$$\frac{c_1}{c_B} = 1 + \frac{\pi a^2 s}{A c_B}\left[\left(\frac{r_0}{a}\right)^2 - 1\right] \quad (2)$$

From (1) r_0/a is calculated and from (2) c_1/c_B is calculated. Then the concentration distribution is calculated from the steady-state logarithmic relationship between c/c_B and r/r_0 in the range ($c = c_1$, $r = a$) to ($c = 0$, $r = r_0$). For evaluating experiments we have to calculate Dt/a^2 for given values of $A/\pi a^2$, s/c_B and r_0/a or alternatively c_1/c_B by using (2), and a stepwise procedure in calculating the integral in (1).

For the method introduced by the present author (method II) we get the corresponding equations (eq. 28 and 20 in ref. 2).

$$\frac{Dt}{a^2} = -\frac{A}{4\pi a^2}\int_1^{c_1/c_B} \frac{1 - (r_0'/a)}{c_1'/c_B}\,d(c_1'/c_B) - \frac{s}{2c_B}\int_1^{r_0/a} \frac{1 - (r_0'/a)}{c_1'/c_B}\,d(r_0'/a) \quad (3)$$

$$\frac{c_1}{c_B} = \frac{\frac{A}{\pi a^2} - \frac{s}{c_B}\left[1 - \left(\frac{r_0}{a}\right)^2\right]}{\frac{A}{\pi a^2} + \frac{1}{3}\left[2 - \left(\frac{r_0}{a}\right) - \left(\frac{r_0}{a}\right)^2\right]} \quad (4)$$

Equations 3 and 4 are applied just as (1) and (2) and the concentration calculated from a second degree relationships between c/c_B and r/r_0 in the range previously indicated. Thus the calculations are not more troublesome than for method I. The absence of logarithmic factors simplifies the work in method II and the integral (3) can be exactly evaluated by introducing (4). However in practice it is often more convenient to use the differential form of (3) and (1) and calculate D for a series of time intervals $t \rightarrow t + \Delta t$.

It is of course important to compare the accuracy of the two methods. It has been indicated[2] that method II gives a satisfactory accuracy as the "affinity" s/c_B is large. This seems also to be valid for method I as specially demonstrated by Crank (Fig. 4[1]) for the case $Dt/a^2 = 9/16$, $s/c_B = 10$, $A/\pi a^2 = 21$. It was confirmed by the present author that method II was just as good as method I at the larger values of s/c_B corresponding to dyeing experiments. But Crank also has compared the results from method I with his "exact" calculations for the case (Fig. 4[1]) $Dt/a^2 = 9/16$, $s/c_B = 2$, $A/\pi a^2 = 5$. We have made the corresponding evaluation using our method II and the results obtained are compared in Table I.

TABLE I

	"Exact" value[1]	Method I[1]	Method II[2]
r_0/a	0.317	0.222	0.314
Fractional total concn. at			
$r/a = 0.314$	0.664	.714	.667
$r/a = .50$	.737	.778	.737
$r/a = .75$	.806	.834	.810
$r/a = 1.00$	.856	.874	.859

Apparently the results from method II are in excellent agreement with the "exact" results, while method I differs significantly, as also pointed out by Crank.

(1) F. Crank, *Trans. Faraday Soc.*, **53**, 1083 (1957).

(2) B. Olofsson, *J. Text. Inst.*, **47**, T464 (1956).

TABLE II

VALUES OF Dt/a^2 CALCULATED FOR AN INFINITE BATH

E = "Exact" values, I = calculations by method I, II = calculations by method II

	Plane sheet			Cylinder			Sphere		
s/c_B	E	I	II	E	I	II	E	I	II
		$x_0/a = 0.75$			$r_0/a = 0.75$			$r_0/a = 0.75$	
1	0.041	0.031	0.039	0.038	0.029	0.036	0.035	0.026	0.033
2	.072	.063	.070	.067	.057	.064	.061	.052	.059
5	.167	.156	.164	.152	.142	.150	.141	.130	.139
10	.323	.313	.320	.295	.285	.293	.273	.260	.272
∞		II/I = 1.000			II/I = 1.006			II/I = 1.019	
		$x_0/a = 0.50$			$r_0/a = 0.50$			$r_0/a = 0.50$	
1	0.162	0.125	0.156	0.138	0.101	0.129	0.118	0.083	0.111
2	.289	.250	.281	.241	.202	.233	.205	.167	.202
5	.666	.625	.656	.548	.504	.545	.460	.417	.475
10	1.290	1.250	1.281	1.049	1.009	1.066	.887	.833	.931
∞		II/I = 1.000			II/I = 1.033			II/I = 1.094	
		$x_0/a = 0.25$			$r_0/a = 0.25$			$r_0/a = 0.25$	
1	0.366	0.281	0.352	0.274	0.191	0.258	0.219	0.141	0.214
2	0.653	0.564	0.633	0.475	0.382	0.469	.370	.281	.394
5	1.496	1.406	1.477	1.057	0.955	1.102	.828	.703	.934
10	2.907	2.813	2.883	2.036	1.911	2.156	1.543	1.406	1.835
∞		II/I = 1.000			II/I = 1.104			II/I = 1.281	
		$x_0/a = 0$							
1	0.650	0.500	0.625						
2	1.158	1.000	1.125						
5	2.660	2.500	2.625						
10	5.167	5.000	5.125						
∞		II/I = 1.000							

To get a general idea about the applicability of the two approximation methods the conditions applied in their evaluation should be considered. For method I the concentration–distance (c–r) curve at some time t is wholly fixed by the two parameters $c = c_1$ (at the boundary $r = a$) and $r = r_0$ (corresponding to $c = 0$), and these parameters are determined to fit the boundary conditions of diffusional flow. For method II the c–r curve gets another degree of freedom by the assumption $c = a_0 + a_1 r + a_2 r^2$. To get a fixed curve another boundary condition must be applied and this is really the integrated form of the condition at $r = a$. These two forms of the same boundary condition (*cf.* (10) and (12) in ref. 2) are not equivalent in the approximation procedure, as one of them is deduced from the other by applying the original (time-dependent) diffusion equation. However, in applying the integrated boundary condition the c–r curve is approximated with a straight line and thus the accuracy of the calculations decreases, as the real c–r curve increases in curvature at small s-values.

For a plane sheet method I really suggests a linear c–x curve (21).[1] Thus we might suppose that the second degree curve used for calculation of D by method II provides a greater accuracy. For this case eq. 3 is still valid, if we substitute (Crank's symbols)

$$r = x,\ A/2\pi a = l \qquad (5)$$

but eq. 4 must be exchanged with

$$\frac{c_1}{c_B} = \frac{\frac{l}{a} - \frac{s}{c_B}\left(1 - \frac{x_0}{a}\right)}{\frac{l}{a} + \frac{1}{2}\left(1 - \frac{x_0}{a}\right)} \qquad (6)$$

To demonstrate the accuracy of the approximation methods, we have made some calculations for an infinite bath ($l/a \to \infty$). From (3), (5) and (6) we get $c_1/c_B \to 1$ and $l/a.\mathrm{d}(c_1/c_B) \to (s/c_B + 1/2)\ \mathrm{d}(x_0/a)$ and finally

$$\frac{Dt}{a^2} = \left(\frac{s}{c_B} + \frac{1}{4}\right) \times \frac{1}{2}\left(\frac{x_0}{a} - 1\right)^2 \qquad (7)$$

Calculations by method (II) from (7) are compared with calculations by method (I) from (24)[1] and "exact" calculations by Crank (Table II[7]) in Table II. Evidently our assumption on the accuracy of the approximation is verified.

For the cylinder case the increasing curvature of the c–r curve with decreasing r is observed in the steady-state approximation (8).[1] This influences the accuracy of method II and it already was proposed earlier[2] to restrict calculations to $r_0/a > 0.30$ (deeper penetration also corresponds to very small changes in external bath concentration, if the bath ratio is not too small). In applying the "integrated boundary condition" with the linear c–r curve in method II, however, the error because of the curvature is compensated to an appreciable extent, as the contribution of the volume element at distance r to the total sorbed quantity is $(c + s)\ 2\ \pi\ r\ dr$, thus decreasing in proportion to r. In Table II we have made calculations in analogy to those for the plane sheet and the results give some idea about the decreasing accuracy as r_0/a decreases.

For the sphere the same sort of discussion is applicable. There is still larger increase of curvature with decreasing r, *cf.* (17),[1] and in spite of the compensation because of the rapidly decreasing volume elements $4\pi r^2 dr$ the error of method II increases

more rapidly with decreasing r_0/a than for the cylinder as demonstrated in Table II (now A in eq. 3 is substituted with $V/2a$). Also from the formal point of view method I is less troublesome than method II.

We conclude that the approximation method suggested[2] is very useful for a plane sheet to get a great accuracy. It has formal advantages to the steady-state approximation method for a cylinder and also a greater accuracy in the range indicated here. But it has no formal advantage to the steady-state approximation method for a sphere and a greater accuracy in a rather narrow range.

PROTON NUCLEAR SPIN RESONANCE SPECTROSCOPY. XI. A CARBON-13 ISOTOPE EFFECT

By George Van Dyke Tiers

Contribution No. 166 from the Central Research Dept., Minnesota Mining & Mfg. Co., St. Paul 19, Minnesota

Received October 16, 1959

Recently a nuclear spin resonance (n.s.r.) "isotope effect" of C^{13} upon attached fluorine atoms has been discovered.[1] The rather unexpectedly large shifts were always found to be in the direction corresponding to greater shielding by C^{13} than by C^{12}. Though no shift was found for protons, the much smaller effect anticipated by analogy with the deuterium shifts[2] would not have been detected.

As both the sign and the relative magnitude of such a C^{13} effect might prove theoretically interpretable, a more elaborate experimental procedure has been used in the present work.

Experimental

The compounds studied were examined neat in the customary 5 mm. o.d. sample tubes, from which air had been swept by means of a brisk stream of bubbles of prepurified nitrogen; however, air-saturated $CHCl_3$ and $(CH_3)_4Si$ were found to give the same results. The C^{13} isotopic isomers were present at their natural abundances.

The n.s.r. spectrometer and measurement techniques have been described.[3] For the present study separate reference compounds were not employed, the exceedingly strong sharp signal from the normal (C^{12}) compound being used instead; "image" lines (also called "side-bands") are readily produced from it by audio-oscillator modulation of the magnetic field. When C^{13} is present, the proton signal is split by it into a doublet, the coupling constant being *ca.* 100 to 250 c./sec. The positions of these two weak C^{13} satellite lines are measured, separately, relative to the strong C^{12} central peak by use of the "image" lines.[3] The small but reproducible difference found in each case results from the isotopic shift, as otherwise the high- and low-field C^{13} components would be equally spaced from the C^{12} central line.

Errors random in nature were counteracted by multiple repetition of measurements; all data have been used and weighted equally. Measurements were made over a three-week period. At each session six sweeps were run on each of the two C^{13} lines for each of the compounds studied. In addition to the routine alternation of sweep direction,[3] which virtually eliminates errors due to differential saturation or to "ringing" of the signals, in most cases care was taken in the magnet cycling to obtain a "flat" field and hence very symmetrical peaks for both directions of sweep; sweep rates also were controlled to be equal (within 10%) in both directions. Subsequent examination of the data failed to reveal any significant effect of over- or under-cycling or of unequal sweep rates, or of the degree of resolution upon the magnitude or direction of the C^{13} effect. It should be emphasized that optimal resolution was not attained, nor was bad resolution tolerated. "Ringing" was never observed for any of the image lines, or for the C^{13} satellites of $(CH_3)_4Si$, but was attained at the C^{13} lines of the other compounds in about half of the measurements. The widths of the image signals at half-maximum were 0.70 to 0.85 c./sec. in nearly all cases, while the C^{13} satellites (when not ringing) were, if anything, narrower than the corresponding C^{12} images, except for $(CH_3)_4$ Si, for which they averaged *ca.* 0.12 c./sec. wider. The effect of sweep direction is fairly large, the C^{13} isotope effect appearing to be larger by 0.002_2 p.p.m. when the sweep is toward decreasing field, or smaller by the same amount when the opposite sweep is used exclusively. Although such error was avoided, it would not have concealed the isotope effect.

Table I

The Excess N.S.R. Shielding, $\Delta\tau$, Produced by C^{13}, Relative to C^{12}, in Several Compounds

Compound	No. of meas.	$\Delta\tau$, p.p.m.[a] (C^{13}—C^{12})	$J(C^{13}H)$, c/s[b]	Shielding value, τ[c]
$(CH_3)_4Si$	18	+0.0042	118.20	10.000
CH_3I	18	+ .0012	151.17	7.843
CH_2Cl_2	12	+ .0042	178.24	4.720
$CHCl_3$	18	+ .0059	209.17	2.755

[a] Standard deviation of the averaged value was ±0.0012 p.p.m. in each case. [b] Standard deviation of the averaged value was ±0.09 c./sec. in each case. [c] Measured in dilute solution in CCl_4, as described in ref. 3.

Results and Discussion

The results presented in Table I demonstrate a small but statistically significant excess shielding by C^{13} in three molecules, namely, $CHCl_3$, CH_2Cl_2 and $(CH_3)_4Si$. In the case of CH_3I the shift is not large enough to be considered as established. The center of the doublet corresponding to protons attached directly to C^{13} is found at shielding values higher by *ca.* 0.004 p.p.m. than the line due to the normal (C^{12}) compound. This effect is of the same sign but only about 1/40 as large as the corresponding effect upon fluorine.[1] The same ratio, 1/40, has been observed for the deuterium isotope effect upon proton and fluorine shieldings.[2] It appears unrelated to the ratios found for the coupling constants in the same compounds, *ca.* 1/2 for $J(C^{13}\text{–H})/J(C^{13}\text{–F})$ and *ca.* 1/4 for $J(\text{D–H})/J(\text{D–F})$.

The data in Table I seem to indicate a significant variability in the magnitude of the effect. The variation observed is not simply related either to the coupling constants, to the relative shieldings, or even to the number of substituents; however, the experimental uncertainty is such as not to warrant more detailed studies at this time.

The conclusions reached above are of course entirely dependent upon the successful elimination of directed error in the measurements. Potential errors and the precautions taken have already been discussed in the Experimental section. There may well be further, unrecognized, sources of error; for example, treatment of the $C^{13}HCl_3$ spectrum as an "AX" case rather than as an "AB" case[4] in fact must result in an apparent excess shielding by C^{13}, even if there were no isotope effect. By

(1) P. C. Lauterbur, private communication; I am indeed grateful for this advance information, without which it is unlikely that the present work would have been begun.

(2) G. V. D. Tiers, *J. Am. Chem. Soc.*, **79**, 5585 (1957), *J. Chem. Phys.*, **29**, 963 (1958).

(3) G. V. D. Tiers, This Journal, **62**, 1151 (1958).

(4) J. A. Pople, W. G. Schneider and H. J. Bernstein, "High-Resolution Nuclear Magnetic Resonance," McGraw-Hill, Book Co., Inc., New York, N. Y., 1959, pp. 118–123.

algebraic manipulation of the relations appropriate to the two cases, the error is shown to be only 0.00001 p.p.m. for $CHCl_3$, and should be equally negligible for the other molecules studied.

The most serious effect of bad resolution should be an increase in random errors, with the result that the C^{13} effect would be rendered highly uncertain. If resolution varied substantially with sweep direction, a directed error might be produced; however, no evidence for such could be found by careful analysis of the data. The apparently poor resolution of the C^{13} satellites for the $(CH_3)_4Si$ (as judged by the excess line width, *ca.* 0.12 c./sec., observed for them) is actually due to the exceedingly weak spin-spin coupling between protons on C^{13} and those on C^{12}. This splitting becomes observable as a result of the "effective chemical shift" produced by the magnetic moment of individual C^{13} atoms upon their attached protons. The coupling constant, $J(C^{12}H_3SiC^{13}H_3)$, must be approx. 0.12 c./sec., the multiplet being assumed to be 10-fold, with binomial intensity distribution; $J = (0.90^2 - 0.78^2)^{1/2}/3.6$.

Acknowledgment.[1]—I am indebted to Donald Hotchkiss for the excellent careful operation of the n.s.r. equipment so necessary in this work.

THE STANDARD ELECTRODE POTENTIAL OF THE QUINHYDRONE ELECTRODE FROM 25 to 55°[1]

BY JOHN C. HAYES[2] AND M. H. LIETZKE

Contribution from the Chemistry Division, Oak Ridge National Laboratory, Oak Ridge, Tennessee

Received October 17, 1959

Since the discovery[3] and development[4,5] of the quinhydrone electrode, it has found frequent use as a substitute for the hydrogen electrode for *p*H measurements. The electrode is convenient to use and it gives results which are easily reproducible.[6,7] The earlier research established the fact that measurements with the electrode in certain solutions contained a "salt error,[5] which was due[8] to a change in the ratio of the activity of hydroquinone and quinone caused by the presence of other dissolved substances in solution. While other investigations were concerned with the "salt-error," they also established the normal potential of the quinhydrone electrode,[9] as well as the normal potentials of the hydroquinhydrone and the quinoquinhydrone electrodes.[10]

Harned and Wright[11] determined the normal electrode potential of the quinhydrone electrode from 0 to 40° by combining their data with activity coefficients determined by Harned and Ehlers[12] by a different method.

In the present investigation the standard electrode potentials of the quinhydrone electrode were measured from 25 to 55 at 5° intervals, using a Ag–AgCl reference electrode. The establishment of standard electrode potentials at each interval allows the direct calculation of activity coefficients at these temperatures.

In the calculations, it has been assumed that the cell reaction is

$$\text{Quinone} + 2HCl + 2Ag \rightleftharpoons \text{Hydroquinone} + 2AgCl \qquad (1)$$

The electromotive force for this reaction is given by the Nernst equation in the form.

$$E = E^0_{\text{cell}} + \frac{RT}{F} \ln a_{HCl} \qquad (2)$$

Since the quinhydrone used is an equimolar compound of quinone and hydroquinone, and since these substances are non-electrolytes of low solubility in contact with the solid, their activities should be constant. At higher temperatures, the solubility of quinhydrone becomes appreciable (7 g. per 100 g. H_2O),[2] but as long as the ratio of the activities of quinone and hydroquinone is nearly constant, these activities may be neglected. Therefore, the Nernst equation may now be written

$$E = E^0_{\text{cell}} + \frac{2RT}{F} \ln m_{HCl}\gamma_{HCl} \qquad (3)$$

If one assumes that

$$\ln \gamma = \frac{-S\sqrt{I}}{1 - A\sqrt{I}} + BI \qquad (4)$$

where A and B are parameters and I = ionic strength, $S = 1.17202\ (23375.2/DT)^{3/2}$, and D = dielectric constant of water (at temperature T), determined by the Åkerlöf equation[13] then equation 3 may be rearranged to give

$$E - \frac{2RT}{F} \ln m + \frac{2RT}{F} \frac{S\sqrt{I}}{1 + A\sqrt{I}} = E^0 + \left(\frac{2RT}{F} B\right) I \qquad (5)$$

If the quantities on the right are equated to $E^{0\prime\prime}$, then

$$E^{0\prime\prime} = E - \frac{2RT}{F} \ln m + \frac{2RT}{F} \frac{S\sqrt{I}}{1 + A\sqrt{I}} \qquad (6)$$

The E^0 at any one temperature may be determined by extrapolating the $E^{0\prime\prime}$ values to zero ionic strength. In this work, however, the parameters A and B and the values of E^0 in equation 5 were determined by a non-linear least squares method on a high speed computer (the ORACLE).

Materials and Apparatus

Quinhydrone.—The quinhydrone used in this project was Eastman No. 217, recrystallized from water heated to

(1) This paper is based upon work performed for the Atomic Energy Commission at the Oak Ridge National Laboratory operated by Union Carbide Corporation.

(2) Research Participant for the Summer, 1959, from Hamline University, St. Paul, Minnesota.

(3) F. Haber and R. Russ, *Z. physik. Chem.*, **47**, 257 (1904).

(4) F. S. Granger and J. M. Nelson, *J. Am. Chem. Soc.*, **43**, 1401 (1921).

(5) E. Biilman, *Ann. Chim.*, [9] **15**, 109 (1921).

(6) J. L. R. Morgan, O. M. Lammert and M. A. Campbell, *J. Am. Chem. Soc.*, **53**, 454 (1931).

(7) E. Biilman and A. L. Jensen, *Bull. soc. chim.*, **41**, 151 (1927).

(8) S. P. L. Sörensen, M. Sörensen and K. Linderstrom-Lang, *Ann. Chim.*, **16**, 283 (1921).

(9) F. Hovorka and W. C. Dearing, *J. Am. Chem. Soc.*, **57**, 446 (1935).

(10) H. I. Stonehill, *Trans Faraday Soc.*, **39**, 67 (1943).

(11) H. S. Harned and D. D. Wright, *J. Am. Chem. Soc.*, **55**, 4849 (1933).

(12) H. S. Harned and R. W. Ehlers, *J. Am. Chem. Soc.*, **55**, 2179 (1933).

(13) G. C. Akerlof and H. I. Oshry, *J. Am. Chem. Soc.*, **72**, 2844 (1950).

65°. The recrystallized product was dried overnight in a vacuum desiccator. The quinhydrone gave a melting point at 168 ± 1°.

Nitrogen.—All operations involving quinhydrone were done in an atmosphere of nitrogen. The bubbling of nitrogen into the cell during e.m.f. measurements not only gave an inert atmosphere but also provided stirring of the solution.

Hydrochloric Acid.—Stock solutions of hydrochloric acid were prepared from Fisher Certified Reagent Hydrochloric Acid. Concentrations were determined by titration of the solutions with standard alkali. Densities were determined by weighing a certain volume of solution. The concentrations then were expressed in terms of molalities to eliminate corrections for the change in volume at different temperatures.

Ag–AgCl Electrodes.—The silver–silver chloride electrodes were prepared according to the method described by Greeley.[14]

Cell Measurements.—The cell potentials were measured with a vibrating reed electrometer (Model 30, Applied Physics Corp.) used as a null instrument. Potentials were read from a potentiometer (type B, The Rubicon Co.) using a Brown Recorder to indicate equilibrium conditions. The cell was held in a constant temperature bath (controlled to ±0.02°) by means of a brass tube holder which had holes drilled in it to facilitate thermal equilibriun. The tube holder also shielded the cell from any environmental capacitance.

Experimental

The cells, without the quinhydrone, were allowed to equilibrate for at least one hour in an atmosphere of N_2. Measurements of potential were started from 5 to 10 minutes after the quinhydrone had been added. Equilibrium voltages were considered constant when they did not change more than 0.2 mv. in a half-hour period. Equilibrium voltages often were observed within 15 minutes and remained essentially constant for as long as 2 or 3 hours.

Discussion of Results

The E^0 values for the Ag-AgCl, quinhydrone cell from 25 to 55° are listed in Table I. The best value of the parameter A in equation 4 was found to be 1.5.

TABLE I

THE Ag-AgCl-QUINHYDRONE CELL

	25°	30°	35°	40°	45°	55°
E^0	0.4771	0.4762	0.4762	0.4765	0.4771	0.4770
$\left(\frac{2RT}{F}B\right)^a$	0.0096	0.0148	0.0120	0.0052	0.0062	0.0118

[a] This term is defined in equation 5.

TABLE II

STANDARD ELECTRODE POTENTIALS OF THE QUINHYDRONE ELECTRODE

25°	30°	35°	40°	45°	55°
0.6995[a]	0.6953	0.6919	0.6886	0.6854	0.6776
.6995[b]	.6953	.6918	.6885	.6854	.6776
.6994[15]	.6952	.6919	.6885	.6885	.6776
.6997[11]	.6960	.6923	.6886		
.6994[9]					

[a] Based on this investigation plus E^0 values for Ag–AgCl from Harned and Ehlers; see also Bates "Electrometric *p*H Determinations, Theory and Practice," John Wiley and Sons, Inc., New York, N. Y., 1954. [b] Based on this investigation plus E^0 values for Ag–AgCl from Greeley.[14]

The standard electrode potentials of the quinhydrone electrode have based based on the E^0 values of the Ag–AgCl electrode from the values of Harned and Ehlers,[12] as well as those of Greeley[14] (which were measured in this Laboratory). As shown in Table II, these values agree usually to within 0.1 mv.

(14) R. S. Greeley, Ph.D. Thesis, University of Tennessee, May 22, 1959.

TABLE III

ACTIVITY COEFFICIENTS OF HCl

m	1[a]	2[12]	25° 3[15]	4[14]	5[16]	6[17]
0.001	0.9654	0.9656	0.9650		0.9653	0.9650
.002	.9524	.9521	.9520		.9525	.9519
.005	.9287	.9285	.9283	0.9284	.9287	.9280
.01	.9048	.9048	.9045	.9044	.8757	.9040
.02	.8754	.8755	.8753		.8301	.8747
.05	.8295	.8304	.8308	.8310	.8310	.8296
.1	.7923	.7964	.7967	.7972	.7938	.7958
m			30°			
0.001	0.9652	0.9650	0.9648			
.002	.9521	.9515	.9518			
.005	.9284	.9275	.9274			
.01	.9047	.9034	.9034			
.02	.8759	.8741	.8741			
.05	.8319	.8285	.8291			
.1	.7981	.7940	.7946			
m			35°			
0.001	0.9648	0.9647				
.002	.9515	.9513				
.005	.9274	.9268				
.01	.9033	.9025				
.02	.8737	.8731				
.05	.8279	.8265				
.1	.7916	.7918				
m			40°			
0.001	0.9642	0.9643	0.9642			
.002	.9508	.9505	.9507			
.005	.9261	.9265	.9268			
.01	.9011	.9016	.9026			
.02	.8701	.8715	.8735			
.05	.8208	.8246	.8283			
.1	.7792	.7891	.7927			
m			45°			
0.001	0.9639	0.9644				
.002	.9503	.9504				
.005	.9253	.9261				
.01	.9001	.9008				
.02	.8690	.8704				
.05	.8194	.8232				
.1	.7780	.7872				
m			55°			
0.001	0.9631	0.9636				
.002	.9493	.9497				
.005	.9240	.9240				
.01	.8987	.8990				
.02	.8676	.8680				
.05	.8192	.8195				
.1	.7801	.7829				

[a] Results of this investigation.

The activity coefficients of hydrochloric acid are listed in Table III. These values agree closely with those obtained by other investigators. The largest deviations occur at 40 and 45°, yet they are still less than 1%. Agreement is unusually good at the other temperatures. Hence it appears that the quinhydrone electrode may be used in activity coefficient measurements in a manner similar to the hydrogen electrode.

(15) R. G Bates and V. E. Bower, *J. Research Natl. Bur. Standards*, **53**, 283 (1954).

(16) T. Shedlovsky, *J. Am. Chem. Soc.*, **72**, 3680 (1950).

(17) G. J. Hills and D. J. G. Ives, *J. Chem. Soc.*, 318 (1951).

Acknowledgment.—The authors wish to thank Dr. R. W. Stoughton for interesting discussions in connection with this work.

THERMOCHEMISTRY OF POTASSIUM PERMANGANATE, POTASSIUM MOLYBDATE, POTASSIUM CHLORATE, SODIUM CHLORATE, SODIUM CHROMATE AND SODIUM DICHROMATE

BY THOMAS NELSON, CALVIN MOSS AND LOREN G. HEPLER[1]

Contribution from Cobb Chemical Laboratory, University of Virginia Charlottsville, Va.

Received October 20, 1959

Heats of solution of $KMnO_4$(c), $KClO_3$(c), $NaClO_3$(c) and Na_2CrO_4(c) and the heat of reaction of $Na_2Cr_2O_7$(c) with excess OH^-(aq) have been determined as part of an undergraduate research program. These heats have been used for calculation of standard heats of formation of K_2MoO_4(c), Na_2CrO_4(c) and $Na_2Cr_2O_7$(c) and standard partial molal entropies of MnO_4^-(aq) and ClO_3^-(aq).

Experimental

The solution calorimeter used for these determinations has been described.[2-4] All calorimetric determinations were carried out at 25.0 ± 0.2° with 950 ml. of water or solution in the calorimeter.

All of the salts were prepared for use in the calorimeter by recrystallization of the appropriate reagents and all except $NaClO_3$ and $KClO_3$ were analyzed by common volumetric methods. Some samples were dried in vacuum desiccators and some in an air oven.

Results

Heats of solution of $KMnO_4$(c), K_2MoO_4(c), $KClO_3$(c), $NaClO_3$(c) and Na_2CrO_4(c) are given in Tables I–V. In each table, ΔH refers to the reaction

$$\text{salt(c)} = \text{salt(aq)} \qquad (1)$$

TABLE I

HEATS OF SOLUTION OF $KMnO_4$(c)

Moles $KMnO_4 \times 10^3$/950 ml. H_2O	ΔH(kcal./mole)
4.810	10.42
5.687	10.39
6.345	10.43
6.570	10.44
7.187	10.42
9.9158	10.44

TABLE II

HEATS OF SOLUTION OF K_2MoO_4(c) IN 10^{-3} *M* OH^-(aq)

Moles $K_2MoO_4 \times 10^3$/950 ml. soln.	ΔH(kcal./mole)
0.5741	−0.82
1.100	− .79
1.359	− .82
1.623	− .79
1.746	− .75
1.784	− .77
2.022	− .73

TABLE III

HEATS OF SOLUTION OF $KClO_3$(c)

Moles $KClO_3 \times 10^3$/950 ml. H_2O	ΔH(kcal./mole)
4.245	9.87
6.822	9.92
7.770	9.85
11.04	9.90
12.93	9.91
16.16	9.90

TABLE IV

HEATS OF SOLUTION OF $NaClO_3$(c)

Moles $NaClO_3 \times 10^3$/950 ml. H_2O	ΔH(kcal./mole)
0.9260	5.21
1.032	5.21
1.062	5.23
1.178	5.23
1.263	5.24
2.270	5.24

TABLE V

HEATS OF SOLUTION OF Na_2CrO_4(c) IN 10^{-3} *M* OH^-(aq)

Moles $Na_2CrO_4 \times 10^3$/950 ml. soln.	ΔH(kcal./mole)
0.5632	−4.42
.6645	−4.44
.9791	−4.42
1.016	−4.39
1.137	−4.43
1.408	−4.36

Heats of reaction of $Na_2Cr_2O_7$(c) with a small excess of aqueous NaOH as in the equation

$$Na_2Cr_2O_7(c) + 2OH^-(aq) = 2Na^+(aq) + 2CrO_4^-(aq) + H_2O(l) \qquad (2)$$

are given in Table VI.

TABLE VI

HEATS OF SOLUTION OF $Na_2Cr_2O_7$(c) IN OH^-(aq)

Moles $Na_2Cr_2O_7 \times 10^3$/950 ml. soln.	Moles $OH^- \times 10^2$	ΔH(kcal./mole)
2.087	1.0	−21.36
2.646	1.0	−21.34
4.302	1.5	−21.33
4.640	1.5	−21.49
5.106	2.0	−21.36
6.549	1.5	−21.23
6.567	1.8	−21.32
8.566	2.5	−21.33
10.482	2.5	−21.26

Heats of dilution of $KClO_3$(aq) and $NaClO_3$ have been taken from National Bureau of Standards Circular 500[5] and heats of dilution of $KMnO_4$(aq), K_2MoO_4(aq) and Na_2CrO_4(aq) have been estimated from heats of dilution[5] of $KClO_4$(aq), K_2SO_4(aq) and Na_2SO_4(aq), respectively. Standard heats of solution calculated from these heats of dilution and data in Tables I–V are given in Table VII. The standard heat of reaction which is also given in Table VII is based on the data in Table VI and estimated heats of dilution. Our estimates of total maximum uncertainties are indicated by ±.

(1) Alfred P. Sloan Foundation Research Fellow.

(2) R. L. Graham and L. G. Hepler, *J. Am. Chem. Soc.*, **78**, 4846 (1956).

(3) C. N. Muldrow, Jr., and L. G. Hepler, *ibid.* **79**, 4945 (1957).

(4) M. M. Birky and L. G. Hepler, to be published.

(5) "Selected Values of Chemical Thermodynamic Properties," Circular 500, National Bureau of Standards, 1952.

TABLE VII

STANDARD HEATS OF SOLUTION

Salt	ΔH(kcal./mole)
$KMnO_4$	10.41 ± 0.06
K_2MoO_4	−0.95 ± .10
$KClO_3$	9.89 ± .06
$NaClO_3$	5.18 ± .06
Na_2CrO_4	−4.57 ± .10
$Na_2Cr_2O_7$ (reaction 2)	−21.37 ± .18

Thermodynamic Calculations

Brown, Smith and Latimer[6] have determined the entropy of $KMnO_4$(c) at 298°K. to be 41.04 cal./deg. mole and have calculated from solubility data that the standard free energy of solution of $KMnO_4$(c) is 1710 cal./deg. mole. We have combined these data with our heat of solution and the NBS[5] standard partial molal entropy of K^+(aq) to obtain ΔS^0 = 29.2 cal./deg. mole for the entropy of solution of $KMnO_4$(c) and 45.7 cal./deg. mole for the standard partial molal entropy of MnO_4^-(aq). This latter entropy differs from the NBS[5] value (45.4) because we have used our heat of solution rather than that of Roth and Becker[7] whose work was carried out at 16.6 and 21.6° and with more concentrated solutions.

The heat of formation of K_2MoO_4(c) has been calculated to be −357.3 kcal./mole from our heat of solution and the heats of formation of $MoO_4^=$(aq)[2] and K^+(aq).[5]

The standard free energy of solution of $KClO_3$(c) has been calculated to be 1.19 kcal./mole from the solubility[8,9] and the activity coefficient[9] in saturated solution. We have used this ΔF^0 with our ΔH^0 to calculate the entropy of solution, ΔS^0 = 29.1 cal./deg. mole. This ΔS^0 and the entropies of $KClO_3$(c)[10] and K^+(aq)[5] lead to 38.8 cal./deg. mole for the standard partial molal entropy of ClO_3^-(aq). Earlier heats of solution[5] were carried out at temperatures lower than 25° and with solutions more concentrated than ours.

Standard heats of formation of Na_2CrO_4(c) and $Na_2Cr_2O_7$(c) have been calculated to be −318.6 and −468.8 kcal./mole, respectively, from our heat of solution of Na_2CrO_4(c) and our heat of solution of $Na_2Cr_2O_7$(c) in OH^-(aq) as in equation 2. Heats of formation of $CrO_4^=$(aq),[11] Na^+(aq),[5] OH^-(aq)[5] and H_2O(l)[5] have been used in these calculations.

The standard partial molal entropies of MnO_4^-(aq) and ClO_3^-(aq) may be combined with other thermodynamic data[5] to obtain standard free energies of formation and oxidation potentials and the heats of solution of $KMnO_4$(c), $KClO_3$(c) and $NaClO_3$(c) may be combined with other heat data[5] to obtain heats of formation.

Acknowledgment.—We are grateful to the National Science Foundation for financial support, to the Alfred P. Sloan Foundation for a research fellowship for one of us, to Mr. Richard Jesser for doing much of the work on K_2MoO_4 and to Mr. Merritt Birky for assistance with some of the calorimetric experiments.

(6) O. L. I. Brown, W. V. Smith and W. M. Latimer, *J. Am. Chem. Soc.*, **58**, 2144 (1936).

(7) W. A. Roth and G. Becker, *Z. physik. Chem.*, **A159**, 27 (1932).

(8) A. Seidell, "Solubilities of Inorganic and Metal Organic Compounds," D. Van Nostrand Co., Inc., New York, N. Y., 1940.

(9) J. H. Jones and H. R. Froning, *J. Am. Chem. Soc.*, **66**, 1672 (1944).

(10) W. M. Latimer, P. W. Schutz and J. F. G. Hicks, Jr., *ibid.*, **56**, 88 (1934).

(11) L. G. Hepler, *ibid.*, **80**, 6181 (1958).

SEPARATION OF WAXES FROM PETROLEUM BY ULTRACENTRIFUGATION

BY C. W. DWIGGINS AND H. N. DUNNING

U. S. Department of the Interior, Bureau of Mines, Bartlesville, Oklahoma

Received October 23, 1959

The colloidal properties of asphalts have long been recognized.[1] More recently, the colloidal nature of crude petroleum has been established by ultracentrifugation.[2] The results of these studies emphasized the presence of asphaltic materials and of some inorganic residues in the sediment. Other studies have shown that asphaltenes are sedimented during ultracentrifugation and contribute largely to the viscosities of the ultracentrifugal fractions.[3]

However, studies in this Laboratory show that the sediment from several crude oils contains relatively large amounts of waxes. Although the presence of microcrystalline waxes in crude oils has been known for several years,[4] there have been no reports of the sedimentation of these waxes during ultracentrifugation.

Four crude oils, from Oklahoma, Texas, and Kuwait, were ultracentrifuged for 3 hours at an average force of 60,000 times gravity in a Beckman Model L ultracentrifuge equipped with a No. 40 angle-head rotor. The shortest practical period was used to minimize asphaltene sedimentation. The sediments were drained of oils and suspended in chloroform with ultrasonic agitation.

Then the chloroform suspensions were centrifuged for 2 hours at an average force of 40,000 times gravity. During this centrifugation, waxy materials accumulated at the top of the tubes, most of the residual oils were dissolved in the chloroform, and inorganic materials sedimented to the bottom of the tubes. This purification process was repeated.

The waxy materials thus obtained were dried, melted, and allowed to cool for X-ray diffraction studies. Softening points ranged from 80 to 90°. The waxy material obtained from Texas Wilcox oil was only slightly colored; those from the other oils were darker but still translucent.

X-Ray diffraction patterns of the waxy materials from the four crude oils are similar and resemble those of waxes reported in the literature. In Fig. 1, the X-ray diffraction pattern of the waxy material centrifuged from the Kuwait crude oil is compared to that of a carefully purified, high-melting-point, microcrystalline wax stock, "190 Special," similar to Petrolite C-1035 produced by the Bareco Wax Co., division of Petrolite Corp.

The X-ray diffraction pattern of the waxy material is distinct and in good agreement with that of the pure wax. These X-ray diffraction data

(1) J. Pfeiffer and R. N. Saal, THIS JOURNAL, **44**, 139 (1940).

(2) B. R. Ray, P. A. Witherspoon and R. Grim, *ibid.*, **61**, 1296 (1957).

(3) H. N. Dunning, I. A. Eldib and R. J. Bolen, presented at the Division of Colloid Chemistry, Am. Chem. Soc. Meeting, Atlantic City, N. J. (September 16, 1959).

(4) J. W. Horne and J. W. Watkins, Bureau of Mines Technical Paper 715, 1949, 47 pp.

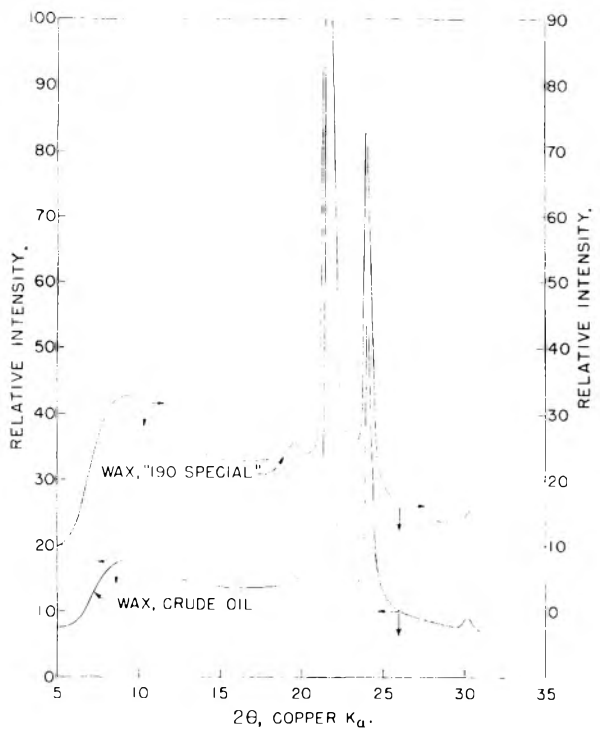

Fig. 1.—X-Ray diffraction patterns of wax ultracentrifuged from crude oil and of commercial, high-melting point wax.

are rather positive proof that the materials centrifuged from crude oils, as described above, are waxes. Their softening points and lack of solubility in solvents such as hydrocarbons and chloroform indicate that they are of relatively high molecular weight. The ease with which these waxes were ultracentrifuged from petroleum indicates that they were present as unstable colloids, probably in a suspended microcrystalline form.

These results indicate that the sediment obtained from ultracentrifugation of petroleum often contains relatively large amounts of wax in addition to the asphaltic materials previously identified.[2,3] Such waxes must be taken into account during interpretation of ultracentrifuge data based on sediment obtained. Because the centrifugal forces used are in the range of supercentrifuges, the centrifugal method may prove commercially applicable for clarification of crude oils or refinery stocks and for the preparation of high-molecular-weight waxes.

THE HEATS OF COMBUSTION OF SOME COBALT AMMINE AZIDES

BY TERENCE M. DONOVAN, C. HOWARD SHOMATE AND TAYLOR B. JOYNER

Chemistry Division, Research Department, U. S. Naval Ordnance Test Station, China Lake, California.

Received October 30, 1959

There has been recent interest in the thermodynamics and kinetics of metallic azides.[1] Previously the heat of formation of thallium azide was determined in this Laboratory.[2] During the course of a study of the thermal decomposition of some cobalt ammine azides it was thought desirable to have values of their heats of formation and the present study resulted.

Experimental

Materials.—The compounds were prepared and purified by previously described methods.[3-6] X-Ray powder patterns were used to identify all compounds except $[Co(NH_3)_3(N_3)_3]$. Corroborating evidence of the composition of $[Co(NH_3)_6](N_3)_3$ and $[Co(NH_3)_5N_3](N_3)_2$ was obtained during the course of kinetic studies of their thermal decomposition.[7] Explosions prevented similar studies of the remaining compounds. The very explosive $[Co(NH_3)_3(N_3)_3]$ was obtained by individual preparations each yielding enough material (*ca.* 400 mg.) for a single combustion. This was carefully washed but not recrystallized because of the rapid hydrolysis in warm water.[4] In view of these difficulties, some uncertainty must be attached to the reported ΔH_f^0 of this compound.

Measurements.—The measurements were made with calorimetric equipment described previously.[8,9] Benzoic acid (N.B.S. sample No. 39g) was used in determining the energy equivalent of the calorimeter which was 2789.36 ± 0.43 cal. deg.$^{-1}$ for all determinations. All weighings were reduced to vacuum and all heat values are expressed in defined calories (1 cal. = 4.1840 abs. joules).

X-Ray powder patterns of the solid residues showed the lines of CoO and Co_3O_4 only, except in the case of $[Co(NH_3)_3(N_3)_3]$ where the lines of cobalt metal also were evident. Average values of the O:Co ratios as determined by reducing the residue samples in a stream of H_2 at 700° are: $[Co(NH_3)_6](N_3)_3$, 1.1232; $[Co(NH_3)_5N_3](N_3)_2$, 1.1577; *cis*-$[Co(NH_3)_4(N_3)_2]N_3$, 1.1235; *trans*-$[Co(NH_3)_4(N_3)_2N_3$, 1.1253; and $[Co(NH_3)_3(N_3)_3]$, 0.8401. All the energy values were corrected to correspond to cobalt as the free metal in the final product using 57.1 kcal. mole^{-1} as the heat of formation of CoO and 35.7 kcal. g. atom^{-1} as the energy of combination of the excess oxygen.[10]

The exhaust gases were tested for oxides of nitrogen and carbon monoxide spectrographically and the bomb washings were tested for soluble cobalt with KOCN. Observation of the bomb washings showed no starting material which in all cases except the $[Co(NH_3)_3(N_3)_3]$ consisted of highly colored water-soluble material.

A 360-ml. Parr double-valve oxygen bomb with 1 ml. of water was flushed for 15 minutes with oxygen at slightly greater than atmospheric pressure and then filled to 30 atmospheres for the combustions. Corrections were made for the ignition wire and fuse material. The observed values for the heat of the bomb process were corrected to obtain values for the energy of the idealized combustion reaction in which all the reactants and products were in their standard states at 25° and no external work was performed. The corrections, which included those for the formation of nitric acid, were made as described by Hubbard, Scott and Waddington.[11]

Results

The determined heats of combustion are: $[Co(NH_3)_6](N_3)_3$, −645.5 ± 0.3; $[Co(NH_3)_5N_3](N_3)_2$, −562.8 ± 0.4; *trans*-$[Co(NH_3)_4(N_3)_2]N_3$, −500.3 ± 0.8; *cis*-$[Co(NH_3)_4(N_3)_2]N_3$, −500.8 ± 0.4,

(1) B. L. Evans, A. D. Yoffe and Peter Gray, *Chem. Revs.*, **59**, 515 (1959).

(2) W. S. McEwan and M. M. Williams, *J. Am. Chem. Soc.*, **76**, 2182 (1954).

(3) M. Linhard and H. Flygare, *Z. anorg. allgem. Chem.*, **262**, 328 (1950).

(4) M. Linhard and M. Weigel, *ibid.*, **263**, 245 (1950).

(5) M. Linhard, M. Weigel and H. Flygare, *ibid.*, **263**, 233 (1950).

(6) T. B. Joyner, D. S. Stewart and L. A. Burkardt, *Anal. Chem.*, **30**, 194 (1958).

(7) To be reported by Taylor B. Joyner and Frank Verhoek.

(8) W. S. McEwan and M. W. Rigg, *J. Am. Chem. Soc.*, **73**, 4725 (1951).

(9) M. M. Williams, W. S. McEwan and R. A. Henry, THIS JOURNAL, **61**, 261 (1957).

(10) B. J. Boyle, F. G. King and K. C. Conway, *J. Am. Chem. Soc.*, **76**, 3835 (1954).

(11) W. N. Hubbard, D. W. Scott and G. Waddington, THIS JOURNAL, **58**, 152 (1954).

TABLE I

COMBUSTION DATA

Compound	Sample wt., g. vacuum	$-\Delta Hc^\circ$ kcal./mole	ΔHf°, kcal./mole
$[Co(NH_3)_6](N_3)_3$	0.9934	645.64	
	1.0006	644.86	
	1.0010	646.44	
	1.0062	644.98	
	0.9889	645.76	
		mean 645.5 ± 0.3	30.7
$[Co(NH_3)_5N_3](N_3)_2$	1.0009	562.59	
	1.0000	562.73	
	0.9998	563.00	
	1.0011	563.86	
	1.0048	561.70	
		mean 562.8 ± 0.4	50.4
cis-$[Co(NH_3)_4(N_3)_2]N_3$	0.5001	500.36	
	.5048	500.36	
	.5109	500.51	
	.5189	500.42	
	.4991	502.22	
		mean 500.8 ± 0.4	90.9
trans-$[Co(NH_3)_4(N_3)_2]N_3$	0.4976	502.04	
	.4977	501.70	
	.5118	500.42	
	.5137	499.20	
	.5096	498.03	
		mean 500.3 ± 0.8	90.4
$[Co(NH_3)_3(N_3)_3]$	0.4200	404.2	
	0.4593	402.1	
		mean 403.2 ± 1.0	95.7

$[Co(NH_3)_3(N_3)_3]$, -403.2 ± 1.0 kcal. mole^{-1}. The heats of formation of these compounds were calculated using $-68{,}316$ and $-94{,}059.6$ (at. wt. C = 12.011) cal. mole^{-1} as the heats of formation of water and carbon dioxide, respectively. These values are listed in the last column of Table I.

As some difficulty was encountered in obtaining complete combustion preliminary calculations were made of the standard deviation of the mean for each set of determinations and any runs which exceeded the mean value by more than three times the standard deviation were discarded.

Because of the difficulties mentioned above in the preparation of $[Co(NH_3)_3(N_3)_3]$ and the fact that only two acceptable determinations were made of its heat of combustion, the reported value should be considered preliminary.

THE HEAT OF COMBUSTION OF THULIUM[1]

BY ELMER J. HUBER, JR., EARL L. HEAD AND CHARLES E. HOLLEY, JR.

Los Alamos Scientific Laboratory of the University of California, Los Alamos, New Mexico

Received October 31, 1959

This paper is a continuation of the series[2] reporting measurements of the heats of formation of the rare earth oxides. The method, involving the determination of the heat evolved from the combustion of a weighed sample of the metal in a bomb calorimeter at a known initial pressure of oxygen, has been described.[3] The same units and conventions are used here.

Thulium Metal.—Thulium metal was obtained from two sources, Ames Laboratory, A.E.C., Ames, Iowa (Ames) and The Michigan Chemical Co., Saint Louis, Michigan (M.C.). The analyses of the samples were made at this Laboratory and are summarized in Table I.

TABLE I

ANALYSIS OF THULIUM METAL—% IMPURITIES

	C	H	O	N	Mg	Ca	Ta	Sm
Ames	0.090	0.009	0.020	0.006	0.04	0.10	..	1.0
M.C.	0.075	0.037	0.230	0.009	0.05	0.10	1.05	..

No other metallic impurities were detected spectrochemically. The thulium metal from Ames thus contained about 1.27% impurities, the M.C. metal, 1.55%. Assuming that the non-metallic impurities were combined with the thulium as the carbide, hydride, nitride and oxide, the Ames material was 96.69 mole % metal and the M.C. material, 93.66 mole %. (Atomic weight Tm = 168.94.) The X-ray lattice constants for the M.C. material were slightly greater than expected, possibly indicating the presence of rare earths of lower atomic number in solution.

Combustion of Thulium.—A 10 mil diameter fuse wire of magnesium was used to ignite the thulium. The thulium was burned on sintered discs of thulium oxide in oxygen at 25 atm. pressure. The metal showed no gain in weight when exposed to O_2 at 25 atm. pressure for one hour. Combustion varied from 88.67 to 99.67% of completion. The average initial temperature was 25.2°. The two series of runs are summarized in Table II.

TABLE II

THE HEAT OF COMBUSTION OF THULIUM

Mass Tm burned, g.	Wt. Mg, mg.	Wt. Tm_2O_3, g.	Joules/deg, total[4]	ΔT, °K.	Energy from Firing, j.	Energy from Tm, j./g.	Dev. from mean
			Ames				
2.1404	7.00	70.2	10020.2	1.2210	15.1	5628.2	5.2
1.9987	7.29	67.6	10019.3	1.1477	10.6	5658.1	24.7
2.3099	6.15	59.0	10017.0	1.3117	7.7	5619.2	14.2
1.7425	6.94	60.6	10017.5	0.9967	10.3	5625.8	7.6
2.0488	7.11	55.8	10016.2	1.1685	15.4	5630.4	3.0
2.1125	6.15	59.8	10014.6	1.2060	13.8	5638.9	5.5
				Av.		5633.4	10.0
				Stand. dev.			5.6
			M.C.				
2.2753	6.75	49.6	10014.6	1.2694	12.5	5508.5	1.7
1.9130	7.09	46.8	10013.9	1.0750	10.5	5530.3	20.1
2.0456	7.31	46.1	10013.7	1.1462	11.2	5517.3	7.1
2.0316	7.42	46.3	10013.7	1.1353	12.9	5499.4	10.8
1.9019	6.20	39.1	10011.9	1.0642	12.5	5515.1	4.9
2.2207	6.39	39.1	10011.9	1.2381	11.7	5505.7	4.5
2.2905	6.28	33.1	10010.3	1.2757	16.7	5500.3	9.9
2.0385	6.76	17.6	10014.1	1.1383	10.5	5504.9	5.3
				Av.		5510.2	8.0
				Stand. dev.			3.65

The two values must be corrected for the impurities present.

Correction for Impurities.—The calculated percentage composition of the thulium metal (Ames) by weight is as follows: Tm metal, 97.77; TmH_2, 0.76; Tm_2O_3, 0.16; TmN, 0.08; C, 0.09; Mg, 0.04; Ca, 0.10; Sm, 1.0. The heat of combustion of this thulium metal corrected for impurities is 5,595.4 joules/g. or 0.67% smaller than the un-

(1) This work was done under the auspices of the A.E.C.

(2) See E. J. Huber, Jr., E. L. Head and C. E. Holley, Jr., THIS JOURNAL, **61**, 1021 (1957), for reference to earlier papers in the series.

(3) E. J. Huber, Jr., C. O. Mathews and C. E. Holley, Jr., *J. Am. Chem. Soc.*, **77**, 6493 (1955).

(4) The specific heat of Tm_2O_3 is estimated as 0.26 joule/g./deg.

corrected value.[5] If the combustion products, H_2O, NO_2 and CO_2, are assumed to react with the oxide to form the hydroxide, nitrate and carbonate, the calculated value would be decreased by an additional 0.36%.

The calculated percentage composition of the thulium (M.C.) is Tm metal, 93.62; TmH_2, 3.14; Tm_2O_3, 1.85; TmN, 0.118; C, 0.075; Mg, 0.05; Ca, 0.10; Ta, 1.05. The heat of combustion of this sample corrected for impurities is 5,564.4 joules/g. or 0.98% larger than the uncorrected value. Reactions between the combustion products would decrease this value by 2.43%.

Whereas the original combustion values differed by 2.2%, the corrected values differ by 0.6%.

Calculation of the Uncertainty.—The uncertainty to be attached to each of the corrected values includes the uncertainty in the energy equivalent which is 0.04%, the uncertainty in the calorimetric measurements which is 0.20% (Ames) and 0.13% (M.C.), and the uncertainty introduced in the correction for impurities which is estimated to be 0.39% (Ames) and 0.40% (M.C.). The combined uncertainties become 0.44 and 0.42%.

Composition of the Thulium Oxide.—The oxide formed was tan in color. An X-ray pattern showed it to have a cubic structure with a = 10.490 Å.

Heat of Formation of Tm_2O_3.—Using methods of calculation reported elsewhere,[3] the heat of formation of Tm_2O_3 is $\Delta H_{25}^\circ = -1894.8 \pm 8.3$ and -1884.3 ± 7.9 kjoules/mole for the two samples of thulium metal used. Combining and weighing these values yields a figure of 1888.8 ± 5.7 kjoules/mole or 451.4 ± 1.4 kcal./mole. This value is quite close to that observed for the heat of formation of erbium oxide ($\Delta H_f = -453.59 \pm 0.45$ kcal./mole).[6] No literature values for thulium are available for comparison.

Acknowledgments.—The authors wish to acknowledge the valuable assistance of F. H. Ellinger, H. D. Cowan and D. Pavone in the analytical work. They also appreciate the courtesy of Dr. F. H. Spedding of the Ames Laboratory, A.E.C., for loaning the oxide and one sample of the metal.

(5) The heats of formation of TmH_2 and TmN are estimated at −45 and −75 kcal./mole. The heats of combustion of graphite (to CO_2), Ca (to CaO), Mg (to MgO), and Sm (to Sm_2O_3) are taken as 33,000, 15,800, 24,670 and 6020 joules/g., respectively. The heats of formation of H_2O(g) and NO_2 are taken as −58 and +8 kcal./mole.

(6) E. J. Huber, Jr., E. L. Head and C. E. Holley, Jr., THIS JOURNAL, **60**, 1582 (1956).

THE THERMODYNAMICS OF THE REACTION $Cr(OH_2)_6^{+3} + Br^- = Cr(OH_2)_5Br^{+2} + H_2O$ IN AQUEOUS SOLUTION OF IONIC STRENGTH = 2.0 M[1]

BY JAMES H. ESPENSON AND EDWARD L. KING

Department of Chemistry, University of Wisconsin, Madison, Wisconsin

Received October 31, 1959

The present study of ion association to form the complex ion[2] $Cr(OH_2)_5Br^{+2}$ is possible despite the very low stability of the species because of its inertness. Although less than one per cent. of the chromium(III) is converted to $Cr(OH_2)_5Br^{+2}$ in the solutions studied in this work, the trace of chromium(III) present in this form can be quantitatively separated from $Cr(OH_2)_6^{+3}$ by an ion-exchange procedure. The influence of one per cent. ion association of an electrolyte MX_3 on any colligative property of the solution would be so slight as to defy its use in the determination of the extent of ion association. This is due not to the impossibility of making measurements of the appropriate accuracy but rather to the impossibility of accurately defining the properties expected of an electrolyte solution which contains a completely dissociated electrolyte at a moderate concentration.

Doubly-distilled water was used in the preparation of all solutions. Chromium(III) perchlorate was prepared by the reduction of reagent grade chromium(VI) oxide with formic acid in perchloric acid solution; it then was recrystallized twice from perchloric acid solution. Sodium perchlorate, obtained from the G. F. Smith Chemical Co., was recrystallized twice from water. A solution of hydrobromic acid was prepared by treating potassium bromide with concentrated perchloric acid, the precipitated potassium perchlorate then being removed by filtration through sintered glass.

Solutions of three different stoichiometric compositions were prepared and equilibrated for times long relative to the time required for equilibrium to be established. In some cases, solutions were pre-equilibrated at a higher temperature; equilibrium at the temperature of interest then was approached from the opposite side. The equilibrated samples were effectively quenched, and a lowering of the electrolyte concentration was simultaneously accomplished, by dilution of measured volumes 3- to 5-fold with ice-cold water (T = 0–5°). The chilled solution, with an electrolyte normality of ~0.4–0.8, was passed through a short column of Dowex-50 resin (X-12, 50–100 mesh) and followed by chilled 0.8 M perchloric acid. The chromium (III) species of charge + 3, $Cr(OH_2)_6^{+3}$, was held in the resin phase as shown by the presence of the dark band which had barely moved from the top of the column, and all species of lower charge were contained in the eluant. It has been shown that inappreciable chemical change occurs in the quenched samples during this separation procedure. The eluant was analyzed for chromium by treatment with sodium hydroxide pellets and hydrogen peroxide. The resulting chromate ion was determined spectrophotometrically.[3] It was assumed that the only chromium(III) species which came through the ion exchange separation procedure was $Cr(OH_2)_5Br^{+2}$. The relative constancy of the value of the equilibrium quotient, $Q_1 = [CrBr^{+2}]/[Cr^{+3}][Br^-]$,[4] calculated on this basis demon-

(1) This work was supported in part by a grant from the United States Atomic Energy Commission (Contract AT(11-1)-64, Project No. 3)

(2) It is assumed that the coordination number of chromium(III) is six in monobromochromium(III) ion. A green crystalline hexahydrate of chromium(III) bromide is known (M. A. Recoura, *Compt. rend.*, **110**, 1029, 1193 (1890); N. Bjerrum, *Ber.*, **40**, 2917 (1907)); presumably this contains the ion $Cr(OH_2)_4Br_2^+$. If analogous to the species in crystalline green chromium(III) chloride hexahydrate, it is the *trans* isomer (E. L. King, Sr. M. J. M. Woods, O. P., and H. S. Gates, *J. Am. Chem. Soc.*, **80**, 5015 (1958)).

(3) G. W. Haupt, *J. Research Natl. Bur. Standards*, **48**, 414 (1952).

TABLE I

VALUES OF $Q_1 = [CrBr^{+2}]/[Cr^{+3}][Br^-]$ AS A FUNCTION OF TEMPERATURE AT $I = 2.00\ M$

Soln. compn.[a]			
$[Br^-]$	0.509	0.875	1.324
$[Cr^{+3}] + [CrBr^{+2}]$	.126	.105	0.106
$[H^+]$	.512	.473	.512
$[Na^+]$	.737	.900	.857
Temp., °C.	Values of $Q_1 \times 10^{-5}$[b,c]		
0.0	0.97	0.93	0.98
25.0	2.26	2.25	2.23
34.7	2.85	2.85	2.86
45.2	3.63	3.83	3.74

[a] A formula in brackets represents the molarity of the species. In each solution, perchlorate ion was present at the concentration required for electroneutrality. [b] Each tabulated value of Q_1 is the average of two to four independent measurements. The average difference of the independent measurements from the average values was 1.5%. [c] The values of $Q_1 \times 10^5$ calculated for these temperatures using $\Delta H_1 = +5.1$ kcal. and $\Delta S_1 = 4.9$ e.u. are 0.98, 2.09, 2.79 and 3.67, respectively.

strates the correctness of the assumption. A summary of the results is given in Table I.

The approximate constancy of Q_1 if the medium is changed by the substitution of bromide ion for perchlorate ion at constant ionic strength is taken to indicate that: (a) the activity coefficient quotient $\gamma_{+3}\gamma_{-1}/\gamma_{+2}$, with the subscripts indicating the ionic charges, is constant with this medium change; (b) outer-sphere association of $Cr(OH_2)_6^{+3}$ and Br^- does not occur to an appreciable extent, and (c) as stated above, an inappreciable amount of $CrBr_2^+$ is formed. It must be admitted that the observed results could also be the consequence of a mutual cancellation of these several factors.

The temperature coefficient of Q_1 yields the values, $\Delta H_1 = 5.1$ kcal. and $\Delta S_1 = 4.9$ e.u. The approximately 100-fold lower stability of $CrBr^{+2}$ (with respect to Cr^{+3} and Br^-) relative to the analogous stability of $CrCl^{+2}$ is largely a consequence of the less positive value of ΔS_1. (For the reaction $Cr^{+3} + Cl^- = CrCl^{+2}$ in 3.7 M $HClO_4$, $\Delta H = 6.1$ kcal. and $\Delta S = 17.2$ e.u.[5])

(4) For convenience, water molecules will not always be shown in the first coördination shell of chromium(III).

(5) H. S. Gates and E. L. King, *J. Am. Chem. Soc.*, **80**, 5011 (1958).

COMMUNICATIONS TO THE EDITOR

CATALYTIC OXIDATION OF HYDROGEN SULFIDE TO SULFUR OVER A CRYSTALLINE ALUMINOSILICATE

Sir:

We have discovered that a synthetic crystalline aluminosilicate, known commercially as 13X molecular sieve,[1,2] is a particularly active catalyst for the oxidation of hydrogen sulfide with air. When gaseous sulfide was passed over the powdered zeolite in open air at room temperature, free sulfur was deposited on the catalyst surface initially, and the immediate evolution of heat was observed. Within seconds the catalyst became incandescent and the gas stream ignited.

Further studies were made using a tubular glass reactor which was fitted with a coarse-porosity sintered disc for holding approximately 1 g. of catalyst powder. A glass jacket surrounded the reaction zone and contained 1-methylnaphthalene, b.p. 245°, which served as a coolant. Hydrogen sulfide and air were introduced to the reactor at flow rates of 360 and 960 ml. per minute, respectively, corresponding to stoichiometric ratios of hydrogen sulfide and oxygen for sulfur formation. On admitting the gases at room temperature the catalyst turned yellowish-brown in color, changing to a cobalt-blue color which persisted. During this color transformation sulfur started condensing below the disc; within five minutes the coolant was refluxing slowly. Mass spectrometry gave the effluent gas composition as 98.1 mole % nitrogen and 1.2 mole % argon. The reaction was continued for 110 hours to yield a total of 2100 g. of sulfur. Several times during this period the reaction was stopped, the reactor cooled to room temperature and reaction started again by the introduction of more of the gas mixture. When the reaction was interrupted, the intense blue coloration of the catalyst disappeared. Occasionally small portions of the used catalyst had a permanent light blue color. X-ray diffraction of the used catalyst indicated retention of a major part of the crystallinity. No measurable loss of catalyst activity was noted throughout the experiment.

A gaseous mixture of 30 mole % hydrogen sulfide, 26 mole % methane, 9 mole % oxygen and 35 mole % nitrogen underwent a preferential oxidation of the hydrogen sulfide when passed over the catalyst. Clean, odorless sulfur was produced. Analysis of the effluent gas by mass spectrometry indicated no loss or oxidation of methane while from 95 to 100% of the oxygen was consumed.

The oxidation of hydrogen sulfide to sulfur has been catalyzed previously by bauxite,[3] by soda-lime[4] and by nickel and cobalt sulfides supported on alumina.[5] Bauxite, the most widely used of these catalysts, cannot initiate reaction at room temperature as does the aluminosilicate catalyst, nor does bauxite effect the high conversions observed in our studies.

(1) Obtained from the Linde Company; see D. W. Breck, W. G. Eversole and R. M. Milton, *J. Am. Chem. Soc.*, **78**, 2338 (1956).

(2) R. M. Barrer, F. W. Bultitude and J. W. Sutherland, *Trans. Faraday Soc.*, **53**, 1111 (1957).

(3) For example, see H. Grekel, *Oil Gas J.*, **57**, No. 30, 89 (1959).

(4) H. N. Dunning, U. S. Patent 2,760,848 (1956).

(5) J. Lefebvre, *Bull. soc. chim. France*, 564 (1959).

Since the crystalline aluminosilicate is a one-component catalyst, as distinguished from multi-component or amorphous catalysts, an opportunity is afforded for detailed study of the compositional and structural factors which impart catalytic activity for this reaction.

SOCONY MOBIL OIL COMPANY
RESEARCH DEPARTMENT GEORGE T. KERR
PAULSBORO, NEW JERSEY GEORGE C. JOHNSON

RECEIVED FEBRUARY 25, 1960

INTRACRYSTALLINE AND MOLECULAR-SHAPE-SELECTIVE CATALYSIS BY ZEOLITE SALTS

Sir:

We have found unexpected intrinsic catalytic activities on synthetic crystalline inorganic zeolite salts.[1,2]

The sodium aluminosilicate isostructural with faujasite, known as "13X,"[3] is more active for the cracking of normal paraffins than conventional silica–alumina cracking catalysts (10% Al_2O_3, 420 m.^{2}/g. surface area). If one replaces most of the Na^+ by Ca^{++}, the cracking activity is further increased (Table I). The products from the Ca^{++} form resemble those from silica–alumina. However, the products from the Na^+ form are free of branched-chain structures.

TABLE I

n-DECANE CRACKING, 3 HR. OPERATION, 470°, τ = 9 SEC., 1 ATM.

Catalytic Solid	% Decane converted	Iso-butane: *n*-butane ratio	Iso-pentane: n-pentane ratio	Olefins in cracked products, wt. %
Silica-alumina	25	3.1	3.0	37
Na-aluminosilicate, X	32	0.0	0.0	62
Ca-aluminosilicate, X	39	1.1	2.4	30

In contrast with its high catalytic activity for the cracking of paraffins, the Na^+ form is inactive for the dealkylation of isopropylbenzene even at 510°; however, the Ca^{++} form produces extensive conversion at 465°. Alpha-pinene undergoes no reaction when refluxed with the Na^+ form, but is converted extensively to camphene by the Ca^{++} salt.

The observed cracking activities are unexpected because of the common view that "acidity" is a requirement and the common experience of poisoning by alkali and alkaline earth metals on conventional silicious cracking catalysts.[4]

We believe that the locus of catalytic activities resides in the extensively developed interstices of the X crystal. These interstices are accessible to all molecules with critical diameters less than *ca.* 9Å., *i.e.*, to all of the reactant and product molecules described above.

We have been able to demonstrate molecular-shape-selective catalysis by utilizing intrinsic catalytic activities described above, or artificially incorporated catalytic materials within salt forms of the A zeolite, known as "molecular sieves,"[5] having "port" sizes of 4 to 5 Å. Such observations, in addition to providing an unusual type of catalytic selectivity, support the concept of "intracrystalline catalysis," in contrast to activity of the exterior surface of crystals.

With the Ca^{++} form of the A crystal, we have carried out the selective dehydration of 1-butanol in the presence of isobutyl alcohol. Conventional silica–alumina catalyst dehydrates both alcohols at comparable rates. In contrast to the Ca^{++} form of the "X" crystal, we observed cracking of only *n*-paraffins over this solid to only straight chain products, consistent with molecular sieve action which does not allow egress of isomeric products.

As an example of imparted activity, molecular-shape-selective hydrogenation catalysts have been prepared by incorporation of platinum in the A crystal. We have selectively hydrogenated 1-butene in a mixture of 1-butene and 2-Me-propene. In a mixture of equal volumes of 1-butene, isobutene and hydrogen, at 25° with a contact time of *ca.* 0.1 sec., 50% of only the 1-butene was converted to butane. A platinum on alumina catalyst converted approximately equal quantities of both olefins.

Not *all* catalytic activities exhibited by the zeolites need be intracrystalline. For example, with an A zeolite of 4Å. port size we have observed catalysis for the hydration of ethylene oxide to ethylene glycol and polyglycols with no hindrance effect of port size in evidence. Here the catalytic activity appears to be located at the external surface of the crystallites.

In conventional surface catalysis the termination of a three-dimensional solid structure is considered to be the locus of activity. For these zeolites, the concept of surface loses its conventional meaning and the molecular participants can find themselves exposed to unusual coulomb fields.

We wish to acknowledge contributions made to various phases of the above work by R. W. Maatman, R. L. Golden, E. Mower, and G. T. Kerr.

SOCONY MOBIL OIL COMPANY, INC.
PAULSBORO LABORATORIES P. B. WEISZ
PAULSBORO, N. J. V. J. FRILETTE

RECEIVED FEBRUARY 25, 1960

(1) D. W. Breck, *et al.*, *J. Am. Chem. Soc.*, **78**, 2338 (1956).
(2) R. M. Barrer, *et al.*, *Trans. Faraday Soc.*, **53**, 1111 (1957).
(3) Linde Air Products Co., Tonawanda, New York.
(4) *E.g.*, A. G. Oblad, *et al.*, "Advances in Catalysis," Vol. III, Academic Press, New York, N. Y., 1951, pp. 199–247.
(5) D. W. Breck, *et al.*, *J. Am. Chem. Soc.*, **78**, 5963 (1956).

THE NATURE OF THE SPECIES RESPONSIBLE FOR THE LONG WAVE LENGTH ABSORPTION BAND IN ACIDIC SOLUTIONS OF OLEFINS

Sir:

Distinctly different electronic spectra are obtained from solutions of arylalkenes in strongly acidic and weakly acidic media. Thus, while solutions of 1,1-diphenylethylene (DPE) in concentrated sulfuric acid exhibit only the spectrum ($\lambda_{max.}$ = 423 mμ; ϵ = 4.7 × 10^4 cm.$^{-1}$ mole^{-1} liter) due to the expected methyldiphenylcarbonium ion,[1] solutions in weakly acid media, *e.g.*, sulfuric–

acetic acid mixtures, show[2] an additional intense absorption at 600 mμ, ($\epsilon \sim 10^4$ cm.$^{-1}$ mole^{-1} liter). Similar spectra are obtained when DPE is chemisorbed on the acidic surface of a silica–alumina cracking catalyst.[3] It has been suggested[2b] that this long wave length peak corresponds to a non-classical carbonium ion (Pi Complex). However, recent British work,[4] as well as some of our own, has indicated that this probably is not the case. It is the object of this communication to offer evidence leading to the conclusion that this anomalous absorption band is due to the formation of an oxidation product whose properties closely resemble those of aromatic radical ions.[5]

(1) **Kinetic Evidence.**—Reproducible kinetic measurements were made on the rate of formation of the species corresponding to the 600 mμ absorption peak from DPE in a solvent system composed of sulfuric acid, acetic acid and monochloroacetic acid. The over-all kinetic behavior showed that the formation of this species involved an induction period, autocatalysis and a competing decomposition process. While the experimental data have not, so far, yielded to detailed kinetic analysis, the data are suggestive of a free radical chain mechanism. Moreover, the observed rates could be increased by over 100-fold by addition of trace amounts of oxidizing agents such as H_2SeO_4, $H_2S_2O_8$ and $K_3Fe(CN)_6$.

(2) **Spectrophotometric Evidence.**—It was found that DPE could be reduced by Li, Na, K or Ca in tetrahydrofuran in the absence of air to produce either a blue (excess olefin) or red (excess metal) solution. These solutions were interconvertible. Similar behavior was observed with $C_6H_5C{=}CHC_6H_5$, $C_6H_5C{=}CC_6H_5$, $C_6H_5C{=}CH{-}CH{=}CC_6H_5$ and has been reported previously[6] with $C_6H_5CH{=}CHC_6H_5$. Furthermore, the blue solution produced a virtually identical spectrum having a single absorption maximum within 5 mμ of that produced (600 mμ) in the acid solution. As has been noted previously,[5a] this symmetry in behavior is predicted from the simple MO theory of Hückel.[7]

(3) **Magnetic Evidence.**—The solutions of the negative ion were found to be paramagnetic and it was demonstrated that spin concentration followed the spectral intensity of the blue color. A single strong, sharp resonance line was obtained having a width of less than 10 gauss centered at $g = 2.00$. An essentially identical e.p.r. signal was obtained from a solution of DPE and $SbCl_5$ in CH_2Cl_2 (positive ion), whose optical spectrum was observed to be identical to that of the mixed acid solution. It has been noted previously,[4] that paramagnetism cannot be observed in sulfuric acid–acetic acid solutions containing the blue species formed from DPE. In the present work this was confirmed, although failure to observe a signal here might be attributed to the high conductivity and dielectric loss of the solvent system employed. Nevertheless, e.p.r. spectra have been obtained from polynuclear aromatic systems[5] in 98% H_2SO_4. Furthermore, no e.p.r. resonance was observed when DPE was adsorbed on the surface of a silica–alumina catalyst, even when the latter was colored an intense blue.

From the above discussion it appears evident that the species responsible for the 600 mμ absorption peak, formed when DPE is adsorbed on a silica–alumina cracking catalyst, is an oxidation product of the olefin. It is tempting to suggest that this species is a positive radical ion, but on this basis the absence of paramagnetism remains to be explained. Work on this problem is continuing and a more detailed report will be made later.

Thanks are due to Drs. A. J. Saraceno and D. E. O'Reilly of Gulf Research and Development Company for helpful discussions and to the former for the e.p.r. determinations. This work was sponsored by the Gulf Research and Development Company as a part of the research program of the Multiple Fellowship on Petroleum.

MELLON INSTITUTE HARRY P. LEFTIN
PITTSBURGH 13, PENNSYLVANIA W. KEITH HALL

RECEIVED JANUARY 26, 1960

(1) (a) A. G. Evans and S. D. Hamann, *Proc. Roy. Dublin Soc.*, **25**, 1939 (1950); A. G. Evans, *J. Appl. Chem.*, London, **1**, 240 (1951); (b) V. Gold and F. L. Tye, *J. Chem. Soc.*, 2172 (1952); V. Gold, B. W. V. Hawes and F. L. Tye, *ibid.*, 2167 (1952).

(2) (a) V. F. Lavrushin, *Zhur. Obshchei Khim.*, **26**, 2697 (1956); (b) A. G. Evans, N. Jones, P. M. S. Jones and J. H. Thomas, *J. Chem. Soc.*, 2757 (1956); A. G. Evans, P. M. S. Jones and J. H. Thomas, *ibid.*, 104 (1957).

(3) (a) H. P. Leftin and W. K. Hall, Abstracts of Papers, 135th National Meeting, A.C.S., Chicago, September, 1958, p. 34S; (b) A. N. Webb, Preprints, Div. of Pet. Chem., **4**, C171, 135th National Meeting, A.C.S., Boston, April (1959).

(4) J. A. Grace and M. C. R. Symons, *J. Chem. Soc.*, 958 (1959).

(5) (a) S. I. Weissman, E. de Boer and J. J. Conradi, *J. Chem. Phys.*, **26**, 963 (1958); (b) A. Carrington, F. Dravnieks and M. C. R. Symons, *J. Chem. Soc.*, 947 (1959).

(6) D. E. Paul, D. Lipkin and S. I. Weissman, *J. Am. Chem. Soc.*, **78**, 116 (1956).

(7) E. Hückel, *Z. Physik*, **70**, 204 (1931).

SEPARATION OF HYDROGEN, HYDROGEN DEUTERIDE, AND DEUTERIUM BY GAS CHROMATOGRAPHY

Sir:

A great deal of interest has been shown in the last few years in attempts to separate the isotopes of hydrogen by the methods of gas chromatography. Glueckauf and Kitt[1] separated pure deuterium from hydrogen by displacement chromatography in a column containing palladium black, but indicated that separation by gas-elution chromatography would not be possible. Thomas and Smith[2] did obtain partial resolution of hydrogen and deuterium mixtures by gas-elutionchromatography on such a column; however, the palladium catalyzed the equilibrium between hydrogen, deuterium and hydrogen deuteride, so that only the pure isotopes can be obtained. Moore and Ward[3] reported the separation of orthohydrogen from parahydrogen, and partial separation of

(1) E. Glueckauf and G. P. Kitt, in D. H. Desty, "Vapor Phase Chromatography," Butterworths Scientific Publication, London, 1957, pp. 422–427; E. Glueckauf and G. P. Kitt, in the "Proceedings of the International Symposium on Isotope Separation," Interscience Publishers, Inc., New York, N. Y., 1958, pp. 210–226.

(2) C. O. Thomas and H. A. Smith, *J. Phys. Chem.*, **63**, 427 (1959).

(3) W. R. Moore and H. R. Ward, *J. Am. Chem. Soc.*, **80**, 2909 (1958).

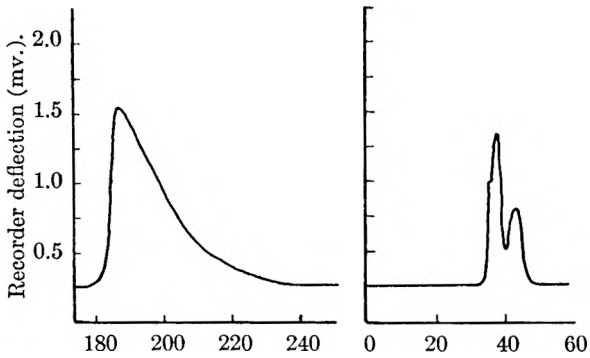

Fig. 1.—Elution curves for hydrogen isotopes on chromia–alumina column with neon carrier at 77°K. The left curve is a deuterium peak with an activated column after introduction of a mixture of H_2, HD, and D_2. Tue H_2 and HD peaks appeared after 114 and 133 minutes. The right curve shows the H_2, HD, and D_2 overlapping peaks when the column is deactivated.

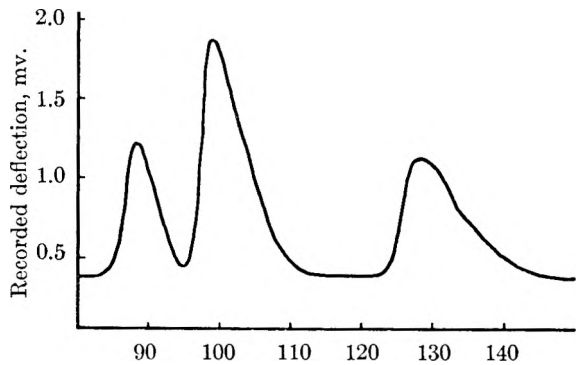

Fig. 2.—Elution curves for hydrogen i6otopes on partially deactivated chromia–alumina column with neon carrier at 77°K. The sample was introduction as a mixture of H_2, HD, and D_2

orthodeuterium from paradeuterium at 77°K. by means of an activated alumina column and employing helium as the carrier gas. Van Hook and Emmett[4] also studied gas chromatography of these isotopes and spin forms on alumina at −195° but were unable to obtain complete separation of the isotopes. Ohkoshi, Fujita and Kwan[5] separated hydrogen deuteride and deuterium by employing a Linde molecular sieve column and hydrogen as the carrier at 77°K. However, none of these workers has succeeded in obtaining quantitative separation of hydrogen, hydrogen deuteride, and deuterium.

Such separation has now been accomplished through the use of a chromia–alumina column operated at 77°K., with neon as the carrier gas. When the packing in a 12-ft. column is freshly activated, the peaks obtained with neon flow rates of 35 cc. per minute are separated by as much as one hour. A recorder trace of a deuterium peak obtained in this manner is shown in Fig. 1. It should be noted that while the peak front is reasonably sharp, there is a considerable amount of tailing evident. When the same column is deactivated by treatment with water, symmetrical peaks are obtained, but hydrogen, hydrogen deuteride, and deuterium peaks overlap, as is shown in Fig. 1. An intermediate situation has been obtained by partially deactivating the column with water, which results in complete separation of hydrogen, hydrogen deuteride, and deuterium, as shown in Fig. 2. The analysis of a known mixture of the three isotopic forms showed that each component can be determined with standard deviations of 0.5 to 1.0 per cent.

Complete details of the column preparation and experimental procedures, as well as a report of work with other columns, will be submitted in the near future.

This work was supported by the United States Atomic Energy Commission.

CHEMISTRY DEPARTMENT HILTON A. SMITH
THE UNIVERSITY OF TENNESSEE
KNOXVILLE, TENNESSEE PAUL P. HUNT

RECEIVED JANUARY 26, 1960

(4) W. A. Van Hook and H. Emmett, private communication of work to be published.

(5) S. Ohkoshi, Y. Fujita and T. Kwan, *Bull. Chem. Soc., Japan*, **31**, 770 (1958).

PHYSICAL PROPERTIES OF CHEMICAL COMPOUNDS—II

Number 22 in
Advances in Chemistry Series

This is a continuation of R. R. Dreisbach's compilation of physical properties of organic compounds (Advances 15). The present volume includes accurate data on 476 acylic compounds not hitherto published. It also includes parameters which can be used for interpolating and extrapolating the determined data for practically all of the compounds listed.

Cloth bound—486 pages plus index—$6.50

order from:
Special Issues Sales
American Chemical Society
1155 16th Street, N. W.
Washington, D. C.

22 types of Safety Enclosures for Handling Hazardous Substances

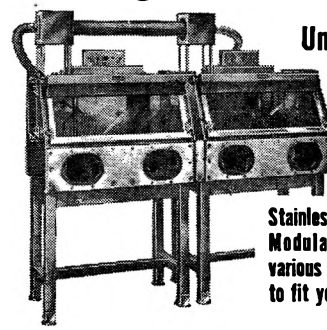

Unitized SAFETY ENCLOSURES

Stainless Steel, All Purpose: Modular adaptability with various adaptor accessories to fit your needs.

DRY RADIOACTIVE WASTE CONTAINER

All-welded stainless steel construction with stainless steel inner container.

Write for illustrated folder describing these and 20 other kinds of enclosures. S. Blickman, Inc., 9003 Gregory Avenue, Weehawken, New Jersey.

BLICKMAN SAFETY ENCLOSURES

Look for this symbol of quality Blickman-Built

Literature Resources for Chemical Process Industries

Designed To Help Both The *New* And The *Experienced* Searcher Of Literature Find What He Wants

Discusses various information sources with 13 articles on market research, 7 on resins and plastics, 6 on textile chemistry, 10 on the food industry, 10 on petroleum, and 13 on general topics, plus 34 pages of index.

order from:
Special Issue Sales
American Chemical Society
1155 Sixteenth Street, N.W.
Washington 6, D.C.

Number 10 in
Advances in Chemistry Series

edited by the staff of
Industrial and Engineering Chemistry

582 pages—paper bound—$7.50 per copy

Announcing the second edition of . . .

THE RING INDEX

A List of Ring Systems Used in Organic Chemistry

by ***AUSTIN M. PATTERSON***
LEONARD T. CAPELL
DONALD F. WALKER

Until this book first appeared in 1940 there was no single source in any language where structural formulas, names and numberings of the thousands of parent organic ring systems could be found.

FEATURES

This new edition of the Ring Index lists 7727 organic ring systems—almost a hundred percent increase over the first edition. The book now has been enlarged to 1456 pages to cover the abstracted literature through 1956. Each ring system contains: (1) A structural formula showing the standard numbering system in accord with the 1957 Rules for Organic Chemistry of the IUPAC. (2) Other numberings that have appeared in the literature. (3) A serial number which identifies the system. (4) The preferred name and other names given to the system. (5) Identifying references to the original literature.

ARRANGEMENT

The ring systems are arranged from the simplest to the most complex, beginning with single rings, then systems of two rings and so on up to twenty-two ring complexes.

USES

The Ring Index is an indispensable reference work for organic chemists and for others who have to do with cyclic organic compounds. Some of its uses are: (1) Determining accepted structure of a ring system. (2) Finding name or names of the system if structure is known. (3) Finding the numbering of a system. (4) Identifying a system if there are two or more isomeric forms. (5) Discovering what systems have been reported in the literature and where. (6) Naming and numbering a newly discovered ring system. (7) As a reference book in teaching.

Cloth bound **1456 pages** **$20.00**

Order from

Special Issues Sales Department, American Chemical Society
1155 Sixteenth Street, N.W., Washington 6, D. C.

1156